

7-25-2008

The Effect of Active Site Mutations on the Homodimeric Behavior of the PvuII Restriction Endonuclease

Grigorios A. Papadakos

University of Missouri-St. Louis, gap4z3@umsl.edu

Follow this and additional works at: <https://irl.umsl.edu/dissertation>

 Part of the [Chemistry Commons](#)

Recommended Citation

Papadakos, Grigorios A., "The Effect of Active Site Mutations on the Homodimeric Behavior of the PvuII Restriction Endonuclease" (2008). *Dissertations*. 546.

<https://irl.umsl.edu/dissertation/546>

This Dissertation is brought to you for free and open access by the UMSL Graduate Works at IRL @ UMSL. It has been accepted for inclusion in Dissertations by an authorized administrator of IRL @ UMSL. For more information, please contact marvinh@umsl.edu.

The Effect of Active Site Mutations on the
Homodimeric Behavior of the PvuII Restriction Endonuclease

A Dissertation

By

Grigorios A. Papadakos

Submitted to the Office of Graduate studies of

The University of Missouri St.Louis

In partial fulfillment of the requirements for the degree of

DOCTOR OF PHILOSOPHY

August 2008

Major subject: Biochemistry

Abstract

The Effect of Active Site Mutations on the Homodimeric Behavior of the PvuII Restriction Endonuclease

(August 2008)

Grigorios A. Papadakos, B.S., University of Athens, Greece

Chair of Committee: Dr. C. M. Dupureur

The PvuII restriction endonuclease, a homodimer of two 18 kDa subunits, belongs to the type II family of restriction enzymes. As a part of the *Proteus vulgaris* RM system, it specifically cleaves the 5'-CAGICTG-3' sequence in the presence of Mg²⁺ ions. Located in the active site of PvuII, Tyrosine 94 has previously been shown to be involved in the metal ion binding by the enzyme. The profile of the Ca²⁺ dependence of the DNA binding to the Y94F variant is shown to be clearly biphasic. The application of a sequential binding model yielded two weak binding constants in the upper phase with a coupling energy ($\Delta G^{\circ}_{\text{coop}}$) at -0.3, while two tight binding constants are shown for the lower phase with -1.4 kcal/mole interaction energy. The similar metal binding pattern between the Y94F and the WT PvuII for Mg²⁺, Ca²⁺, Tb³⁺ and Eu³⁺ in the absence of DNA is also shown. The application of ¹H-¹⁵N HSQC spectroscopy in the presence of Ca²⁺ and DNA and the chemical denaturation of the Y94F variant confirm the conformational impact of Tyr94. It is concluded that the removal of the aromatic

hydroxyl group of Tyr94 slightly repositions the metal ions in the active site of PvuII affecting the intra and/or inter-subunit interactions among the metal binding sites.

The single chain (SC) PvuII bearing a covalent linker between the two subunits is utilized in the exploration of the modes of cooperativity among the metal binding sites. The heterodimeric WTIE68A-SC PvuII was prepared and studied in parallel to the WT-SC homodimer. Global analysis of DNA binding isotherms at different Ca^{2+} concentrations for the WTIE68A-SC variant returned an intra-subunit $\Delta G^{\circ}_{\text{coop}}$ at +1.6 and +1.0 kcal/mole in the absence and presence of DNA, respectively. Combined with similar analysis for the WT-SC variant, the corresponding values for the inter-subunit $\Delta G^{\circ}_{\text{coop}}$ are shown at -2.8 and -1.1 kcal/mole for the occupation of two sites simultaneously. The sequential binding of metal ions in the absence and presence of DNA is overall unfavorable with significant negative interaction being observed between the metal sites. It is shown that the effect of Ca^{2+} ions on DNA binding is greater than the effect of the DNA on the affinity for metal ions. The cleavage of plasmid DNA under single turnover conditions reveals a similar dependence of the nicking and linearization rates on the concentration of Mg^{2+} ions for the WT-SC and the WTIE68A-SC PvuII. The series of events leading to the linear product (DNA association, nicking, release of the intermediate, re-association and linearization) in the presence of metal ions in one PvuII subunit is not significantly slower than the synchronized double strand cleavage in the presence of metal ions in both PvuII subunits.

Στους πολυαγαπημένους μου γονείς και αδέρφια

Αθανάσιο, Ελένη, Ευγενία και Νικόλαο

ACKNOWLEDGEMENTS

I would like to express my gratitude to my advisor Prof. Cynthia Dupureur. I am really indebted to her for the opportunity that she gave me to work on my projects. Her guidance and mostly the understanding and flexibility that she provided me have been invaluable towards the completion of my graduate studies. I would like to sincerely thank Prof. Wesley Harris for providing his fluorimeter when it was needed most. I am grateful for his availability and helpful advice and suggestions in all stages of my research. I would also like to express my gratitude to Prof. Michael Henzl for the availability of his calorimeter and the very influential and informative discussions on the thermodynamics of protein-ligand interactions. His constructive criticism has been very helpful in calorimetry and many related experiments. Many thanks are due to Prof. Chung Wong who always had time to discuss my computational and programming questions. I really appreciate his valuable and precise advice, which correctly oriented me many times. I thank Prof. George Gokel for allowing me to use the calorimeter in his lab. My sincere thanks go to the members of the Gokel lab especially Megan, Wei, Rachel and Alex who have always been very helpful and supportive. My sincere gratitude goes to the late Prof. Andras Simoncsits for his generous donation of the single chain PvuII gene. I would like to thank my committee members Prof. James Chickos, Wendy Olivas and Wesley Harris for reading my manuscript and also for their helpful comments.

Special thanks go to Dr. Lori Bowen, my previous labmate in the Dupureur lab who introduced me to the lab and had been an excellent colleague to work with. My deepest and warmest gratitude goes to my current labmates Dr. Fuqian Xie, Charulata

Prasannan, Supratik Dutta and Binod Pandey. Apart from working together I really enjoyed and appreciated their invaluable friendship. I would also like to express my thankfulness to Dr. Claire Brook, Florencia Lopez Leban and Roxanna Contreras for their strong support and friendship. Many thanks also go to my good friends Dr. Colin White and Aileen Bongat. It has really been a pleasure.

I would not have completed this thesis unless for the endless and loving support of my family: Athanasios, Eleni, Eugenia and Nikolaos. In spite of the long distance they have always been so close through their encouragement and understanding. As a least sign of acknowledgement I would like to dedicate this work to them.

Finally I would like to thank the Department of Chemistry and Biochemistry in the University of Missouri St.Louis for the opportunity in graduate studies that I was provided and the NIH for the financial support of my projects.

TABLE OF CONTENTS

	Page	
ABSTRACT	ii	
DEDICATION	iv	
ACKNOWLEDGEMENTS	v	
TABLE OF CONTENTS	vii	
LIST OF FIGURES	ix	
LIST OF TABLES	xiii	
LIST OF SCHEMES	xiv	
CHAPTER I	INTRODUCTION	
1.1	Introduction to allosteric cooperativity	1
1.2	The Restriction endonucleases	8
1.3	Introduction of heterologous phenotypes in the subunits of oligomeric proteins	34
1.4	Overview of Dissertation	42
CHAPTER II	MATERIALS AND METHODS	
2.1	Enzyme preparation	44
2.2	DNA preparation	53
2.3	Metal ion stock preparation	56
2.4	DNA Binding assays	57
2.5	Metal Binding assays	62
2.6	DNA cleavage experiments	72
2.7	Conformational analysis	75

CHAPTER III	TYR94 OF THE PvuII ENDONUCLEASE	
3.1	Introduction	79
3.2	Methods	86
3.3	Results	93
3.4	Discussion	125
CHAPTER IV	THE SINGLE CHAIN PvuII ENDONUCLEASE	
4.1	Introduction	135
4.2	Methods	144
4.3	Results	150
4.4	Discussion	189
REFERENCES		209
VITA		218

LIST OF FIGURES

		Page
Figure 1.1	Schematic representation of allosteric cooperativity	2
Figure 1.2	A. Schematic representation of the MWC and KNF models	4
	B. Energy diagram for the binding of ligands X and Y to protein A	
Figure 1.3	A. The defense system of the bacterial cells towards phage invasion	10
	B. DNA cleavage sites of type II restriction endonucleases	
Figure 1.4	The structure of the functional subunit in type II restriction endonucleases	12
Figure 1.5	The structure of the EcoRV endonuclease in the presence of cognate and non-cognate DNA.	14
Figure 1.6	A. A generic mechanism for the phosphodiester hydrolysis performed by the type II restriction endonucleases	18
	B. Schematic of the phosphodiester cleavage pattern followed by the PvuII endonuclease	
Figure 1.7	A. The structure of the PvuII endonuclease in the presence of cognate DNA and Ca ²⁺ ions	20
	B. Detail of the PvuII active site residues	
Figure 1.8	A. The locations of the Tyr residues in the PvuII endonuclease dimer	29
	B. Superposition of the active site residues of PvuII in the absence and presence of Ca ²⁺ ions	

	Page	
Figure 1.9	The potential species formed in the case of dimeric proteins	35
Figure 2.1	Purification of the WT E68A single chain PvuII	52
Figure 2.2	A. The duplex oligonucleotide sequences applied to the DNA binding and conformational analysis experiments	54
	B. Structure of the Hexachlorofluorescein dye used in the fluorescence anisotropy experiments	
Figure 2.3	DNA binding to WT E68A single chain PvuII followed by fluorescence anisotropy	59
Figure 2.4	DNA binding to WT single chain PvuII followed by nitrocellulose filter binding	61
Figure 2.5	The structure of the tetrapotassium salt of Mag Fura-2 and the excitation spectra of the chromophore	63
Figure 2.6	Stepwise cleavage of plasmid DNA by PvuII	74
Figure 3.1	The octahedral coordination of the Ca^{2+} ions within the PvuII active site in the WT PvuII-cognate DNA- Ca^{2+} complex	80
Figure 3.2	The interface of the PvuII subunits and the cognate DNA in the D34G PvuII-cognate DNA co-crystal structure	82
Figure 3.3	Differential binding of the Mg^{2+} ions across the WT PvuII subunits	84
Figure 3.4	The dependence of the DNA association constants on the concentration of Ca^{2+} ions for the WT PvuII	94
Figure 3.5	The profiles of the DNA association constants as a function of the	97

	Page
	Ca ²⁺ concentration for the WT and the Y94F PvuII
Figure 3.6	Error intervals for the profile of the DNA association constants versus the Ca ²⁺ concentration of the Y94F PvuII 98
Figure 3.7	The independent fits of the two phases of the DNA binding profile of the Y94F PvuII 100
Figure 3.8	Ca ²⁺ binding to Y94F PvuII 104
Figure 3.9	Mg ²⁺ binding to Y94F PvuII 108
Figure 3.10	Emission spectrum of Tb ³⁺ bound to PvuII 111
Figure 3.11	Tb ³⁺ binding to Y94F PvuII 112
Figure 3.12	Eu ³⁺ binding to Y94F PvuII 113
Figure 3.13	The dependence of the GdnHCl denaturation on the concentration of the WT PvuII dimers 117
Figure 3.14	GdnHCl induced denaturation of the Y94F PvuII 120
Figure 3.15	Overlays of the ¹ H- ¹⁵ N HSQC spectra of the WT and Y94F PvuII 123
Figure 3.16	Overlays of the ¹ H- ¹⁵ N HSQC spectra in the presence of Ca ²⁺ and cognate DNA for the WT and Y94F PvuII 126
Figure 4.1	The structure of the single chain PvuII endonuclease 139
Figure 4.2	The approaches followed in the preparation of heterodimers in restriction endonucleases 141
Figure 4.3	Ca ²⁺ binding to the WT E68A-SC PvuII 152
Figure 4.4	Ca ²⁺ binding observed by Tyr-sensitized Tb ³⁺ luminescence 159
Figure 4.5	The Ca ²⁺ dependence of the DNA association constants in the 164

	Page
	WT and variants of PvuII
Figure 4.6	Energetic diagram of ΔG° for the DNA association with the WT PvuII variants (native and SC) 169
Figure 4.7	DNA binding to the WT/E68A-SC PvuII 172
Figure 4.8	DNA binding to the WT-SC PvuII 173
Figure 4.9	Diagram of ΔG° for the association of the WT-SC and WT/E68A-SC PvuII with DNA at different Ca^{2+} compositions 176
Figure 4.10	The intra and inter-subunit interaction among the metal binding sites in the WT-SC PvuII 181
Figure 4.11	Overlays of the WT and WT-SC PvuII ^1H - ^{15}N HSQC spectra 182
Figure 4.12	Cleavage of Litmus 28i by the WT-SC PvuII 186
Figure 4.13	The Mg^{2+} dependence of the nicking (k_1) and linearization (k_2) rates of Litmus 28i by the WT-SC and WT/E68A-SC PvuII 188
Figure 4.14	The environment of the Glu68 side chain in the WT PvuII-complex with cognate DNA. 195
Figure 4.15	Superposition of the structures of the WT PvuII under different complexation states 203

LIST OF TABLES

		Page
Table 2.1	The sequences of the oligonucleotides used as primer sets for mutagenesis and sequencing	45
Table 2.2	The macroscopic association constants for the Mg ²⁺ binding sites of PvuII, used in the fitting model of the Mg ²⁺ binding data	65
Table 3.1	DNA binding to the WT PvuII and Y94F PvuII	96
Table 3.2	Ca ²⁺ binding to Y94F PvuII	105
Table 3.3	Lanthanide binding to Y94F PvuII observed by Tyrosine sensitized lanthanide spectroscopy	114
Table 3.4	Dependence of the GdnHCl induced denaturation on the WT PvuII dimers concentration	119
Table 4.1	Ca ²⁺ binding to the single chain PvuII variants	154
Table 4.2	Tb ³⁺ binding to the single chain PvuII variants	161
Table 4.3	The DNA dissociation constants for the WT, WT-SC, WT/E68A-SC and E68A PvuII at different Ca ²⁺ concentrations	165
Table 4.4	The apparent Gibbs free energies for the DNA-PvuII complexes at different Ca ²⁺ ion concentrations	167
Table 4.5	Ca ²⁺ and DNA binding properties of the single chain variants of PvuII	174
Table 4.6	Single turnover reaction rates for the cleavage of the Litmus 28i plasmid by the single chain PvuII variants	187
Table 4.7	The metal saturation of the E68A subunit in the E68A homodimers	192

LIST OF SCHEMES

	Page	
Scheme 2.1	The preparation of heterodimeric PvuII variants	47
Scheme 2.2	The script used in Scientist for fitting of the Mg^{2+} -PvuII binding data	66
Scheme 3.1	The sequential occupation of the metal binding sites of the WT PvuII in the presence of DNA	88
Scheme 3.2	The sequential occupation of the metal binding sites of the Y94F PvuII in the presence of DNA	92
Scheme 3.3	Energetic diagrams for the interactions between the metal ion binding sites in the presence of DNA	103
Scheme 4.1	The linked equilibria describing the metal and DNA binding to the single chain PvuII variants	146
Scheme 4.2	The sequential occupation of the metal binding sites of the single chain PvuII variants in the presence of DNA	149

CHAPTER I

INTRODUCTION

1.1 Introduction to allosteric cooperativity

Cells have evolved in a manner that a myriad of regulatory procedures have been developed through which the cellular system carries out its multiple functions. The nucleic acid processes (including transcription, splicing and translation), covalent modifications (such as phosphorylation), several protein-protein interactions and protein interactions with other molecules, and apoptosis are only a few of the regulatory pathways that serve as mechanisms of the cellular functions. The outcome of all these regulatory functions is the maintenance of the cellular homeostasis, the control of cellular metabolism, the transmission of signals, the cell mobility and many more processes characteristic of living and interacting cells. However what underlies all these cellular regulatory functions is the allosteric cooperativity of proteins (Bray, et al., 2004).

The term allostery refers to the coupling of conformational changes between two binding sites, which reside in distant positions on a protein molecule (**Fig 1.1**). If the ligands of the two communicating sites are identical then the linkage is called homotropic, while in the opposite case it is called heterotropic (Wyman, et al., 1990). Depending on the feedback that is to be transmitted by the binding of the first ligand, the affinity of the protein for the second ligand may increase or decrease. The property of communication between distant residue is more universal and not restricted to ligand binding (Koshland, et al., 2002). The stability of the tertiary structure of protein molecules depends on allosteric interactions, while similar communication among amino acids regulates the adoption of a secondary structure of the polypeptide chain

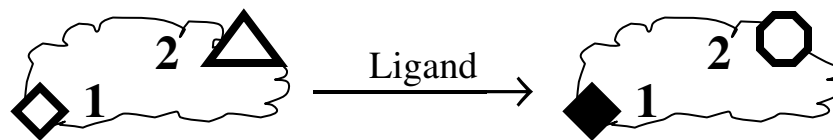


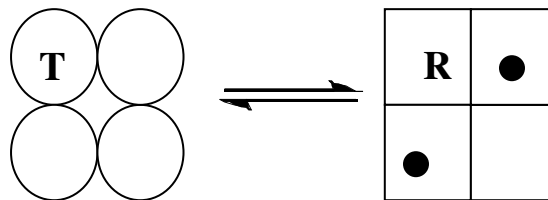
Figure 1.1 Schematic representation of allosteric cooperativity. The conformational change undergone at a distant site on the event of ligand binding is shown. The two distant sites are denoted as 1 (rhombic) and 2 (triangle and circle). The binding site 1 is vacant (white) and occupied (black). Upon binding of ligand at site 1 there is a switch in the conformation of the binding site 2. This conformational change results in alteration of the affinity of site 2 for its ligand.

(Di Cera 1998). Allostery had been initially reasoned as the underlying cause for the mechanism of inhibition of metabolic enzymes such as in the pathway of pyrimidine biosynthesis where uracil and cytosine (the end-products of the pathway) inhibit an enzyme early in the pathway (Pardee, et al., 1956). In this case and also in other metabolic enzymes (e.g., (Adelberg, et al., 1953)), it was noted that the inhibitory ligand was not structurally similar to the substrate of the pathway and thus the binding of the two ligands probably occurs at distinct sites. It is known now that the communicating sites may be found at different domains within the same polypeptide chain or at different subunits in multi-subunit proteins and also across multi-molecular arrays of proteins (Bray, et al., 2004).

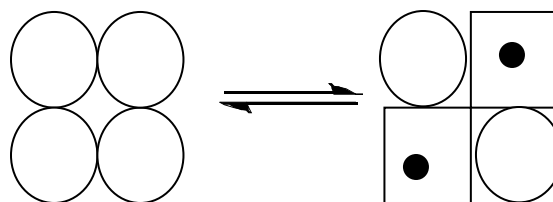
1.1.1 Models describing the allosteric cooperativity

In order to describe ligand-induced protein allostery, two models have been developed based on the observations made for the O₂ binding to hemoglobin: the Monod-Wyman-Changeux model (MWC), (Monod, et al., 1963) and the Koshland-Nemethy-Flimer model (KNF), (Koshland, et al., 1966) (**Fig.1.2A**). Led by the observation of a distinct conformation of hemoglobin in each of the deoxy- and oxy- states, the MWC (concerted) model states that the hemoglobin tetramer assumes concertedly either of the two states (T or R) i.e., all the subunits are in the same conformation at the same time (Monod, et al., 1963). The allosteric systems were consequently described as symmetrical oligomers consisting of identical subunits. Since the MWC model describes the two states as uniform for all the subunits, it practically involves only the case of affinity increase for the binding of ligands following the binding of the first one (positive

A MWC model



KNF model



B

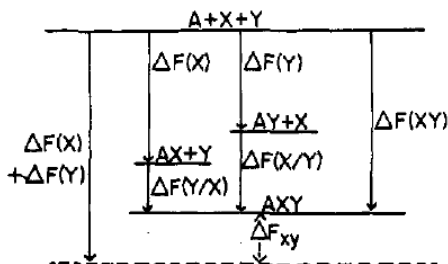


Figure 1.2 A. Schematic representations of the Monod-Wyman-Changeux (MWC) (*top*) (Monod, et al., 1963) and the Koshland-Nemethy-Flimer (KNF) (*bottom*) models (Koshland, et al., 1966). The two states T (non-ligated) and R (ligated) are noted in the MWC model while the corresponding circles (non-ligated state) and squares (ligated state) are noted in the KNF model. The ligand is represented by the black circle.

B. Energy diagram for the binding of ligands X and Y to protein A (adapted from (Weber 1972)). The total free energy of binding both ligands $\Delta F(XY)$ is equal to the sum of the coupling free energy ΔF_{XY} and the free energies of each ligand bound independently $\Delta F(X)$ and $\Delta F(Y)$ ($\Delta F(XY) = \Delta F(X) + \Delta F(Y) + \Delta F_{XY}$). The coupling free energy ΔF_{XY} in turn is equal to the $\Delta F_{XY} = \Delta F(X/Y) - \Delta F(X) = \Delta F(Y/X) - \Delta F(Y)$ where $\Delta F(X/Y)$ is the free energy of binding X in the presence of bound Y and $\Delta F(Y/X)$ is the free energy of binding Y in the presence of X. The conformations of A in the four species (A free, AX, AY, AXY) are not considered equivalent.

cooperativity). In the KNF (sequential) model the ligand binding is described as sequential such that the binding of one ligand molecule induces the adoption of an active conformation of a single subunit, and this change is transmitted to the neighboring subunits, leading to the change in their affinity for subsequent ligand molecules. Essentially the conformational change depends on whether there is a bound ligand in a subunit, and not all the subunits are regarded as conformationally equivalent at the same time (Koshland, et al., 1966). Using the MWC terminology, there can be TR states in the KNF model and not exclusively T or R states. The KNF model evidently permits the effect of the binding of one ligand to be the hindrance of the binding of a subsequent ligand (negative cooperativity) unlike the MWC model.

According to Weber, the binding of ligands to all proteins represents the shift of the equilibria among the populations that the protein molecules can be found in their dynamic ensembles (Weber 1972). The dynamic ensemble was hypothesized after the investigation of the difference of the free energies between the states of ligand bound to an unliganded protein molecule and the one when the protein is already occupied with another ligand, assuming different conformations of the polypeptide chain (**Fig. 1.2B**). It is demonstrated that in the case of negative cooperativity, the conformation adopted by the protein molecule would be dictated by both the bound ligands (and of course depend upon their concentrations). Extrapolating the concept of ligands to the environment of the protein molecules (e.g. protons and other ions) it can be seen that some of them would respond in a non-cooperative manner upon the binding of a protein ligand. Thus due to the solution conditions, a protein cannot assume a unique conformation upon ligand binding. The perturbation of the set of pre-existing equilibria of protein conformations is

done at the expense of free energy at the binding of the first ligand (Weber 1972).

The space of the states of differential stability assumed by a polypeptide chain during its folding may be represented by an energy landscape known as a folding funnel. The folding funnel depicts all the possible conformations according to their stability, which translates into the formation of hills representing high energy states and valleys representing favorable low energy states (Ma, et al., 1999). The bottom of the funnel represents the most favorable states, which are energetically similar if the bottom is not rugged but differing significantly in energy if the bottom is not smooth. The energy differences reflect the stability of the corresponding conformations and consequently the flexibility of the structures. High-energy barriers among states reflect more rigid structures while higher flexibility is shown among conformers with low-energy barriers between them. The flexibility of the protein results from the backbone, domain and amino acid side chain mobilities, which characterize the different conformers. Extending the pattern of the pre-existing equilibria among different conformational states during protein folding to the binding of a ligand, the theory of the dynamic ensemble, is demonstrated (Ma, et al., 1999). The binding of the ligand occurs preferentially to specific conformers and shifts the equilibrium to the most stable conformer in the presence of the ligand. The application of the folding funnel concept to ligand binding contrasts the “lock and key” and “induced fit” theories by Fischer and Koshland, respectively, initially applied to enzyme-substrate interactions which suggested a single conformation of the protein either pre-existing or introduced by the substrate, respectively (Koshland 1958). As a consequence of their conformational substates, all proteins may be classified as either flexible or stiff depending on the local energy minima

around their native states and accordingly potentially allosteric or not. Thus the property of allostery is inherent to all protein molecules and as such the addition of a ligand or mutation can turn a protein molecule allosteric even if its kinetic properties (under native conditions) do not predict this (Gunasekaran, et al., 2004).

This description of cooperativity practically involves all proteins either multimeric or not. Weber had noted that in all proteins the binding of a ligand leads to the introduction of interactions at the binding site that are transmitted through the polypeptide chain and affect local structures of the chain that are less stable than others. In addition to this transmission of the strain due to the bound ligand, the interface between subunits is also a mediator of the strain in multimeric proteins (Weber 1972). In addition to ligand binding, the introduction of mutations even distant to the ligand binding site or the flexible part of the protein that mediates the strain propagation also shifts the pre-existing conformational equilibria.

Molecular dynamics simulations and NMR experiments have proven the flexibility of the protein structure and the population shift upon ligand binding in several systems. Indicative is the case of the homodimeric biotin carboxylase component of the acetyl CoA carboxylase of *E. coli*, whose apo- and holo-structures were determined in solution by triple resonance experiments (Roberts, et al., 1999). By obtaining through space NOE connectivities, the backbone amide dynamics were probed by acquisition of distance restraints, leading to the overlay of the structures of the biotinyl domain in the presence and absence of biotin. It was demonstrated that the two states of the domain had adopted different conformations attributed to the flexibility of the structure at positions far from the biotin binding site (Roberts, et al., 1999). The shift in the

conformation population in the dehydrofolate reductase (DHFR) of *E. coli* was shown via calculations of the energy couplings between individual or groups of amino acids (Pan, et al., 2000). The coupling between individual amino acids was defined to describe how the alterations through point mutations would be propagated while the coupling between groups of residues describes the propagation of alterations upon ligand binding (Pan, et al., 2000). To explore these energy couplings, the residue specific connectivities were introduced, which correlated the probabilities of the states of the residues or groups of residues in the folded state. It was demonstrated that a loop 15 Å from the folate binding site was destabilized upon binding of folate, while the residues around this loop were not energetically coupled to the binding site. Essentially the binding of the ligand showed that the dynamics of the molecule becomes more intense at the event of the binding and thus the molecule does not acquire absolute conformations but dynamically sweeps through all possible conformations of the ensemble (Pan, et al., 2000).

The inherent character of allostery as described makes it evident that even in the absence of a perturbation (mutation or ligand binding), the polypeptide chain is intrinsically dynamic. The protein molecules adopt a variety of conformational changes while maintaining their principal fold either simultaneously rearranging groups of residues or through intrinsically disordering a subunit at the local level and also by domain movements (Bahar, et al., 2007).

1.2 The Restriction endonucleases

The restriction endonucleases comprise a family of nucleases specifically occurring in the proteome of bacteria. The invasion of phages to the bacterial cells led to

the evolution of these highly specific and effective nucleases as part of the Restriction-Modification (RM) system that performs the cleavage and subsequent degradation of the DNA of the invading phage (**Fig. 1.3A**). The bacterial host DNA is protected from the cleavage action of the endonuclease by methylation at the specific endonuclease sites by a methyltransferase, the counter partner enzyme of the RM system (Pingoud, et al., 2001).

1.2.1 The type II restriction endonucleases

The subfamily of the type II restriction endonucleases is comprised of mainly homodimeric nucleases, which have been further classified into types according to their cleavage mode. They may recognize palindromic (e.g. 5'-GAT|ATC-3' for EcoRV and 5'-CAG|CTG-3' for PvuII), or asymmetric substrate sites (e.g. 5'-GGATGN₉|NNNN-3' for FokI), and cleave within the recognition site (e.g. PvuII and EcoRV) or at a specific distance from it (e.g. FokI) producing either blunt (e.g. PvuII) or sticky ends (e.g. G|AATTC for EcoRI) at the substrate DNA (**Fig. 1.3B**). Although in most type II restriction endonucleases all the enzyme subunits possess nuclease activity there is the exception of NaeI which is shown to involve an endonuclease and a topoisomerase domain (Conrad, et al., 1989; Colandene, et al., 1998).

The specificity of the type II restriction endonucleases is demonstrated by the fact that the enzymes scan the bacterial genome whose size ranges from 0.6-10 Mbp and bind with nanomolar affinity to their cognate sequence, which in turn ranges from 4-6 bp. The magnitude of the binding to a specific sequence ranges from 10^3 - 10^7 fold higher than the magnitude of the binding to a non-cognate sequence (Jen-Jacobson 1997). It was

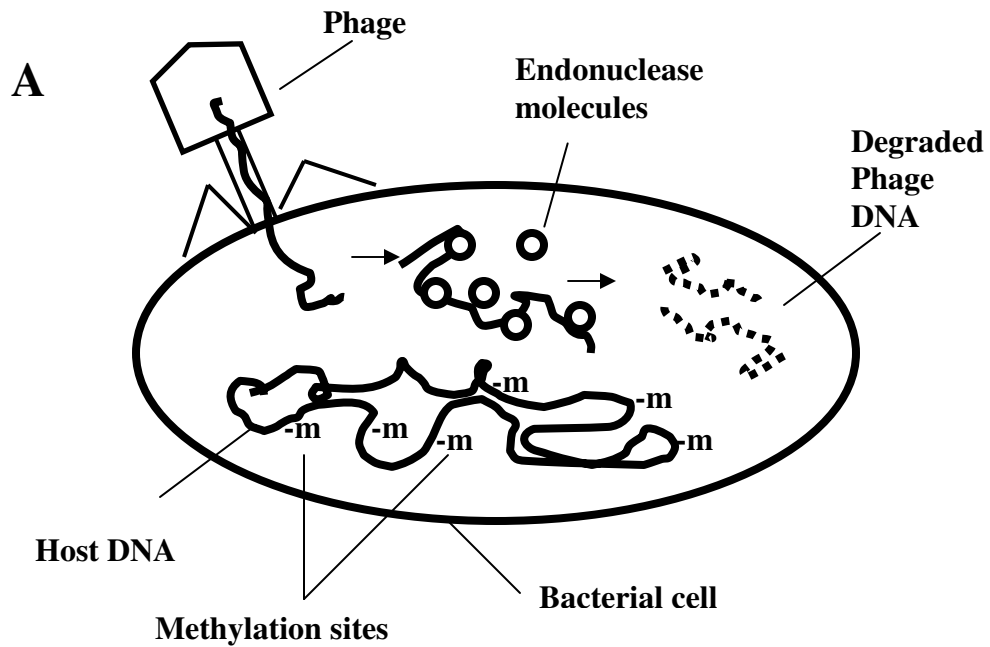


Figure 1.3 A The defense system of the bacterial cells towards phage invasion. The endonucleases bind to their specific sequences on the phage genetic material and cleave it while the corresponding sites at the host DNA remain intact due to methylation at specific bases. B. DNA cleavage sites of type II restriction endonucleases. The cognate palindromic scissile sites of EcoRV and EcoRI and the production of blunt and sticky ends on the DNA substrate are shown respectively.

initially believed that DNA binding proteins discriminate their cognate sequences along the polynucleotide chain by direct hydrogen bonding to the DNA bases (direct readout). This was based on the fact that there is clear distinction on the geometric and electrostatic pattern of two hydrogen bonds potentially formed between a polypeptide chain and purines or pyrimidines that can lead to discrimination among the bases (Seeman, et al., 1976). However the co-crystal structures of type II restriction endonucleases with their cognate DNA have demonstrated the presence of water mediated hydrogen bonding to the DNA bases and hydrogen bonds to the phosphate backbone that contribute to the site recognition (indirect readout) (Winkler, et al., 1993; Athanasiadis, et al., 1994; Deibert, et al., 1999)

Although the primary sequences of the type II restriction endonucleases show very little sequence homology, the structure of these polypeptide chains has been proved to acquire a similar pattern (Venclovas, et al., 1994). Through the comparison of the crystal structures of EcoRI and EcoRV in the presence of cognate DNA the enzymes have been described to be including a common motif in their core consisting of five β strands sandwiched between two α helices (**Fig. 1.4**) (Venclovas, et al., 1994). It was later shown through the development of more crystal structures that irrespective of their lack of sequence homology and also of their mode of cleavage (production of blunt or sticky ends) the motif in the core is preserved and the catalytic site of the enzyme is included into it (Pingoud, et al., 2001). Two families of type II endonucleases have emerged (Pingoud, et al., 2001), a classification due to the structural similarities among enzymes that approach the minor groove of the DNA substrate producing blunt ends (EcoRV family) and the structural similarity among the ones that approach the major

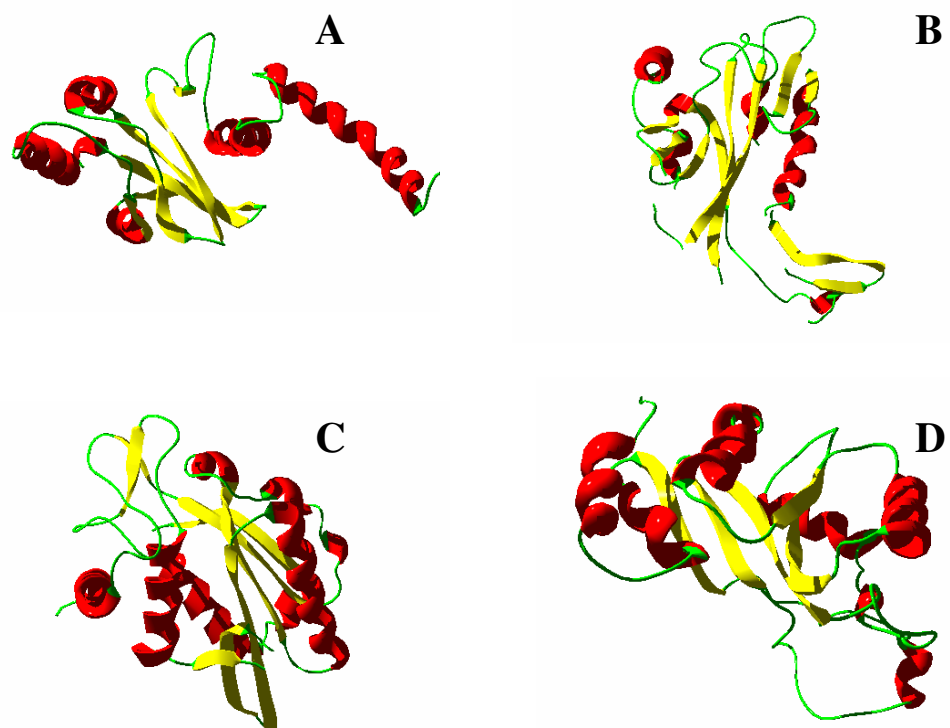


Figure 1.4 The structure of the functional subunit in characteristic members of the type II family of restriction endonucleases. The sandwiched five stranded β sheet (*yellow*) between the two α helices (*red*) is shown for (A) PvuII, (B) EcoRV (EcoRV family) and (C) BamHI, (D) MunI (EcoRI family) adopted from the crystal structures in pdb files 1PVI, 1AZ3, 1BAM, 1D02 respectively.

groove of DNA producing sticky ends (EcoRI family).

The individual subunits come together in dimers or tetramers symmetrically positioned in pairs on the sides of dimerization interfaces. Several sizes of buried surface area ranging from 800-4800 Å² (due to their structural diversity) have been calculated between enzyme subunits based on crystal data of type II restriction endonucleases (Pingoud, et al., 2001). It is evident that the domains that participate in the subunit dimerization are of crucial importance, since they modulate the formation of the DNA binding pocket, correctly positioning the enzyme against the double stranded DNA substrate. Single amino acid substitutions at the dimerization interface result in poor enzyme activity as demonstrated in the case of the W220A variant of the tetrameric Cfr10I where the tetramerization is disrupted (Siksnys, et al., 1999).

In the process of the cognate sequence recognition, the type II restriction endonucleases diffuse linearly on the substrate, forming weak complexes with non-cognate sequences. Water molecules and counterions are excluded from the interface between the protein and the DNA, which involves an area ranging from 2000-4000 Å² buried between the two macromolecules (Pingoud, et al., 2001). Upon substrate binding there are approximately 15-20 direct hydrogen bonds to the DNA bases formed and also other water-mediated or not (e.g. van der Waals) contacts to the DNA bases and backbone. The DNA binding cleft holds the substrate while the catalytic core within each subunit is activated by a conformational change transmitted from the site of the DNA contacts. The conformational response due to the contacts to the cognate DNA has been shown for EcoRV where binding to the specific sequence leads to greater closure of the DNA binding cleft than in the case of non-specific DNA (**Fig. 1.5**)

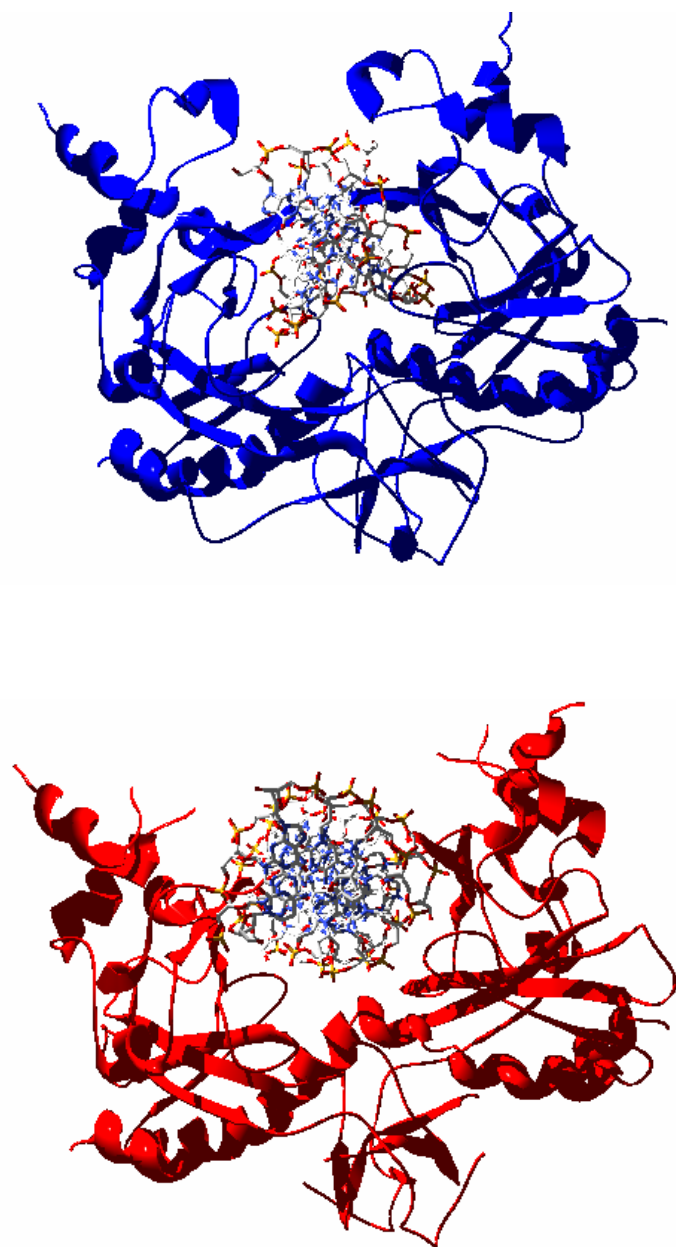


Figure 1.5 The structure of the EcoRV endonuclease in the presence of cognate (top) and non-cognate DNA (bottom). The difference in the closure of the DNA binding cleft is evident in the two different DNA substrates. Adopted from the pdb 2RVE and 4RVE for the non cognate and cognate DNA sequences respectively, (Winkler, et al., 1993).

(Winkler, et al., 1993). The adoption of a conformation that encircles the two strands of the substrate induces major or minor conformational alterations on the DNA as well. For example, in the co-crystal structures with DNA of PvuII and BamHI, minimal distortion on the corresponding substrates is shown where the DNA in both cases retains the B form (Cheng, et al., 1994; Newman, et al., 1995). However the major groove is compressed while the minor groove is widened and a kink of $\sim 50^\circ$ at the phosphate backbone located at the central TA site of EcoRV is observed in the presence of a cognate decamer (Winkler, et al., 1993). Similarly in the case of MunI an overall DNA bend of $\sim 20^\circ$ is observed at the central tetranucleotide AATT (MunI scissile site: 5'-CAATTG-3') while both the major and minor grooves are widened (Deibert, et al., 1999). In both cases the distortions from the B-DNA structure facilitate the unwinding of the DNA and the unstacking of the bases bringing the scissile phosphate ester bonds closer to the active site (Pingoud, et al., 2001). It is shown that the DNA distortion for EcoRV is necessary for the formation of the specific DNA-enzyme complex, as the non-specific DNA sequence in complex with EcoRV still maintains the B form (Winkler, et al., 1993). However as already noted this does not hold for all the members of the family of type II restriction endonucleases.

1.2.2. Metal ion dependence of the catalytic activity of type II restriction endonucleases

As members of the wider family of metallonucleases, the type II restriction endonucleases possess catalytic activity through the coordination of divalent Mg^{2+} ions. Although several transition metals and lanthanide ions have been proposed to facilitate the hydrolysis of phosphodiester bonds when properly ligated, the metallonucleases

natively ligate Mg^{2+} , which intracellularly can be found approximately at 0.5 mM (Cowan 1998; Sreedhara, et al., 2001). It has to be noted that the Ca^{2+} ions can be coordinated within the nuclease active site and promote the binding to the specific DNA sequence although they do not support the catalysis of the substrate DNA as it has been shown for a series of type II restriction endonucleases (Cowan 1998).

As previously shown through crystallography, the type II restriction endonucleases and related nucleases to EcoRV all possess the PD..D(E)XK sequence motif located in the second and third β sheets of the motif surrounded by the two α helices (**Fig. 1.4**) (Pingoud, et al., 2005). In all the restriction endonuclease systems, the application of site directed mutagenesis on the residues included in the motif has shown that the catalytic activity of the enzymes is abolished. This is due to the impaired DNA binding by the variants of these enzymes since the affinity to cognate sequences in the presence of saturating Ca^{2+} concentrations is significantly lower than affinity to the corresponding wild type enzymes (Pingoud, et al., 2005). Thus located in the active site of the restriction endonucleases, the conserved residues of the PD...D(E)XK motif comprise the catalytic machinery of the type II restriction endonucleases with the acidic Asp and Glu contributing to the ligation of metal ions and the basic Lys participating in the DNA hydrolysis (Pingoud, et al., 2005).

The ligation of the native Mg^{2+} ions to the type II restriction endonuclease active site through the conserved acidic residues of the PD..D(E)XK motif has been similarly shown in other nucleic acid processing enzymes which include acidic residues in their Mg^{2+} binding sites such as the RNA polymerase and the Ribonuclease H (Cowan 1998). Crystal structures in the presence of Ca^{2+} , Mg^{2+} or Mn^{2+} exhibit participation of several

water molecules within the coordination sphere of the metal ion. Accordingly, based on the interactions of the metal cofactor with the DNA substrate and the enzyme mediated interactions through these water molecules, several hydrolytic mechanisms that involve the participation of the metal-ligated water molecules have been proposed (**Fig. 1.6A** shows a generic two-metal ion mechanism), (Pingoud, et al., 2005).

Despite the fact that the binding of EcoRV to substrate DNA does not require metal ions (although there is no preference to the cognate sequence) (Taylor, et al., 1991), Mg^{2+} ions are required for recognizing the specific DNA sequence (Thielking, et al., 1992), while Ca^{2+} ions at high concentrations also increase the specificity (Vipond, et al., 1995). In the case of EcoRI the apo enzyme binds preferentially to its cognate sequence (Vipond, et al., 1995), and the presence of Mn^{2+} ions does not exhibit any sequence discrimination (Hsu, et al., 1978). It has been shown that PvuII requires Ca^{2+} ions to promote the formation of high affinity enzyme:DNA complexes and also to distinguish its cognate sequence (Nastri, et al., 1997; Conlan, et al., 2002). Essentially in the case of the type II restriction endonucleases, Ca^{2+} ions increase the specificity to the cognate DNA sequence but there is not a single pattern regarding the modulation of specificity led by Mg^{2+} , Mn^{2+} or even in the apo enzymes. There are enzymes which exhibit the necessary specificity in the absence of Mg^{2+} ions or in the catalytic step when Mg^{2+} ions are already bound (Pingoud, et al., 2001).

1.2.3 The PvuII endonuclease

The PvuII endonuclease is a type IIP restriction enzyme that recognizes and cleaves the palindromic sequence 5'-CAGICTG-3', producing blunt ends and releasing

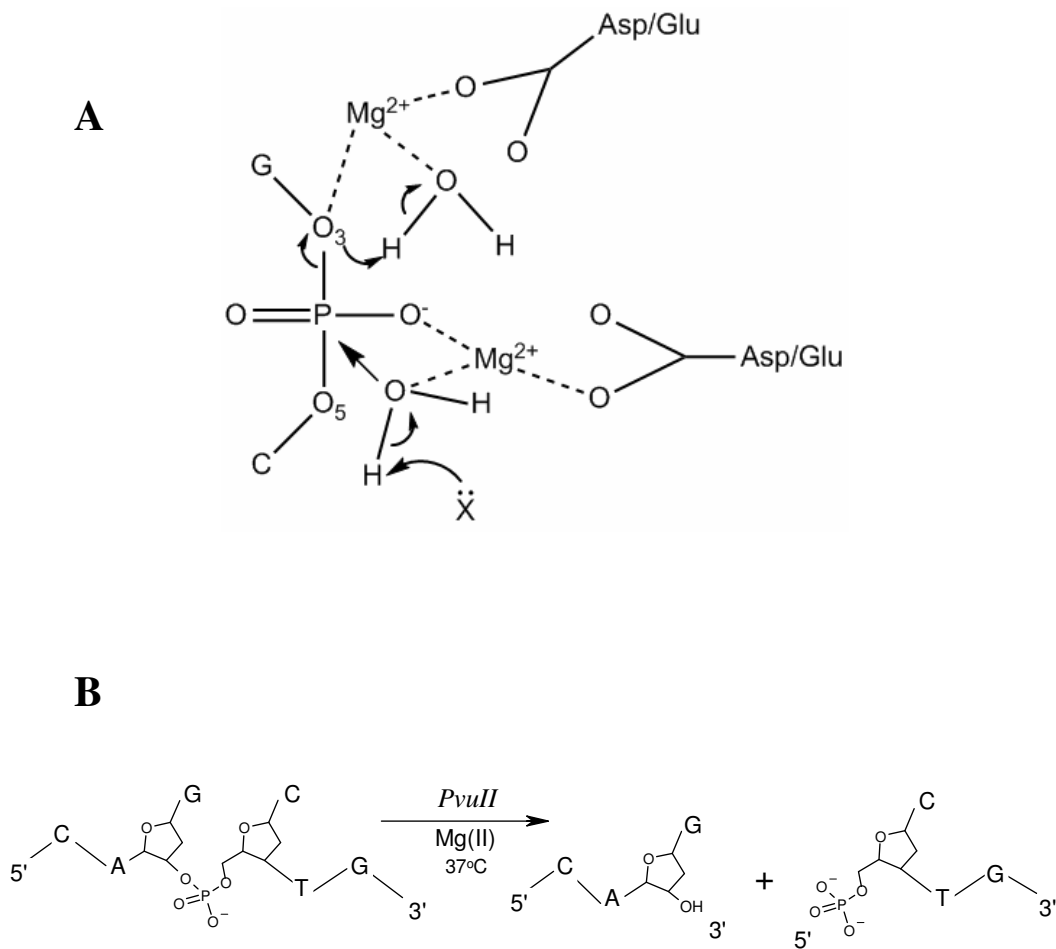


Figure 1.6 A A generic mechanism for the phosphodiester hydrolysis performed by the type II restriction endonucleases. The conserved Asp and Glu of the PD..D(E)XK motif are shown ligating the Mg^{2+} ions, which in turn ligate the attacking and protonating water molecules. A nucleophile X offers its electrons to prepare the nucleophilic OH⁻, which attacks the backbone phosphorus. G and C represent the scissile DNA base pair. The release of the substrate with the free 3'-OH and the 5'-phosphate (as shown in B for PvuII) results in inversion of the phosphorus configuration.

B Schematic of the phosphodiester cleavage pattern followed by the PvuII endonuclease. The 6 bp scissile site 5'-CAG|CTG-3' is symmetrically cleaved in the middle and the released product at the scissile GC base pair along with its complement form a blunt end of the nucleotide sequence.

the hydrolysed phosphate ester to the scissile G base as shown in (**Fig. 1.6B**). PvuII is a homodimer consisting of two identical subunits (**Fig. 1.7A**) and utilizes Mg^{2+} ions as a cofactor for the hydrolysis of the substrate DNA. PvuII belongs in the PD..D(E)XK family of type II endonucleases and utilizes Asp58, Glu68 and Lys70 as parts of the conserved motif to perform the binding of the metal cofactor and the binding and cleavage of the substrate DNA (**Fig. 1.7B**). The coordination of metal ions within the active site of PvuII has been demonstrated both crystallographically and also in solution (Jose, et al., 1999; Dupureur, et al., 2000; Horton, et al., 2000; Spyridaki, et al., 2003; Bowen, et al., 2004).

The crystal structure of PvuII in the presence of Mg^{2+} ions has been examined in the absence of DNA and a single metal ion had been observed per enzyme subunit (Spyridaki, et al., 2003). In the presence of cognate DNA though, the ligation of two Ca^{2+} ions has been shown with each metal ion adopting an octahedral coordination within the active site (**Fig. 1.7B**) (Horton, et al., 2000). In the presence of either Mg^{2+} or Ca^{2+} the acidic residues of the PD..D(E)XK motif participate in the ligation of the metal ions in all the crystal structures examined.

1.2.4 Metal ion coordination to the active site of PvuII

Studies have been performed for the binding of the alkaline earth metal ions and also for the transition metal Mn^{2+} and the lanthanides Tb^{3+} and Eu^{3+} to PvuII in the absence of DNA (Jose, et al., 1999; Dupureur, et al., 2000; Bowen, et al., 2004). Direct calorimetric titrations for Ca^{2+} and Mn^{2+} provided evidence for the ligation of two metal ions to the PvuII active site. The fit of the data to a model of two sets of independent

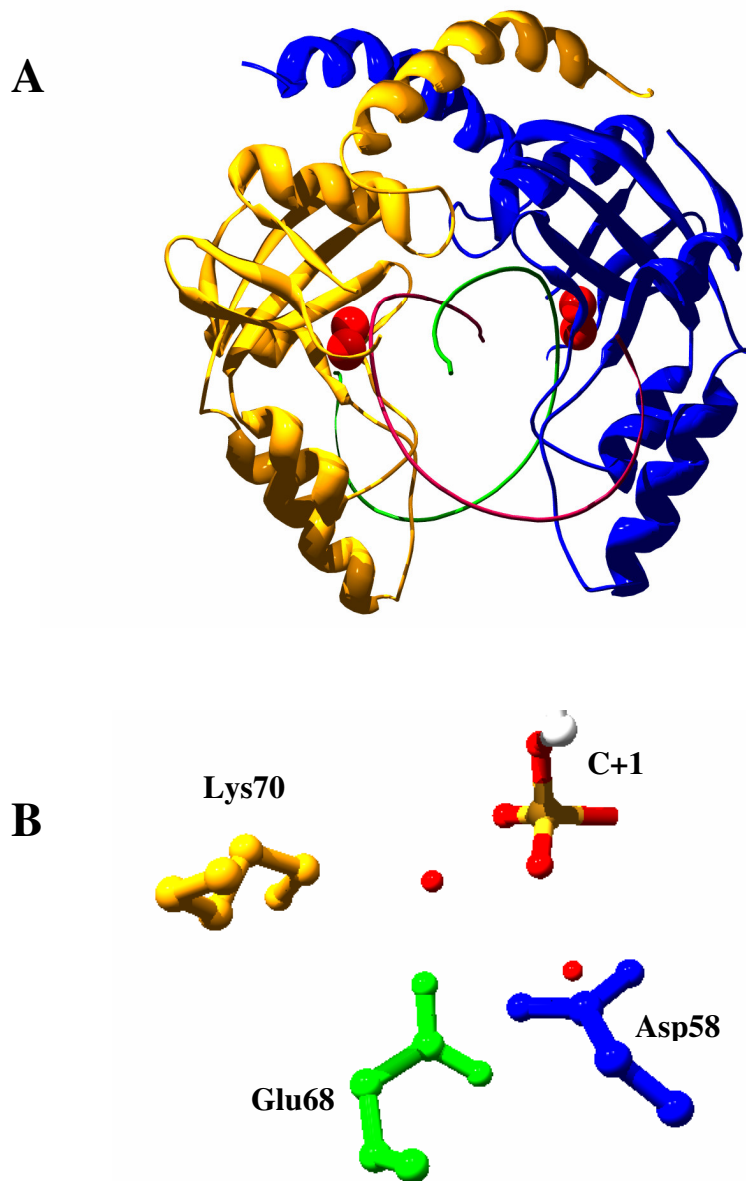


Figure 1.7 A. The structure of the PvuII endonuclease in the presence of cognate DNA and Ca^{2+} ions. The two subunits are shown in *blue* and *yellow* while the two DNA strands are shown as *green* and *red* ribbons and the Ca^{2+} ions as *red* spheres. The catalytic core consisting of the five β -sheets surrounded by the two α -helices includes the catalytic center of the enzyme ligating the metal ions. The conformation of the DNA is induced such that the scissile site is positioned deep into the active site participating in the coordination of the Ca^{2+} ions.

B. Detail of the PvuII active site residues. The conserved Asp58, Glu68 and Lys70 in accordance with the PD..D(E)XK motif are shown along with the two octahedrally coordinated Ca^{2+} ions. Both structures are adopted by the pdb 1F00 (Horton, et al., 2000).

binding sites returned two binding constants at 0.12 ± 0.08 mM and 2.1 ± 0.14 mM and a stoichiometry close to unity for each Ca^{2+} site (Jose, et al., 1999). The same approach in the case of Mn^{2+} returned a set of two metal ions binding at 1.6 ± 0.3 mM, supportive of the binuclear coordination environment within the enzyme active sites irrespective of the type of the metal ion. These data are in full accordance with the crystallographic data as they demonstrate an affinity for Ca^{2+} ions in the absence of cognate DNA. As an additional evidence of the participation of the PD..D(E)XK motif in the ligation of the metal ions in the absence of DNA, the metal binding properties of the E68A and D58A variants of PvuII have been examined. In the case of both variants, the direct titrations of Ca^{2+} to millimolar concentrations of enzyme monomers did not produce sufficient amounts of heat to verify the binding of the metal ions to the active site (Jose, et al., 1999). As such both E68A and D58A were considered as not effective in Ca^{2+} binding, a behavior attributed to the deprivation of the carboxylic groups of the corresponding residues. The same behavior was observed for the E68A mutant in the case of Mn^{2+} ions. However, in the case of the D58A variant, direct titrations of Mn^{2+} reproducibly produced heats resulting in the fitting of the results to a set of independent equivalent sites with a binding constant at 2.0 ± 0.3 mM and a stoichiometry above unity (Jose, et al., 1999). Thus the ability of ligating Mn^{2+} is compensated by the active site environment in the absence of the D58A side chain. Collectively the characterization of the binding properties of the particular PvuII variants in the case of Ca^{2+} and Mn^{2+} supports the active participation of the carboxylic groups of D58 and E68 in the ligation of the metal ions. The binding of the native Mg^{2+} ions has been explored through direct titrations observed by NMR, utilizing the quadrupolar ^{25}Mg nucleus. Although the data

are not sufficient for the discrimination between two and one site binding models, the fit to a Hill equation returned a Hill coefficient equal to 1.4, which is consistent with the simultaneous binding of two Mg^{2+} ions with an apparent binding constant at 1.9 mM (Dupureur, et al., 2000). Similar to the above analysis for the active site acidic residues, the same approach for the Mg^{2+} binding to the two variants D58A and E68A was applied. The application of the Hill model to the D58A data returned a Hill coefficient at 0.7 and a binding constant at 3.6 ± 0.5 mM, which indicates a somewhat weaker binding of Mg^{2+} ions (similar pattern to the binding of Mn^{2+}) than the WT PvuII, although the binding is not abolished as in the case of Ca^{2+} ions (Dupureur, et al., 2000). However the case was not the same for the E68A variant. With a binding constant approximately at 40 mM, the binding of Mg^{2+} ions was barely detectable (Dupureur, et al., 2000).

The investigation of the metal binding properties of the E68A and D58A variants in the absence of cognate DNA lead to the conclusion that the geometry of the active site ligands in the absence of the D58 carboxylic group is adapted in a quite flexible manner to accommodate the coordination of Mg^{2+} and Mn^{2+} but not Ca^{2+} ions. This is also supported from the Mg^{2+} binding data collected as a function of pH, which fitted to a model describing two ionizable groups implicated in the binding of the metal ions to the D58A variant also shown in the case of the WT PvuII (Dupureur, et al., 2000). Despite the ligation of the catalytically necessary Mg^{2+} ions, the metal ions are probably not appropriately positioned to effectively participate in the substrate hydrolysis. The specific activity of the D58A variant on λ DNA is only 0.14 % of the specific activity of the WT PvuII (Dupureur, et al., 2000). On the contrary the active site cannot provide the necessary geometric compensation in the absence of the E68 side chain so that the active

site ligands are not effectively repositioned and the ligation of all the investigated metal ions is abolished. However the specific activity for the E68A variant on λ DNA was found at 2.6 % of the WT PvuII value. This shows that although the fractional saturation for Mg^{2+} is only 20 % at the turnover conditions applied (Dupureur, et al., 2000), this fraction of bound metal ions still supports the hydrolytic activity of the enzyme despite their possible mispositioning as compared to the active site in the WT PvuII.

The binding of the lanthanide ions Tb^{3+} and Eu^{3+} to the WT PvuII has also been examined by observation of the tyrosine sensitized luminescence. Isotherms obtained by the direct titration of PvuII to either Tb^{3+} or Eu^{3+} were fitted to a sequential binding model and two binding constants were assigned. For Tb^{3+} a high affinity site at $2.3 \pm 1.7 \mu M$ and a site of lower affinity at $117 \pm 46 \mu M$ were obtained, while the same pattern was observed for Eu^{3+} with two sites at $1.4 \pm 0.6 \mu M$ and $223 \pm 161 \mu M$ (Bowen, et al., 2004). The presence of two lanthanide ions within the PvuII active site was confirmed by the observation of Eu^{3+} direct excitation spectra, which were applied to line shape analysis. Two peaks were assigned to a strong and a weak Eu^{3+} site, which were populated with respect to a low and a high Eu^{3+} concentration. The fractional occupancies of the sites were obtained by the corresponding peak areas, and their ratio was found in accordance with the calculated ratio using the binding constants measured by the tyrosine sensitized luminescence approach (Bowen, et al., 2004). Thus similarly to Ca^{2+} , the geometry of the ligands within the active site allows the accommodation of a pair of lanthanide ions. However in spite of the similarities in ionic sizes and also between the radii of the complexes of hexacoordinated Ca^{2+} and heptacoordinated Ln^{3+} , the binuclear complexes within the PvuII active site probably do not involve all the same ligands. The binding of

Eu³⁺ ions to the E68A PvuII variant returned a weak Eu³⁺ site with an affinity at ≥ 100 μM , which could not be further pursued due to solubility restrictions at higher lanthanide concentrations. However a Eu³⁺ site at a position similar to the weak site in the case of the WT PvuII was occupied at high concentration of the lanthanide. It was concluded then that the Eu³⁺ ions may occupy the weak site in the absence of the carboxylate of Glu68, although the strong site necessitates the presence of the Glu68 side chain (Bowen, et al., 2004). It is evident though that the Glu68 is not a bridging ligand of the two active site metal ions in the case of Eu³⁺ (probably in general for the trivalent lanthanides), in contrast to the case of the ligation of Ca²⁺ where both the divalent metal ions were coordinated by Glu68 (Horton, et al., 2000). Due to the fact that the carboxylate group occupies less volume than two distinct oxygen ligands (Kay, et al., 1972) and only one Eu³⁺ ion is apparently ligated to it, the distance between the two Eu³⁺ ions in the WT PvuII must be greater than the distance between the two Ca²⁺ ions. As the lanthanide ions show a preference for more than six ligands compared to the divalent alkaline earth metals (Sinha, et al., 1983) it is evident that the ligands that participate in the ligation of each type of metal ion differ both in kind and number.

1.2.5 The DNA binding properties of the PvuII endonuclease

The critical residues at the catalytic, DNA recognition and dimerization domains of PvuII have been well-identified. Gel shift assays utilizing a radiolabeled 65mer containing the PvuII cognate site have been performed to monitor the effect of these residues in DNA binding (Nastri, et al., 1997). In the presence of 10 mM Ca²⁺ ions, no DNA complexation was observed for the D58A and E68A variants, while the K70A

mutant maintained its DNA binding ability. The histidine residues in the His83His84His85 triplet, which were shown in the crystal structure of D34G PvuII to be participating in critical hydrogen bonding at the DNA binding cleft (Cheng, et al., 1994), were independently substituted with alanine. The variants bound well to the cognate DNA, proving that the His triplet is not necessary for DNA binding (Nastri, et al., 1997). The same result was shown for Asp34, which has been shown along with His84 to be the only two residues that contact the scissile GC base pair. Except for the D34G variant, the specificity of PvuII, to cognate DNA was supported in all the His→Ala substitutions mentioned above. The substitution of other residues accessory to DNA binding such as Ser81, Thr82, Asn140 and Asn141, which contact the bases adjacent to the scissile GC base pair (Cheng, et al., 1994), were also shown to be indispensable for the PvuI-DNA complexation (Nastri, et al., 1997). It has been shown that the WT PvuII does not support DNA binding in the absence of metal ions as observed by gel shift assays (Nastri, et al., 1997). The metal ion dependence of the DNA binding properties of PvuII has been explored by observation of the DNA complex formation by nitrocellulose filter binding and fluorescence anisotropy measurements (Conlan, et al., 2002). The binding constant for the PvuII-DNA association at metal saturating conditions was measured and a value ranging between 53-125 pM was shown for different cognate oligonucleotide sequences (Conlan, et al., 2002; Conlan, et al., 2002). The picomolar affinity at saturating metal was also shown previously for BamHI and EcoRV (Engler, et al., 1997; Engler, et al., 2001). The high affinity for the DNA is promoted by the metal ions, since under metal free conditions a binding constant approximately at 300 nM was reported (Conlan, et al., 2002; Conlan, et al., 2002). Hill analysis of the DNA association constants provided an

apparent Ca^{2+} association constant at 2.9 ± 1.9 mM and a Hill coefficient at 3.5 ± 0.2 (Conlan, et al., 2002). The binding of DNA to the WT PvuII and the active site variant E68A has also been examined in the presence of several alkaline earth metal ions and also in the presence of lanthanides and transition metals shown previously not to promote DNA hydrolysis (Bowen, et al., 2003). Similar to the low picomolar affinity for DNA achieved in the presence of high Ca^{2+} concentrations, the trivalent Eu^{3+} and Tb^{3+} used at 10 mM also lead to a thousand-fold affinity increase. More modestly but still stimulating the DNA binding by PvuII, the divalent Ba^{2+} , Sr^{2+} , and Cd^{2+} support an increase of the PvuII-DNA affinity by 20-200 fold compared to the metal free conditions (Bowen, et al., 2003). However it was shown that even an abundance of divalent Zn^{2+} does not promote the formation of the PvuII-DNA complex to an extent significantly higher than the metal free conditions. It is evident from the dependence of the DNA binding properties of PvuII on the nature of the metal ions ligated to the enzyme active site that the formal charge and thus the electrostatics and also the preference for ligands prevail in supporting the PvuII-DNA association. On the other hand, the ionic radius does not primarily influence the metal-ligand contacts formed within the active site and thus the DNA binding is not dependent on it. This is evident from the fact that the cleavage-supporting Mg^{2+} , Mn^{2+} , Co^{2+} have similar ionic radii to Zn^{2+} (~ 0.9 - 1.0 Å depending on the number of ligands), although the latter does not even stimulate DNA binding (Bowen, et al., 2003). It has to be mentioned though that there is a possibility for the affinity to DNA (in the presence of the cleavage supporting metal ions mentioned) to be lower than the picomolar supported by Ca^{2+} and the trivalent lanthanides to allow for efficient turnover (Xie Fuqian, PhD Dissertation, 2008). In order to monitor the dependence of the

specificity of the PvuII-DNA binding process on the metal ion properties a non-cognate DNA binding was also studied in the presence of Ca^{2+} , Tb^{3+} , Ba^{2+} and Cd^{2+} ions. In order to establish the active site positioning of the metal ions and thus the support of DNA binding due to active site contacts, the E68A PvuII variant was employed in DNA binding experiments (Bowen, et al., 2003). The DNA affinities in the presence of Ca^{2+} and Tb^{3+} were lowered by 400 and 140-fold, respectively, indicating the significance of the Glu68 carboxylate in the ligation of these metal ions and the formation of contacts to the DNA emanating from the active site in the presence of Ca^{2+} and Tb^{3+} . The E68A PvuII-DNA affinity was only 17-fold reduced compared to the WT PvuII in the presence of Ba^{2+} , while it remained the same as in the case of the WT PvuII in the presence of Cd^{2+} (Bowen, et al., 2003). These data gave rise to speculation that Ba^{2+} and Cd^{2+} bind to different locations than in the active site and the PvuII-DNA contacts are not primarily metal-mediated emerging from ligated metal ions within the active site.

For all the other tested ions the preference of PvuII for the cognate DNA sequence was significantly lower than the observed in the case of Ca^{2+} . In the case of Tb^{3+} ions the affinity to the non-cognate sequence was higher than in the presence of Ca^{2+} , clearly indicating that due to their properties, the lanthanide ions efficiently support contacts with the non-specific sequence, which would otherwise (in metal free conditions or in the presence of other metal ions) not be favored. In the presence of Cd^{2+} , the affinity for both the cognate and non-cognate sequences are similar, while in the presence of Ba^{2+} , the affinity to the non-cognate sequence is similar to the one in the presence of Ca^{2+} but the ~300-fold drop in the affinity to the specific sequence results in a specificity factor comparable to Tb^{3+} . In contrast to Tb^{3+} though, the Ba^{2+} ions cannot promote the

necessary contacts within the active site even in the presence of the cognate sequence.

The examination of the DNA binding specificity of PvuII focusing on the contribution of active site residues and residues at the DNA binding interface was previously performed (Nastri, et al., 1997). The binding to DNA sequences differing at the central base pair of the cognate sequence was observed by gel shift assays. It was demonstrated that the His83His84His85 triplet and the active site Lys70 along with Glu55 do not contribute to the specificity of the DNA binding process as the corresponding site-directed variants retained their specificity. However the implication of the Asp34 carboxylate in the contacts determining the DNA binding specificity was clearly shown by the compromised DNA binding specificity of the D34G variant (Nastri, et al., 1997). In the same study, the D34G variant was found equivalently active to the WT PvuII as demonstrated by their identical cleavage patterns of λ DNA and their cleavage efficiencies. The PvuII DNA binding properties have thus exhibited strong dependencies on the metal ion cofactor and the integrity of the enzyme structure with the mutations on critical residues having an effect on the DNA binding process as significant as the metal ion substitution.

1.2.6 Tyrosine residues in the PvuII endonuclease

The PvuII endonuclease contains ten Tyr residues (**Fig. 1.8A**) (Athanasiadis, et al., 1994). Through the crystallization of the enzyme with and without cognate DNA and metal ions, three of these tyrosines (Tyr67, Tyr94 and Tyr124) have been shown to be positioned near the active site of the enzyme (Athanasiadis, et al., 1994; Cheng, et al., 1994; Horton, et al., 1998; Horton, et al., 2000). More specifically the phenolic group of

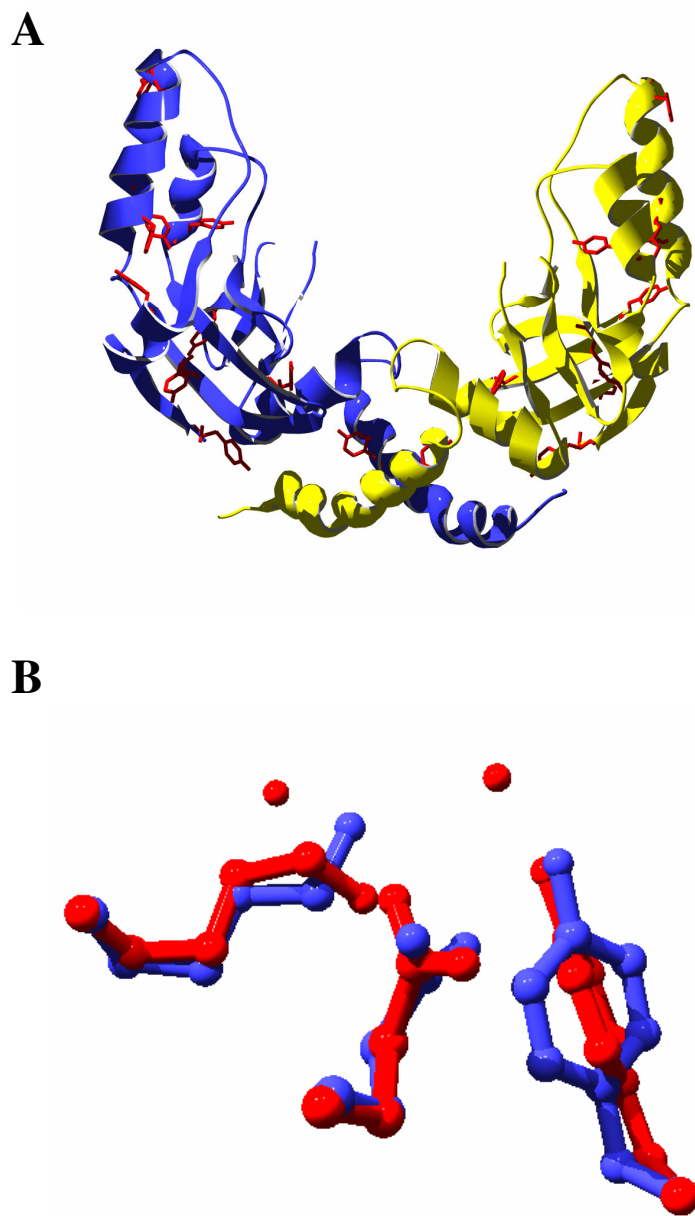


Figure 1.8. A. The locations of the Tyr residues in the PvuII endonuclease dimer. The two subunits are shown in blue and yellow while the ten Tyr residues per enzyme subunit are highlighted (adopted by the pdb file 1PVI). B. Superposition of the Glu68, Lys70 and Tyr94 in co-crystal structures of PvuII with cognate DNA in the absence (*blue*, pdb 1PVI) and presence of Ca^{2+} ions (*red*, pdb 1F0O). The red spheres represent the metal ions in the 1F0O structure.

Tyr124 has been shown to be at a distance of 8 Å away from the carboxylic group of the catalytic Glu68, while the distance of the phenolic ring of Tyr67 from Glu68 is about 13 Å. Due to its adjacent position, the orientation of the latter phenolic ring is opposite to the active site. The crystal structures resolved up to date show that the dimerization interface of the PvuII homodimer does not involve any critical Tyr residue (Athanasiadis, et al., 1994; Cheng, et al., 1994). The seven Tyr residues not in proximity to the active site have not been individually set under investigation, and thus the potential of their exact participation in the adoption of a conformation of the enzyme monomeric subunit is not known. However the relative perturbation of the phenolic ring of all ten Tyr residues of PvuII has been evaluated for the WT PvuII and active site variants upon metal ion ligation in the presence and absence of cognate DNA (Dupureur 1999; Dupureur, et al., 1999; Dupureur, et al., 2001). The incorporation of 3-fluorotyrosine in PvuII was performed, and the fluorine nuclei were observed by application of ^{19}F NMR spectroscopy. No spectral perturbation upon Mg^{2+} binding was shown but the raising of peak degeneracy and perturbation on the chemical shifts of the fluorine peaks was shown in the case of Ca^{2+} and Mn^{2+} , the latter being accompanied by line broadening as well (Dupureur, et al., 1999). Distinct spectral differences were shown between Ca^{2+} and Mn^{2+} , which support the presence of distinct chemical environments and thus positioning of the Tyr residues in response to the ligation of each metal ion. The addition of DNA to WT PvuII did not have any effect on the ^{19}F spectrum of the enzyme, which is identical to the one obtained for the apo WT PvuII (Dupureur 1999). Taking into account the low micromolar binding constants of the WT PvuII for the 6-mer and 12-mer cognate sequences used in this study under metal free conditions the fluorine spectra proved the

weakness of the interaction and the lack of formation of the complex at the applied concentrations (Dupureur 1999). However the addition of Ca^{2+} to the mixture of the WT PvuII and the cognate DNA sequence resulted in the shifting of the six resonances compared to the apo enzyme spectrum, while an extended degeneracy of the resonances was also observed (Dupureur 1999). It should be noted that the perturbed spectrum of the WT PvuII- Ca^{2+} -DNA complex shows extensive differences compared to the Ca^{2+} -PvuII complex. The six observed chemical shift perturbations were regarded to involve the four Tyr residues located within 10 Å from the PvuII active site, in proximity to the metal ions and the cognate DNA. It is evident that the conformational adaptation of the enzyme in the WT PvuII-DNA complex as reported by the Tyr side chains is due to the cooperative effect of the metal ions and the DNA on the enzyme. The conformation of the WT PvuII responds globally to the tertiary complexation as shown by the perturbation affecting the whole group of the ten Tyr residues. However, the conformational perturbation sensed by the Tyr residues in PvuII is not sufficient to assign structural or functional roles in the Tyr residues.

Focusing on the PvuII active site and the three Tyr residues located at its proximity, speculations can be made regarding their potential participation in the formation of the PvuII- Ca^{2+} and WT PvuII- Ca^{2+} -DNA complexes. Due to the distances and orientations of Tyr67 and Tyr124 relative to the active site acidic residues, the participation of Tyr94 to the enzyme complexation is the most probable as crystal structure data indicate (Athanasiadis, et al., 1994; Cheng, et al., 1994). In the structure of the apoenzyme (pdb: 1PVU, (Athanasiadis, et al., 1994)), there are no water molecules in the vicinity of the aromatic hydroxyl group of Tyr94 and consequently no hydrogen

bonds involving Tyr94, despite the fact that the residue is located 3 Å away from the Asp58 carboxylate and less than 5 Å away from the carboxylate of Glu68 and the ε-NH₂ of Lys70. In the presence of DNA, the crystal structure of PvuII (pdb:1PVI, (Cheng, et al., 1994)) showed that Tyr94 is located at the same distance from Glu68 and Lys70, while the scissile phosphate of the cytosine in the central GC base pair is at 3.4 Å from the Tyr94 aromatic hydroxyl group. However there are no water molecules mediating the contact to the scissile phosphate. Moreover in the presence of Ca²⁺ ions in the PvuII-DNA co-crystal structure (pdb:1F0O, (Horton, et al., 2000)), the Tyr94 side chain is positioned towards the carboxylate of Glu68 and the ε-amino group of Lys70 at similar distances (2.9 and 4.1 Å respectively) to the 1PVI structure (**Fig. 1.8B**). In addition the Ca²⁺ ions are shown to be located at 5.35 and 5.8 Å, respectively, from the aromatic hydroxyl group of Tyr94. Although not directly ligated, one Ca²⁺ ion is bound to a water molecule, which in turn is located 3.5 Å away from the aromatic hydroxyl of Tyr94 and 3.3 Å from the scissile phosphate. This particular interaction is the first evidence of the role of Tyr94 in the native enzyme in the presence of metal ions and cognate DNA. The simultaneous implication of the specific water molecule in DNA hydrogen bonding and metal ligation leads to the hypothesis that the Tyr94 phenolic ring takes the supportive role of positioning the specific water molecule and stabilizing this tertiary interaction, which is practically promoted by the metal ions since the Tyr94-water-DNA network did not occur in 1PVI. It should be noted that in all the above-mentioned crystal structures PvuII always appeared as a symmetrical homodimer and no severe discrepancies were observed between the structures of the enzyme subunits, which were thus considered identical. However in a crystal structure of PvuII in the presence of Mg²⁺ ions, the

enzyme subunits were shown to be ligating a single metal ion per subunit in an asymmetric manner (pdb: 1H56, (Spyridaki, et al., 2003)). One Mg^{2+} ion was ligated to Asp58 and Glu68 in one subunit and also participating in hydrogen bonding to water molecules. In the other subunit the aromatic hydroxyl group of Tyr94 was a direct ligand of the Mg^{2+} ion, while the coordination sphere also included the side chain of Thr82 and two water molecules (Spyridaki, et al., 2003). Essentially the metal ion is connecting the catalytic with the DNA recognition site and Tyr94 participates in the network that supports these contacts. An attempt to demonstrate the potential role of the aromatic OH of Tyr94 as emerged from this WT PvuII crystal structure was made by substitution of Tyr94 with Phe and application of the resulting mutant in turnover experiments under steady state conditions. The variant was shown to be accumulating a nicked intermediate of the plasmid substrate applied. The quantification of the dependence of the obtained rates as a function of the Mg^{2+} concentration returned a single metal ion participating per enzyme homodimer and an overall trend of a 10-fold decrease in the rates observed compared to the WT PvuII. This behavior was consistent with the observed asymmetric positioning of the Tyr94 side chain in the crystal structure and led to the conclusion that the Tyr94 mediates the entrance of the Mg^{2+} ions to the PvuII active site in response to intersubunit signaling between the two active sites. Thus the substitution of the residue results in the loss of the communication between the two PvuII monomers. Similar crosstalk impairment across the endonuclease subunits has been previously observed in the case of the EcoRV endonuclease. Substitutions of amino acids involved in catalysis and also in direct and indirect readout were performed in one subunit only (Stahl, et al., 1996; Stahl, et al., 1998). The impact of these mutations on the enzyme activity was

monitored, and it was demonstrated that the amino acids directly contacting the scissile bases and thus performing the base recognition mediate the communication across the subunits (Stahl, et al., 1996). In the case of PvuII similar activity results have been obtained by the introduction of the D34G mutation in one subunit of the enzyme (Simoncsits, et al., 2001). Cleavage experiments under steady state conditions were applied to demonstrate the accumulation of nicked intermediate and the lack of orchestrated cleavage of both DNA strands in the presence of the mutation in one subunit only (Simoncsits, et al., 2001). The production of heterodimeric enzymes in the case of PvuII was performed by the covalent linkage of the subunits, while in the case of EcoRV the two subunits of different phenotype were purified from the mixture of dimers of exchanged subunits by sequential affinity chromatographies (Stahl, et al., 1996; Simoncsits, et al., 2001).

1.3 Introduction of heterologous phenotypes in the subunits of oligomeric proteins

The effect of the introduction of different phenotypes across subunits in multi-subunit proteins has long been under investigation in a wide variety of proteins. The covalent linkage of the different subunits has been mainly exploited for this purpose although the modification of subunits and their subsequent association without linkage has also been performed (**Fig. 1.9**). The covalent linkage is not only of great assistance in the study of the effect of a site-directed substitution of an amino acid, which would be mutated in all the identical subunits if these are not connected. The design of novel protein molecules combining the individual functions of their linked subunits in hybrid molecules is maybe the most significant outcome of such an approach. For example, the

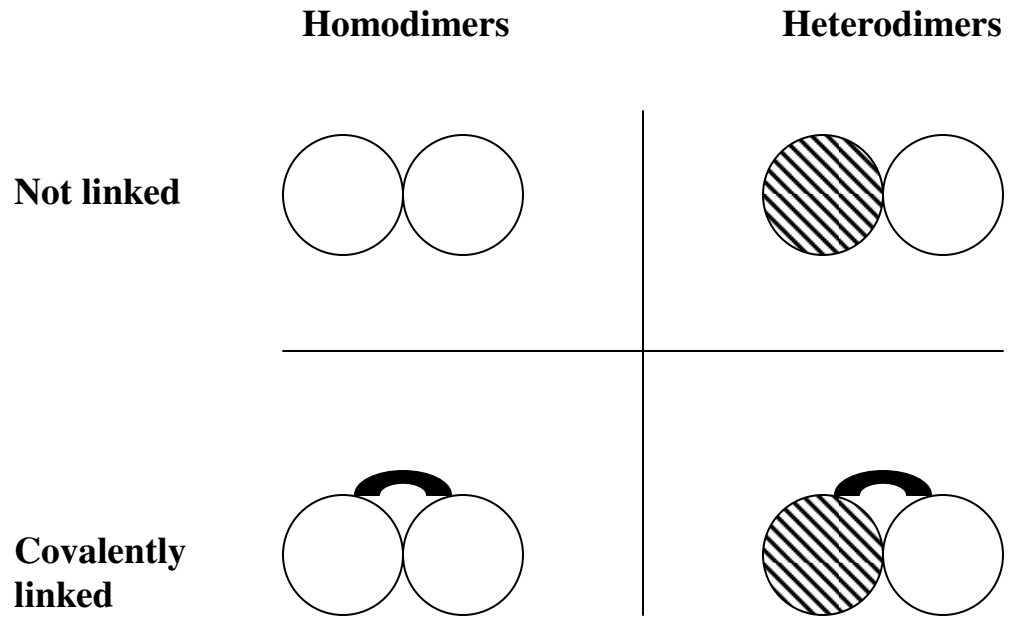


Figure 1.9 The potential species formed in the case of dimeric proteins. The covalent linkage of the two subunits facilitates the formation of heterodimeric variants without concern about the exchange of subunits (Simoncsits, et al., 2001). However the preparation and separation of heterodimers in mixtures of exchanged subunits has also been performed and the resulting heterodimers are not covalently linked (e.g. (Stahl, et al., 1996; Stahl, et al., 1998)).

production of antigen binding properties has been performed with the aim of overcoming the problem of non specific binding of intact antibodies in the cell imaging (Bird, et al., 1988). The antigen binding proteins (merely a F_{ab} fragment) consisting of the V_L and V_H chains of the antibody were linked through an optimized linker. The resulting F_{ab} fragments retained the specificity and affinity of their starting monoclonal antibody for the corresponding antigens, providing a paradigm on effectively combining the intact antibody fragments (Bird, et al., 1988). The effect of the nature and length of the linker to the stability and antigen affinity of these single chain (sFv) fragments was explored for the linked species produced from the F_{ab} of a monoclonal antibody for fluorescein (Pantoliano, et al., 1991). There is a decrease in conformational entropy resulting from the presence of the linker, which reduces the translational and rotational degrees of freedom for the dimer. It is argued that this entropic effect results in the observed two-state unfolding independent of the concentration of the monomers. Moreover the more hydrophilic in composition and greater in length is the linker the more stable is the resulting sFv (Pantoliano, et al., 1991). Following a similar aim the engineering of the homodimeric CuZn superoxide dismutase, which is structurally similar to the immunoglobulins with respect to their Greek key β barrel folds, has been performed (Hallewell, et al., 1989). The human immunoglobulin 19 residue hinge between the F_{ab} and F_c domains was utilized to connect the SOD subunits in order to provide independence in the folding of the subunits without any effect on their activities. The covalently connected subunits were shown to oligomerize, a condition allowed by the flexibility of the hinge while the oligomers were in turn shown to be circulating longer in the blood, which was initially speculated. The linker permitted the application of non-

covalent interactions among the dimers such that their hydrophilic surfaces are combined in different topologies and thus lead to oligomerization. This was not applicable in the case of joining the two subunits head-to-tail (Hallewell, et al., 1989).

The investigation of the activity of fused subunits in the *E. coli* glycyl-tRNA synthetase has been performed utilizing the covalent head-to tail linkage of the individual α and β chains of the protein (possessing a α -2, β -2 structure), which are not active individually but only in the tertiary structure (Toth, et al., 1986). The linker composed of six amino acids was shown to have minimal effect in the aminoacylation and ATP exchange activities. This proved the hypothesis that the subunits need not be separate for the enzyme to be active when the local conformation at the fusion region is minimally perturbed to exhibit no influence in the activity (Toth, et al., 1986).

Extensive hybridization has been performed in the DNA binding domains of transcription factors by covalent linkage among the monomers to serve a wide variety of aims. In the class of the leucine zipper transcription factors, the protein is a homodimer of two α helices, the dimerization of which leads to the formation of a coiled coil. The occurrence of leucine residues located every seven residue repeats has been shown (Oas, et al., 1990). The dimerization of the two α helices has been demonstrated as the determinant of the DNA binding properties of the protein since it regulates the position of the N-terminus of the protein towards the DNA, surrounding the DNA like a scissors (Oas, et al., 1990). Based on this property of the leucine zipper, several engineering approaches have been applied to manipulate the DNA binding properties of transcription factors utilizing the motif. In the case of the AP-1 transcription factor, comprised of the homologous Jun and Fos oncoproteins to form the functional heterodimeric leucine

zipper (Schmidt-Dorr, et al., 1991), the Jun and Fos proteins have different affinities for the AP-1 DNA sites, and their homodimers are not as efficient in DNA binding. The effect of the dimerization and the properties of the dimerization interface have been explored by performing a fusion of the Jun protein to the DNA binding domain of the Lex-A repressor, which contains a helix-turn-helix motif (Schmidt-Dorr, et al., 1991). The hybrid of the helices of Jun and the Lex-A repressor forms a leucine zipper, which efficiently associates with the Lex-A binding site without any constraint for the linker between the two domains. It was shown through mutational analysis of the residues involved in the dimerization interface that the interactions that optimize the dimerization are mainly hydrophobic. In another example under the same motivation, the GCN4 leucine zipper monomer was fused to the N-terminal DNA binding domain of the λ repressor which also contains a helix-turn-helix motif (Hu, et al., 1990). Similarly it was demonstrated that the hydrophobicity within the zipper is necessary, and the role of leucine is of special importance in the dimerization interface. This was achieved through randomization of residues at specific locations in the interface and examination of the conformation of the hybrids by CD spectroscopy (Hu, et al., 1990). The covalent connection of secondary structure described in the previous cases has also been performed in the case of the reshuffling of the α helices of the RNA-binding ROP protein (Predki, et al., 1995). The ROP protein functions as a dimeric, four-helix bundle protein with loops of variable composition, length and flexibility between pairs of the four helices. The covalent linkage of the dimers has been performed resulting in the joining of two 1-2 dimers in a 1-1-2-2 pattern (where 1 and 2 represent the individual helices in the dimer). Through the conformational characterization of the reshuffled bundle, it was

suggested that the hydrophobic core is maintained and critically directs the stability and active conformation towards the target RNA. It was further suggested that the covalent linkage and the loops between the helices do not actively participate in the tertiary structure of the bundle (Predki, et al., 1995).

The study of the stability of a single chain Arc repressor has been performed with the aim to produce a dimer at low concentrations where the affinity to the target operator can be explored but the protein is dissociated (Robinson, et al., 1996). A G-rich linker between the native subunits was added, and the affinity to the operator was examined. The lock of the dimeric structure through the linker resulted in a stable and cooperatively folding molecule with higher affinity than the wild type for the operator site (Robinson, et al., 1996). The linker is shown to be acting simply as a tether between the subunits holding them together and increasing the stability of the dimer at low concentrations as evidenced by the higher refolding rate for the single chain variant compared to the wild type dimer (Robinson, et al., 1996). The variation of the linker length (ranging from 11-19 residues) and composition in the single chain Arc repressor have proved the significance of these factors in the folding and unfolding rates and thus to the stability of the linked dimer (Robinson, et al., 1998). High Ala content was shown to introduce rigidity to the linker and a more restricted space of conformations scanned by the dimer during refolding, while the hydrogen bonding offered by Ser residues allows for extension of the conformational space and greater flexibility. Meanwhile Gly-rich linkers were shown to also provide conformational flexibility but reduce the overall stability of the dimer (Robinson, et al., 1998). A quantitative approach of the effect of the linker in single chain dimers on their stability as compared to the wild type was given by

correlating the probability density for the end-to-end distance of the two monomers with the ratio of the stability constants of the linked and native dimers (Zhou 2001).

In a similar case to the Arc repressor where insignificant dimer accumulation occurs at the low concentrations required to show the high DNA binding affinity, the λ Cro repressor protein has been covalently linked and the properties of the resulting homodimer have been explored (Jana, et al., 1998). In addition to linkers of 8-16 amino acids, site directed mutagenesis was utilized to introduce a Cys residue at the dimerization interface and the two subunits were connected through a disulfide bridge. The S-S covalently dimerized protein was shown to be of similar affinity to the non-linked protein despite the sufficient population of the dimer. The presence of the linker though resulted in greater thermal stability and higher affinity towards the cognate DNA, which was attributed to high intrinsic affinity of the dimer to the DNA (Jana, et al., 1998).

The folding of the subunits of the dimeric gene V protein has also been studied through covalent linkage of the individual monomers (Liang, et al., 1993). Since the folding rate of the native dimer was shown to be dependent on the concentration of the protein, the subunit association was hypothesized to be rate limiting for the folding process. In order to dissect the folding from the subunit association, a five or six residue linker was applied to join the subunits and the single chain was subjected to unfolding experiments. The higher folding but similar unfolding rate for the single chain dimer compared to the wild type showed the importance of interactions between the subunits, which are pronounced by their locked proximity due to the linker (Liang, et al., 1993).

Another aim pursued by utilization of the covalent linkage between protein

subunits (or secondary structure elements) has been the engineering of the specificity of several nucleic acid binding proteins. The Gal4 transcription factor has been fused to the LexA repressor, and the resulting hybrid effectively bound to the *lexA* operator and transcription was induced as shown by *in vivo* β -galactosidase assays (Brent, et al., 1985). It was thus demonstrated that the specificity of the Gal4 factor can be modulated from its counterpart in the linked hybrid while the repressor action of LexA will be suppressed when combined with a transcription activator. The same purpose of specificity alteration has led to the covalent joining of the N-terminal helices of the helix-turn-helix (HTH) motif of the 434 (cI) bacteriophage repressor (Simoncsits, et al., 1997). The natural linker of 20 residues representing the “turn” in the HTH motif was utilized to perform the connection of the N-terminals which were combined in homodimers and heterodimers, the latter being composed of different phenotypes across the subunits. The homo and hetero dimers bound specifically to symmetric and asymmetric operator sites and all the observed interactions with DNA were shown to be of high affinity (Simoncsits, et al., 1997). Previously the head to tail and tail to tail hybrids of the N terminal subunits 434 repressor were applied to the investigation of the conformation of the covalently linked dimer at the binding of cognate and non cognate sequences (Percipalle, et al., 1995). Following the “helix swap” method (Wharton, et al., 1985), similar fusions of subunits of the 434 and the P22 repressors (each contributing a subunit) have been also utilized to demonstrate the novel specificity for the formed hybrid, which was shown to bind to an hybrid operator of the two native ones (Hollis, et al., 1988). In another case regarding the HTH motif, the λ (cI) bacteriophage repressor was fused simultaneously to the heterodimer of the Fos and Jun leucine zipper α helices forming

hybrids with none, one and two arms towards the λ operator site (Kim, et al., 1995). Evidence was provided for the dependence of the specificity of the resulting tertiary structures on the number of the arms interacting with cognate and non cognate operator half sites (Kim, et al., 1995).

1.4 Overview of the dissertation

Due to the previously reported particular behavior of the Tyr94 side chain and the speculation of the participation of the residue in the communication of the two PvuII subunits the Y94F PvuII was set under investigation. In addition the previously covalently linked single chain PvuII was utilized to prepare the homodimeric WT-SC and the heterodimeric WT/E68A-SC PvuII. The parallel study of the properties of the two variants was performed in an effort to explore the communication across the subunits of the PvuII endonuclease.

Chapter II describes the materials and methods applied to the study of PvuII. Details are provided for the preparation of the samples applied to each technique that was exploited to demonstrate the properties of PvuII.

Chapter III involves the biophysical characterization of the Y94F PvuII variant. Nitrocellulose filter binding and fluorescence anisotropy measurements were applied to study the DNA binding in the presence of Ca^{2+} ions. Isothermal titration calorimetry and a fluorescence competition assay were applied to study the binding of the alkaline earth metals Ca^{2+} and Mg^{2+} respectively in the absence of DNA. The binding of the lanthanide ions Tb^{3+} and Eu^{3+} to the enzyme in the absence of DNA was also observed through their Tyr-sensitized luminescence. The stability of the Y94F PvuII was also studied through

denaturation experiments in which the Trp intrinsic fluorescence of the enzyme was observed. Additional information on the conformational adoption by the Y94F PvuII is also provided by application of ^1H - ^{15}N HSQC NMR spectra obtained in the presence of Ca^{2+} ions and cognate DNA.

Chapter IV involves an attempt towards dissecting and quantifying the cooperativity modes across the metal binding sites in the PvuII endonuclease. For this purpose the homodimeric WT and the heterodimeric WTIE68A single chain PvuII variants were prepared in which the binding of metal ions occurs in two or one subunit of the PvuII dimer respectively. The binding of Ca^{2+} in the absence of DNA and also the binding of DNA in the presence of Ca^{2+} is studied in both variants. The DNA cleavage activity of the single chain PvuII variants and its dependence on the concentration of Mg^{2+} ions is also set under investigation.

CHAPTER II

MATERIALS AND METHODS

2.1 Enzyme preparation

2.1.1 Vectors of PvuII

The *E. coli* strain PR1206 was transformed with the vector pBBA5 which carries the gene for the PvuII methyltransferase (Balendiran, et al., 1994). The pBBA5 plasmid (a derivative of pACM8) which offers protection for the expression of the PvuII endonuclease carries the chloramphenicol and kanamycin resistance genes (Balendiran, et al., 1994). The gene for the PvuII endonuclease is included in the vector pBBE3 a derivative of pPR594 in which the gene is placed under the control of the Ptac promoter while the vector also includes the gene for ampicillin resistance (pPR594 is a derivative of pBR322) (Jack, et al., 1991; Balendiran, et al., 1994). The PR1206 strain of *E. coli* transformed with the pBBA5 and also the pBBE3 vector carrying the gene for the Y94F-PvuII were kindly provided by Drs. Paul Riggs and Horacio Natri at New England Biolabs. The introduction of the Y94F mutation to the WT PvuII gene in the pBBE3 vector was performed by use of the set of primers shown in **Table 2.1** and the Quikchange site-directed mutagenesis kit (Stratagene) at NEB. The pRIZ'_{Olac} plasmid (Simoncsits, et al., 1997) carrying the gene for the single chain WT-PvuII was kindly provided by András Simoncsits. The PR1206 strain was used for the expression of all PvuII variants (from both the pBBE3 and pRIZ'_{Olac} plasmids).

2.1.2 Mutagenesis of the single chain PvuII

The pRIZ'_{Olac} vector was created by the commercially available pBR322 plasmid.

Table 2.1. The sequences of the oligonucleotides used as primer sets for mutagenesis and sequencing.

Y94F mutation

Forward: 5' - CCT GTA ATT ATT GCA AAA **TTT** AGA CAA GTA CCT TGG -3'

Reverse: 5' - CCA AGG TAC TTG TCT AAA **TTT** TGC AAT AAT TAC AGG -3'

E68A mutation

Forward: 5' - GCA GGA CAA GAA TAC **GCG** TTA AAA TCA ATA AAC ATA - 3'

Reverse: 5' - TAT GTT TAT TGA TTT TAA **CGC** GTA TTC TTG TCC TGC - 3'

Sequencing (single PvuII copy vectors after mutagenesis)

Forward: 5' - AGT CAC CCA GAT CTA AAT AAA TTA TTA GAG - 3'

Reverse: 5' - GTA AAT CTT TGT CCC ATG TTC CAT TAC A - 3'

Sequencing (single chain PvuII vectors after mutagenesis)

Forward: 5' - GTG AGC GGA TAA CAA TTT CAC ACA GGA GGA - 3'

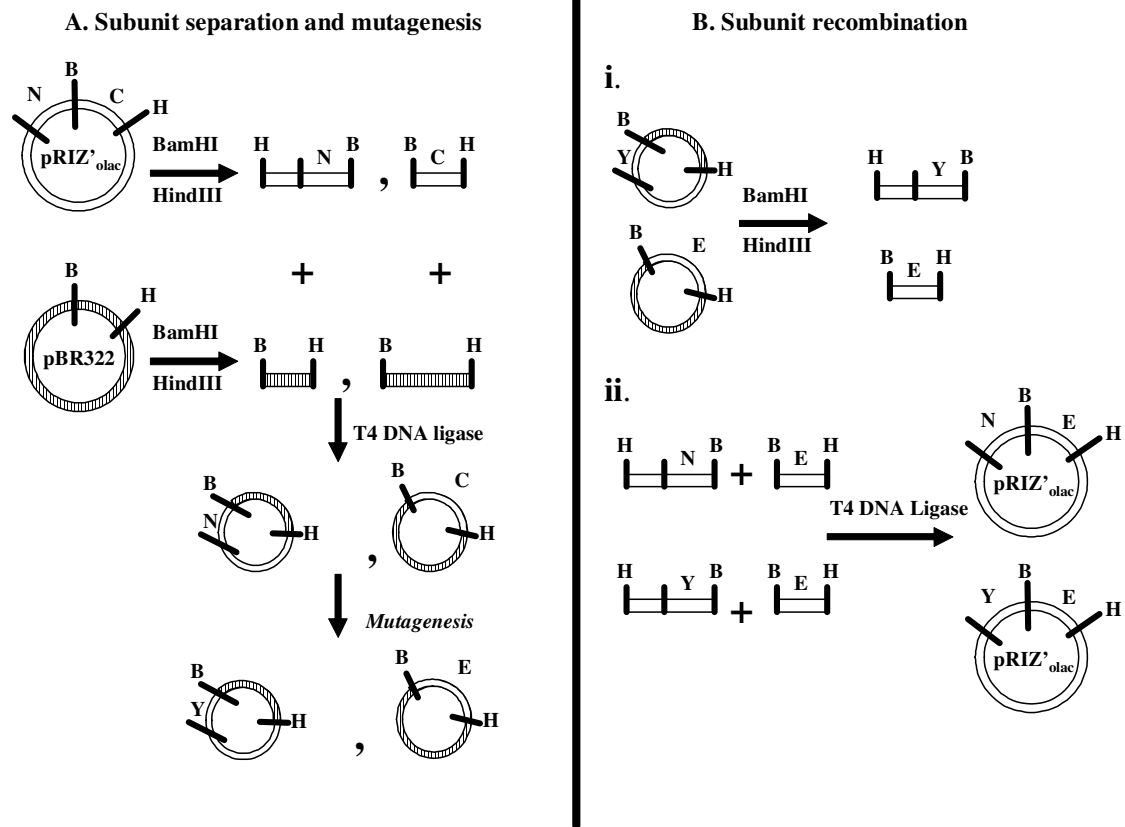
Reverse: 5' - GTC CGC CAC TCG TCA GCA AAG AAG CAA GCT - 3'

The single nucleotide substitutions TAT → TTT for the Y94F mutation and GAG → GCG for the E68A mutation are shown in bold. The sequencing primers span the sequence from the 5' end of the N-terminal subunit to the 3' end of the C-terminal subunit as shown in **Scheme 2.1**.

The pBR322 plasmid was initially modified to result in the pRIZ' vector (Boros, et al., 1986; Simoncsits, et al., 1988; Simoncsits, et al., 1994). The pRIZ' vector was turned into pRIZ'_{O_{lac}} by insertion of the *lacIq-lacprolacZ'*(1-146) region (Simoncsits, et al., 1997). The single chain PvuII was cloned in pRIZ'_{O_{lac}} within a unique NcoI/RcaI site (5' to the first subunit) and a unique HindIII site of the vector (Simoncsits, et al., 2001) (the NcoI/RcaI site was eliminated as the isoschizomers were used). As a derivative of the pBR322 vector the pRIZ'_{O_{lac}} plasmid carries the gene for the ampicillin resistance. The connection of the two subunits was facilitated by the existence of a unique BamHI site designed within the 5'-GAATCCGAAGAA-3' linker sequence (Simoncsits, et al., 2001).

The introduction of different mutations within each subunit required the separation of the two linked subunits. The separation of each subunit from the other and their consequent independent mutagenesis was achieved by utilization of the pBR322 cloning vector. A double BamHI/HindIII digest of pBR322 according to the NEB protocol provided two fragments of distinct sizes at ~0.3 kb and ~5 kb (**Scheme 2.1**). These fragments were gel purified by use of the Qiaquick Gel extraction kit (Qiagen). The pRIZ'_{O_{lac}} vector was similarly double digested by BamHI/HindIII to provide the C terminal subunit (~ 0.47 kb) of the SC-PvuII gene, and the rest of the pRIZ'_{O_{lac}} plasmid (including the N terminal subunit) at a size of about 6kb. These fragments were also gel purified as above. The four fragments from the digest of the pBR322 and pRIZ'_{O_{lac}} plasmids were combined as shown in **Scheme 2.1**: the 0.3 kb pBR322 fragment was ligated to the 6kb fragment of pRIZ'_{O_{lac}} and the 5 kb pBR322 fragment was ligated to the 0.47 kb C terminal subunit of pRIZ'_{O_{lac}}. The ligations were performed by use of the T4

Scheme 2.1. The preparation of heterodimeric PvuII variants. The BamHI and HindIII restriction enzyme sites are denoted as B and H respectively. The N and C terminal WT subunits of the single chain PvuII in the pRIZ'olac plasmid are shown. The Y and E subunits represent the N and C terminal PvuII subunits where the Y94F and the E68A mutations have been introduced.



DNA ligase according to the protocol from NEB.

Each resulting plasmid was then mutated separately. The mutations E68A and Y94F to the C and N terminal subunits respectively were introduced by use of the Quikchange site-directed mutagenesis kit, according to the manufacturer's protocol (Stratagene). The applied primer sets are shown in **Table 2.1**. The primer set shown for Y94F was also applied by Drs. Nastri and Riggs at NEB to introduce the phenotype to both subunits using the pR1206 vector and provide the homodimeric mutant (Papadakos, et al., 2007). Each resulting plasmid bearing a single copy of PvuII was sequenced by use of the primer sets shown in **Table 2.1**. After the verification of the introduction of the mutation to each vector the plasmids were double digested by BamHI/HindIII as previously. Then the reverse procedure to the above (**Scheme 2.1**) was followed in order to religate the subunits and reform the pRIZ'_{O_{lac}} plasmid in its original orientation (N terminal subunit-linker-C terminal subunit). The N-terminal subunit was mutated to Y94F while the C-terminal subunit was mutated to E68A. These were either combined to result in the Y94F|E68A SC PvuII or the E68A subunit was combined with the WT N-terminal subunit to result in the WT|E68A SC PvuII (**Scheme 2.1**). The reformed pRIZ'_{O_{lac}} vectors carrying the heterodimeric single chain PvuII variants were sequenced by use of the primer sets shown in **Table 2.1** to verify the correct orientation of the PvuII subunits. The plasmids carrying the PvuII variants (homodimeric Y94F or heterodimeric single chain variants) were each amplified to 3 mL LB cultures. The resulting DNA was purified by use of the SNAP DNA miniprep kit according to the manufacturer's protocol (Invitrogen).

2.1.3 Transformation

Competent cells of the pR1206 *E. coli* strain were prepared by incubation of the pellet of a 50 mL drug free LB culture of the host cells (grown in the absence of antibiotics) with 0.1 mM CaCl₂. The culture was initiated by an overnight grown 2 mL inoculum. Aliquots of 0.2 mL competent cells in CaCl₂ were used to transform in sterile eppendorf tubes. An approximately 0.5 µL volume of miniprep plasmid DNA was applied and incubated in ice for 45 min. The transformation was performed by heat shock at 42°C for 45 s. LB agar plates supplied with 30 mg/ml sterile filtered ampicillin (Sigma) were used to prepare colonies of the transformed cells.

2.1.4 Expression

A total of ten inocula each at 100 mL, were prepared in autoclaved M9 minimal salt media (22 mM potassium phosphate monobasic, 46 mM sodium phosphate dibasic, 8.6 mM sodium chloride and 18.6 mM ammonium chloride) each by a single colony from the transformation plate. The M9 media were supplemented with 10 mg/mL biotin, 10 mg/mL uracil, 50 mg/mL thiamine, 1 mM CaCl₂, 2 mM MgSO₄, and CAS amino acids (Difco) at 40 mg/mL per amino acid. In the case of the ¹⁵N labeled PvuII, the CAS amino acids were not added. Instead the cultures were started with M9 salts including 1mg/mL of ¹⁵N labeled ammonium chloride (Isotec) while the only amino acid that was added was Met at 40 mg/mL. In both cases (native or ¹⁵N labeled) the cultures were supplemented with 0.5 % glucose and 30 mg/mL sterile filtered ampicillin. After an overnight incubation (37°C under continuous rotary shaking at 220 rpm), the cultures were transferred to 1 L M9 media. At an OD₅₉₀ between 0.6-0.8 the expression was

induced by addition of 360 mg/mL sterile filtered isopropyl thio- β -D-galactoside (Anatrace). After incubation for another 4 h under the same conditions, the cells were harvested and frozen at -20°C . The resulting pellet was between 30-38 g for the expression of the Y94F variant in pBBE from a 10 L culture while the single chain variants in pRIZ'_{O_{lac}} produced 22-27 g from a 10 L culture.

2.1.5 Purification

The harvested cells were resuspended to lysis buffer (50 mM potassium phosphate monobasic, 6 mM β -mercaptoethanol, 1 mM EDTA, pH 7.4) and lysed by application of an SLM Aminco French press. Subsequent centrifugation at 15000 rpm for 10 min resulted in the separation of the higher order cell debris from the nucleic acid-protein mixture. The nucleic acids were then precipitated by addition of 25 % w/v streptomycin sulfate and incubation at 4°C for 45 min. The centrifugation (15000 rpm / 15 min) of the mixture resulted in the isolation of the protein content in the supernatant, which was then precipitated by the addition of ammonium sulfate at 45 % w/v. The mixture was again incubated at 4°C for 1 h to ensure complete precipitation and then the proteins were pelleted. The protein pellet was dissolved in 30 mM potassium phosphate dibasic, 0.1 mM potassium chloride, 1 mM EDTA pH 7.4.

The protein mixture was separated by cation-exchange column chromatography. A 2.5 x 25 cm Econo-column (Bio-Rad) was loaded with cellulose phosphate (Sigma) pre-cycled according to the manufacturer and equilibrated at the same buffer as the protein mixture. The protein mixture was then loaded to the column and the enzyme was eluted by application of a 0.05 mM to 0.8 mM KCl gradient over 1 L at 2 mL/min. The

fractions collected from the phosphocellulose column were subjected to SDS-PAGE analysis and the fractions in which PvuII was present were merged and dialysed against 30 mM potassium phosphate dibasic, 0.1 mM potassium chloride, 1 mM EDTA pH: 7.4. The protein pool was then applied to heparin sepharose (Amersham Biosciences) loaded on a 1.5 x 20 cm Econo-column (Bio-Rad) previously equilibrated at the same buffer as the protein pool. A subsequent SDS-PAGE analysis provided the fractions of purified PvuII (**Fig. 2.1**).

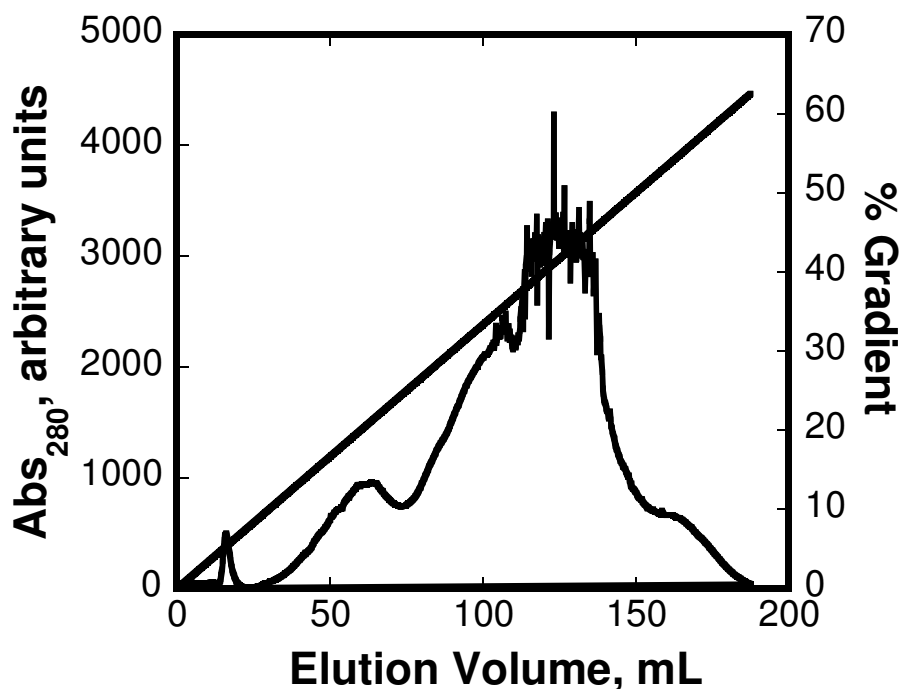
2.1.6 Quantification

The purified enzyme was quantified using the extinction coefficient $\epsilon_{280} = 36,900 \text{ cm}^{-1} \text{ M}^{-1}$ per enzyme subunit obtained by the application of the equation $\epsilon_{280} (\text{M}^{-1} \text{ cm}^{-1}) = (\#\text{Trp})(5,500) + (\#\text{Tyr})(1,490) + (\#\text{Cys})(125)$ (Pace, et al., 1995) for a single PvuII subunit which includes 4 Trp residues, 10 Tyr residues and no Cys residues. The absorbance at 280 nm was converted to enzyme concentration by application of the Beer-Lambert law.

2.1.7 Assay preparation

Before application to any assay the purified enzyme was exhaustively dialysed against metal free buffer. The dialysis of the enzyme was achieved by use of Slide-A-lyzer cassettes (Pierce) with a 10 kDa cutoff membrane under constant stirring for approximately 3 h at 4°C and subsequent application of fresh buffer (about 500 mL) at least two times. In the case of the lanthanide titrations it was observed that the enzyme had greater resistance to precipitation after refreshing the buffer six times during dialysis.

A.



B.

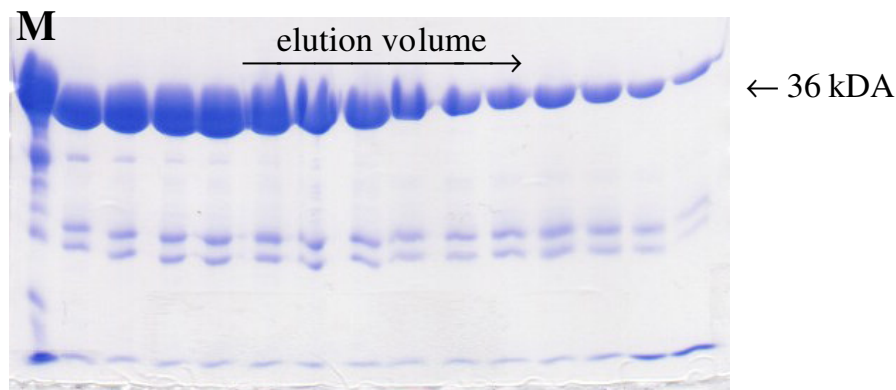


Figure 2.1 Purification of the WTIE68A single chain PvuII. A. The chromatogram of the protein sample applied to the heparin sulfate column. The peak of the absorbance at 280 nm extended from 110 mL (40%) of gradient and above indicates highly concentrated fractions of PvuII. B. The Coomassie stained 12% SDS PAGE of the fractions collected at 110 mL of elution volume and above as shown in A. The marker GAPDH (M.W. at 36 kDa) is denoted as M. The pooled fractions of PvuII contained impurities at less than 10% of the total protein per lane as found by image quantification.

In order to remove the divalent metal ions from the working buffer, a Chelex 100 chelating resin was applied which was precycled and used according to the manufacturer (Sigma). The enzyme was concentrated using Centricon filters with a 10 kDa cutoff membrane (Millipore) and subsequently handled only in plastic lab-ware to avoid metal ion contamination.

2.2 DNA preparation

2.2.1 Oligonucleotide DNA

The sequences of the 14mer non-self complementary and the 13mer self complementary duplex oligonucleotides containing the 5'-CAG|CTG-3' scissile site for PvuII are shown in **Fig. 2.2A**. The 13mer duplex oligonucleotide was prepared by the Biopolymer Synthesis Facility in Caltech and obtained in separate strands purified by reverse phase and ion-exchange HPLC. The duplex DNA was prepared by mixing equimolar amounts of the complementary strands at 95°C and allowing the mixture to cool down to room temperature overnight. The resulting duplex was quantified by application of Beer's law and use of the extinction coefficient of $6600 \text{ M}^{-1}\text{cm}^{-1}\text{nucleotide}^{-1}$. The 14mer oligonucleotide was custom synthesized by IDT Technologies and each non-self complementary strand was obtained in the desalted form, either native or fluorescently labeled. The strands were dissolved in water and then in formamide in 1:1 ratio and purified by 20% polyacrylamide gel electrophoresis. After visualization under UV light the bands were retrieved from the gel and extracted by the use of the Elutrap system (Whatman). The extracted DNA strand was concentrated by the use of Centricon filters with a 3 kDa cutoff membrane (Millipore). The electrophoresis buffer was diluted

A.

Non self complementary 14mer
5'- CAGGCAG CTGCGGA-3'
3'- GTCCGTC GACGCCT-5'
Self complementary 13mer
5'- TGACCAG CTGGTC-3'
3'- ACTGGTC GACCAG-5'

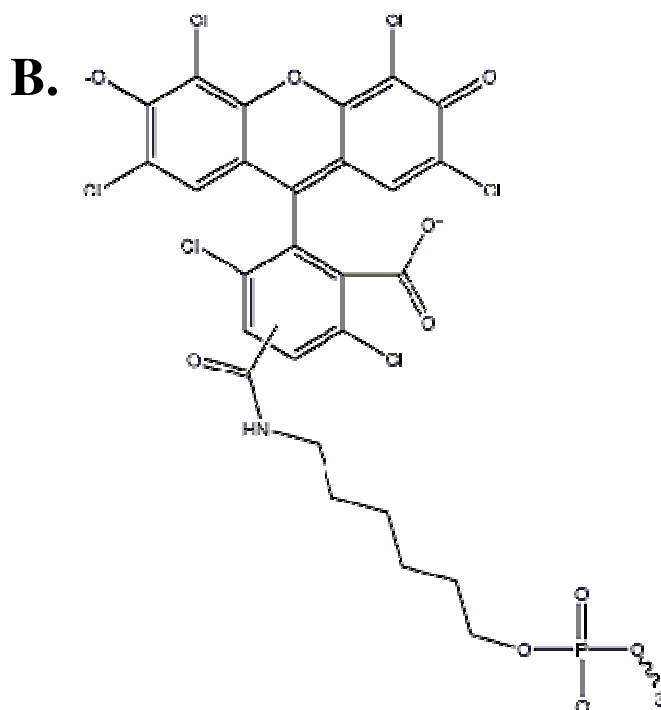


Figure 2.2. A. The duplex oligonucleotide sequences applied in the DNA binding and conformational analysis experiments. The PvuII scissile site is centered within the sequence and shown in bold. B. Structure of the Hexachlorofluorescein dye used in the fluorescence anisotropy experiments as attached to the 5' terminal of the oligonucleotide sequence (taken from IDT DNA).

and any residual metal ions were removed by two successive 10 X dilutions in MQ water each followed by concentration centrifugation. The separate strands were then quantified by use of the provided extinction coefficients (IDT) based on individual base extinction coefficients. The duplex 14mer DNA was prepared and quantified as above.

The native duplex oligonucleotide was ^{32}P radiolabeled at the 5' end as follows. A reaction mixture consisting of 1 μM duplex DNA, 1 unit of T4 Polynucleotide kinase (NEB), and 33 pmol of 3000 Ci/mmol [$\gamma\text{-}^{32}\text{P}$] ATP (Perkin Elmer) was prepared. The reaction was incubated at 37°C for 30 min. Following a 5-fold dilution the labeled oligonucleotide was separated by size exclusion gel filtration using a Sephadex G-50 resin (Sigma). It was assumed that the labeling reaction and the recovery of the labeled oligonucleotide are quantitative. By a subsequent scintillation counting of at least 10,000 cpm for a 1:3000 dilution of the 200 nM DNA stock, the prepared probe was qualified for use.

2.2.2 *Litmus 28i plasmid DNA*

The *E. coli* strain JM109 was transformed with the vector Litmus 28i obtained from NEB. Cultures of the transformed cells were grown in 500 mL of LB media supplemented with 150 mg/mL ampicillin (Sigma). The cell pellet was lysed following a standard alkaline lysis protocol (Sambrook, et al., 1989) and the resulting lysate was applied to purification using the Qiagen plasmid Mega kit (Qiagen) according to the manufacturer instructions.

2.3 Metal ion stock preparation

The metal ion stocks of CaCl_2 and MgCl_2 were prepared by dissolving their hexahydrate puratronic salts (Alfa Aesar) into MQ water. In the DNA binding and kinetic assays the used metal ion stocks were in MQ water. In the metal binding assays the pH of the metal ion stocks was adjusted at 7.4 or 7.7 for Ca^{2+} and Mg^{2+} respectively by use of metal free Hepes or Tris buffer. The ^{25}Mg stock was prepared by dissolving ^{25}MgO into dilute HClO_4 , and then adding Tris buffer to 2 mM and adjusting the pH to 7.7 by use of dilute KOH (Dupureur, et al., 2000). The stocks were quantified by flame absorption spectroscopy on a GBC model 904BT double beam atomic absorption spectrophotometer.

The stocks of the lanthanide ions Tb^{3+} and Eu^{3+} were prepared by dissolving their hexahydrate salts (Sigma) in MQ water. The stocks were quantified by volumetric titration with standard 10 mM EDTA solution (Mallinckrodt) as follows. In a sample cuvette 250 μL of approximately 10 mM lanthanide solution was mixed with 2.5 mL of 100 mM $\text{CH}_3\text{COONH}_4$ at pH 7.2 and 20 μL of 1 mg/mL of Arsenazo dye. The color of the Arsenazo-buffer solution is purple and turns blue at the addition of the lanthanide sample. The sample is titrated with the EDTA standard solution until the endpoint is reached (sample color turns back to purple). The concentration of the lanthanide sample is calculated using **Eq. 2.1** where $[\text{Ln}]$, $[\text{EDTA}]$ are the concentrations of the lanthanide

$$[\text{Ln}] = [\text{EDTA}](\text{volume EDTA})/(\text{volume Ln}) \quad (2.1)$$

and the standard EDTA (10 mM) respectively, the volume of the (Ln) sample is 250 μL and the EDTA volume required to reach the end point is measured (Fritz, et al., 1958).

2.4 DNA Binding assays

In order to monitor the dependence of the PvuII-DNA association constants on the concentration of Ca^{2+} ions, DNA binding titrations were performed by either monitoring fluorescence anisotropy or radioactivity of appropriately labeled DNA as above. In all measurements the solution conditions were 50 mM Tris-HCl and pH 7.5 at 25°C. To ensure independence on the ionic strength this was corrected by NaCl at 130 mM for all the metal ion concentrations examined.

2.4.1 Fluorescence Anisotropy

The experiments were performed on a Fluorolog 3 spectrofluorimeter (HJY) equipped with excitation and emission polarizers. The temperature was maintained at 25°C by continuous thermostating of the working quartz cuvette (NSG Scientific) through an external water bath. The binding of PvuII to the 5'-HEX labeled 14mer DNA sequence shown in **Fig. 2.2B** was monitored by excitation of the fluorophore at 540 nm and recording of the intensities (through excitation and emission polarizers) parallel and perpendicular to the excitation beam either at 556 nm through a single grating monochromator or through a 550 nm cutoff filter (Oriol). The resulting intensities were applied to **Eq. 2.2** through which the anisotropy values were calculated.

$$A = \frac{I_{\parallel} - I_{\perp}}{I_{\parallel} + 2I_{\perp}} \quad (2.2)$$

The sample volume (DNA in buffer) was set at 2.1 mL and the addition of the titrant (PvuII) was ended approximately at 210 μL while each added titrant volume was corrected for dilution. The sample was under constant stirring in order to reduce the

photobleaching of the fluorophore. For each added enzyme aliquot an equilibration period of 5 min was allowed before the measurement was performed. Three anisotropy readings were obtained for each enzyme aliquot, each with an integration time of 2 s. These were averaged to provide the final anisotropy value and fitted as shown in **Fig. 2.3**.

2.4.2 Nitrocellulose filter binding

Nitrocellulose filters (Whatman) and also Bio-dot filter papers (Bio-Rad) were initially soaked for 15 min in buffer of the same composition as the titration buffer but not in Puratronic CaCl₂. The titration was performed in arrays of binding reactions each at 400 μL in 96-well microtiter plates where each titration array consisted of 12 points and performed in duplicate. Throughout the array the unlabeled and 5'-³²P radiolabeled duplex oligonucleotide (in the working buffer) were added at a constant concentration and the enzyme concentration (also in the working buffer) was varied. After a 10 min incubation period at 25°C, the arrays were loaded in 200 μL duplicates on the nitrocellulose filter, which was already assembled along with the filter papers on the Bio-dot slot-blot apparatus (Bio-Rad). The samples were vacuum-filtered, washed with another 200 μL of the working buffer and dried. The nitrocellulose filter was wrapped in Saran-wrap and exposed to a phosphorimager screen (Amersham) for at least 7 h. The screen was scanned on a Storm phosphorimager scanner (Amersham) and the resulting image was quantified by use of the ImageQuant software (Amersham). The slot positions were selected to be of equal area for consistency throughout the titration and each image was background corrected. The quantification resulted in an Excel file in which the whole series of the 48 slots are included. These are split in pairs accordingly to provide

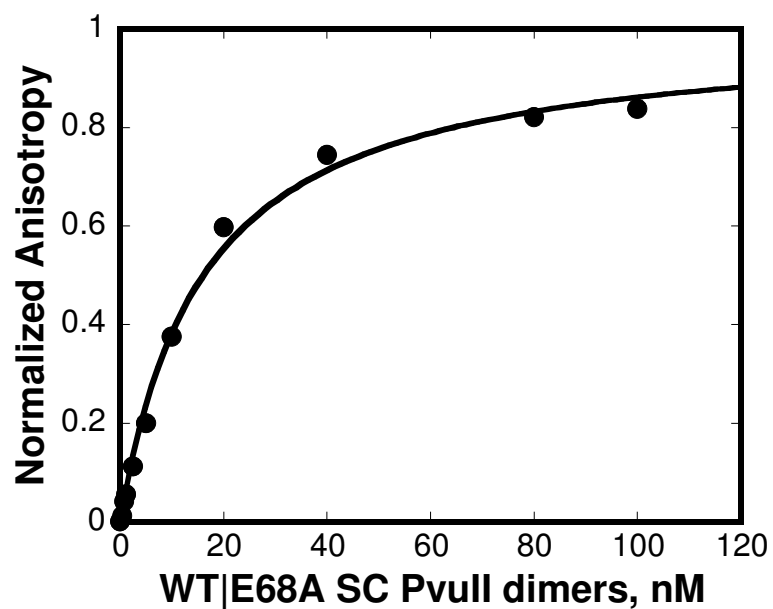


Figure 2.3 DNA binding to WT|E68A single chain PvuII followed by fluorescence anisotropy. Titration of 10 nM duplex non self-complementary HEX labeled 14mer performed at 50 mM Tris-HCl, 127 mM NaCl, 1 mM CaCl₂, pH 7.5 at 25°C. Fit to Eq. 2.1 yields a binding constant of 16.1 nM.

the points of the two titrations performed per nitrocellulose filter. The image of a series of points on a nitrocellulose filter and the corresponding fit of the obtained isotherm are shown in **Fig. 2.4**.

The isotherms obtained by the DNA binding assays were normalized to unity to provide the endpoint of each titration assuming that the observed endpoint coincided with the actual saturation of the titrate. The data were then fitted to **Eq 2.3** which describes a 1:1 binding isotherm in which L is the concentration of the enzyme, K_a is the stoichiometric association constant of the enzyme:DNA interaction and θ is the fraction of the bound DNA.

$$\theta = \frac{K_a L}{1 + K_a L} \quad (2.3)$$

In every Ca^{2+} concentration tested, DNA binding constants were obtained by three or more independent measurements at different DNA concentrations. These binding constants were averaged and the averages were plotted against the Ca^{2+} concentrations. The resulting tertiary plots were treated as isotherms representing the Ca^{2+} ion saturation of the enzyme subunits in the presence of cognate DNA. In both the WT and the Y94F PvuII homodimers it was assumed that the metal binding unit is the enzyme dimer with n metal binding sites and an Hill (all-or-nothing) model according to **Eq. 2.4** was applied to fit the data. In **Eq. 2.4**, E denotes the enzyme dimers, M represents the metal ions which are allowed to bind with up to an 1: n stoichiometry (dimers:metal ions) and EM_n represents the metal bound enzyme species.



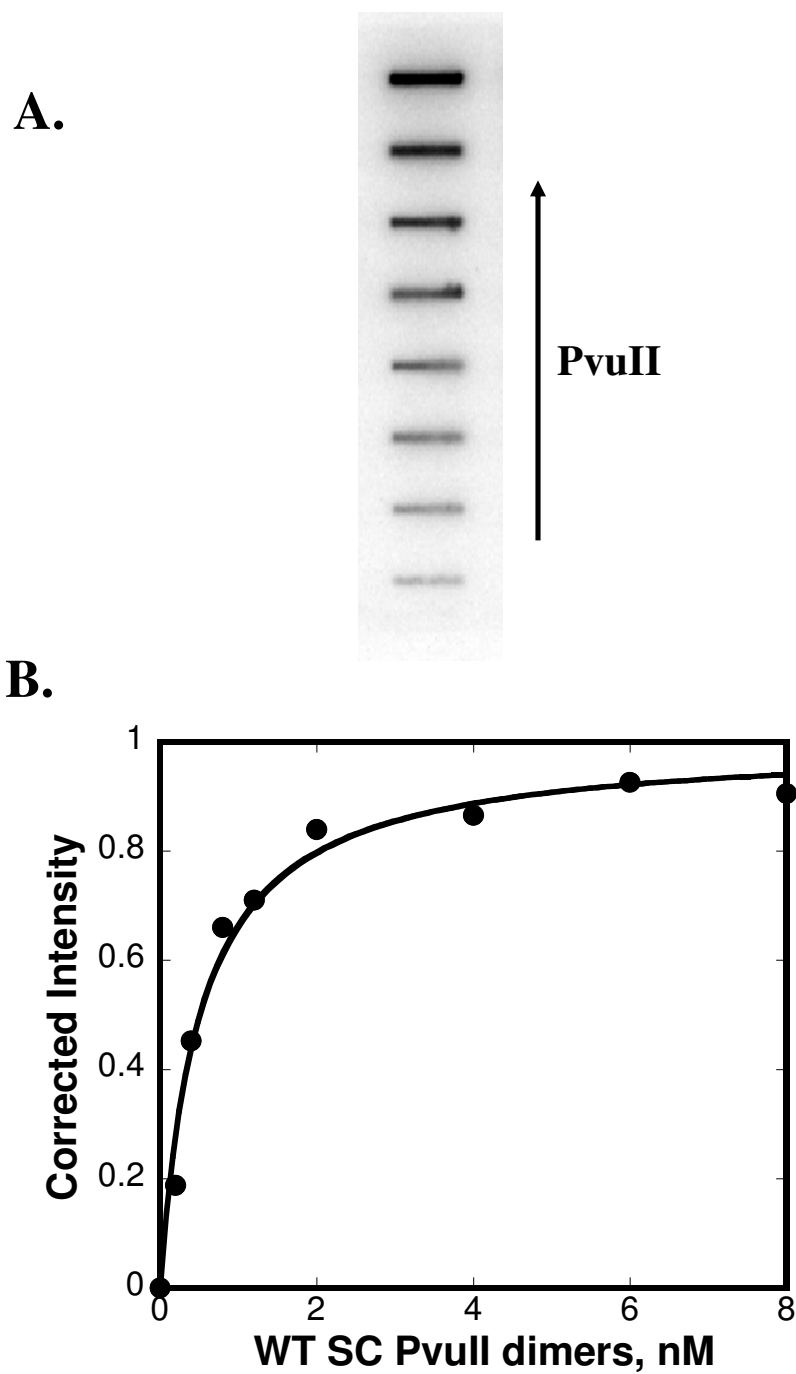


Figure 2.4 DNA binding to WT single chain PvuII followed by nitrocellulose filter binding. A. The increase in the intensity of the radioactivity retained on the nitrocellulose filter is shown as the concentration of PvuII increases. B. Fit of the corrected intensities to **Eq. 2.1** yields a binding constant equal to 0.5 nM. Titration of 300 pM ^{32}P radiolabeled non self complementary duplex 14mer performed at 50 mM Tris-HCl, 115 mM NaCl, 5 mM CaCl_2 , pH 7.5 at 25°C.

The apparent dissociation constant K_d for the reaction of **Eq. 2.4** is given in **Eq. 2.5** and is related to the site-specific dissociation constant $K_{0.5}$ for each of the n sites as shown accordingly in **Eq. 2.5** (Weiss 1997). The affinity of each site $K_{0.5}$ is equal to the concentration of the metal ions at half saturation of the enzyme dimers.

$$\theta = \frac{K_a [M]^n}{1 + K_a [M]^n} = \frac{\left(\frac{[M]}{K_{0.5}}\right)^n}{1 + \left(\frac{[M]}{K_{0.5}}\right)^n} \quad (2.5)$$

The fitting to all equations was performed with the software Kaleidagraph (Synergy).

2.5 Metal Binding assays

2.5.1 Mag Fura-2 competition fluorescence

The binding of the native Mg^{2+} ions to Y94F PvuII was performed by a fluorimetric competition assay utilizing the commercially available Mg^{2+} ion indicator Mag Fura-2 (Invitrogen). Mag Fura-2 has been extensively applied as an intracellular indicator of Mg^{2+} ions in a variety of cells (Johnson 1998). The salt of the indicator (**Fig. 2.5A**) is cell impermeable and can be used in Mg^{2+} detection in vitro. The binding of Mg^{2+} ions to Mag Fura-2 results in a spectral shift of the indicator when irradiated with UV light (**Fig. 2.5B**). The intensities of the excitation spectra at 325 nm (ion-complexed form) and 370 nm (free indicator) can be used to calculate their ratio, which is directly proportional to the fraction of the Mg^{2+} bound chromophore, while not dependent on the total concentration of the chromophore. The sample of the competition assay was prepared in a nitric acid cleaned quartz cuvette at 380 μ L consisting of Mag Fura-2 (varying from 50-200 μ M), and Y94F PvuII monomers (varying from 0.2-0.5 mM) in 50

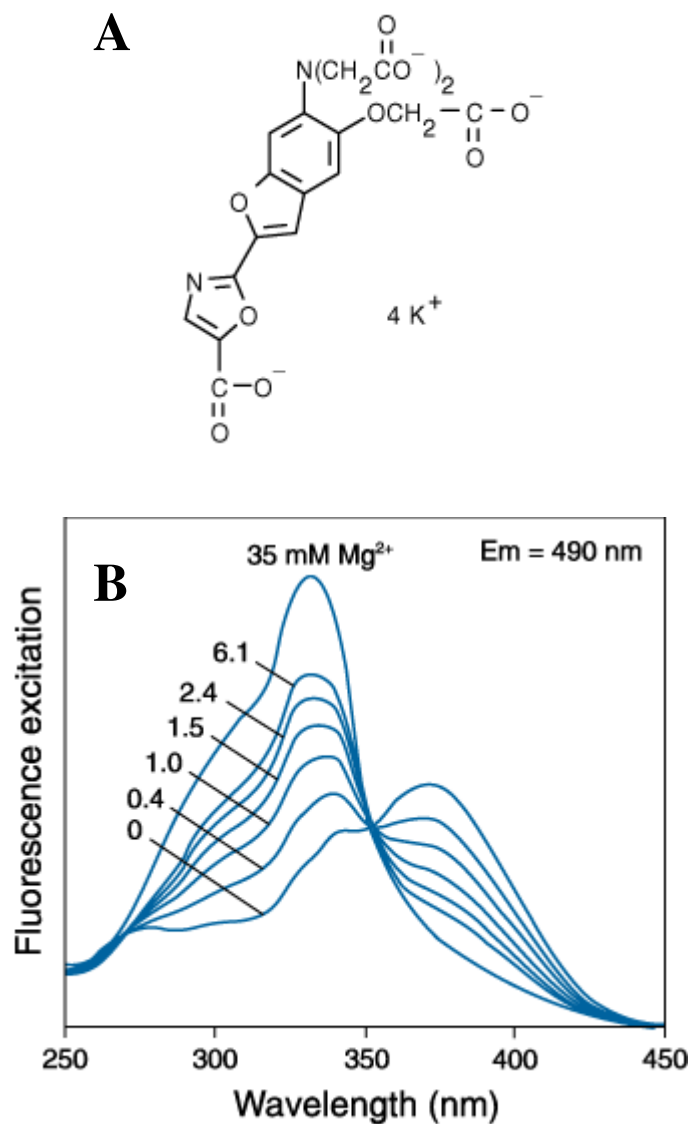


Figure 2.5. The structure of the tetrapotassium salt of Mag Fura-2 (A) and the excitation spectra of the chromophore (B) (Invitrogen). The spectra show the increase of the intensity at 325 nm and the corresponding decrease at 370 nm upon Mg^{2+} binding. The presence of the chromophore in two states (Mg^{2+} complexed and free) in equilibrium result in the isosbestic observed around 350 nm.

mM Tris-HCl, 400 mM KCl, pH 7.7 at 25°C. The high ionic strength was applied to ensure the solubility of the enzyme and its lack of aggregation at the high working concentrations. The sample was titrated with Mg²⁺ stock prepared at pH 7.7 with Tris buffer and an equilibration period of 5 min was allowed after the addition of each Mg²⁺ aliquot under constant stirring. The recording of the excitation spectra was performed on a Fluoromax-3 spectrofluorimeter (HJY) from 250 to 480 nm with an increment of 1 nm and an integration time of 1 s. Assuming the partition of the Mg²⁺ ions between the indicator and the PvuII monomers the recorded data can be fitted to the models shown in **Table 2.2** to extract the Mg²⁺-Y94F PvuII binding constants. Further assuming the saturation of Mag Fura-2 with Mg²⁺ ions at the endpoint of each titration, the data were normalized and fitted using the script shown in **Scheme 2.2** on the software Scientist 3.0 (Micromath). The Mg²⁺ binding constant to Mag Fura-2 is 1.9 mM under the conditions reported by the manufacturer (115 mM KCl, 20 mM NaCl, 10 mM Tris, pH 7.05, at 22°C). The same binding constant (2 mM) was measured by the direct titration of Mg²⁺ to the indicator at the PvuII-Mg²⁺ binding conditions mentioned above and applied to the models of **Table 2.2**. The titration of 100 μM Y94F PvuII monomers to 20 μM Mag Fura-2 in the absence of Mg²⁺ ions did not result in wavelength shifts in the excitation spectra of the indicator, indicating no interference of the enzyme with the observed signal.

2.5.2 Tyrosine sensitized fluorescence of lanthanide ions

The lanthanide ion binding was monitored via energy transfer following the direct excitation of the tyrosine residues in the proximity of the enzyme active site. Direct

Table 2.2 The macroscopic association constants for the Mg^{2+} binding sites of PvuII, used in the fitting model of **Scheme 2.2**.

Model	PvuII- Mg^{2+} association constants
One site	$K_a = \frac{[\text{EM}]}{[\text{E}][\text{M}]}$
Two sequential sites	$K_{a1} = \frac{[\text{EM}]}{[\text{E}][\text{M}]}, K_{a2} = \frac{[\text{EM}_2]}{[\text{EM}][\text{M}]}$
Hill	$K_a = \frac{[\text{EM}_n]}{[\text{E}][\text{M}]^n}$

The concentration of free PvuII monomers is denoted as E, while M is the free metal ion concentration and EM, EM_2 , EM_n are the concentrations of the corresponding metal bound species and n is the Hill coefficient. The expressions of the association constants were applied to the script shown in **Scheme 2.2** for the binding of Mg^{2+} to PvuII.

Scheme 2.2 The script used in Scientist for fitting of the Mg^{2+} -PvuII binding data.

Independent Variables: Mt

Dependent Variables: Θ , M, C, E, (EM, *or* EM, EM₂ *or* EM_n), MC

Parameters: Kc, (Ka *or* Ka₁, Ka₂), Et, Ct

MC = C·M·Kc

EM = M·E·Ka *or* EM = M·E·Ka₁, EM₂ = EM·M·Ka₂ *or* EM_n = Mⁿ·E·Ka

Mt = M+MC+EM *or* M+MC+EM+2·EM₂ *or* M+MC+EM_n

Ct=C+MC

Et=E+EM *or* E+EM+EM₂ *or* E+EM_n

0<M<Mt

0<E<Et

0<C<Ct

$\Theta=(MC/Ct)$

//Initial conditions

Mt=0

The total and free concentrations of PvuII, Mg^{2+} , and Fura-2 are denoted as Et, Mt and Ct and E, M, C respectively. The fraction of the Mg^{2+} bound Fura-2 is denoted as Θ while the binding constant of the complex is denoted as Kc and its value is fixed at 1.9 mM.

titrations of the lanthanide ions to metal free PvuII were performed in 5 mM Hepes, 400 mM KCl, pH 7.5 at 25°C. The solubility of the enzyme in the presence of either Tb³⁺ or Eu³⁺ allowed the titration of PvuII from 0.05 to 10 μM monomers with a maximum of 40 μM of lanthanide ions. As previously described, the purpose of the applied experimental conditions was to avoid the interference of the buffer to the observed signal and maximize the solubility of the enzyme in the presence of the lanthanides (Bowen, et al., 2004).

The emission spectra of the lanthanide ions involve multiple peaks in the visible region as a result of transitions between states of the f^n configuration (Horrocks 1993). In the case of Tb³⁺, the intensity at 543 nm (peak maximum) corresponding to the $^5D_4 \rightarrow ^7F_5$ transition was the signal for the enzyme bound metal, while in the case of Eu³⁺ the intensity at 614 nm (peak maximum) from the $^5D_0 \rightarrow ^7F_2$ transition was observed (Bowen, et al., 2004). After excitation of the enzyme tyrosine residues at 274 nm for Tb³⁺ and 282 nm for Eu³⁺, the emission spectra were recorded from 450 to 650 nm for Tb³⁺ and from 510 to 710 nm for Eu³⁺. All spectra were recorded on a Fluoromax-3 spectrofluorimeter (HJY) with a 1 nm increment over an integration period of 1s. The sample was allowed to equilibrate for 5 min after each metal aliquot addition under constant stirring. The measurements were performed through an emission cutoff filter (Andover) at 450 nm to prevent the Rayleigh scattering. This occurs as part of the excitation beam at 274 or 282 nm is scattered off the sample and second order diffracted at the emission monochromator. This would be observed as a peak at twice as much as the corresponding excitation wavelength and thus interfere with the measured signal (Lakowicz 2006). The specificity of the assay i.e. the observed signal reporting for the

binding of the lanthanide ions specifically at the PvuII active site, was confirmed as described previously (Bowen, et al., 2004) via competition of Ca^{2+} ions for the PvuII active after saturation with Tb^{3+} ions. The competition assay was performed by titrating Ca^{2+} to a sample consisting of 2 μM PvuII monomers and 20 μM Tb^{3+} at the conditions mentioned above. In all the lanthanide titrations a parallel control experiment was performed by titration of equal volumes of lanthanide to the working buffer only. The intensities of the control titration were subtracted from the sample intensities at the corresponding volumes to correct for the buffer contribution to the observed signal. The observed intensities were normalized to unity assuming saturation of the applied enzyme monomers, and fitted to **Eq. 2.5, 2.6** and **2.7** describing the Hill model, n equivalent independent sites (with a K_a , association constant) and two non equivalent independent sites (with a K_1 , K_2 association constants) respectively (L is the total lanthanide concentration and the binding constants of **Eq. 2.4** and **2.5** are intrinsic). The fitting was performed using Kaleidagraph (Synergy).

$$\theta = \frac{nK_a L}{1 + K_a L} \quad (2.6)$$

$$\theta = \frac{K_1 L}{1 + K_1 L} + \frac{K_2 L}{1 + K_2 L} \quad (2.7)$$

The Tyr-sensitized Tb^{3+} luminescence was also applied to measure the binding constant of a single Ca^{2+} binding site in PvuII. Since the utilization of Tb^{3+} ions under the experimental conditions does not allow for the saturation of a second Tb^{3+} site in PvuII the working concentrations for the Ca^{2+} competition experiments was 2 μM monomers

and the Tb^{3+} ions at 18-20 μM . As such a low micromolar site of Tb^{3+} is populated and Ca^{2+} is applied to compete for Tb^{3+} in the enzyme active site. In the competition model that describes the system, the binding polynomial is expressed in terms of the two metal bound enzyme species (i.e. PvuII-Tb^{3+} and PvuII-Ca^{2+}). Since the fraction of the enzyme bound Tb^{3+} is observed the data are fitted to **Eq. 2.8** without being previously normalized, while the vertical asymptote of the resulting hyperbola is taken as a parameter and fitted for along with the apparent Ca^{2+} binding constant. In **Eq. 2.8** the concentrations of the corresponding ions is denoted while the parameters K_1 and K_2 represent the association constants for Tb^{3+} and Ca^{2+} respectively.

$$\theta = \frac{K_1[\text{Tb}^{3+}]}{1 + K_1[\text{Tb}^{3+}] + K_2[\text{Ca}^{2+}]} \quad (2.8)$$

2.5.3 Isothermal titration calorimetry

Isothermal calorimetric titrations have been performed to characterize the binding of Ca^{2+} ions to PvuII. The titrations for the Y94F and WTIE68A-SC variants were performed on a VP-ITC calorimeter (Microcal) whereas the titrations for the WT-SC PvuII were performed on an Omega MC2 calorimeter (Microcal). The titrations were performed in 5 mM Hepes, 400 mM KCl, pH 7.5 at 25°C. The high ionic strength is applied to enhance the stability of the enzyme under the experimental conditions while the applied buffer provides the least contribution to the observed heats. The metal ion stock was buffered with Hepes at pH 7.5 to further minimize the interference of the buffer to the signal. Direct titrations were performed applying 1.41 mL of enzyme (50 to 500 μM monomers of Y94F PvuII, 0.75 to 1.5 mM monomers of WTIE68A SC PvuII and

0.5 mM WT-SC PvuII monomers) as titrate in the sample cell which were then titrated with Ca^{2+} . Before each experiment all the solutions were degassed at 25°C by use of a Thermovac apparatus (Microcal). After the thermal equilibration period, the metal ligand was added to the enzyme in 5 μL injections, each one over a duration time ranging from 12.56-20 s with a 3-4 min equilibration time. The stirring rate of the buret was set at 310 rpm. A control experiment was performed by titrating Ca^{2+} to buffer corresponding to each direct titration of Ca^{2+} to PvuII. The processing of the data was performed by use of the Microcal Origin software (Microcal). The areas of the raw differential power versus time were integrated and the obtained heats were used to calculate the enthalpies per mole of injectant, which were plotted versus the molar ratio of Ca^{2+} /PvuII monomers. The obtained average ΔH for the baseline was subtracted from the ΔH of each datapoint of the metal-to-enzyme titration to correct for the heat of dilution. The first datapoint in each titration (with injection volume at 2 μL) was always subtracted before fitting as it entails high uncertainty due to the diffusion of the titrant in the buret while the system tends to the initial thermal equilibration (VP-ITC manual). In the case of the Y94F PvuII the corrected heats were normalized to unity and the corresponding molar ratios were converted to the concentration of titrating Ca^{2+} ions. The resulting isotherms were fitted in the case of the Y94F PvuII with the software Kaleidagraph (Synergy) to **Eq. 2.3** (one site model), **2.5** (Hill model) and **2.9** (two site model) where L is the concentration of the titrating Ca^{2+} and θ is the fraction of the metal bound enzyme. **Eq. 2.9** describes a stepwise two-site model of the macroscopic association constants K_1 and K_2 for the corresponding steps. In the case of the Single-chain PvuII variants the data were fitted with the models provided by the Microcal Origin software (Microcal). The obtained

heats from the integrated data (cumulative heats, Q_i as described in **Eq. 2.10**) are used to calculate the heats per injection (q_i) (**Eq. 2.11**) to

$$\theta = \frac{K_1L + 2K_1K_2L^2}{1 + K_1L + K_1K_2L^2} \quad (2.9)$$

$$Q_i = V_o[E_t] \sum_j^n \Delta H_j \theta_j \quad (2.10)$$

which the data are fitted. The cumulative heat Q_i after the i -th injection is associated with the cell volume V_o , the total concentration of the titrate (enzyme, E_t) after the i -th injection and the molar binding enthalpy ΔH_j for each enzyme site occupied by j ligands while the enzyme bound fraction is θ_j as shown in **Eq. 2.10** (Microcal Origin manual).

$$q_i = Q_i - Q_{i-1} + \frac{dV(Q_i - Q_{i-1})}{2V_o} \quad (2.11)$$

As shown in **Eq. 2.11**, the heat for the i injection (q_i) is calculated from the difference of the cumulative heats of binding Q_i and Q_{i-1} between the previous and the current injection corrected for the heat associated with the displaced volume between the two injections (where dV is the injection volume and V_o the cell volume). The fractions of the metal bound enzyme (θ) shown in **Eq. 2.3**, **Eq. 2.7** and **Eq. 2.9** are also applied in the Origin models describing the occupation of one site, two independent sites and the sequential occupation of two sites respectively. To explore the binding of Ca^{2+} ions in the E68A subunit of the WT|E68A-SC heterodimer the ITC direct Ca^{2+} titrations a model utilizing the metal bound enzyme fraction shown in **Eq. 2.12** was applied describing the presence of two independent equivalent sites within the WT subunits and one site within the E68A subunit. An additional model (enzyme fraction shown in **Eq. 2.13**) which describes the

presence of two independent equivalent sites in each subunit of the WT/E68A-SC PvuII was also applied. The corresponding association constants for the metal ion sites in the WT and E68A subunits are denoted as K_1 and K_2 respectively.

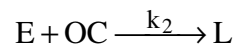
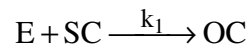
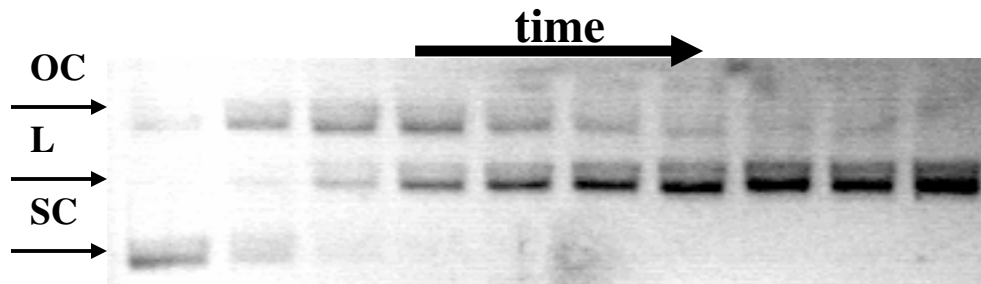
$$\theta = \frac{2K_1L}{1 + K_1L} + \frac{K_2L}{1 + K_2L} \quad (2.12)$$

$$\theta = \frac{2K_1L}{1 + K_1L} + \frac{2K_2L}{1 + K_2L} \quad (2.13)$$

2.6 DNA cleavage experiments

The dependence on the concentration of the native Mg^{2+} ions of the DNA cleavage rates of the single chain PvuII variants was examined. The plasmid Litmus 28i carrying a single scissile site for PvuII was used as a substrate in cleavage reactions under single turnover conditions of 2 μ M enzyme monomers and 0.3 μ M duplex DNA. The reactions were carried out in 50 mM Tris-HCl, pH 7.5 at 37°C while the ionic strength was maintained at 130 mM by addition of NaCl at the different Mg^{2+} concentrations. The Litmus 28i DNA was pre-incubated with Mg^{2+} and the reaction was initiated by the addition of metal free enzyme. The reaction was stopped by bringing the reaction aliquots to EDTA after mixing at a 1:1 ratio with agarose stop dye (420 mM EDTA, 40 % sucrose and 0.25% bromophenol blue). The separation of the nicked plasmid intermediate (OC), the linearized plasmid (L) and the supercoiled (SC) uncut plasmid was performed by agarose gel electrophoresis using 1.5 % agarose gels. The gels were run for approximately 1 h at 100 V and then stained with a 5 μ g/ml ethidium bromide solution. The image of the stained gel was taken by use of a Molecular Image station

440CF (Kodak) and saved as an 8-bit TIFF file (**Fig. 2.6**). Densitometric analysis of the DNA forms in the digital images of the gels was performed using the public domain, free software IMAGEJ (Image processing and analysis in Java, <http://rsb.info.nih.gov/ij/>) by which the area under the peaks was quantified for each of the observed DNA forms. The total amount of DNA per lane was calculated and was used to obtain the fractions of each of the f_{OC} , f_L and f_{SC} . The supercoiled form of the plasmid DNA due to its restriction in unwinding binds less ethidium bromide than the linear and nicked forms (Bennett, et al., 1989). In separate measurements of the amount of DNA by quantifying either the SC or L form, it was found that the difference of the two quantities was not larger than 12 %. As such the differential binding to ethidium bromide does not affect the quantification of the different DNA forms. Due to the presence of the nicked intermediate (OC) and the lag in the appearance of the linear (L) form of the plasmid, the kinetic model applied for the cleavage of the plasmid DNA includes two sequential steps described by the rate constants k_1 and k_2 , respectively, for the formation of the OC form and the formation of the L form (**Fig. 2.6**). The fractions of the three DNA forms SC, OC, and L are described by **Eq. 2.14-2.16** shown in **Fig. 2.6**. By the use of Scientist 3.0 (Micromath), the three quantified fractions were simultaneously fit by least squares to the above three equations. Independent R^2 values for each data set (fraction vs time) and also for the simultaneous fit were obtained. The quality of the fits is determined based on the R^2 for the overall fit. The Litmus 28i preparations contained non-specifically nicked plasmid whose presence interferes with the specifically nicked plasmid, which is to be observed. In order to correct for the contaminating amount of the OC form, the total fraction f_{OC} of open circles was corrected by subtracting (at each timepoint of a reaction), the fraction of the



$$f_{SC} = \exp(-k_1 t) \quad (2.14)$$

$$f_{OC} = [k_1 / (k_2 - k_1)] [(\exp(-k_1 t) - \exp(-k_2 t))] \quad (2.15)$$

$$f_L = 1 + [1 / (k_1 - k_2)] [(k_2 \exp(-k_1 t) - k_1 \exp(-k_2 t))] \quad (2.16)$$

Figure 2.6. Stepwise cleavage of plasmid DNA by PvuII. The three forms of the plasmid DNA (SC, OC and L) and the enzyme (E) are shown. The integration of the $d[SC]/dt$ and $d[OC]/dt$ differentials result in the corresponding fractions while the fraction of the linear form (L) results from the difference $1 - f_{SC} - f_{OC}$.

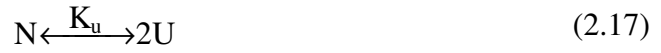
initial OC which is processed. Since the disappearance of the initial non-specifically nicked plasmid depends only on the rate of the first step (k_1), its processing is described by the product $[OC]_0 \exp(-k_1 t)$ which is subtracted at each timepoint ($[OC]_0$ is the initial fraction of open circles at $t = 0$) (King, et al., 1989).

2.7 Conformational analysis

2.7.1 Conformational stability studies

The free energy for the unfolding of PvuII was measured by monitoring the changes of the intrinsic Tryptophan fluorescence after chemical denaturation. A series of mixtures of 1 μ M PvuII dimers with guanidinium hydrochloride (ICT) from 0 to 6 M were prepared in 50 mM Epps, 100 mM KCl, pH 7.7 at 25°C. The concentration of the Gdn-HCl stock solution was measured by refractive index (Nozaki 1972). In another series of mixtures the denaturant was added in buffer (without enzyme) at the same concentrations as in the enzyme samples. Both series were incubated overnight at room temperature. The following day, the intrinsic tryptophan fluorescence of the solutions was measured on a Fluoromax-3 spectrofluorimeter (HJY). Each measurement was performed in a quartz cuvette of 1 mL under the constant wavelength mode where the emission at 330 nm was monitored after excitation at 290 nm. The band pass of the instrument was set at 2.5 nm, and the cuvette holder was constantly thermostated by an external water bath at 25°C. Each measurement was repeated in triplicate and the average of the intensities was used. Following the measurement of each sample and the corresponding control, the cuvettes were reused after scrupulous rinsing with MQ water and drying with ethanol. The intensity of each control was subtracted by the intensity of

the corresponding sample to provide the data points of each denaturation curve. In the two-state model for the unfolding of PvuII the equilibrium between the native dimer N (concentration in subunits) and the unfolded monomeric subunit U is assumed as shown in **Eq. 2.17**. The fraction of the unfolded protein, is proportional to the measured



signal, i.e., the decreasing intrinsic fluorescence and provides the equilibrium constant between the two forms of the enzyme at each denaturant concentration (Gittelman, et al., 1990). The intensity of the observed Trp fluorescence I_{obs} at a given denaturant concentration is the weighted sum of the intensities of the folded (I_f) and unfolded (I_u) forms of the enzyme at the same denaturant concentration and the fraction of the unfolded enzyme θ_u is given by **Eq. 2.18**.

$$\theta_u = \frac{I_{obs} - I_f}{I_u - I_f} \quad (2.18)$$

The equilibrium constant for the denaturation K_u is given by the expression in **Eq. 2.19**, from which the expression of θ_u in **Eq. 2.20** is derived where P_{tot} is the enzyme concentration in enzyme subunits. Substituting the value of K_u from **Eq. 2.21** in **Eq. 2.20**

$$K_u = \frac{2[P_{tot}]\theta_u^2}{1 - \theta_u} \quad (2.19)$$

$$\theta_u = \frac{\sqrt{K_u^2 + 8K_u[P_{tot}]} - K_u}{4[P_{tot}]} \quad (2.20)$$

$$\Delta G^o = - RT \ln K_u = \Delta G^{H_2O} - m[\text{denaturant}] \quad (2.21)$$

yields an expression of $\theta_u = f([\text{denaturant}])$ which is used to perform least squares fit of the θ_u values derived from **Eq. 2.18** as a function of the denaturant concentration. The fitted parameters are the $\Delta G^{\text{H}_2\text{O}}$ (free energy at zero denaturant concentration) and the m value that reflects the susceptibility for denaturation by the denaturant (Gittelman, et al., 1990).

2.7.2 ^1H - ^{15}N HSQC spectroscopy

The effect of the binding of the Ca^{2+} cofactor and also of cognate DNA on the conformation of the several variants of PvuII was performed by ^1H - ^{15}N Heteronuclear Single Quantum Coherence spectroscopy. The PvuII samples were prepared at 650 μM monomers in 25 mM Tris-HCl, 200 mM KCl, 10% D_2O , pH 7.7 at 25°C. The applied ionic strength ensured the solubility of the enzyme at its high concentration and also minimal interference of the dielectric constant of the sample with the tuning of the probe. Spectra were collected for the apo-enzyme, for the PvuII- Ca^{2+} complex in the presence of 10 mM CaCl_2 and also of the ternary PvuII- Ca^{2+} -cognate DNA complex after addition of 1 equivalent of the self complementary 13mer duplex shown in **Fig. 2.2A**. The spectra were collected on a 600 MHz Varian Inova spectrometer at Washington University. Both conventional and Transverse Relaxation Optimized Spectroscopy (TROSY) HSQC spectra were acquired. The ^1H chemical shifts were referenced using DSS and the ^{15}N chemical shifts were referenced indirectly from the ^1H chemical shifts. The ^1H spectral width was 8000 Hz while the ^{15}N spectral width was 1800 Hz. The conventional HSQC spectra were obtained by 64 scans of 1024 points for ^1H and 100 points for the ^{15}N dimension. The TROSY spectra were obtained at 128 scans. The

observed FID in both dimensions was weighted by a phased sine bell function in combination with line broadening before Fourier transformation to improve the signal to noise ratio and also the peak resolution. In each of the 2D spectra obtained the sum of the cross-peak intensities was calculated by use of NIH Image 1.63 (NIH). The ratio of the resulting intensities between two overlapping spectra was applied at the corresponding intensities as a normalization factor. In the overlap of two spectra the reference intensity is calculated as the sum of the intensities of the common cross-peaks plus the intensities of the non-overlapping cross peaks (of either of the two individual spectra). The fraction of the intensities of the common cross-peaks divided by the reference intensity provides the overlapping area between the two spectra (Dupureur 2005).

CHAPTER III

TYR94 OF THE PvuII ENDONUCLEASE

3.1 Introduction

The PvuII endonuclease, a dimer of identical subunits performs the metal-assisted phosphodiester hydrolysis of its cognate DNA sequence 5'-CAGICTG-3' after a number of contacts have been made between the metal ions, the amino acids within and remotely to the active site and the DNA substrate. As a member of the family of endonucleases carrying the PD..(D/E)XK motif, the active site of the PvuII endonuclease consists of the catalytic residues Asp58, Glu68, and Lys70 which have been confirmed through crystallographic and biochemical studies (Nastri, et al., 1997; Horton, et al., 2000) (**Fig. 3.1 Top**). Close to and positioned towards the active site of PvuII is the aromatic hydroxyl group of Tyr94.

In two distinct cases of PvuII crystal structures, Tyr94 has been implicated as critical within the enzyme active site. In the case of the crystal structure of D34G PvuII (pdb: 3PVI) with cognate DNA and no metal ions, the hydroxyl group of Tyr94 is involved in water-mediated interactions with the phosphate groups of the central GC base pair of the scissile site (Horton, et al., 1998). As mentioned above, such an interaction is not observed in the case of the WT PvuII-DNA co-crystals (pdb 1PVI). The carboxylate of Asp34 is positioned at the dimerization interface of the enzyme and involved in the recognition of the central GC base pair of the scissile site through direct and water mediated contacts to the DNA (Horton, et al., 1998). The mutation D34G would thus disrupt the DNA contacts that ensure the specificity for the scissile site. This was previously confirmed in activity assays where the D34G mutant was applied

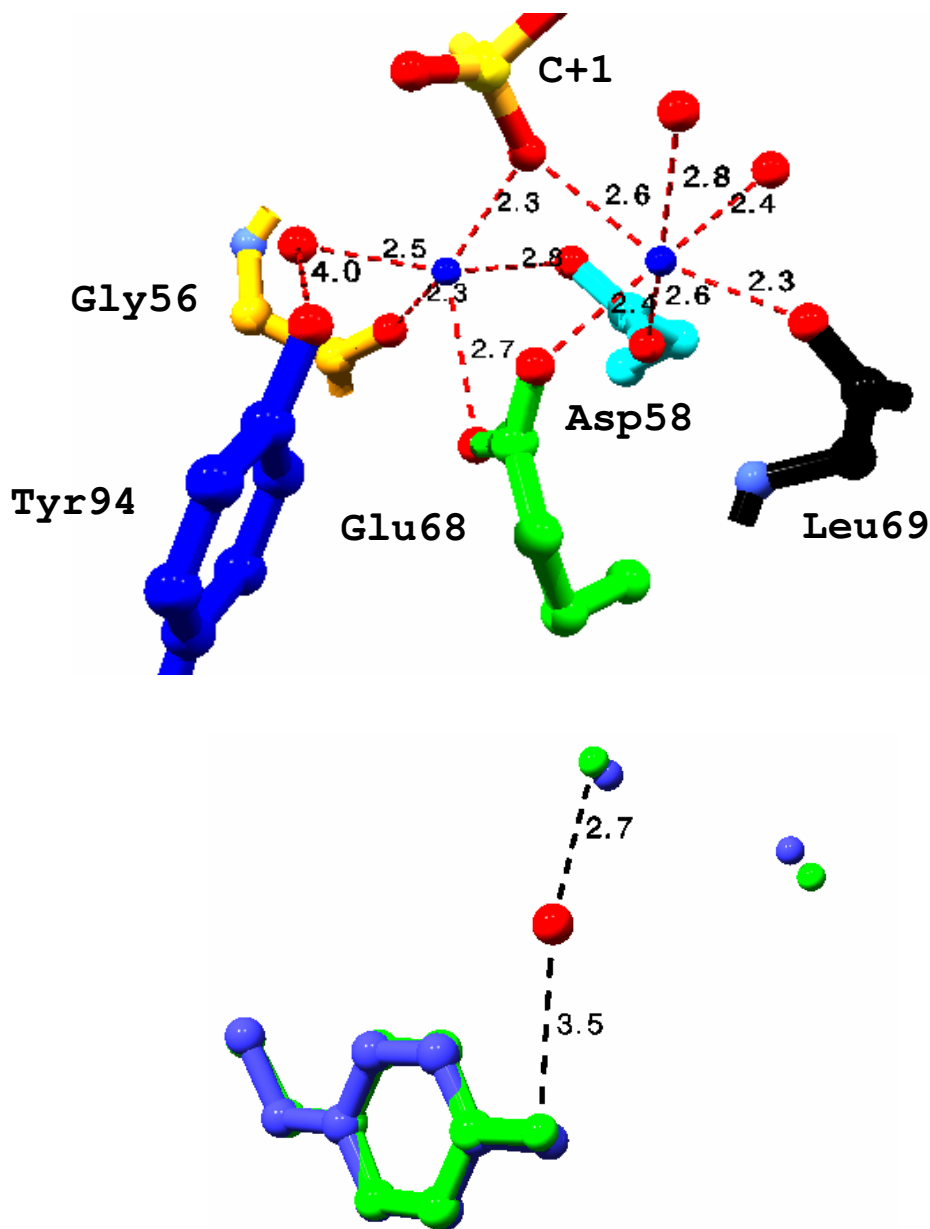


Figure 3.1. The octahedral coordination of the Ca^{2+} ions within the PvuII active site in the WT PvuII-cognate DNA- Ca^{2+} complex (pdb 1F00 (Horton, et al., 2000)). *Top:* the active site of subunit A (Horton, et al., 2000). The coordination of the Ca^{2+} ions is shown as described in the text. The proximity of Tyr94 to the Ca^{2+} ligated water molecule is shown. *Bottom:* superposition of the Tyr94 and Ca^{2+} ion pairs across the enzyme subunits. The lack of the water molecule at 3.49 Å from Tyr94 in subunit B is shown. *Legends:* *Top.* Ca^{2+} (Blue), H_2O (Red), *Bottom.* Subunit A (Blue), Subunit B (Green), H_2O (Red)

(Nastri, et al., 1997). The active role of Tyr94 is assisted by the hydrogen bonding network of the His83-His84-His85 triad which is extended in the case of the D34G mutant (**Fig. 3.2**) (Horton, et al., 1998) (the His triad is present at the dimerization interface and critical in the catalytic efficiency of the enzyme (Nastri, et al., 1997)). This extension is obviously compensating for the lost contacts of Asp34 to the substrate DNA. As a result the phenolic ring of Tyr94 is positioned at the interface of the DNA recognition region and the catalytic region of the DNA (Horton, et al., 1998). In essence in D34G PvuII, a variant in which the specific DNA sequence cannot be recognized, it is shown that water molecules in one subunit only orient the phenolic ring of Tyr94 in such a manner that this makes contacts to the substrate DNA. The participation of Tyr94 close to the active site in such a manner (Horton, et al., 1998) showed for the first time the flexibility of the PvuII polypeptide chain around Tyr94. The aromatic ring is readily positioned to partially compensate for lost DNA contacts. The D34G PvuII-DNA crystal structure is also the first example where the pronounced position of Tyr94 led the authors to assume that the residue directs the position of the metal ions after their entry to the PvuII active site (Horton, et al., 1998). However the assumption that the active site residues and also Tyr94 position the metal ions can be readily made by examination of the WT PvuII complex with cognate DNA in the presence of Ca^{2+} (pdb 1F00) (Horton, et al., 2000) (**Fig. 3.1**). In this structure the octahedral coordination of the metal cofactors is resolved. Within the metal ion coordination spheres (distances under 3 Å from each metal center) are the carboxylate groups of Glu68 and Asp58, the backbone carbonyl oxygen atoms of Gly56 and Leu69, several water molecules and the oxygen of the scissile phosphate (Horton, et al., 2000). In this active site conformation the Tyr94 is 5.4

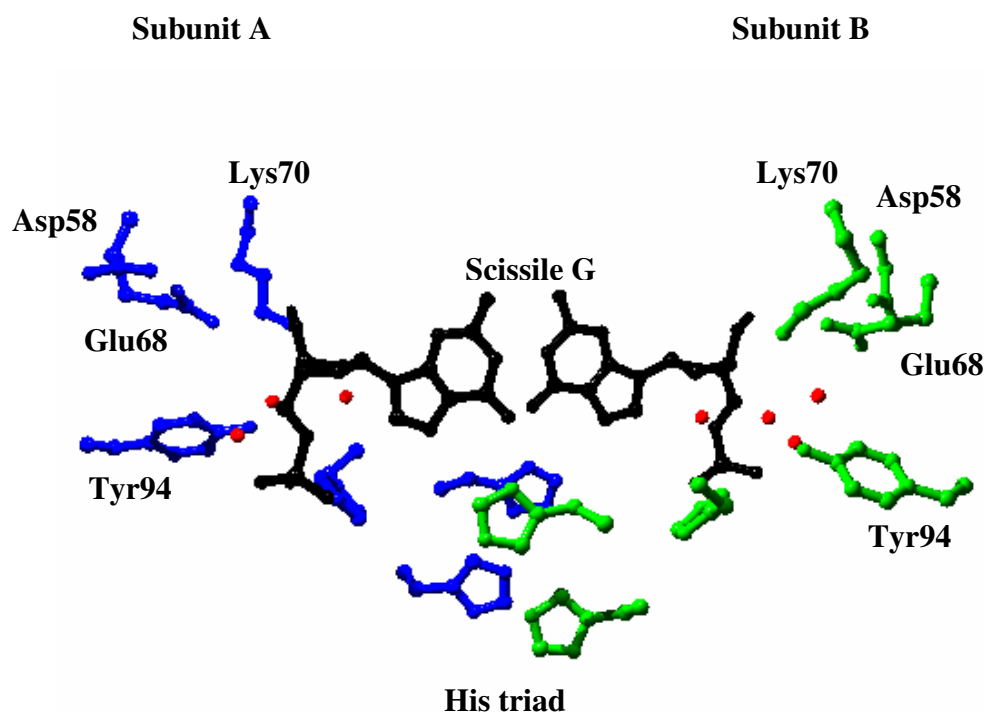


Figure 3.2. The interface of the PvuII subunits and the cognate DNA as previously shown in the D34G PvuII-cognate DNA co-crystal structure (pdb 3PVI (Horton, et al., 1998)). The PvuII subunits are denoted as A (*blue*) and B (*green*) while the DNA (*black*) and the H₂O molecules are also shown (*red*). The asymmetry that is developed in the active site conformation across the subunits is evident by the lack of a water molecule in subunit B within the hydrogen bonding network extending from the His83-His84-His85 triad and also from the different conformation of the Asp58 in the two subunits. The Tyr94 side chain in each subunit is clearly ligated to the water molecules of the His triad hydrogen bond network.

and 5.9 Å away from each Ca²⁺ ion, but only 3.49 Å away from the a water molecule coordinated to one of the Ca²⁺ ions (**Fig. 3.1**). The overlap of the Tyr94 residues and the metal ion positions across the PvuII subunits in the 1F0O structure is significant. However the position of the water ligand of the Ca²⁺ ion in close proximity to Tyr94 is asymmetrical across the subunits. Despite this asymmetry the hypothesis about the role of the side chain of Tyr94 is raised due to the clear positioning close to the Ca²⁺ ions.

The involvement of Tyr94 in the positioning of the metal ions was also assumed by the examination of another crystal structure of the WT PvuII in the presence of the native Mg²⁺ ions and in the absence of cognate DNA (**Fig. 3.3**) (pdb:1H56) (Spyridaki, et al., 2003). In this crystal structure, there is also asymmetry observed across the enzyme subunits similar to the 3PVI structure of the D34G PvuII shown before (Horton, et al., 1998). In this PvuII-Mg²⁺ complex, one subunit possesses only one Mg²⁺ ion, which is coordinated by Asp58, Glu68 and two water molecules. One of these metal bound water molecules is hydrogen bonded to Lys70 and Tyr94, which is in turn hydrogen bonded to Thr82. Similarly the other subunit possesses a single Mg²⁺ ion which is coordinated directly by the aromatic hydroxyl group of Tyr94, the hydroxyl group of Thr82 and two water molecules (Spyridaki, et al., 2003). The authors also in this case speculated that Tyr94 is found in the way of the Mg²⁺ ion as it enters the enzyme active site and that the exact metal positioning is what Tyr94 contributes to and thus the crystal structure is regarded as an intermediate instant towards the final positioning of the Mg²⁺ ion (Spyridaki, et al., 2003). The resulting general assumption from the overview of the 3PVI and 1H56 structures of PvuII is that the Tyr94 at nearly physiological conditions is indeed in such a position that it contributes to an overall conformation that stabilizes the

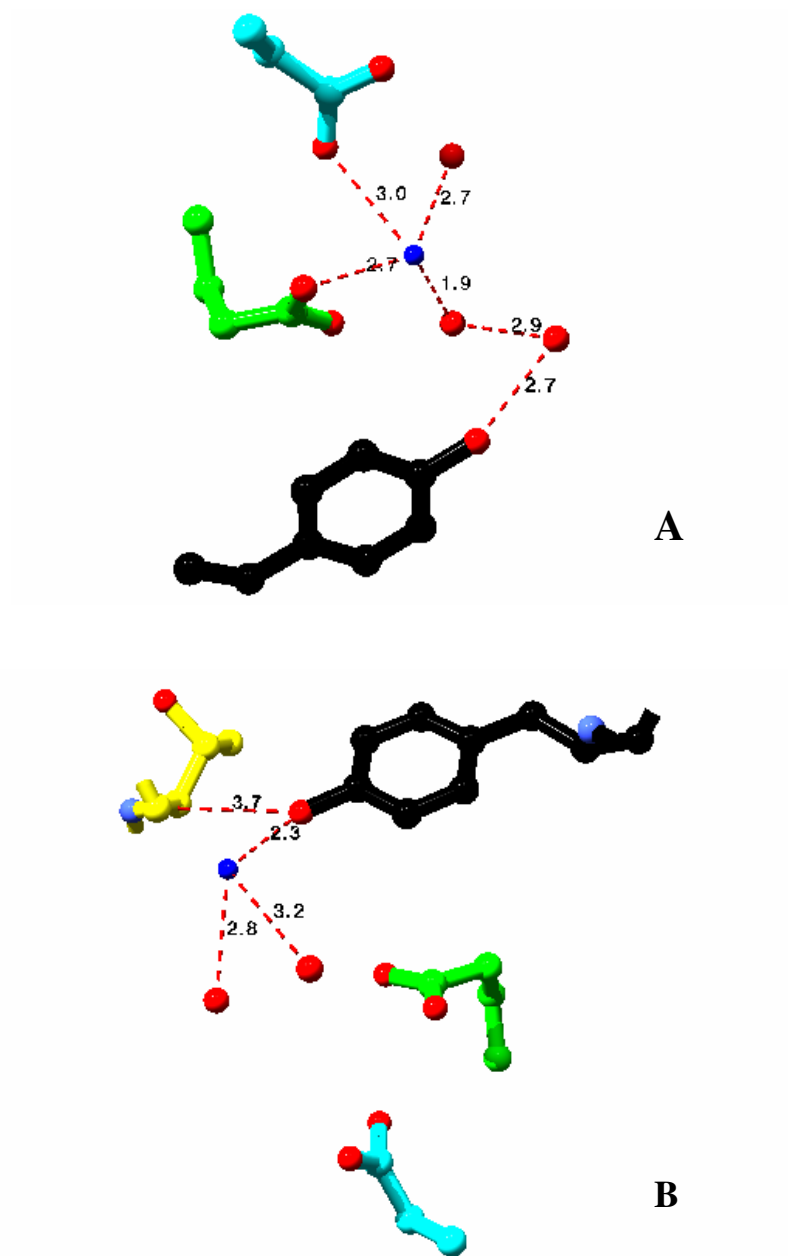


Figure 3.3. Differential binding of the Mg^{2+} ions across the WT PvuII subunits (pdb 1H56) (Spyridaki, et al., 2003). The subunits are denoted as A and B, (Asp58 (Cyan), Glu68 (Green), Tyr94 (Black), Thr82 (Yellow), Mg^{2+} (Blue), H_2O (Red)). In subunit A the active site residues Asp58, Glu68 and water molecules ligate the Mg^{2+} ion while Tyr94 points away from the metal ion. In subunit B the Tyr94 is ligated directly to Mg^{2+} while the active site residues are not within the Mg^{2+} coordination sphere. The distances shown are in Å.

metal ions against the substrate DNA and vice versa. It is not clear in both studies whether the metal ion positioning is performed by Tyr94 or the DNA actually orients the metal ions within the active site and Tyr94 only supports the network of the formed contacts (assumed by the 1F0O structure and the observation of the Tyr94-water-Ca²⁺ contact).

Certainly the pair of metal ions and the octahedral coordination around their centers drives the conformational adoption of the active site but also the enzyme, the DNA and the water molecules participate. Tyr94 contributes to this synergistic event (the adoption of an active site conformation) where the position and role of each of the components is communicated through its interactions with its counterparts. The emerging question is whether the contribution of Tyr94 to this network of cooperative interactions can be explicitly defined.

The first approach to show the effect of the Tyr94 side chain on the ligation of the Mg²⁺ native ions was performed by plasmid DNA cleavage under steady state conditions (Spyridaki, et al., 2003). The cleavage experiments were performed as a function of the concentration of Mg²⁺ and indicated the direct concerted cleavage of both strands of the duplex substrate by the WT PvuII. The data were fitted to a Hill equation describing the observed rate as a function of the metal bound fraction of the enzyme, which returned a n_H equal to 3.6 for the WT PvuII in accordance with four metal ions occupying the enzyme dimer. In the case of the Y94F variant, the accumulation of a nicked intermediate was shown, which was linked to the non-concerted character of the behavior of the two subunits of the Y94F homodimer (Spyridaki, et al., 2003). The 10-fold decrease of the steady state cleavage rates was shown for the Y94F PvuII compared to

the WT PvuII, while the n_H fitted to 1.1 for the variant was consistent with the presence of one Mg^{2+} ion per Y94F PvuII dimer. The occupation of the enzyme subunit by a single metal ion is consistent with the lower cleavage rate and also with the observation of the nicked intermediate (Spyridaki, et al., 2003).

However the DNA cleavage data of the Y94F variant do not imply a direct role for the aromatic hydroxyl group, but rather refer to the overall behavior of the dimer on the substrate cleavage. The result definitely does not associate with the WT PvuII crystal structure 1H56, which sparked the implication of Tyr94 in the metal ion ligation (Spyridaki, et al., 2003). The exact involvement in the active site of the enzyme of the Tyr94 side chain cannot be extracted from the reported kinetic analysis. The ternary metal-DNA-enzyme complex and their constructive interactions need to be dissected and quantified with respect to Tyr94.

It is the purpose of this study to explore the functionality of the Y94F PvuII endonuclease, monitoring the response of the enzyme to metal ions either directly or through the metal dependence of the DNA processing. It is hypothesized that the separate study of the different functions of the enzyme in the presence of the Y94F mutation would provide insights into the Tyr94 behavior. The conformational impact of the Tyr94 is also examined under the hypothesis that the role of the aromatic hydroxyl group is to adopt a position that leads to a functional PvuII active site.

3.2 Methods

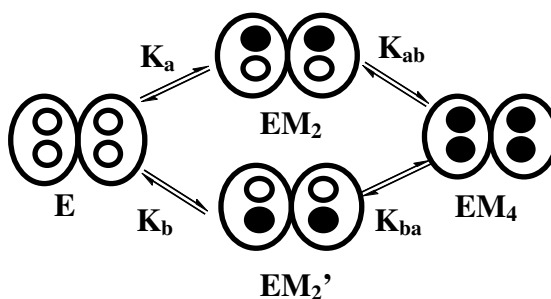
The methods utilized are described in Chapter II. The following analysis applies to the DNA binding data described for the WT and Y94F PvuII in this chapter.

3.2.1 Analysis of the metal dependence of the DNA binding to PvuII

Assuming the presence of two classes of metal binding sites for the WT PvuII in the presence of DNA, **Scheme 3.1** can be used to describe the associated macroscopic and microscopic binding constants. In this case the term “microscopic” is not used strictly to describe the intrinsic binding constant of a single site. Instead it is applied here referring to a class of two sites and thus distinguishing each pair of sites from the other regarding their location within the subunits. Each of the two metal ions would have to occupy a PvuII subunit and not one subunit simultaneously considering the homodimeric nature of the enzyme. The homodimeric character dictates that the two subunits (native or mutant) are characterized by equal probability in binding metal ions at a given metal ion concentration. As such, a sequential model describing the occupation of two sites within a subunit as a first step with a second set of sites being subsequently occupied in the other subunit cannot be considered. In the model shown in **Scheme 3.1**, the first set of sites (two metal ions) is assumed to be filled with a macroscopic K_1 binding constant in an all-or-nothing (Hill) fashion, since the order of filling and the affinities of the sites cannot be further discriminated. In the next step, the second class of sites is filled (two metal ions) in a similar mode, and the macroscopic constant K_2 is assigned. The occupation of the last two metal sites involves the communication of the sites across and within the PvuII subunits. The modes of cooperativity cannot be distinguished in either of the two binding steps. However the synergy between the two classes of sites can be calculated as follows.

As shown in **Scheme 3.1**, the free energy difference between the initial metal free and the final metal bound state (four metal ions) in terms of the observed macroscopic

Scheme 3.1 The sequential occupation of the metal binding sites of the WT PvuII in the presence of DNA. The binding of four metal ions to the PvuII homodimers is shown in accordance to the two classes of sites model. The enzyme species at the different metal stoichiometries are denoted as E (metal free), EM_2 and EM_2' (two metal ions in two different position sets) and EM_4 (four metal ions). The fit of the DNA binding data to **Eq. 3.5** is under the assumption that all the Enzyme-Metal species shown contribute equally to the observed DNA binding signal. The macroscopic binding constants K_1 and K_2 and the microscopic binding constants K_a , K_b , K_{ab} and K_{ba} are shown.



● Occupied site ○ Vacant site



binding constants K_1 and K_2 would be $\Delta G^\circ = -RT \ln K_1 K_2$. Similarly this energy difference can be expressed in terms of the macroscopic constants K_a , K_b , K_{ab} , K_{ba} which describe sequential filling of the two classes of sites and its value would be $\Delta G^\circ = -RT \ln K_a K_{ab} = -RT \ln K_b K_{ba}$ as shown in **Scheme 3.1**. Since the two expressions of the free energy are equivalent, the observed K_1 and K_2 can be expressed as shown in **Eq. 3.1** and **Eq. 3.2** (Weber 1975; Linse, et al., 1987; Wyman, et al., 1990).

$$K_1 = K_a + K_b \quad (3.1)$$

$$K_1 K_2 = K_a K_{ab} \Rightarrow K_2 = \frac{K_a K_{ab}}{K_a + K_b} \quad (3.2)$$

The fraction of the metal bound sites (θ) would then be expressed as in **Eq. 3.3**, where the EM_2 , EM_2' , and EM_4 are the concentrations of the corresponding species of **Scheme 3.1** and E_f is the concentration of the free enzyme dimers (Wyman, et al., 1990).

$$\theta = \frac{\text{moles of occupied sites}}{\text{moles of total sites}} = \frac{2EM_2 + 4EM_4}{4(E_f + EM_2 + EM_2' + EM_4)} \quad (3.3)$$

Substitution of the K_a , K_b , K_{ab} , K_{ba} binding constants in **Eq. 3.3** results in the form of θ in **Eq. 3.4**. By use of **Eq. 3.1**, **3.2**, **3.4**, the expression in **Eq. 3.5** is extracted which is used to fit the normalized DNA association constants as a function of the Ca^{2+} concentration for the WT PvuII. The fit was performed using Kaleidagraph (Synergy).

$$\theta = \frac{K_1 M^2 + 2K_1 K_2 M^4}{2(1 + K_1 M^2 + K_1 K_2 M^4)} \quad (3.4)$$

In the expression of θ in **Eq. 3.5**, a general two-site model is assumed that describes the

sequential binding of four metal ions in pairs (two classes) involving their macroscopic

$$\theta = \frac{(K_a + K_b)M^2 + 2K_a K_{ab} M^4}{2(1 + (K_a + K_b)M^2 + K_a K_{ab} M^4)} \quad (3.5)$$

binding constants (bottom of **Scheme 3.1**). The coupling energy between the two classes of metal sites ($\Delta\Delta G_{\text{coop}}^{\circ}$) is defined as the difference of the free energy (ΔG_a° or ΔG_b°) for the occupation of a class of sites when the other class is unoccupied, from the free energy (ΔG_{ab}° or ΔG_{ba}°) for the occupation of the same class of sites when the other class is already occupied as shown in **Eq. 3.6**.

$$\Delta\Delta G_{\text{coop}}^{\circ} = \Delta G_{ba}^{\circ} - \Delta G_a^{\circ} = -RT \ln\left(\frac{K_{ba}}{K_a}\right) \quad (3.6)$$

Note that the energy difference between the two states is expressed in terms of the K_a and K_{ba} constants and not in terms of the K_1 , K_2 . However the combination of **Eq. 3.1**, **3.2**, **3.6** provides the expression for the $\Delta\Delta G_{\text{coop}}^{\circ}$ shown in **Eq. 3.7** where n is the ratio K_b/K_a .

$$\Delta\Delta G_{\text{coop}}^{\circ} = -RT \ln\left(\frac{K_2(1+n)^2}{K_1 n}\right) \quad (3.7)$$

Assuming that there is no preference for the occupation of the first set of metal binding sites across the PvuII subunits the two binding constants K_a and K_b can be considered to be equal. Under this assumption, $n = 1$ in **Eq. 3.7** and $\Delta\Delta G_{\text{coop}}^{\circ}$ is given by **Eq. 3.8** (Weber 1975; Linse, et al., 1987).

$$\Delta\Delta G_{\text{coop}}^{\circ} = -RT \ln\left(\frac{4K_2}{K_1}\right) \quad (3.8)$$

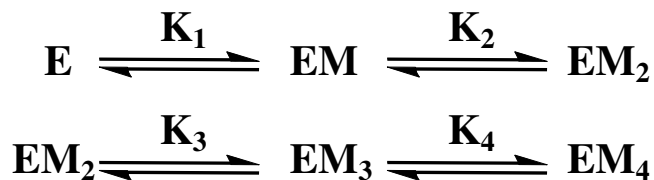
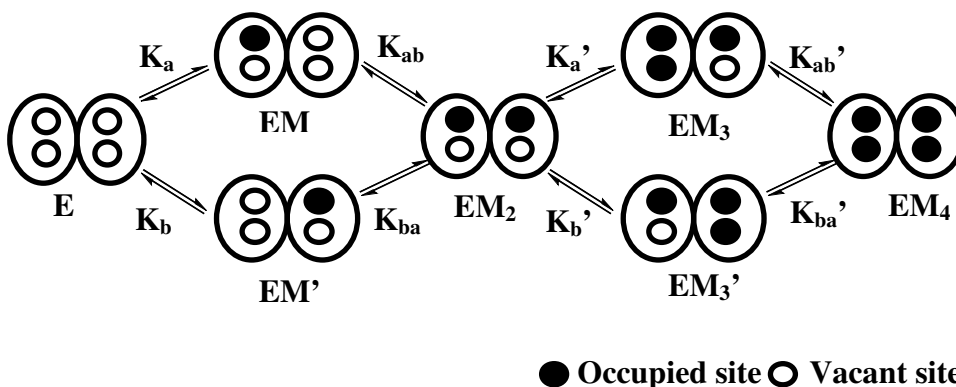
In the case of a homodimer where two phases are observed in a metal ion titration it may be assumed that each phase represents a distinguished class of metal ion sites each one

involving the binding of two metal ions. Accordingly DNA binding data for each of these phases can be fitted to **Eq. 3.9**, which describes the sequential binding of two metal ions without discrimination between the homodimer subunits (involving the macroscopic binding constants K_1 and K_2). The model of the sequential binding of two metal ions (representing each class of sites) is shown in **Scheme 3.2**. In the case of the second class of sites the macroscopic constants K_1 and K_2 in **Eq. 3.9** and also in **Eq. 3.8** for the energy difference between the two sites are substituted by the macroscopic constants K_3 , K_4 as described in **Scheme 3.2**.

$$\theta = \frac{K_1M + 2K_1K_2M^2}{2 + 2K_1M + 2K_1K_2M^2} \quad (3.9)$$

It has to be noted that the K_a , K_b , K_{ab} and K_{ba} (regarded as intrinsic for each class of sites and distinguished by the prime sign for the second class of sites in **Scheme 3.2**) metal binding constants cannot be independently measured in a homodimer like PvuII which accommodates two metal ions per monomeric subunit. However the macroscopic binding constants can be measured and cumulatively provide the energy difference between two states of the enzyme, i.e. the energy between the enzyme bound to four metal ions and the metal free enzyme or between the two metal ions bound state and the metal free state as shown in **Schemes 3.1** and **3.2** respectively. The sums of the energies (observed or intrinsic) of the two steps (between the initial and final state) are equal. Essentially two energetically unequal states are defined and two pathways leading from the initial to the final state are followed. It is the goal of this approach to associate the cooperativity defined by the energy difference between the two states and expressed by the K_a , K_b , K_{ab} and K_{ba} constants with the fitted values for K_1 and K_2 .

Scheme 3.2 The sequential occupation of the metal binding sites of the Y94F PvuII in the presence of DNA. The enzyme species at the different metal stoichiometries are denoted as E (metal free), EM and EM' (one metal ion in two different position sets), EM₂ (two metal ions each in a different subunit), EM₃ and EM₃' (the third metal ion in different subunit in each case) and EM₄ (four metal ions). The fit of the DNA binding data to **Eq. 3.9** is under the assumption that all the Enzyme-Metal species shown contribute equally to the observed DNA binding signal. In this case the binding constants $K_a(K_a')$, $K_b(K_b')$, $K_{ab}(K_{ab}')$, and $K_{ba}(K_{ba}')$ for the two classes of sites are intrinsic while the K_1 , K_2 and K_3 , K_4 are macroscopic.



3.3 Results

3.3.1 The dependence of the PvuII-cognate DNA association on Ca^{2+} ions

It has been previously shown for a number of type II restriction endonucleases that the divalent Ca^{2+} ions support DNA-endonuclease association but not DNA cleavage (Vipond, et al., 1995; Lagunavicius, et al., 1997; Gormley, et al., 2000). The Ca^{2+} -DNA-endonuclease complex has been considered substantially stable (Engler, et al., 1997), which makes the Ca^{2+} ions suitable for DNA binding experiments in the presence of divalent metal ions. The binding of the WT PvuII to cognate DNA has been previously performed as a function of the Ca^{2+} concentration using the cognate non-self complementary 14mer duplex (Chapter II) as a substrate (Conlan, et al., 2002). Through fluorescence anisotropy and filter binding experiments, the measured DNA association constants ranged from 330 nM under metal free conditions to 125 pM for 10 mM Ca^{2+} at 50 mM Tris-HCl, pH 7.5, 25°C and constant ionic strength of 130 mM using NaCl (Conlan, et al., 2002). In addition to the 6000-fold increase in DNA affinity due to Ca^{2+} , the profile of the association constants shows a sigmoidal dependence on the metal ion concentration (**Fig. 3.4**) (Conlan, et al., 2002). The observed sigmoidicity is indicative of the cooperative behavior of the ternary Ca^{2+} -PvuII-DNA complex. Performing a Hill analysis and fitting to **Eq. 2.5**, an site-specific dissociation constant $K_{0.5}$ for Ca^{2+} equal to 3.0 ± 0.2 mM can be readily obtained along with an n_H equal to 3.5 ± 0.15 as previously reported (Conlan, et al., 2002) and also shown in **Table 3.1**. However it can be assumed that there are two non equivalent metal ion sites within a single enzyme subunit and thus taking into account the homodimeric nature of PvuII there would be two classes of metal ion sites across the enzyme dimer as shown in **Scheme 3.1**. In this

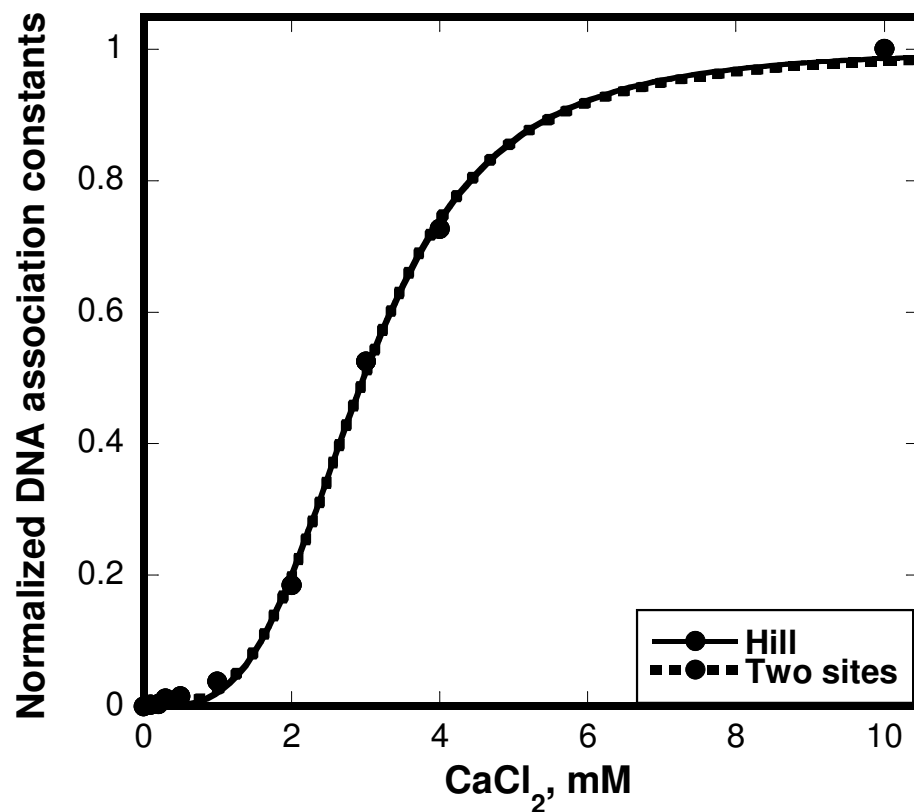


Figure 3.4. The dependence of the DNA association constants on the concentration of Ca^{2+} ions for the WT PvuII (Conlan, et al., 2002). The data were normalized prior to fitting assuming saturation of the metal binding sites at 10mM Ca^{2+} . The Hill model returned n_H equal to 3.5 ± 0.15 . The fitting parameters of the two applied models are shown in **Table 3.1**.

scheme it is also assumed that the filling of each class of metal sites occurs in an all-or-nothing (Hill model) fashion. Fitting the WT-PvuII DNA binding data to **Eq. 3.5** the macroscopic Ca^{2+} binding constants for the two classes of sites are found equal to 6.0 ± 0.8 mM and 1.5 ± 0.2 mM also shown in **Table 3.1**. The application of K_1 and K_2 to **Eq. 3.8** returned a value for the lower limit of the interaction free energy between the two classes of sites $\Delta\Delta G_{\text{coop}}^{\circ}$ equal to -2.5 kcal/mole (at 25°C). The four Ca^{2+} ion sites cannot be further distinguished in the case of the WT PvuII since the metal site interactions within each subunit and also among them contribute to the overall calculated energy.

The fluorescence anisotropy and filter binding experiments with the HEX labeled and the ^{32}P radiolabeled 14mer respectively, were also performed for the Y94F PvuII. The conditions were identical to those of the WT PvuII. The relationship between the DNA binding affinities and the metal saturation of the Y94F subunits is characterized by two phases as seen in **Fig 3.5**. The measurements were performed through fluorescence anisotropy up to 0.1 mM Ca^{2+} and filter binding was applied in all the metal concentrations above 0.1 mM. At 0.1 mM Ca^{2+} measurements with both techniques were applied providing equivalent binding constants. The lower phase is well defined by the plateau at the points between 0.5 and 2 mM Ca^{2+} at which point the errors do not overlap with the next immediate points at 2.5 mM Ca^{2+} (negligible error at this point) and 3 mM Ca^{2+} (**Fig. 3.6**). Evidently the affinity to the 14mer DNA is higher for the Y94F variant than for the WT PvuII up to 2 mM Ca^{2+} , at which point the shape of the WT sigmoidal plot becomes steep (**Fig. 3.5 inset**).

The two distinct phases may be indicating the existence of two distinct classes of metal binding sites. If this is the case then part or all of the interaction energy between

Table 3.1 DNA binding to the WT PvuII and Y94F PvuII.

WT PvuII		
	Hill^a	Two sites
n_H	3.5 ± 0.1	
K_1 (mM)	3.0 ± 0.2	6.0 ± 0.8
K_2 (mM)		1.5 ± 0.2
$\Delta\Delta G_{\text{coop}}^{\circ}$ (kcal/mol)		-2.5
χ^2	0.001	0.001
R^2	0.999	0.999

Y94F PvuII		
	Hill^b	
	upper phase	lower phase
n_H	1.1 ± 0.2	1.5 ± 0.4
K_1 (mM)	1.25 ± 0.3	0.14 ± 0.02
χ^2	0.023	0.017
R^2	0.983	0.991

	Two sites	
	upper phase	lower phase
K_1 (mM)	0.8 ± 0.3	0.23 ± 0.09
K_2 (mM)	1.8 ± 0.6	0.08 ± 0.03
$\Delta\Delta G_{\text{coop}}^{\circ}$ (kcal/mol)	-0.3	-1.4
χ^2	0.024	0.018
R^2	0.982	0.991

The macroscopic association constants and Hill coefficients are provided from fitting to the corresponding models. The $\Delta\Delta G_{\text{coop}}^{\circ}$ energies are calculated through the application of the binding constants to **Eq. 3.8**. (a): (Conlan, et al., 2002), (b): (Papadakos, et al., 2007)

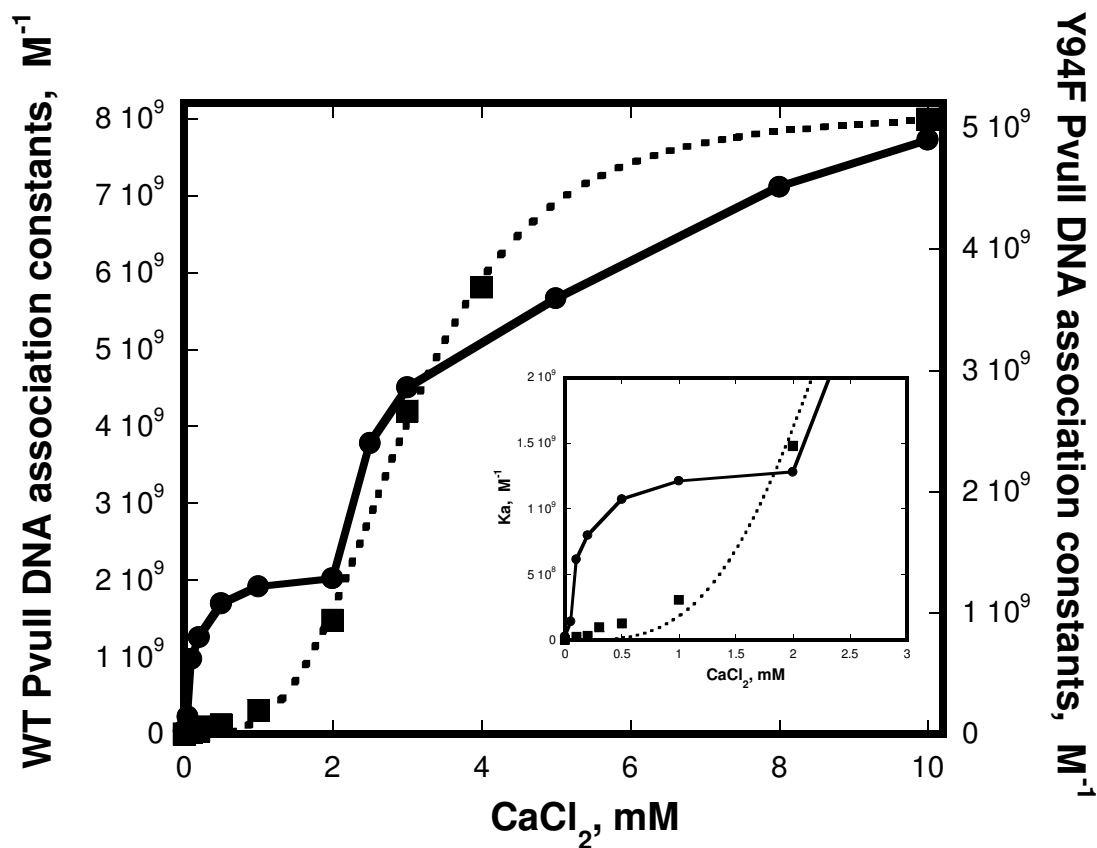


Figure 3.5. The profiles of the DNA association constants as a function of the Ca^{2+} concentration for the WT and the Y94F PvuII (Conlan, et al., 2002; Papadakos, et al., 2007). The WT data are shown for comparison and the fit to the Hill model (*dotted line*) is shown as in **Fig 3.4**. In the case of the Y94F data (*continuous line*) the line is not a fit. The lower overall affinity to the DNA is evident for the Y94F PvuII. The inset is a detail of the overlap at the $[\text{Ca}^{2+}]$ range between the 0 and 3 mM on the same y-scale.

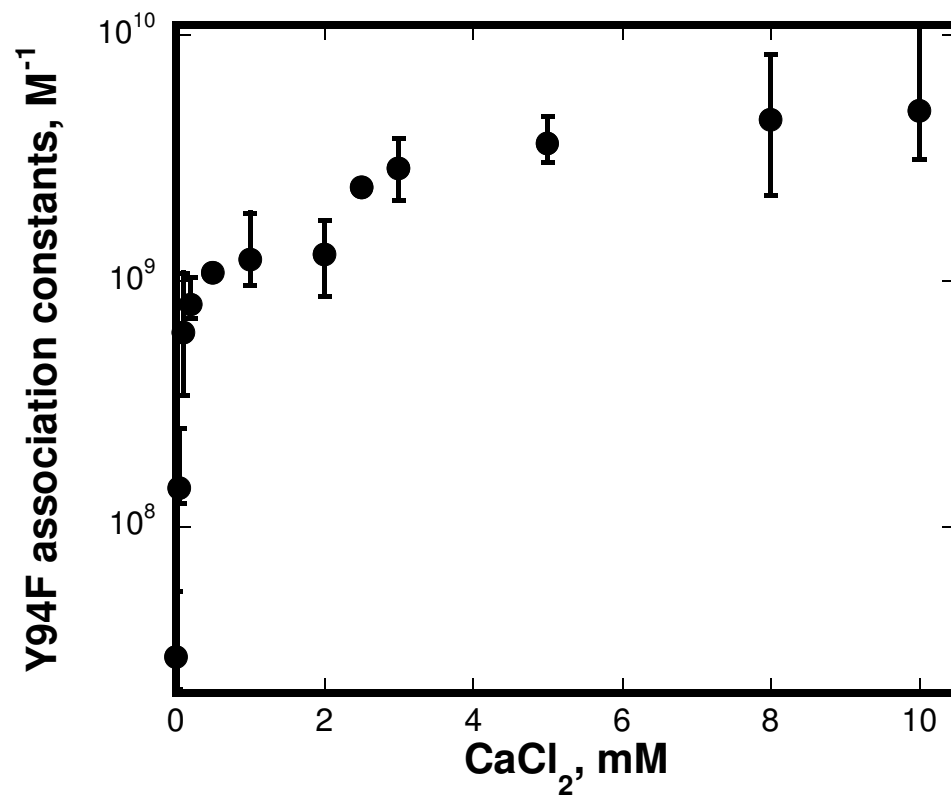


Figure 3.6. Error intervals for the profile of the DNA association constants versus the Ca^{2+} concentration of the Y94F PvuII (**Fig. 3.5**). At 2.5 mM Ca^{2+} the error is negligible and the plateau up to 2 mM Ca^{2+} is well defined. Clearly the overall plot is biphasic.

the two classes of sites ($\Delta\Delta G_{\text{coop}}^{\circ}$) in the WT PvuII (-2.7 kcal/mole) is removed in the case of the Y94F variant. For the analysis of the biphasic data according to the models described in *Methods*, the following considerations were made. The upper phase of the biphasic DNA binding plot of the Y94F PvuII is normalized with respect to the DNA association constants and also with respect to the Ca^{2+} concentrations. The 2 mM Ca^{2+} concentration is assumed as the lowest point of the phase and the 10 mM Ca^{2+} point is accordingly normalized to 8 mM. This normalization is under the assumption of independence between the two classes of sites on the biphasic profile.

Each of the phases was applied to Hill analysis and fit to **Eq. 2.5** providing the Ca^{2+} apparent association constants and Hill coefficients shown in **Table 3.1**. Indeed the fitted Hill coefficients at 1.5 ± 0.4 and 1.1 ± 0.2 (**Table 3.1** and **Fig. 3.7**) suggest the occupation of the Y94F-PvuII homodimers with at least two metal ions at low Ca^{2+} concentrations and a stepwise occupation of another two metal ion sites at higher Ca^{2+} concentrations. For the first two metal ion sites an apparent binding constant at 135 ± 22 μM has been calculated while at the higher phase the data fitted to a 125 ± 30 μM binding constant (**Table 3.1**). The two apparent binding constants show great consistency with the previously reported Ca^{2+} binding constants to WT-PvuII in the absence of cognate DNA (0.12 mM and 2.1 mM by a two classes of sites model) (Jose, et al., 1999). Whether the two metal ion sites of a class of sites are distributed across the subunits or not is not possible to distinguish. The model in **Scheme 3.2** presents the scenario in which the homodimeric nature of the enzyme is taken into account and the involved uncoupling into classes as observed in the biphasic profile is symmetrically affecting the metal ion site occupation.

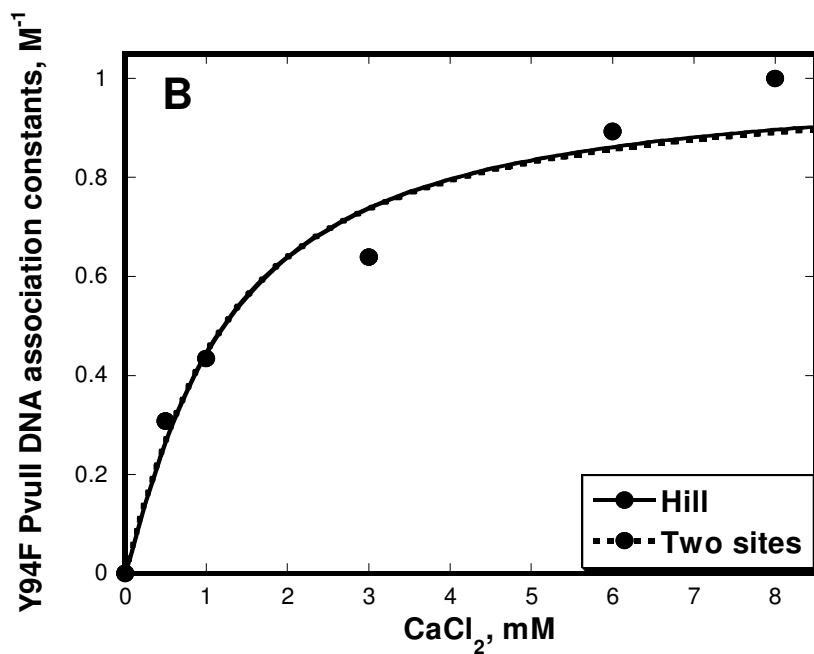
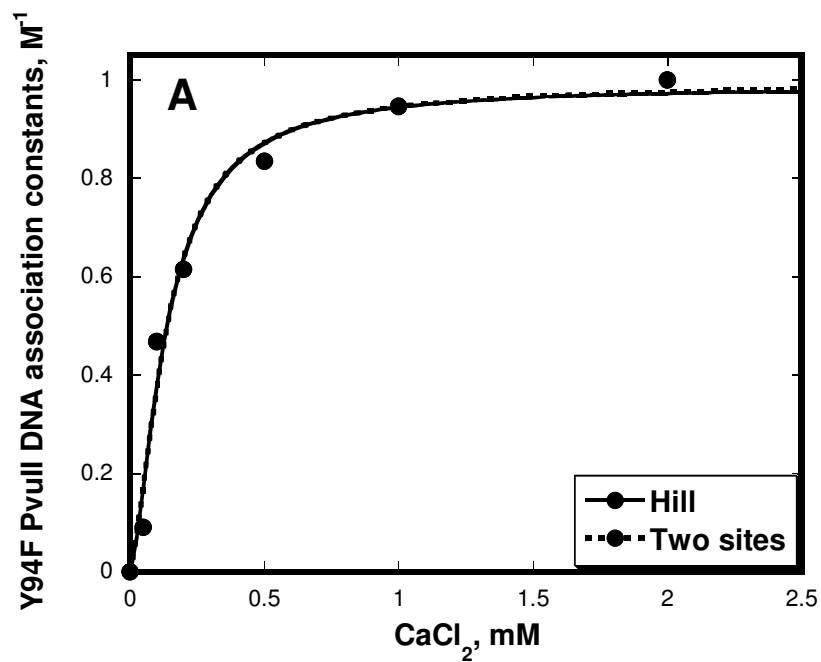


Figure 3.7. The independent fits of the two phases of the DNA binding profile of the Y94F PvuII. The lower phase of **Fig. 3.4** (A) and the upper phase (B) are shown. The upper phase is normalized as described in the text. The Hill coefficients are 1.5 ± 0.4 and 1.14 ± 0.2 for the lower and upper phases respectively.

Further analysis of each of the two phases has been applied to characterize each class of sites. Assuming a two-site model for each of the phases (**Scheme 3.2**) the data can be fitted to **Eq. 3.9 (Fig. 3.7)**. This approach returned the values shown in **Table 3.1**. The fit of the upper phase data yielded values of K_1 and K_2 equal to 0.8 ± 0.3 mM and 1.8 ± 0.6 mM, respectively, while the lower phase yielded the corresponding 0.23 ± 0.09 mM and 0.08 ± 0.03 mM as shown in **Table 3.1**. The free energies of the communication between the macroscopic sites are ΔG_{coop}^1 equal to -0.3 kcal/mole and ΔG_{coop}^2 equal to -1.4 kcal/mole for the upper and lower phases respectively. The points of each phase applied to the fit are not sufficient to provide high confidence on the fitted values in contrast to the WT PvuII where the whole profile is simultaneously fitted.

Taking into account the homodimeric nature of PvuII, the $\Delta\Delta G^\circ$ value represents the interaction energy between the two metal ion sites across the two PvuII subunits for each of the classes of sites (in each phase) of the Y94F PvuII-DNA binding profile. The results suggest that after the occupation of one metal ion in one enzyme active site, the occupation of the active site of the enzyme in the opposite subunit by one metal ion is favored by 1.4 Kcal/mole. This set of sites (lower phase) is uncoupled from the second set of sites (upper phase). The energy of their interaction is not known in the case of the Y94F mutant although it is estimated to be -2.5 kcal/mole for the WT PvuII. It may be assumed that there is still a partial communication characterized by a fraction of the 2.5 kcal/mole or that the interaction is impaired. In the second set of sites in the Y94F PvuII after the third metal ion is bound to one of the enzyme active sites, the binding of the fourth metal ion is favored by 0.3 kcal/mole. It is shown that despite the fact that the absolute magnitude of the energetic levels of the intrinsic binding constants is not known,

the followed approach returns the lower limit of the energy of interaction between these levels. The calculated $\Delta\Delta G^\circ$ values are graphically shown in the energetic diagrams of **Scheme 3.3**. The apparent uncoupling of the metal binding sites imposed by the Y94F mutation facilitates the study of the interaction between the sites in the presence of DNA to a greater extent than in the WT PvuII. The structural outcome of the absence of the aromatic hydroxyl group of Tyr94 in the DNA binding process is required for the uncoupling of the metal binding sites. As previously involved as a direct Mg^{2+} ligand even without cognate DNA (Spyridaki, et al., 2003), Tyr94 may indeed be directly implicated in the coordination of metal ions which eventually affects the DNA association dependence on Ca^{2+} .

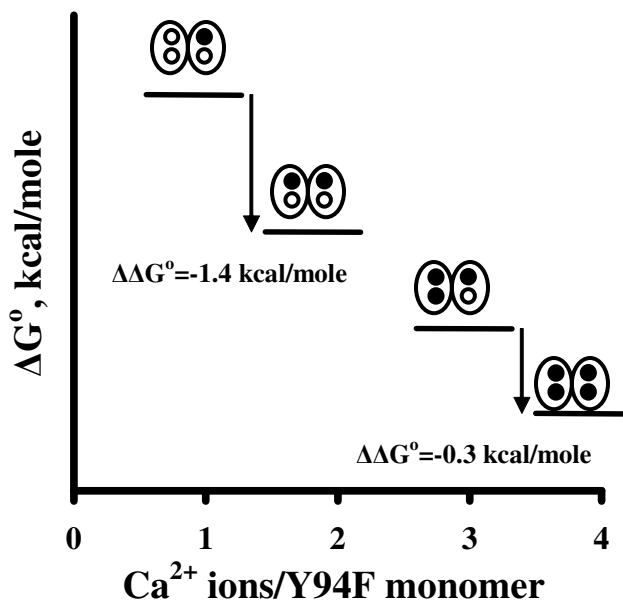
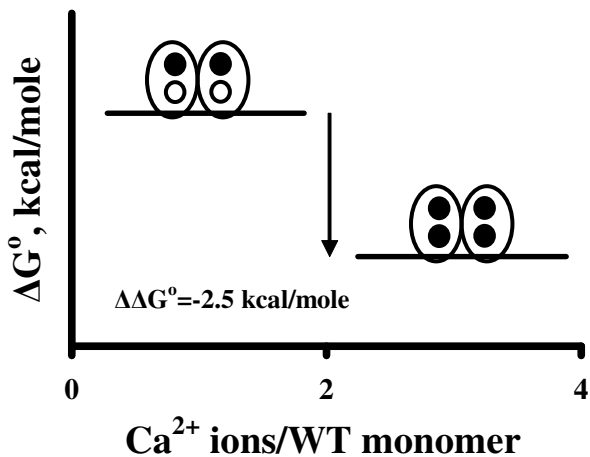
3.3.2 The metal binding properties of Y94F PvuII in the absence of DNA.

In order to elucidate the role of the aromatic hydroxyl group of Tyr94 as a metal ion ligand within the active site of PvuII the Y94F variant was applied in metal binding assays for Ca^{2+} , Mg^{2+} , and the lanthanides Tb^{3+} and Eu^{3+} in the absence of cognate DNA.

3.3.2.1. Ca^{2+} binding to Y94F PvuII

To characterize the binding of Ca^{2+} by Y94F PvuII, isothermal titration calorimetry was applied. The normalized heats obtained were fitted to the Hill model (**Eq. 2.5**) and also to models for one and two metal sites (sequential) per enzyme monomer (**Eq. 2.3** and **2.8** respectively). Raw and integrated ITC data of the titration of 500 μ M Y94F PvuII monomers are shown in **Fig. 3.8** while the summary of the fitted results is shown in **Table 3.2**. The existence of two exothermic binding sites for Ca^{2+} is

Scheme 3.3. Energetic diagrams for the interactions between the metal ion binding sites in the presence of DNA. The free energy levels (ΔG° axis in arbitrary units) shown, represent the $\Delta\Delta G^\circ$ values as they are calculated from **Eq. 3.8** for the WT (*top*) and Y94F (*bottom*) PvuII dimers. The free energy associated with the coupling between the two sets of sites in WT PvuII is partially or totally abolished due to the Y94F mutation.



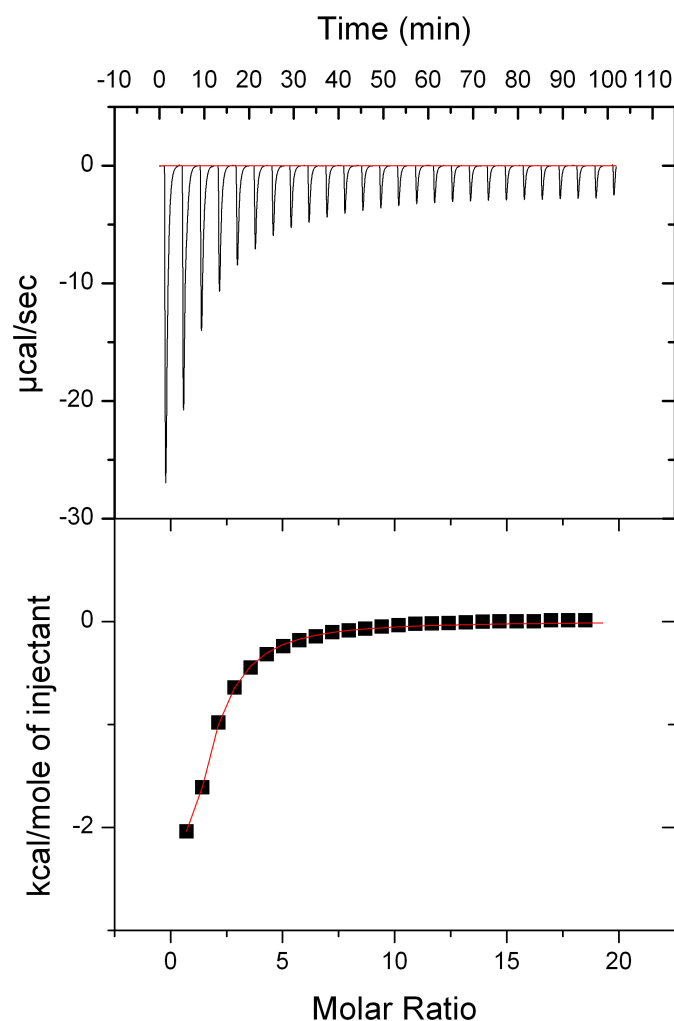


Figure 3.8 Ca^{2+} binding to Y94F PvuII. Representative ITC isotherm of 500 μM PvuII monomers vs 12.5 mM Ca^{2+} obtained at 25°C (*Top panel*: raw, *Bottom panel*: integrated ITC data). The calorimetric isotherms were fit to the models described in Chapter II. The line at the *bottom panel* is drawn to guide the eye. The best fit of the data to the model describing two independent classes of sites yielded K_1 and K_2 equal to 0.1 ± 0.04 mM and 3.9 ± 0.9 mM respectively.

Table 3.2 Ca^{2+} binding to Y94F PvuII. The integrated calorimetric data were normalized and fit to the models shown in Chapter II.

	Model		
	One site	Two sites	Hill
n	1	2	1.6
K₁ (mM)	0.9 ± 0.01	0.1 ± 0.04	5.2 ± 4.6
K₂ (mM)		3.9 ± 0.9	
	One site	Two sites	Hill
n	1	2	1.4 ± 0.1
K₁ (mM)	0.38 ± 0.26	0.28 ± 0.2	0.68 ± 0.38
K₂ (mM)		3.8 ± 0.4	
R²	0.984	0.985	0.966
χ²	0.035	0.033	0.077

n represents the number of sites or the Hill coefficient accordingly. The top panel includes the data obtained by the titrations of 500 μM Y94F PvuII monomers while the data from the experiment involving 50 μM monomers are shown in the bottom panel.

confirmed by the characteristic endpoint of the titration appearing at a molar ratio of $[\text{Ca}^{2+}] / [\text{PvuII monomers}]$ higher than two (**Fig. 3.8**) which is typical in the characterization of two site systems by ITC (Jose, et al., 1999; Henzl, et al., 2003). The fit to the one site model provided a K_d of 0.9 ± 0.01 mM, while the Hill model provided a K_d of 5.2 ± 4.6 mM with a Hill coefficient n_H of 1.6, suggesting the titration of at least two Ca^{2+} ions per PvuII active site. The fitting of the data to the sequential two site model returned K_1 and K_2 equal to 0.1 ± 0.04 mM and 3.9 ± 0.9 mM, respectively. The two-site and mainly the Hill model provide fitted values with greater statistical confidence than the one-site model. The individual fits to the Hill and two-site models provided R values at 0.998 and χ^2 values at 0.0022, which are superior to the corresponding 0.974 and 0.04 values for the one site model, respectively. As is the case for the WT PvuII where the calorimetric data are consistent with the presence of two Ca^{2+} ions per enzyme active site (Jose, et al., 1999) the fit of the data involving 0.5 mM enzyme monomers to models describing two sites for Y94F PvuII also support a $\text{Ca}^{2+}:\text{PvuII}$ active site stoichiometry equal to 2:1. In addition, the low millimolar binding constants obtained from all the models are similar to the binding constants obtained for the Ca^{2+} titration to WT PvuII for one set of two equivalent sites (1.3 ± 0.14 mM) and also for two sets of independent sites (0.12 ± 0.08 mM and 2.1 ± 0.14 mM).

Essentially the calorimetric data indicate that the removal of the aromatic hydroxyl group of Tyr94 does not affect the stoichiometry and affinity of Ca^{2+} ions to the PvuII active site. In order to explore the presence of a binding site with an apparent affinity around 100 μM as obtained by the fit to the two-site model, 50 μM Y94F PvuII monomers were titrated at 25°C by ITC under the same conditions. The obtained data

were fitted to the same models and the results are shown in **Table 3.2**. The best fit to the two-site model returned a Ca^{2+} site with an affinity at 0.28 ± 0.2 mM and a second site at 3.8 ± 0.4 mM. The data are consistent with the existence of a high micromolar site as hypothesized and as previously shown for the WT PvuII (0.12 ± 0.08 mM) (Jose, et al., 1999). Although the high affinity site was not explored further and the data shown represent a single experiment, it is evident that the Ca^{2+} binding behavior of the Y94F PvuII is almost identical to the WT PvuII.

3.3.2.2. Mg^{2+} binding to Y94F PvuII

In order to characterize the binding of the native Mg^{2+} ions to Y94F PvuII in the absence of cognate DNA, the commercially available magnesium indicator Mag Fura-2 was utilized. A competition assay was set up involving the titration of Mg^{2+} ions into a mixture of enzyme and the chromophore. This results in the partition of the total concentration of the metal ions to three states (i.e., free in solution, bound to the chromophore and bound to the enzyme). The observed wavelength shifts in the excitation spectra of Mag Fura-2 in the presence of Y94F PvuII from 250-480 nm at 490 nm emission report the Mg^{2+} bound state of the chromophore (**Fig 3.9A**). The measured signal (intensity ratio $I_{325/370}$) is modulated by the partition of the total Mg^{2+} concentration to which the active site of PvuII participates. The ratiometric measurement results in the acquisition of the isotherm shown in **Fig. 3.9B** where Y94F PvuII monomers are fixed at 250 μM while the indicator is set at 200 μM and their mixture is titrated to 40 mM Mg^{2+} . Titrations were performed with Y94F PvuII and the chromophore at the concentration ranges mentioned in Chapter II. Simulations using the three models were performed

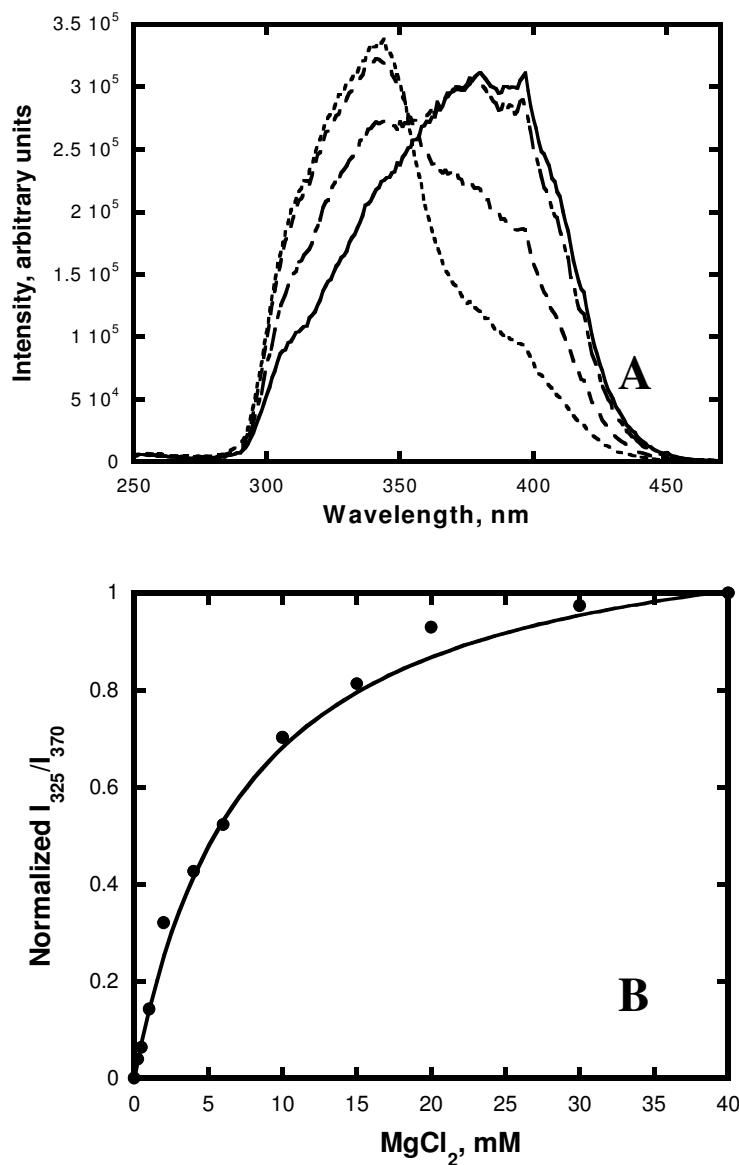


Figure 3.9. Mg²⁺ binding to Y94F PvuII. A. Excitation spectra of 200 μM Mag Fura-2 obtained in the presence of 250 μM PvuII monomers and increasing concentrations of Mg²⁺ (0 mM (—), 1 mM (— · —), 10 mM (---), 50mM (·····)). The spectra were collected between λ_{ex}: 250-480 nm at λ_{em}: 490 nm and slits at 1 nm. B. The corresponding isotherm to the spectra is shown in A. The ratio of the intensities I₃₂₅/I₃₇₀ vs the Mg²⁺ concentration is normalized and fitted to the models described in Chapter II. The best fit of the data to the Hill competition model yielded n_H equal to 1.4 and K_d at 0.4 ± 0.2 mM for the Mg²⁺ binding sites.

applying binding constants ranging from low millimolar to high nanomolar affinity for each Mg^{2+} site of PvuII. For Mag Fura-2 concentrations between 0.1 and 0.5 mM and PvuII monomer concentrations between 0.2 and 1 mM, the obtained isotherms were identical to the models of one-site and two independent sites. Essentially the experimental concentrations for these two models resulted in isotherms that did not permit the exploration of the corresponding binding constants due to the fact that the complexation of Mg^{2+} ions to PvuII would not perturb the Mg^{2+} -chromophore equilibrium in order to sufficiently discriminate between the models. It would be necessary to use enzyme concentrations far higher than are experimentally feasible. However, applying the 2 mM binding constant for the Mg^{2+} :chromophore complex and also n_H equal to 1.4 to the Hill model, the fitting of the three datasets returned an average of 0.4 ± 0.2 mM binding constant for the binding of Mg^{2+} to PvuII (**Fig. 3.9B**). The fit to the Hill model suggests the presence of two metal ions within the Y94F PvuII active site, although at a lower affinity than in the case of the WT PvuII (1.9 ± 0.4 mM) (Dupureur, et al., 2000).

3.3.2.3. *Tb³⁺ and Eu³⁺ binding to Y94F PvuII*

Similar in ionic radius and also having identical coordination preferences with the divalent Ca^{2+} ions, the trivalent lanthanide ions Tb^{3+} and Eu^{3+} have been extensively applied as Ca^{2+} substitutes in Ca^{2+} binding systems to characterize their metal binding properties (Horrocks 1993; Huheey, et al., 1993). The spectroscopic information on the metal binding properties of the lanthanides can be acquired either by their excitation spectra after their direct excitation or by their emission spectra after indirect excitation by

nearby tyrosine residues (Bowen, et al., 2004). The latter approach was followed for the characterization of the metal binding sites of the Y94F PvuII. The characteristic spectrum obtained by the emission of the lanthanide ion after the addition of 20 μM Tb^{3+} to 2 μM Y94F PvuII monomers is shown in **Fig. 3.10**. The intensities of the peak at 543 nm were collected and corrected for the buffer interference. The same was applied in the case of Eu^{3+} , and the intensity of the characteristic peak at 614 nm was utilized as the observable. The corrected intensities were normalized and plotted against the concentrations of the corresponding lanthanide ion corrected for dilution. Typical isotherms obtained for Tb^{3+} and Eu^{3+} are shown in **Fig. 3.11** and **3.12**. The data for each metal ion were fitted to a Hill model and also to one-site and two-site models as described in Chapter II. The results are summarized in **Table 3.3** where the averages of the individual fitted values at different concentrations of Y94F PvuII monomers are shown. The fits of the data for the Tb^{3+} binding to Y94F PvuII resulted in similar fit quality (**Fig. 3.11**) among the models (with a slight deviation for the Hill model) for all the enzyme concentrations applied. This is observed at the identical patterns of the residuals shown in **Fig. 3.11** except for the Hill model for which the deviation of the residuals is greater and thus represents the poorest fit of the four models applied. The χ^2 and R^2 values in **Table 3.3** also show the superiority of the three models over the Hill model. The averages of the fitted binding constants for all models (**Table 3.3**) reveal the presence of a low micromolar binding site for Tb^{3+} consistent with the previously observed Tb^{3+} site at $2.3 \pm 1.7 \mu\text{M}$ obtained for the WT PvuII (Bowen, et al., 2004). The metal ion working concentrations were limited to 40 μM , with Y94F PvuII concentrations up to 10 μM monomers exhaustively dialysed as described in Chapter II.

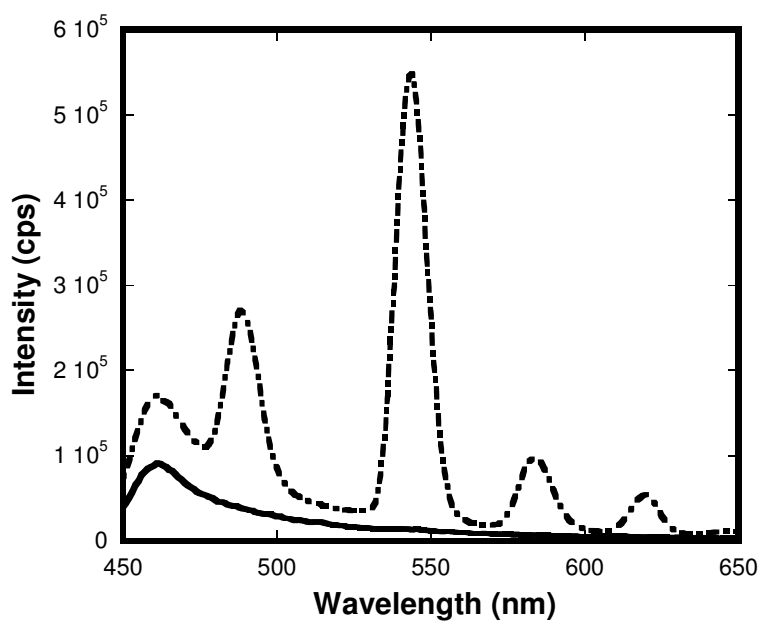


Figure 3.10. Emission spectrum of Tb³⁺ bound to PvuII. The characteristic profile of the Tb³⁺ emission (dashed line) is observed by excitation of the protein at 274 nm while the spectra are collected between 450-650 nm through a 450 nm cutoff filter (slits at 6 nm). Y94F PvuII concentration is 2 μM monomers (apo-enzyme spectrum represented by the continuous line) while the Tb³⁺ concentration is 20 μM in 5 mM Hepes, 400 mM KCl, pH 7.5.

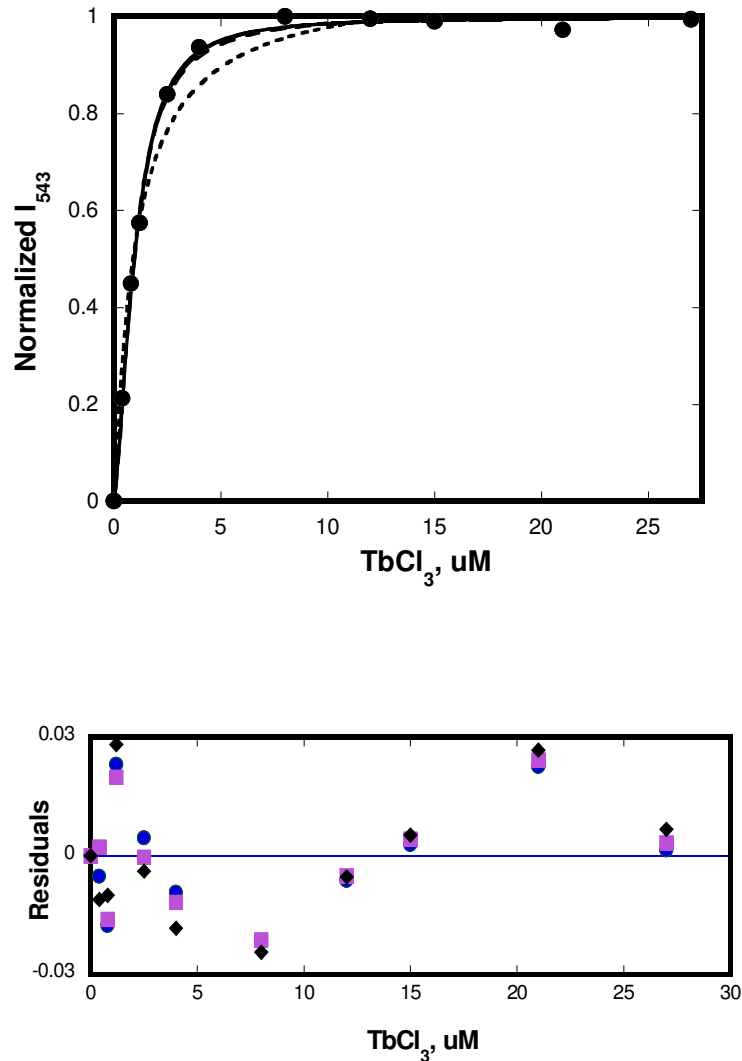


Figure 3.11 Tb^{3+} binding to Y94F PvuII. Typical isotherm of: 0.5 μM Y94F PvuII monomers vs. 27 μM Tb^{3+} (λ_{ex} : 274 nm, λ_{em} : 450-650 nm, slits: 6 nm). The intensities of the characteristic maximum at 543 nm were corrected for the buffer interference and normalized and fitted to the shown models. It is evident from the residuals of the individual fits that there is no discrimination among the models regarding their quality except for the Hill model which does not fit well to the isotherm. This was observed for all the Y94F PvuII concentrations applied to Tb^{3+} binding. *Fit and residuals legend:* (One site —●—), (Two equivalent sites - -○), (Two non equivalent sites —·—■), (Hill ·····◆). The fitted lines of the one site and two equivalent site models coincide.

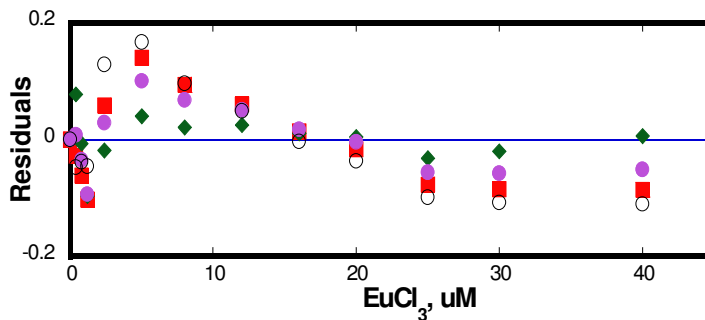
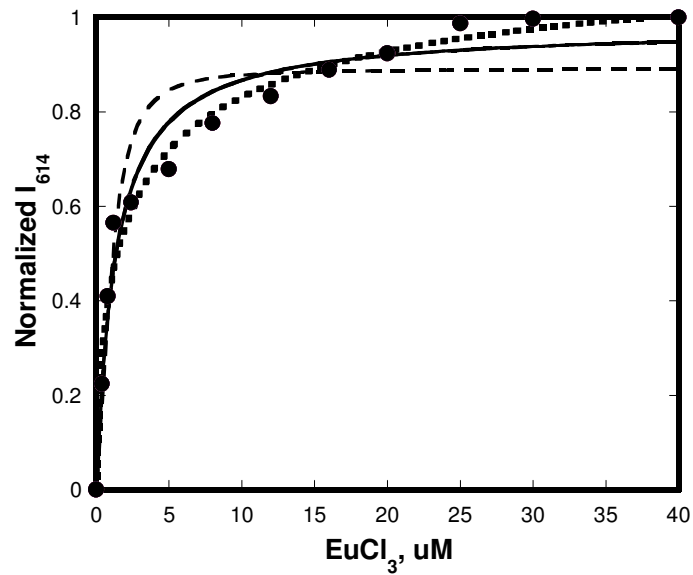


Figure 3.12. Eu^{3+} binding to Y94F PvuII. Typical isotherm, of 1 μM Y94F PvuII monomers vs. 40 μM Eu^{3+} (λ_{ex} :282 nm, λ_{em} : 510-710 nm, slits: 6nm). The intensities of the characteristic maxima at 614 nm were corrected for the buffer interference and normalized and fitted. The residuals of the individual fits support the superiority of the Hill model in the description of the Eu^{3+} binding to Y94F PvuII. A Hill coefficient at 1.5 ± 0.17 and a binding constant at $0.51 \pm 0.17 \mu\text{M}$ was obtained. *Fit and residuals legend:* (One site—●), (Two equivalent sites—○), (Two non-equivalent sites—■), (Hill—◆). The fitted lines of the one site and two non-equivalent site models coincide.

Table 3.3 Lanthanide binding to Y94F PvuII observed by Tyrosine sensitized lanthanide spectroscopy.

Tb³⁺	Y94F			
	Model			
	One site	Two sites		Hill
		Equivalent	Non Equivalent	
n	1	2	2	1.5 ± 0.17
K₁ (μM)	2.2 ± 2.0	5.5 ± 6.2	3.98 ± 4.3	0.51 ± 0.24
K₂ (μM)			77.9 ± 55.4	
χ²	0.031	0.013	0.017	0.156
R²	0.985	0.993	0.992	0.991
	WT			
K₁ (μM)	1.1 ± 0.6		2.3 ± 1.7	
K₂ (μM)			117 ± 46	
R²	0.986		0.988	
	Y94F			
Eu³⁺	Model			
	One site	Two sites		Hill
		Equivalent	Non Equivalent	
n	1	2	2	1.5 ± 0.06
K₁ (μM)	1.2 ± 0.2	1.3 ± 0.6	1.5 ± 0.7	1.3 ± 0.4
K₂ (μM)		4.7 ± 2.0	9.8 ± 9.2	
χ²	0.017	0.01	0.003	0.003
R²	0.994	0.994	0.998	0.998
	WT			
K₁ (μM)	3.3 ± 2.3		1.4 ± 0.6	
K₂ (μM)			223 ± 161	
R²	0.997		0.998	

n represents the number of sites or the Hill coefficient accordingly. The values are averages of the independent fits of seven datasets for Tb³⁺ at Y94F PvuII ranging from 0.25-5 μM monomers. In the case of Eu³⁺ three datasets were independently fitted and averaged at enzyme concentrations between 1-3 μM Y94F PvuII monomers. The statistical parameters χ² and R² are the average values of the applied fits. The WT PvuII data are reproduced (Bowen, et al., 2004)

The poor enzyme solubility at 50 μM Tb^{3+} and above was readily observed with minimal stirring. A lower affinity site similar to the previously shown in the case of WT PvuII at $117 \pm 46 \mu\text{M}$ (Bowen, et al., 2004) would be barely populated. Simulations at 5 μM PvuII monomers from a model describing two independent non equivalent sites with apparent affinities at 2 and 120 μM returned a fraction of ~ 0.18 enzyme monomers occupied by Tb^{3+} at the weak site at a total Tb^{3+} concentration of 40 μM , i.e., $\sim 1.0 \mu\text{M}$ PvuII monomers. Consequently the fits of these experimental data to two site models cannot provide the affinity of a higher micromolar site (above 100 μM) if present. The fits to the two site models rather report the binding constant of a second site as it is actually populated under the experimental conditions at $77.9 \pm 55.4 \mu\text{M}$ (**Table 3.3**). The high error reflects the large uncertainty associated with the value. Simulations provide fractions of enzyme bound to a second Tb^{3+} ion with 22 μM or 80 μM affinity at ~ 0.6 or ~ 0.3 respectively (one Tb^{3+} binding site at 2 μM , 5 μM PvuII monomers, 40 μM Tb^{3+} total concentration). Whatever the affinity of the second site, it is not saturated up to 40 μM Tb^{3+} but the bound fraction perturbs the observed Tb^{3+} binding and this is reflected in the two-site model. The same conclusion comes from the fit to the Hill model for which the statistics are not comparably good but still allow the prediction of a second Tb^{3+} site within the Y94F PvuII active site. This is indicated by the Hill coefficient fitted to 1.5 ± 0.2 while the affinity is $0.51 \pm 0.24 \mu\text{M}$ (**Table 3.3**) which is also at the same range as the high affinity site for the WT PvuII. The data from the Eu^{3+} titrations lead to the same observations. The fits to the one-site and two-site models are not distinguishable with respect to their quality while the Hill model is overall superior. The binding constant of a low micromolar site at $1.2 \pm 0.2 \mu\text{M}$ (one-site model) or $1.3 \pm 0.6 \mu\text{M}$ (two-

site model) is also estimated in the case of Eu^{3+} for the Y94F PvuII similar to the corresponding $3.3 \pm 2.3 \mu\text{M}$ and $1.4 \pm 0.6 \mu\text{M}$ affinities estimated for the WT PvuII (Bowen, et al., 2004). The Hill model provided a binding constant at $1.3 \pm 0.4 \mu\text{M}$ with a coefficient of 1.5 ± 0.06 . This is indicative of the presence of a second metal ion within the active site while the affinity is also similar to the high affinity site of the WT PvuII.

3.3.3 Conformational studies of the Y94F PvuII

3.3.3.1 Measurement of the conformational stability of the Y94F PvuII

In order to estimate the involvement of the Tyr94 to the conformational stability of PvuII, the equilibrium denaturation of the Y94F PvuII variant was studied. As previously described, PvuII contains four Trp residues per subunit, two of which are solvent accessible while the other two are buried (Balendiran, et al., 1994). The intrinsic fluorescence of the buried Trp residues can then be used as a probe of the unfolding state of the enzyme subunit since the solvent exposure of the buried Trp residues results in quenching of the observed fluorescence. The approach was previously described for a series of proteins including the *E. coli* trp aporepressor, the *E. coli* CRP and also the WT PvuII (Gittelman, et al., 1990; Cheng, et al., 1993; Dupureur, et al., 2001). PvuII dimers were equilibrated overnight at different GdnHCL concentrations as described in Chapter II, and the fluorescence of the Trp residues was monitored at 330 nm after excitation at 295 nm. The WT PvuII was initially applied to the analysis and the denaturation curves at 0.1, 0.5, 1.0, 1.5, 2.0 μM PvuII dimers, in 50mM Epps, 100mM KCl, pH 7.7 and 25°C were obtained (**Fig. 3.13**). Within the applied range of concentrations of denaturant and as observed by the Trp fluorescence no stable intermediate was populated. The data were

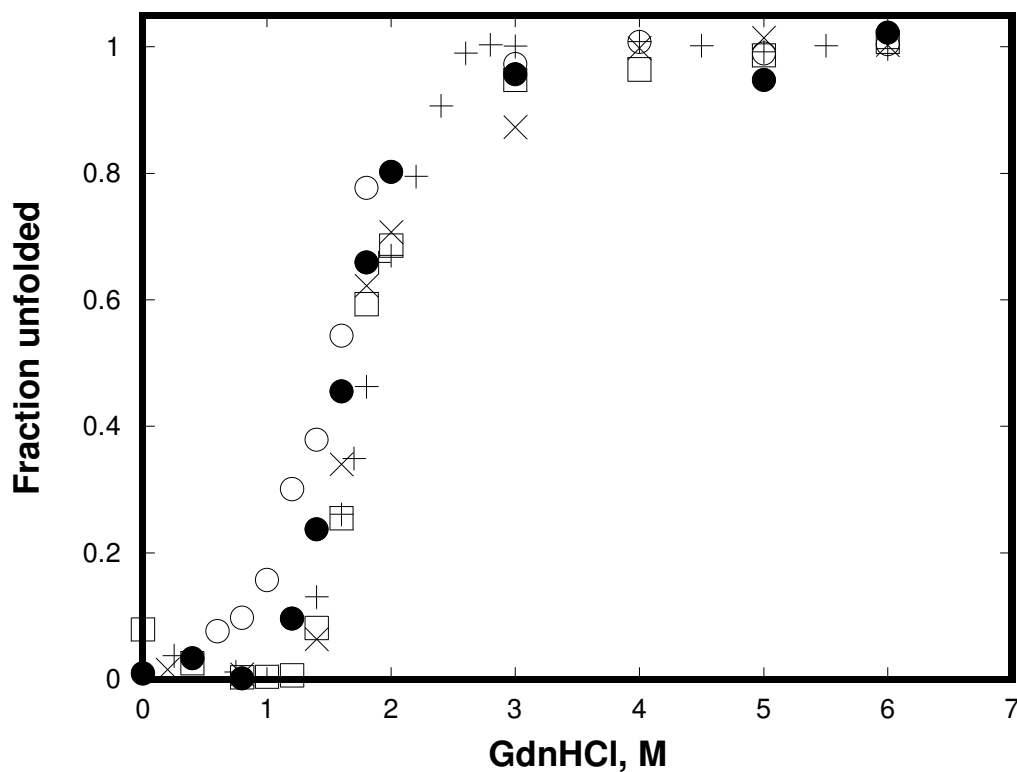


Figure 3.13 The dependence of the GdnHCl denaturation on the concentration of the WT PvuII dimers. The fits of the corresponding curves to the two-state model provide the denaturation parameters shown in **Table 3.4**. All experiments were performed at 50 mM Epps, 100 mM KCl, pH 7.7. Protein concentration: 0.1 (\circ), 0.5 (\square), 1.0 ($+$), 1.5 (\bullet), 2.0 (\times) μ M dimers.

fit to a two-state model as previously described (Neet, et al., 1994; Dupureur, et al., 2001). The extrapolated value of the ΔG_u to the zero denaturant concentration (ΔG^{H_2O}), the concentration of the denaturant at the midpoint of the denaturation transition and the m value for the denaturation susceptibility of the enzyme are shown in **Table 3.4**. The similar stability observed by the parameter values for ΔG^{H_2O} , $D_{0.5}$ and m at the 20-fold concentration range of WT PvuII provides further evidence of the validity of the application of the two-state model in the case of the WT PvuII. It turns out that in the presence of denaturant there are no folded WT PvuII subunits populated and the quaternary (inter subunit) interactions of the dimers are also necessary for the stabilization of the folded subunit (Neet, et al., 1994). In terms of the three state model described in Chapter II for the WT PvuII it should hold that $K_1 \ll K_2$ and thus the two-state model is justified. A characteristic denaturation curve obtained for the Y94F PvuII at 1 μ M dimers and identical experimental conditions to the WT PvuII experiments is shown in **Fig. 3.14**. The biphasic profile obtained, exhibited a plateau at GdnHCl concentrations on average (of three experiments) between 1.8 and 2.6 M whereas the two transitions were observed in the ranges between 1.6-1.8 M and 2.6-3 M GdnHCl. The collapse of the intermediate was observed in multiple trials within a short range of denaturant concentrations above 2.6 M close to the unfolding plateau. Clearly the of the aromatic hydroxyl group of Tyr94 has a pronounced effect on the unfolding route followed by the enzyme dimers. Since the denaturation of the Y94F PvuII results in the stabilization of an intermediate, a three state model analysis would be necessary. The dimer dissociation constant K_1 in this case should be of greater magnitude than the unfolding constant K_2 of the folded monomer. The quaternary interactions (inter-subunit)

Table 3.4 Dependence of the GdnHCl induced denaturation on the WT PvuII dimers concentration.

WT PvuII dimers	ΔG^{H_2O} (kcal/mole)	$D^{1/2}$ (M)	m (kcal/moleM)
0.1	5.7 ± 0.2	1.5	-3.1 ± 0.2
0.5	8.8 ± 0.1	1.8	-4.9 ± 0.004
1	6.7 ± 0.5	1.6	-3.8 ± 0.3
1.5	6.2 ± 0.2	1.6	-4.1 ± 0.1
2	7.1 ± 0.2	1.7	-4.5 ± 0.03

The denaturation curves were obtained at 50 mM Epps, 100 mM KCl, pH 7.7 at 25°C. Parameters obtained by the fit of the denaturation data to a two-state unfolding model as described in Chapter II.

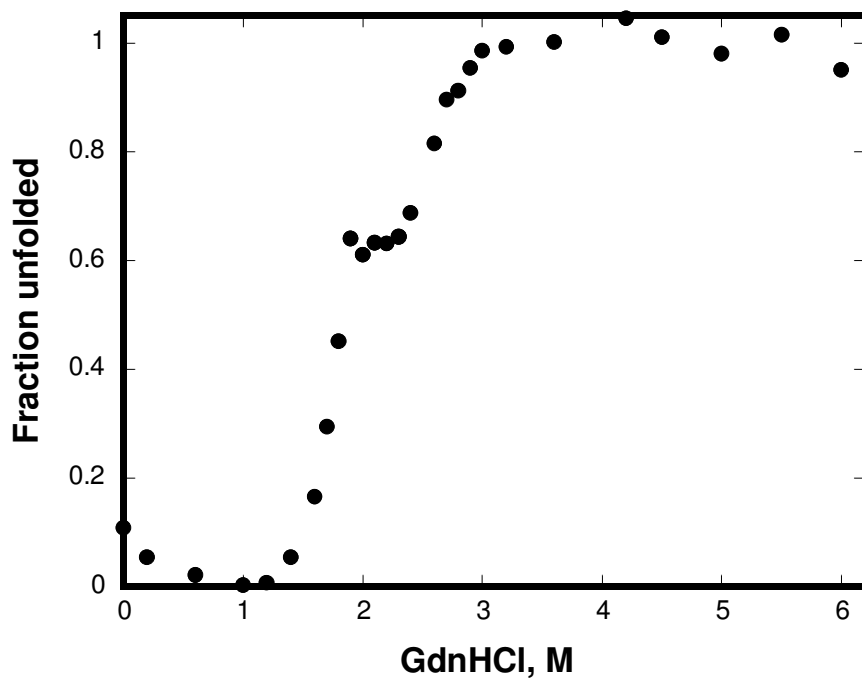


Figure 3.14 GdnHCl induced denaturation of the Y94F PvuII. The enzyme was applied at 1 μ M dimers while the solution conditions were 50mM Epps, 100mM KCl, pH 7.7 and 25°C. The intermediate stabilized at 1.8 M is shown, dissecting the profile in two phases.

that stabilize the native dimer are significantly weaker than the tertiary and secondary interactions that hold the folded structure of the monomeric subunit. The intermediate may have maintained some secondary and tertiary structure similar to its state in the native dimer or it may have structural characteristics similar to the unfolded state. However the fact that the absence of the Tyr94 aromatic hydroxyl group leads to the isolation of the folded monomeric PvuII subunit is directly associated with the involvement of the Tyr94 residue in the unfolding pathway of PvuII.

3.3.3.1 Conformational investigation of the Y94F PvuII by Heteronuclear single quantum coherence NMR

In order to further investigate the conformational implication of the aromatic hydroxyl group of Tyr94, NMR spectroscopy was employed to study the perturbation on the global conformation of PvuII resulting from the absence of the Tyr94 aromatic hydroxyl group. The enzyme was uniformly labeled with ^{15}N by cell growth supplemented with $^{15}\text{NH}_4\text{Cl}$ as the sole nitrogen source as described in Chapter II. The acquisition of the 2D ^1H - ^{15}N HSQC spectra returns the cross peaks of the incorporated ^{15}N nuclei and the corresponding scalar coupled protons (Rule, et al., 2006). Essentially all the backbone amide nitrogen atoms (except for Pro) and the amide and amino groups of the side chains should provide a crosspeak with their corresponding coupled protons. Focusing on the range between 110-160 ppm for the chemical shift of the ^{15}N nucleus and also between 6-9 ppm for the ^1H chemical shift, the corresponding crosspeaks represent the coupled amide nitrogens to their amide protons (backbone, and Gln, Asn side chains) (Rule, et al., 2006). The actual chemical shift ranges are more extended due

to the dispersion that occurs because of the folded structure of the polypeptide chain. The resulting area of the 2D ^1H - ^{15}N spectrum provides a “fingerprint” of the specific chemical shift dispersion of the backbone resonances of a polypeptide chain as folded under the experimental conditions (Rule, et al., 2006). The PvuII endonuclease consists of 157 amino acids in which eight Pro, nine Asn and six Gln residues are included resulting in 180 expected amide crosspeaks. Previously the WT PvuII and active site mutants were applied in conformational studies involving ^{15}N - ^1H HSQC NMR spectroscopy (Dupureur, et al., 2001; Dupureur 2005) and it was concluded that the acquisition of TROSY spectra in a 600 MHz field strength combined with the FID treatment by the combined sine bell function were sufficient to provide the theoretically anticipated number of peaks. The conformational investigation of the impact of the metal ion cofactor and the cognate DNA on the backbone of PvuII based on the overlap analysis of HSQC spectra is followed as previously (Dupureur 2005).

Accordingly it is hypothesized that the fraction of the overlapping backbone amide crosspeaks between two states of the enzyme or between two enzyme variants in the same state reflects the extent of backbone conformational perturbation conferred globally to the enzyme under the conditions examined. The term globally is applied since the specific crosspeak assignments are not available. The participation of the aromatic hydroxyl group of Tyr94 in the overall conformation of the enzyme in the presence of Ca^{2+} ions and also in the presence of cognate DNA is examined as previously for WT PvuII (Dupureur 2005). The characteristic spectra of 650 μM monomers apo WT PvuII and Y94F PvuII in 25 mM Tris, 200 mM KCl, 10% D_2O , pH 7.7, and 25°C are shown in blue and red in **Fig. 3.15A** (Dupureur 2005; Papadakos, et al., 2007).

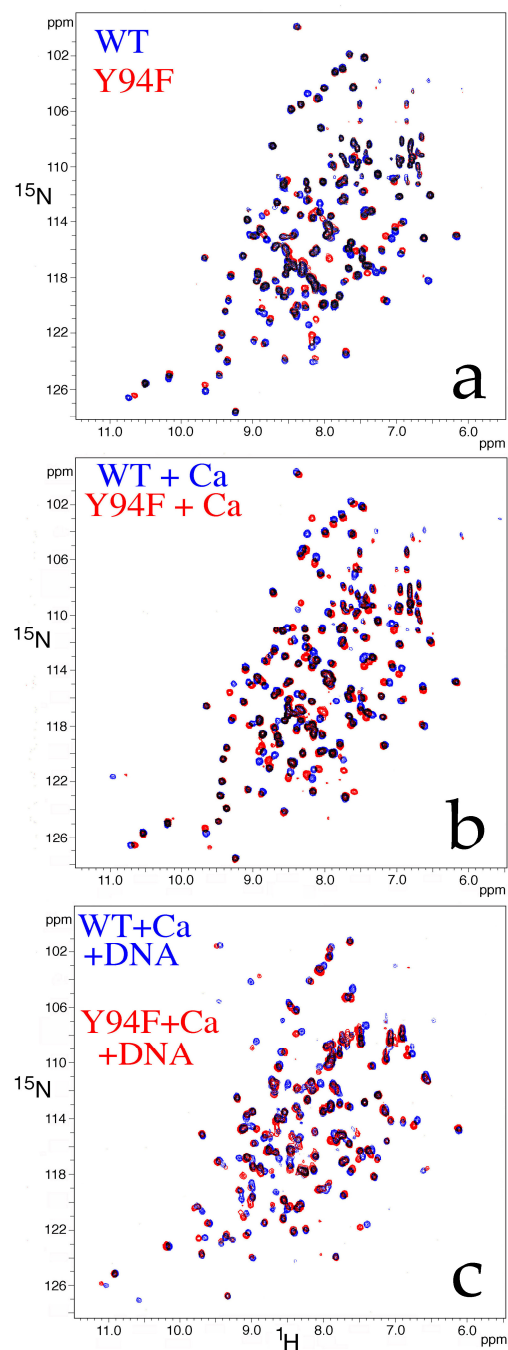


Figure 3.15. Overlays of the ^1H - ^{15}N HSQC spectra of WT and Y94F PvuII. (a) Spectra of the apo-enzymes, (b) in the presence of Ca^{2+} and (c) in the presence of Ca^{2+} and cognate DNA (Blue: WT PvuII, Red: Y94F PvuII). The (a) and (b) spectra are TROSY while the (c) is conventional. The enzyme was applied at 650 μM monomers in 25 mM Tris, 200 mM KCl, 10% D_2O , pH 7.7, and 25°C. Sequential additions of 10 mM Ca^{2+} in (b) and one equivalent of the cognate duplex in (c) are applied. The spectra result from 128 scans with each FID at 1024 (^1H) and 100 (^{15}N) points. The chemical shifts are relative to DSS.

The black resonances represent the overlapping between the two apo structures, which is approximately 70%. The extent of the overlap implies that the folding of PvuII is not significantly affected by the absence of the Tyr94 side chain hydroxyl group. Similarly significant overlap was previously observed between the apo WT PvuII and the apo active site variants D58A, K70A and E68A (Dupureur, et al., 2001), suggesting that the side chains of the corresponding residues have minimal impact on the backbone conformation. In order to monitor the effect of metal ions to the backbone structure of Y94F PvuII the HSQC spectrum of the variant was collected in the presence of Ca²⁺ ions. In **Fig. 3.15B** the overlaid spectra of the Ca²⁺ bound WT and Y94F PvuII are shown in blue and red, respectively. In the case of the WT PvuII the addition of the native Mg²⁺ ions did not lead to significant perturbation between the apo-enzyme and metal bound enzyme states with the overlap between them exceeding 80% (Dupureur 2005). However the addition of Ca²⁺ ions to the apo-enzyme led to a significant decrease in the overlap between the two states which was found at 60% (Dupureur 2005). Except for the backbone perturbation, Ca²⁺-induced local conformational fluctuations have been shown through ¹⁹F-NMR spectroscopy (Dupureur, et al., 1999). The case is similar for the Y94F PvuII, for which the Ca²⁺ ions do not confer significant change in the overlap pattern compared to the apo-enzyme. However as seen in **Fig. 3.15B** there is less overlap between the Ca²⁺ bound WT and Y94F PvuII spectra. This may be regarded as a propagation of the minor deviation already observed between the spectra of the corresponding apo-enzymes rather than as a significant perturbation between the two structures. The fact that the perturbation on the backbone conformation of the Y94F variant by the addition of Ca²⁺ ions is comparable to the WT PvuII may be correlated on

a global level with the calorimetric result for the Ca^{2+} binding to Y94F PvuII.

The actual dramatic effect on the conformation of the Y94F PvuII backbone comes in the presence of the cognate DNA as previously seen in the case of the WT PvuII. (Dupureur 2005). In **Fig. 3.16A**, the overlaid spectra of Ca^{2+} bound and Ca^{2+} -cognate DNA bound Y94F PvuII are shown. The overlap of the cross peaks is 10% while in the case of the corresponding complexes for the WT PvuII (**Fig. 3.16B**) the overlap is approximately 20% (Dupureur 2005). The extensive shift of the crosspeaks is associated with a significant shift in the backbone conformation conferred by the addition of cognate DNA in both variants. That this effect is more intense upon the removal of the aromatic hydroxyl group of Tyr94 supports the involvement of this residue in the adoption of the conformation of the DNA-PvuII complex. Local perturbations in the backbone of the enzyme and also at the environment of the side chain of Tyr94 are not observed. However, the obvious uncoupling of the metal binding sites observed for the Y94F variant would be consistent with an altered global conformation in the presence of DNA compared to the WT PvuII. Evidence for this is provided by the overlay of the DNA bound WT and Y94F PvuII shown in **Fig. 3.15C**. The fraction of the coinciding crosspeaks is 50% between the WT and the Y94F PvuII revealing the different conformation of the structures of the tertiary complexes between the two variants.

3.4 Discussion

The aromatic hydroxyl group of Tyr94 is not a direct metal ligand in the active site of PvuII. This is demonstrated through the extensive characterization of the metal binding properties of the variant Y94F PvuII. The absence of the hydroxyl group of

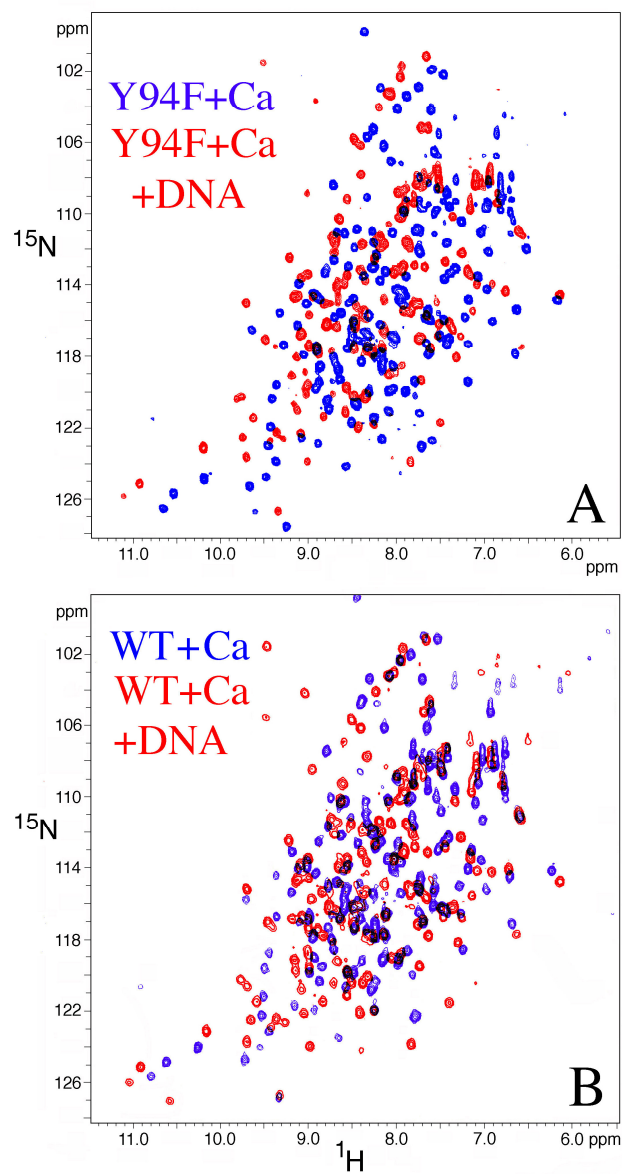


Figure 3.16. Overlays of the ^1H - ^{15}N HSQC spectra in the presence of Ca^{2+} and cognate DNA for the WT and Y94F PvuII. A. Y94F PvuII, B. WT PvuII (*Blue*: Ca^{2+} ions only, *Red*: Ca^{2+} ions and cognate DNA). The enzyme was applied at 650 μM monomers in 25 mM Tris, 200 mM KCl, 10% D_2O , pH 7.7, and 25°C. The Ca^{2+} ions are added at 10 mM Ca^{2+} and the cognate duplex is applied at one equivalent. The spectra result from 128 scans with each FID at 1024 (^1H) and 100 (^{15}N) points. The chemical shifts are relative to DSS.

Tyr94 apparently does not perturb the coordination sphere of Mg^{2+} , Ca^{2+} , Tb^{3+} and Eu^{3+} to such an extent that the discrepancy would be detectable by the applied methods for the binding of these ions to the active site of PvuII. The Y94F PvuII is shown to bind at least one Mg^{2+} ion as shown by the fluorometric competition assay. With an estimated n_H at 1.4 and a binding constant at 0.4 ± 0.2 mM the effect of the Y94F mutation on the ligation of Mg^{2+} is minimal considering the millimolar affinity at 1.9 ± 0.4 mM for each Mg^{2+} ion in the case of the WT PvuII (Dupureur, et al., 2000). Similarly for the divalent Ca^{2+} ions, the calorimetric result of two binding sites at 0.1 ± 0.04 mM and 3.9 ± 0.9 mM in Y94F PvuII does not support deviation from the WT PvuII binding pattern of Ca^{2+} as shown in **Table 3.2**. Additional evidence of the similar binding of metal ions to PvuII in the presence and absence of the Tyr94 hydroxyl group comes from the binding of Tb^{3+} and Eu^{3+} to Y94F PvuII. Although the low micromolar affinity of only one lanthanide ion binding site per enzyme active site is confirmed for the Y94F PvuII (**Table 3.3**), the presence of two binding sites has been demonstrated for the WT PvuII (Bowen, et al., 2004). According to the hypothesis of this study, should the hydroxyl group of Tyr94 coordinate metal ions, the metal binding to DNA free Y94F PvuII would be abolished or partially maintained as previously shown for the E68A variant in the case of Mg^{2+} , Ca^{2+} and Mn^{2+} (Jose, et al., 1999; Dupureur, et al., 2000) and also for the D58A variant in the case of Ca^{2+} (Jose, et al., 1999) where the metal binding acidic residues within the PvuII active site were substituted by alanine. The fact that no significant perturbation is observed in the metal binding properties of the Y94F PvuII in the absence of cognate DNA indicates that the aromatic hydroxyl group of Tyr94 is not a direct metal ligand under these conditions. This comes in direct contrast to the 1H56 crystal structure where

the direct ligation of Mg^{2+} ions to Tyr94 is shown (Spyridaki, et al., 2003). It is noted that the metal binding to Y94F PvuII was observed at pH 7.5 for the lanthanide ions and Ca^{2+} and at pH 7.7 for Mg^{2+} . As reported by pH titrations of Mg^{2+} bound WT PvuII the $pK_{a,app}$ value for metal binding is 6.7 (Dupureur, et al., 2000). Consequently under the experimental conditions, the acidic active site residues are fully deprotonated and apparently available for metal ion ligation. The data for the 1F00 crystal structure collected with crystals grown at pH 6.5 demonstrated the active site of PvuII in the presence of cognate DNA and exhibit two Ca^{2+} ions ligated to Asp58 and Glu68 with the carboxylic groups deprotonated for both residues (Horton, et al., 2000). The side chain of Tyr94 is not present in the octahedral coordination sphere of either Ca^{2+} ion (Horton, et al., 2000). The data for the 1H56 crystal structure were collected with crystals grown at pH 5.0 (Spyridaki, et al., 2003). It is expected that metal ion ligands in the active site of PvuII should be protonated under the crystal growth conditions. Indeed as **Fig. 3.2** shows in subunit B where the metal ion is ligated directly to Tyr94, the Asp58 and Glu68 are not ionized and thus not capable of coordinating the Mg^{2+} ion. This incompetence of the native metal ligands may lead to the adoption of the active site conformation where the hydroxyl group of Tyr94 is involved in the coordination of Mg^{2+} which is probably more favorable energetically under the conditions. However in solution and at physiological pH, the ionization state of the metal ligands more reasonably leads to an active site conformation similar to that reported in the case of the 1F00 structure confirming the metal binding studies in solution for the WT PvuII (Jose, et al., 1999; Dupureur, et al., 2000; Bowen, et al., 2004). An energetically similar active site conformation should be adopted in the case of the Y94F PvuII at physiological pH as shown by the obtained

binding constants obtained for the metal ions studied leading to the stabilization of the metal coordination sphere at a similar energy level to WT PvuII.

Although the Tyr94 is not directly binding metal ions in the active site of PvuII in the absence of cognate DNA, the side chain of the residue is probably essential for the stabilization of the binary PvuII-cognate DNA complex in the presence of Ca^{2+} ions. The DNA binding affinity to Y94F PvuII as a function of the concentration of Ca^{2+} ions provided a biphasic profile implying two modes of dependence of the DNA affinities on the metal ion fractionation. The two independent metal binding events are demonstrated by the lower and the upper phase in **Fig. 3.5** and **Fig. 3.7**. Taking into account the corresponding monophasic profile for the WT PvuII, the assumption of the presence of two classes of sites returned the interaction energy between the two classes of sites. Essentially then the state of the WT PvuII dimers representing the occupation by a third and fourth Ca^{2+} ion sequentially to an initial pair of Ca^{2+} ions is stabilized with respect to the state of the two Ca^{2+} ions initially bound by 2.5 kcal/mole (**Scheme 3.3**). Due to the biphasic profile obtained for the Y94F PvuII (**Fig. 3.5**) this energy is abolished and the second set of sites is occupied independently of the initial set of sites. More interestingly the transition from the first to the second Ca^{2+} ion leads to a stabilized complex by 1.4 kcal/mole whereas the transition between the third and the fourth Ca^{2+} ion leads to further stabilization by 0.3 kcal/mole. In addition to the observed metal classes and coupling energies among sites, the overall stability of the tertiary Ca^{2+} -Y94F PvuII-DNA complex is higher at the lower phase and lower at the upper phase than the corresponding stability of the Ca^{2+} -WT PvuII-DNA complex (**Fig. 3.4**). It is concluded then that the Tyr94 in the presence of DNA is actively involved in the formation of the tertiary complex. This

is further supported by the ^1H - ^{15}N HSQC spectroscopy applied in the presence of Ca^{2+} and cognate DNA. As demonstrated in **Fig. 3.16**, the addition of DNA to the already formed Ca^{2+} -Y94F PvuII resulted in less overlap and thus greater perturbation than in the case of the WT PvuII. Perhaps the adoption of an active site conformation by the Y94F variant significantly different from the WT PvuII results in the different metal binding pattern in the presence of DNA. This difference is supported by the 10% less global overlap between the Ca^{2+} only and Ca^{2+} -DNA spectra compared to the already scattered corresponding spectra of the WT PvuII between the two states. As previously reported, the side chain of Tyr94 is positioned at the interface of the DNA recognition region and the catalytic region of the DNA (pdb 3PVI) (Horton, et al., 1998). The development of the necessary interactions emanating from residues at the DNA recognition region at the introduction of DNA to the Ca^{2+} PvuII complex is probably obstructed or not occurring in the absence of the Tyr94 side chain. It has to be noted that these might not be the only interactions that are disrupted in the case of the Y94F PvuII variant. Evidently the unfolding pathway followed by PvuII without the hydroxyl group of Ty94 is markedly different than in the case of the WT PvuII. The stabilization of the folded subunit (**Fig. 3.14**) indicates a decrease in the impact of the quaternary interactions of the enzyme and the importance of the secondary and tertiary interactions within each PvuII subunit. The quaternary structure of the enzyme must be disrupted probably due to alterations in the interactions at the subunit interface where the implication of Tyr94 is obvious. The outcome of this participation of Tyr94 in the presence of DNA is transmitted to the active site and affects the metal binding properties of the enzyme. In parallel, the lack of quaternary interactions leads to lack of inter-subunit communication, which also might be

contributing to the observed energetic pattern for the metal binding. A similar assumption was previously made for Tyr94, which was considered to position the metal ions at their entrance to the active site (Spyridaki, et al., 2003). However it is demonstrated that the Tyr94 behavior is clearly conformational and not due to direct metal binding.

The presence of the phenolic ring of Tyrosine in critical positions in the structure of nucleases has been extensively shown. In most cases, Tyrosine residues have been found to participate in the DNA binding by the nuclease either in direct contact with nucleotides or not. In EcoRII, another type II restriction enzyme, the effect of Tyr41 in DNA binding is substantial for the enzyme. The Y41A mutant showed greater loss in activity than the active site residue mutants, due to the inefficient binding to DNA (Reuter, et al., 1999) and this contact is supported by photo cross-linking studies showing that Tyr41 is the main crosslinking amino acid to the specific DNA sequence (Mucke, et al., 2002).

EcoRV endonuclease possesses Tyr95 which has been shown to form a weak contact with the phosphates of the cognate DNA sequence and thus contributing to the DNA recognition (Wenz, et al., 1996). EcoRV also contains Tyr129 and Tyr110 with significance in the conformation of the enzyme. Although distant from the active site, Tyr219 is shown to be essential for the DNA binding by the enzyme as the mutation of the residue to Cys resulted in decrease of the DNA affinity even in the presence of Mg^{2+} ions (Jeltsch, et al., 1995). It has been proposed that a third Mg^{2+} site remote to the active site metal ion sites exists in EcoRV and involves the Tyr110 and the Tyr219 which are located along with water molecules in a hydrophilic core surrounding the (-2) phosphate

(Jeltsch, et al., 1995). The MunI endonuclease possess the Tyr53 which participates in a hydrogen bonding network that contacts the C(-1) phosphate and thus contributes to the stabilization of the enzyme:DNA complex (Fuxreiter, et al., 2002). In BglII, the Tyr190 in each monomer is involved in a hydrogen bond network through water molecules to also assist in DNA binding. Meanwhile Tyr99 and Tyr144 in BglII form hydrogen bonds with the phosphates of the cognate DNA sequence (Lukacs, et al., 2000). Similarly, in BamHI the Tyr65 is hydrogen bonded to Asp94 resulting in the maintenance of the conformation of the latter which in turn is coordinated through both metal ions within the active site (Viadiu, et al., 1998).

In the case of the P1 nuclease, which cleaves small single stranded DNA or RNA, the Tyr144 and Tyr155 form a hydrophobic binding pocket that enclose an adenine of its substrate (Romier, et al., 1998). In the XPF-ERCC1 endonuclease, Tyr145 and Tyr152 have been shown, in a co-crystal structure of the ERCC1 domain with cognate DNA, to reside in a groove of conserved residues which promote the DNA binding (Tsodikov, et al., 2005).

In addition to their mostly observed role as serving the contact network towards the target DNA, tyrosines have also been shown as participating in the adoption of the active conformation of nucleases. In the case of the tetrameric *M. jannaschii* t-RNA endonuclease, a hydrophobic core consisting of several residues is formed at the intersubunit surface of two dimers where Tyr 176 is involved. The helix-hairpin-helix domains of the homodimeric Hef nuclease contain Tyr758 which makes multiple contacts with residues around it to promote the interaction of the C-terminal of one subunit with residues of the other subunit (Li, et al., 1998). More specifically Tyr758 forms salt

bridges with the Arg716 through its hydroxyl group and also interacts hydrophobically with Leu719 and Lys720 domains (Li, et al., 1998; Nishino, et al., 2005). Another relevant example is the *Staphylococcal* nuclease, in which Tyr27 lies in the beginning of a β -barrel, making several hydrophobic and hydrogen bonding interactions with residues around it, which in turn contribute to the stability of the overall structure of the formed β -barrel (Bhat, et al., 1997).

The significance of the Tyr side chain and its conformational impact on the interactions of the above mentioned systems is indicative of the critical positioning of the aromatic hydroxyl group also observed for the Tyr94 in the PvuII endonuclease.

Asymmetries observed in the PvuII crystal structures

As mentioned above in the 3PVI PvuII crystal structure, Tyr94 is positioned at the interface of the DNA recognition region and the catalytic region of the DNA (Horton, et al., 1998). Surprisingly this occurs in only one subunit of the D34G homodimer as the hydrogen bonding network is disrupted in the other subunit before the active site and thus it does not allow for similar positioning of Tyr94 (Horton, et al., 1998). There is no evidence that D34G would accumulate a nicked product, as the variant has not been reportedly assayed with plasmid DNA (except for the reference to Litmus 28i in (Nastri, et al., 1997) without however any shown or discussed results). The active site conformation in the 1H56 structure also showed asymmetry as to the position of the Mg^{2+} ion and the amino acids across the subunits. Previously the crystal structures of another two type II restriction endonucleases the BamHI and the EcorV (Kostrewa, et al., 1995; Viadiu, et al., 1998), in the presence of metal ions and DNA were also found to be

asymmetric across their subunits. The asymmetry was treated by the authors as an effect of crystal packing forces and the observed structure was regarded as independent of the actual properties of the Endonuclease-DNA complex (Kostrewa, et al., 1995; Horton, et al., 1998; Viadiu, et al., 1998). Probably the same reasoning can be followed for the crystal structure 1F0O and the asymmetric association of the Tyr94 side chain to the metal sites (**Fig. 3.1**). No such treatment of the observed asymmetry was applied to the 3PVI and 1H56 structures for PvuII (Horton, et al., 1998; Spyridaki, et al., 2003). It has to be emphasized then that the position and environment of Tyr94 in the crystal structures reported for PvuII are not necessarily physiological as they appear.

CHAPTER IV

THE SINGLE CHAIN PvuII ENDONUCLEASE

4.1 Introduction

The PvuII endonuclease contains a single active site within each subunit that accommodates Mg^{2+} ions, utilized to assist the binding and hydrolysis of the 5'-CAG|CTG-3' palindromic sequence (Gingeras, et al., 1981). Specific contacts between the enzyme subunits and each strand of the scissile DNA site, mediated in part by metal ions, lead to the formation of the enzyme:DNA complex (Horton, et al., 2000). The phosphodiester bond hydrolysis occurs simultaneously at the backbone of both strands of the DNA cleavage site (Spyridaki, et al., 2003). The concerted DNA hydrolysis by the two active sites is also observed in the case of other members of the type IIP family (Halford, et al., 1983; Halford, et al., 1988; Taylor, et al., 1989; Dorner, et al., 1994; Sasnauskas, et al., 1999). More specifically in EcoRV, EcoRI and MunI, through cleavage of plasmid DNA the orchestration of the two catalytic events in the DNA strands has been demonstrated to be dependent on the equivalents of metal ions within the active site of the enzyme (Halford, et al., 1983; Halford, et al., 1988; Sasnauskas, et al., 1999).

In the case of PvuII, the binding of two metal ions to each active site in the absence of DNA has been confirmed for the native Mg^{2+} ions (Dupureur, et al., 2000) and also for the Ca^{2+} ions (Jose, et al., 1999), which support the binding to DNA but not its cleavage (Vipond, et al., 1995). In fact, within a PvuII subunit and in the absence of DNA, the two Ca^{2+} binding sites have been shown to be weakly interacting (Jose, et al., 1999), while the cognate DNA binding dependence on Ca^{2+} ions has revealed a

significant heterotropic synergy: the binding constants for DNA span three orders of magnitude between metal-free and metal-saturating conditions (Conlan, et al., 2002). Essentially PvuII represents a highly cooperative system which functions through the simultaneous binding of four metal ions (two per subunit) and the substrate DNA (Conlan, et al., 2002). This has been shown for the WT PvuII by the fit of the profile of the DNA association constants versus the Ca^{2+} concentration to the Hill (all-or-none) model (**Eq. 2.5**), providing a Hill coefficient at 3.5 ± 0.2 per enzyme dimer (Conlan, et al., 2002). The Hill model provides an estimate of the overall cooperativity that is present in the system. In this analysis, no discrimination is made among the intermediate enzyme:metal states (EM_n) that contribute to the final (least) stoichiometry between the enzyme and four metal ions in the presence of DNA, which is however represented by the Hill coefficient. Thus it was appropriately assumed that four metal ions lead to the formation of the high affinity PvuII-DNA complex (Conlan, et al., 2002). Although the application of the Hill model in the case of PvuII requires five species reacting simultaneously, which is physically impossible due to the associated low probability, the estimate of the number of involved ligands is consistent with the number of metal ions physiologically observed in the presence of cognate DNA (**Fig. 3.1**) (Horton, et al., 2000). In reality, the intermediate EM_n species of sequentially or independently bound ligands accumulate significantly due to the magnitude of the intermediate binding constants, which are ignored in the Hill model. Consequently the Hill model can only be applied to describe a system in the case of marked positive cooperativity where the stoichiometric association constant for the highest macromolecule:ligand stoichiometry is larger by orders of magnitude than the association constants for any intermediate species

formed (Weiss 1997). In each intermediate state, which describes the binding of metal occupied enzyme (EM_n) to duplex DNA, the contributions of all implicated modes of cooperativity are included. The metal binding sites (heterotropic cooperativity) may be characterized by intra and/or inter subunit communication, while the interaction of each PvuII subunit with a DNA strand (homotropic cooperativity) is communicated to the opposite subunit and is probably modulated by the different metal ion affinities and stoichiometries of the (EM_n) species.

Focusing on the contribution of the metal ions to the PvuII:DNA association, the energetics of the interactions of the PvuII metal binding sites are investigated when DNA is present. The application of macroscopic metal binding constants allows for the estimation of the cooperativity among the subunits (Weber 1975), but their measurement in the presence of DNA is experimentally challenging. Moreover, it is impossible to directly measure the intrinsic metal binding constants in the absence or presence of DNA, as the metal binding sites within a subunit cannot be independently filled. As shown in the 1F00 structure (**Fig. 3.1**) for WT PvuII in the presence of cognate DNA, the two Ca^{2+} ions are bridged by three ligands (i.e. the carboxylic groups of Asp58 and Glu68 and the phosphate of the scissile Cyt). The substitution of any of these residues results in the abolition of the binding of both metal ions and thus does not allow their independent occupation. This has been shown in the case of the E68A PvuII variant for Ca^{2+} and Mg^{2+} ions (Jose, et al., 1999; Dupureur, et al., 2000), while in the case of Eu^{3+} ions the high micromolar site was maintained (Bowen, et al., 2004). In order to quantify the extent of communication among the metal binding sites, the two modes of communication need to be dissected. Although the intra subunit communication can not

be perturbed the cooperativity (if any) among the subunits can be removed by introducing a mutation to abolish the metal binding in only one subunit.

The preparation and utilization of single chain heterodimeric PvuII variants has been previously reported. A construct of two PvuII subunits has been prepared in which the Tyr157 of the N-terminal subunit in the dimer was covalently linked through a GSGG linker to the Ser2 of the C-terminal subunit covering the distance of 12 Å between the two residues (**Fig. 4.1**). Exploiting the small size and lack of charge of the Gly and Ser residues, the linker had been hypothesized to not perturb the folding and function of the covalent dimer (Simoncsits, et al., 2001). The homodimeric WT single chain (WT-SC PvuII) was characterized via gel shift assay in the presence of Ca²⁺ ions, using oligonucleotides containing the PvuII cognate site. The WT-SC PvuII binding constant for DNA was 120 pM which is identical to the corresponding value of the native WT PvuII at 110 pM (Conlan, et al., 2002). In cleavage experiments under steady state conditions and with different substrates (pBR322 and also λ DNA), the WT-SC PvuII exhibited the same cleavage pattern as the WT PvuII, with similar turnover number (5.8 min⁻¹ versus 12.3 min⁻¹ for the native WT) but lower K_m (3.5 nM versus 5.3 nM for the native WT) due to the lower DNA affinity. Employed also in *in vivo* experiments the WT-SC PvuII was proven as effective as the WT PvuII in the inhibition of proliferation of *E. coli* cells not bearing the methyltransferase complement of the PvuII RM system.

In addition, the single chain WT PvuII showed similar but slightly less activity than the WT PvuII in a λ phage restriction assay performed by utilization of the plasmids expressing the two PvuII variants in *E. coli* cells. The production of a heterodimeric single chain PvuII variant useful in showing that the communication across the enzyme



Figure 4.1 The structure of the single chain PvuII endonuclease as reported in (Simoncsits, et al., 2001) and adopted from the pdb file 1PVI (Cheng, et al., 1994). The two subunits are colored yellow (N-terminal) and green (C-terminal) while the GSGG linker is shown in red. The ribbon structure represents the duplex cognate DNA in complex with PvuII.

subunits leads to the recognition and cleavage of both DNA strands when all DNA contacts are made in both subunits. This was achieved by the application of the WTID34G-SC PvuII in a pBR322 plasmid cleavage assay, which indicated the accumulation of a nicked intermediate and a lower rate of linearization of the substrate DNA which suggests the lack of coordination across the subunits of the heterodimer. Overall these results prove the minimal perturbation conferred by the GSGG linker to the dimerization and functionality of the single chain PvuII construct, making it suitable for the study of heterodimeric PvuII variants.

Another application of the covalent linkage between subunits of a restriction endonuclease is the crosslinking of the EcoRV subunits with artificial crosslinkers not of amino acid constitution (Schulze, et al., 1998). The bivalent crosslinkers involved two maleimide groups (one at each end) separated by several methylene groups thus forming linkers of different lengths (**Fig. 4.2**). The maleimide groups were selectively reacted in the presence of DNA with two specifically engineered Cys residues (one in each subunit) at the arms of the DNA binding site of EcoRV. The exploration of the topology of the enzyme subunits in the binding and cleavage of DNA was pursued with the subunits being fixed at various distances from each other at the different linker lengths.

Heterodimers of the EcoRV endonuclease have also been prepared, aiming to dissect the inter- and intra-subunit communication of the endonuclease dimer. In this case, the two subunits were not covalently linked. Instead two copies of the EcoRV subunit were separately expressed (in the same vector) each bearing either a His-tag or a glutathione S-transferase tag which would facilitate the heterodimer separation through sequential affinity chromatographies (utilizing either Ni-NTA or GSH columns, **Fig. 4.2**)

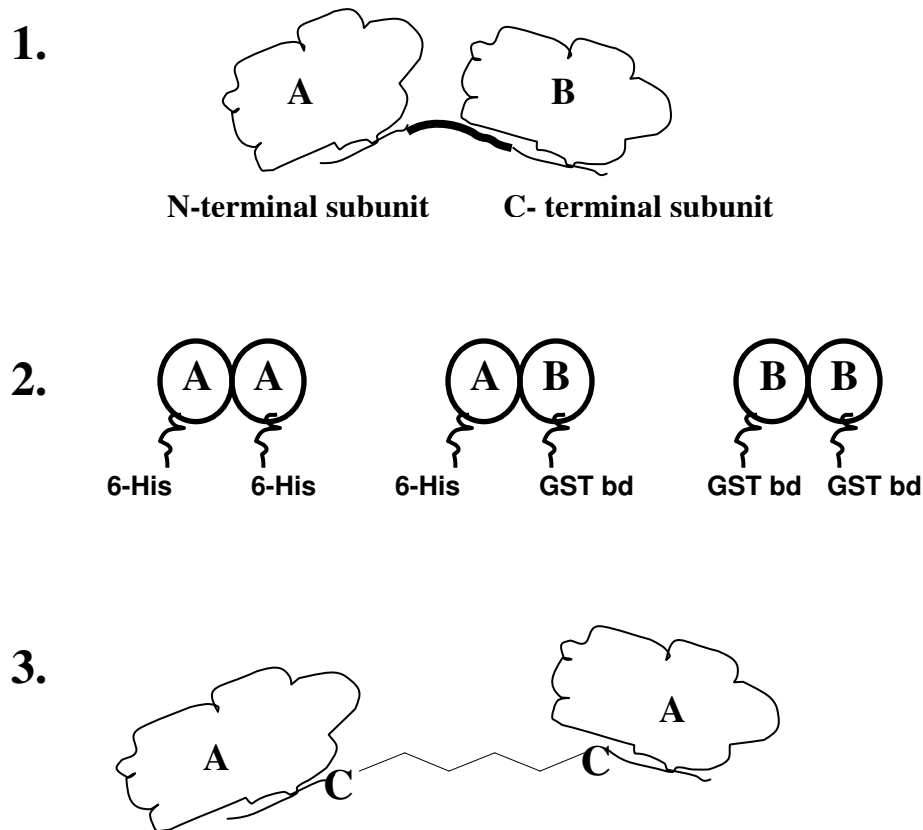


Figure 4.2 The approaches followed in the preparation of heterodimers in restriction endonucleases. The communication across the subunits has been approached by the production of heterodimers bypassing the subunit exchange in two ways. Either the production of heterodimeric variants is performed and their homodimeric counterparts are not expressed as in (1) (covalently linked subunits expressed from double copies of the subunit gene interrupted by the amino acid linker) (Simoncsits, et al., 2001), or each subunit is expressed with an affinity column tag (His-tag or the glutathione binding domain of GST) as in (2) and sequential chromatographies are followed to separate the hetero from the homo-dimers (Wende, et al., 1996; Stahl, et al., 1998). In (3) the covalent linkage of engineered Cys residues (C) with bivalent crosslinkers is shown, where the enzyme is expressed in non-linked homodimers and the linkage occurs in the presence of DNA (Schulze, et al., 1998). This approach was utilized in the investigation of the topology of the enzyme subunits in the enzyme-DNA complex. A and B stand for the different phenotypes of the subunits.

(Wende, et al., 1996; Stahl, et al., 1998). Hybrid dimers involving substitutions of the residues at the DNA recognition interface (e.g. N188Q, T186S) and also in the active site of EcoRV (e.g. D74A) in one subunit (maintaining the WT phenotype in the other) or combined in both subunits were prepared and applied to DNA binding and cleavage experiments (Stahl, et al., 1996; Wende, et al., 1996). The residues involved in the recognition of the specific DNA bases (direct readout) were shown to function cooperatively across the two subunits, since the specificity and cleavage activity was impaired in heterodimers including substitutes of these residues (Stahl, et al., 1996). The residues involved in the indirect readout of the DNA substrate were also set under investigation in the EcoRV endonuclease (Stahl, et al., 1998; Stahl, et al., 1998). The Ala substitutions of the Asp36, Thr37 and Lys38, previously shown to be involved in contacts with DNA bases spanning the scissile site of EcoRV, were combined with the WT or the D90A phenotype and the resulting heterodimers were applied in DNA binding and cleavage experiments (Stahl, et al., 1998). It turned out that T37 and K38 do not influence the specificity and activity of the dimer, but their effect is only upon their own subunit. However D36 is involved in concerted cleavage by the two EcoRV subunits, demonstrating the participation of residues contacting the base pairs adjacent to the scissile site in the communication of the two subunits (Stahl, et al., 1998). As such, the DNA binding sites of the two monomers (providing direct or indirect readout of the DNA) are involved in intersubunit communication, transmitting a conformational signal after the completion of the necessary DNA contacts across the two catalytic centers (Stahl, et al., 1996; Stahl, et al., 1998). The two EcoRV catalytic centers are otherwise perceived as independent (Stahl, et al., 1996; Wende, et al., 1996). Heterodimeric

variants in which the P73G, D74A, D90A, and K92E substitutions of the PD..D(E)XK motif residues are introduced in one subunit (only maintaining the WT phenotype in the other subunit) were prepared and applied in cleavage experiments with the pAT153 plasmid as a substrate. All the heterodimers exhibited approximately half the catalytic efficiency of a fully functional homodimer. Although the affinity to the substrate is not significantly altered, the lack of the active site residues involved in catalysis results in decrease of the turnover number by the heterodimeric EcoRV variants (Wende, et al., 1996).

In another study of the EcoRV endonuclease, the metal dependence of the DNA cleavage under single turnover conditions resulted in the best fit of the cleavage rate profiles to models of multiple metal ions to the enzyme dimers (Groll, et al., 1997). This prompted the exploration of the location of the multiple metal ions in the subunit of EcoRV. In order to exclude the possibility of one metal ion residing in each subunit of the WT EcoRV which would result in the fit of the kinetic profiles in a model supporting catalysis by two metal ions, one of the subunits should be impaired in metal binding. To pursue this, the heterodimeric variant WTID90A EcoRV was prepared as previously described (Stahl, et al., 1996; Wende, et al., 1996), bearing the D90A mutation in one subunits. As a direct metal chelator and necessary in catalysis, the mutation of Asp90 (conserved residue of the PD..D(E)XK motif) would assist the impairment of metal ligation in one subunit. The profile of the cleavage rates of oligonucleotide substrate under single turnover conditions was found as sigmoidal as the WT EcoRV profile with the rates of the heterodimer about two-fold lower than the WT EcoRV. However the profile of the WTID90A variant was also best fit to a model involving two metal ions for

cleavage for which the apparent affinity was similar to the WT EcoRV (0.84 mM versus 1.25 mM for the WT EcoRV). It was thus shown that the two metal ions hypothesized for the WT EcoRV were indeed coordinated simultaneously to each enzyme subunit and not one per subunit as confirmed by the heterodimeric variant (Groll, et al., 1997).

This study aims to address quantitatively the extent of the communication characterizing the PvuII metal binding sites in the presence of cognate DNA and also to approach the homotropic cooperativity observed in the PvuII-Metal-DNA complex. Rationalizing the perturbation of the inter-subunit communication in the presence of the E68A mutation in only one subunit, the production and study of heterodimeric PvuII variants is necessary. For this purpose, the single chain variants WT|E68A-SC and WT-SC PvuII were produced in which the two subunits are covalently linked as previously described (Simoncsits, et al., 2001). The examination of cooperativity was performed by monitoring the dependence of the DNA binding and catalytic activities of the two PvuII variants on the metal ion concentration. In addition, the metal binding affinities in the absence of cognate DNA were measured and the data were globally evaluated for each of the two PvuII variants.

4.2 Methods

4.2.1 Global analysis of the DNA binding data

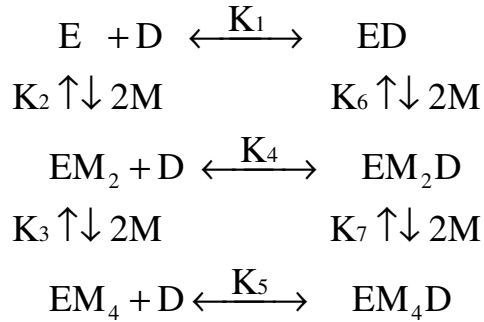
The nitrocellulose filter binding and the fluorescence anisotropy assays were applied in the measurement of the DNA affinity of the PvuII variants as a function of the Ca^{2+} concentration as described in Chapter II. The 14mer duplex oligonucleotide (previously applied in the study of the native WT PvuII) was also applied in identical

solution conditions: 50 mM Tris, pH 7.5 at 25°C with the ionic strength maintained constant by the addition of appropriate amounts of NaCl.

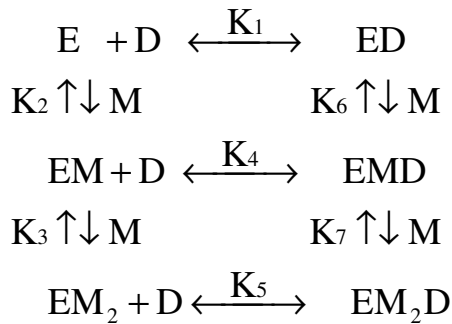
The signal of the DNA binding assays provides only an apparent association constant for the enzyme bound DNA molecules. However, the enzyme dimers are partitioned according to their metal saturation and all the enzyme species (i.e. the metal free enzyme dimers E, the enzyme dimers occupied by one metal ion per subunit EM_2 , and the enzyme dimers occupied by two metal ions per subunit EM_4) are capable of binding to DNA. In order to approach the metal binding constants in the presence of DNA and also the DNA binding constants of each enzyme species, the observed signal would have to be dissected according to the contribution of each enzyme species to the overall DNA binding of the DNA that is observed. The DNA binding was measured as described in Chapter II under metal free conditions, and at Ca^{2+} concentrations from 0-10 mM at least three times and at various DNA concentrations. In the datasets to be fitted, the fraction of the bound DNA in each experiment was converted to the concentration of the bound DNA. The endpoint of each titration was estimated by fitting in each individual dataset the normalized fractions of bound DNA to a 1:1 isotherm. Then the asymptotic limit of the isotherm was regarded as the endpoint and a further normalization to this value of the observed signal was performed. The software Dynafit was used to perform the global fitting. The simultaneous fit of all the datasets was performed by applying the models of linked equilibria shown in **Scheme 4.1**. In each metal binding step, a WT subunit in the WT-SC PvuII is shown to bind a metal ion while the stoichiometry of two metal ions shown refers to the two subunits that simultaneously participate. The applied concentration of the WT-SC PvuII is expressed in dimers;

Scheme 4.1 The linked equilibria describing the metal (M) and DNA (D) binding to the single chain PvuII variants (E). Whereas in both cases (WT-SC and WT|E68A-SC) the concentration of E is applied in dimers, the metal binding equilibrium constants K_2 , K_3 , K_6 , and K_7 correspond to the binding of metal ions in enzyme monomers. Since the thermodynamic cycle provides the energy difference between an initial and a final state irrespective of the followed pathway, the application of the model in Dynafit involved either the K_4 and K_5 DNA binding steps or the K_6 and K_7 metal binding steps. The binding constants for the steps not included in each case are calculated from the product $K_1K_6=K_2K_4$ and $K_4K_7=K_3K_5$, respectively.

WT-SC PvuII



WT|E68A-SC PvuII



however each sequential metal binding constant refers to the binding of a metal ion per enzyme subunit (**Scheme 4.1**) and is equal to the square root of the fitted value. The concentration of the WT subunit in the WT|E68A-SC PvuII is essentially equivalent to the dimer concentration and thus assuming the E68A subunit as metal free, the stepwise metal binding constants refer to the occupation of the WT monomer only (**Scheme 4.1**). For each of the WT-SC and the WT|E68A-SC PvuII, a selection of 15 datasets were fitted. All DNA bound enzyme species (i.e. the ED, EM₂D, EM₄D for the WT-SC and the ED, EMD and EM₂D for the WT|E68A-SC variant) were regarded as equally contributing to the observed signal and thus to the fractionation of the substrate DNA. The equilibrium constants for metal binding in the presence of DNA and DNA binding in the presence of metal ions were approached through the global fit of the data. To pursue this the DNA binding constant under metal free conditions was fixed at the average value obtained by three independent measurements. Additionally the metal binding constants for the first and second metal equivalents in the absence of DNA were fixed at the values obtained by fit of the calorimetric data to the two-site sequential model. The DNA binding equilibria represented by the equilibrium constants K₄ and K₅ in **Scheme 4.1** are the only parameter values that are fitted for. The metal binding constants in the presence of DNA (represented by the equilibrium constants K₆ and K₇ in **Scheme 4.1**), were subsequently calculated applying the fixed and fitted values of the equilibrium constants K₁, K₂, K₃, K₄ and K₅ to the equations $K_1K_6=K_2K_4$ and $K_4K_7=K_3K_5$ emerging from the thermodynamic cycles shown in **Scheme 4.1**. Initial values were applied to the parameters and the system was allowed to converge with an estimation of the parameter error at a 68% confidence interval (one standard deviation). In both single chain variants

the data readily fitted to the obtained values with significantly low standard error. The stabilization of the system through the application of the fixed values K_1 , K_2 and K_3 led to the restriction of the size of the parameter space and the decrease of the number of local minima (Beechem 1992). The achievement of the minimization of the root mean square (RMS) of the residuals was thus facilitated. It has to be noted that in systems of linked equilibria, the covariance of the parameters is high. Essentially the overall binding constant for an MXY system as the one described herein is shown in **Eq. 4.1** (Wyman, et al., 1990).

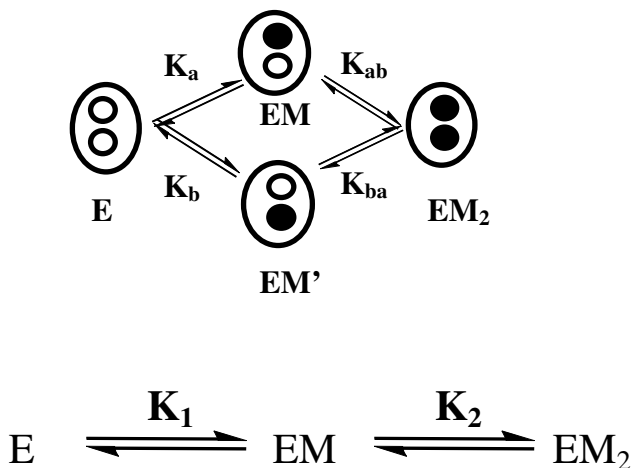
$$K_{\text{obs}} = \frac{\Sigma[E]_{\text{DNA}^{\text{b}}}}{\Sigma[E]_{\text{DNA}^{\text{f}}}} = K_1 \frac{1 + K_6[M] + K_6 K_7[M]^2}{1 + K_2[M] + K_2 K_3[M]^2} \quad (4.1)$$

The K_{obs} expressed as the ratio of the sums of concentrations of the DNA bound and free enzyme species leads to the expression of the corresponding binding polynomials where the binding constants of **Scheme 4.1** (using the WTIE68A-SC stoichiometry) are applied. There is evidently high dependency among the values of the binding constants applied to **Eq. 4.1**, and this high correlation often necessitates the use of assumptions on resolving the system values as previously reported (Kozlov, et al., 2006). The high covariance of the parameters is partly relieved by the application of the fixed values of the K_1 , K_2 and K_3 constants.

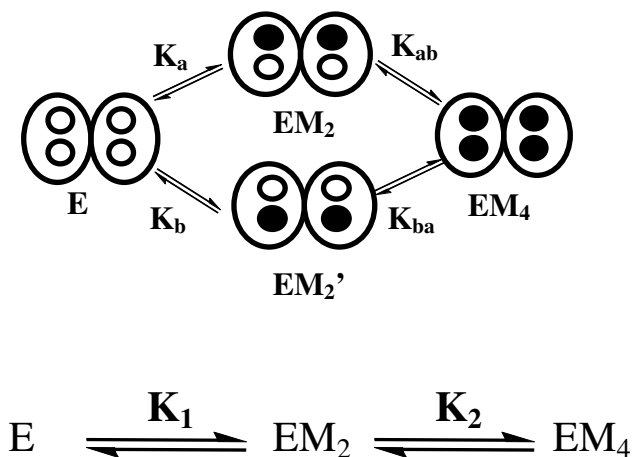
In order to obtain the interaction energies between the metal binding sites in the presence and absence of DNA, the equilibria shown in **Scheme 4.2** are considered for the two single chain PvuII variants. The intrinsic metal binding constants in the case of the WTIE68A-SC variant are denoted as K_a and K_b , while the intrinsic binding constants of

Scheme 4.2 The sequential binding of two metal ions within the WT subunit of (A) the WTIE68A-SC PvuII (intrinsic sites) and four metal ions to the pair of WT PvuII subunits of (B) the WT-SC variant (classes of sites) are shown. The enzyme species at the different metal stoichiometries are denoted as E (metal free), $EM_{(2)}$ and $EM_{(2)}$ ' (one metal ion in each intrasubunit site or two metal ions in two different position sets across the subunits) and EM_4 (four metal ions). The macroscopic binding constants K_1 and K_2 and the microscopic binding constants K_a , K_b , K_{ab} and K_{ba} are shown.

A



B



● Occupied site ○ Vacant site

the sites in the presence of a second metal ion are denoted as K_{ba} and K_{ab} , and the coupling energy between the two metal sites ($\Delta\Delta G_{coop}^{\circ}$) is given by **Eq. 4.1**.

$$\Delta\Delta G_{coop}^{\circ} = \Delta G_{ba}^{\circ} - \Delta G_a^{\circ} = -RT\ln\left(\frac{K_{ba}}{K_a}\right) \quad (4.1)$$

The energy difference between the two states (in the presence and absence of a second ion) is expressed in terms of K_1 , K_2 as in **Eq. 4.2**

$$\Delta\Delta G_{coop}^{\circ} = -RT\ln\left(\frac{K_2(1+n)^2}{K_1n}\right) \quad (4.2)$$

where n is the ratio K_b/K_a , which is further assumed to be equal to unity and leads to the expression shown in **Eq. 4.3** for $\Delta\Delta G_{coop}^{\circ}$.

$$\Delta\Delta G_{coop}^{\circ} = -RT\ln\left(\frac{4K_2}{K_1}\right) \quad (4.3)$$

4.3 Results

In order to introduce a different phenotype in each subunit of the PvuII endonuclease, the construct of the single chain PvuII previously reported was utilized (Simoncsits, et al., 2001). The plasmid pRIZ'_{Olac} encoding for the WT-SC PvuII was obtained and the variant was purified as described in Chapter II. The genes encoding for the two linked subunits were separated by restriction digest, and the C-terminal subunit was subcloned in the pBR322 vector. The E68A genotype was introduced to the separated subunit by PCR, and the mutated subunit was relegated to the N-terminal WT PvuII subunit of the pRIZ'_{Olac} plasmid.

The divalent Ca^{2+} ions have been shown to be successful substitutes for the native Mg^{2+} ions within the active site of PvuII. Crystallographic data in the presence of DNA, show the presence of two Ca^{2+} ions coordinated to the catalytic and neighboring residues

and also water molecules in the PvuII active site (Horton, et al., 2000). These crystal data support the previous measurements (Jose, et al., 1999) of the affinities of two Ca^{2+} ions in the active site of PvuII with a binding constant at 1.3 mM in the absence of DNA. Calcium has also been previously shown as non-supportive of catalysis but assisting the PvuII-DNA association (Nastri, et al., 1997; Conlan, et al., 2002). In order to explore the metal binding content and the interaction of the metal sites of the single-chain PvuII variants, measurements of Ca^{2+} binding have been performed in the absence of DNA, while the apparent binding to Ca^{2+} and Mg^{2+} has been explored in the presence of DNA in binding and cleavage experiments.

4.3.1.1 Ca^{2+} binding in the absence of cognate DNA

In order to obtain the affinity and stoichiometry of Ca^{2+} to the WTIE68A-SC PvuII, direct titrations of CaCl_2 to the apo-enzyme monitored through isothermal titration calorimetry have been performed. The titrations were repeated at 0.375, 0.5, and 0.6 mM WT subunits enzyme monomers (0.75, 1 and 1.2 mM total monomers). From the titration at 0.5 mM WT monomers of WTIE68A-SC, it can be inferred that the binding of Ca^{2+} results in the release of up to 0.2 kcal/mole of Ca^{2+} using the 120 mM metal stock (**Fig. 4.3**). In the case of the WT-PvuII, the titration of 1 mM enzyme monomers with a 120 mM CaCl_2 stock resulted in the release of about 1.5 kcal/mole of Ca^{2+} ions (Jose, et al., 1999). The difference between the binding energies of Ca^{2+} to the two variants is almost 7-fold, while it has to be considered that the WT-PvuII has two metal binding subunits and thus two extra metal binding sites than the heterodimeric WTIE68A-SC (the E68A subunit is considered metal free). Focusing on the latter fact, in a hypothetical

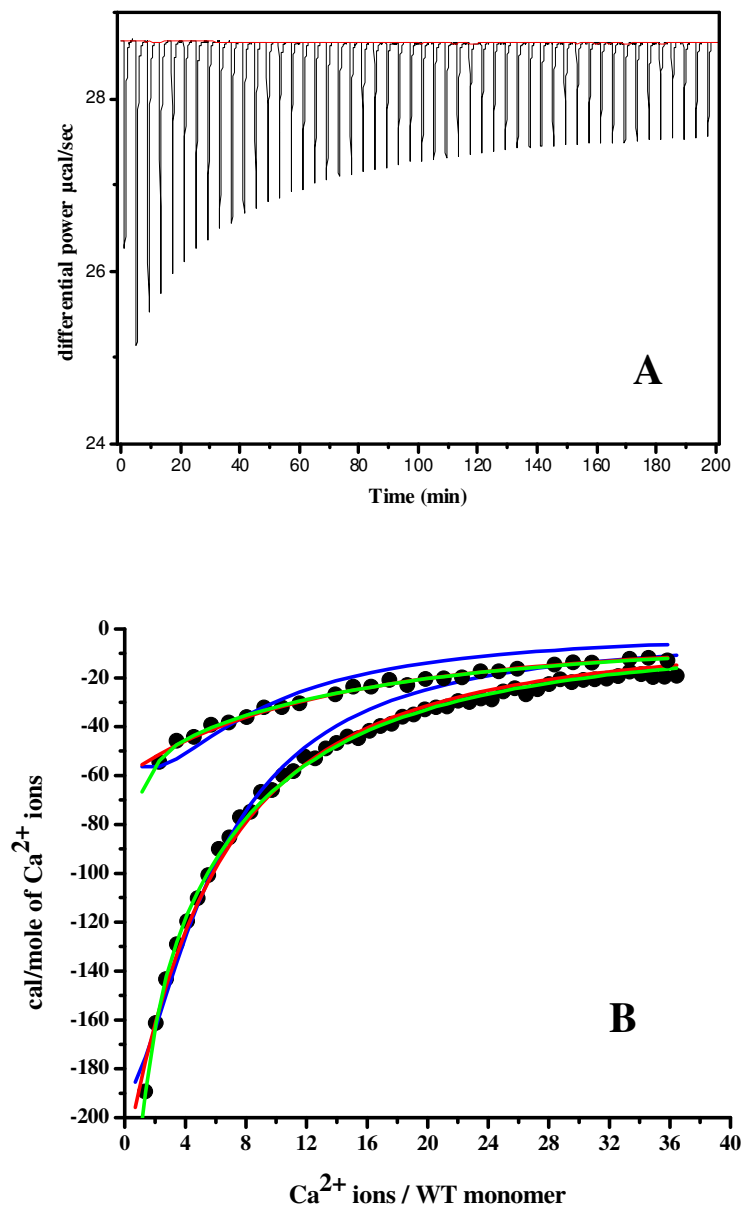


Figure 4.3 Ca^{2+} binding to the WTIE68A-SC PvuII A. Raw ITC data. 50 x 4 μL injections of 120 mM CaCl_2 vs 1 mM PvuII monomers (i.e. 0.5 mM WT monomers and the molar ratio is $[\text{Ca}^{2+}]/[\text{WT subunits}]$) B. Independent fits of the integrated data of the calorimetric titrations of 120 mM CaCl_2 vs 0.75 and 1 mM the WTIE68A-SC PvuII monomers to models describing one site (*red line*), a set of two sequential sites (*blue line*) and a set of two independent sites (*green line*). The experiments were performed in 5 mM HEPES, 400 mM NaCl, pH 7.5 and 25°C.

scheme of independent sites across the two subunits (no inter-subunit communication considered), the metal binding energy for the half functional WT E68A-SC heterodimers should be approximately half of the binding energy of the fully functional homodimeric WT-PvuII (including the intra subunit cooperativity in each case). It is clear that there is communication across the subunits and the effect of this communication is major to the metal ion affinity in the case of the WT-PvuII. The obtained integrated data were fitted to the models provided by Microcal Origin. It is noted that the best-fitted values were obtained by lowering the dependency among the fitted parameters (thus the quality of the fits improved in addition to the minimization of χ^2 value or maximization of R^2) and the final set of values has a unique combination of all these optimized criteria. **Table 4.1** summarizes the calorimetry results for the Ca^{2+} direct titrations presented for comparison along with the WT PvuII previously reported data (Jose, et al., 1999). The data were fitted assuming the E68A subunit as essentially metal free. In this case the applied monomer concentration is equal to the corresponding concentration of the WT subunits only. Two models of independent sites per enzyme subunit were considered: one model describing one class of n sites and another describing two classes of sites, each involving a single site. A model of sequential occupation of two sites is also applied providing two macroscopic binding constants. The fit of the data to the one class of sites model marginally indicates the presence of two Ca^{2+} ions within the WT subunit of the heterodimer ($n=1.0 \pm 0.8$), since the error associated with the value is high. The apparent affinity at 7.3 ± 0.5 mM of these sites is weaker than the value supported for the binding affinity of Ca^{2+} in the presence of a set of sites in the WT PvuII (1.3 ± 0.1 mM), but still a low millimolar binding constant is supported. In the case of two independent sites within

Table 4.1 Ca²⁺ binding to the single chain PvuII variants.

WT E68A-SC	n sites ^{a,b}	Model			
		Two independent sites ^c	Sequential sites ^d	Two WT+One E68A site ^e	Two WT+Two E68A sites ^f
n	1.0 ± 0.8	1+1	2	2+1	2+2
K₁ (mM)	7.3 ± 0.5	3.7 ± 0.2	0.15 ± 0.006	6.6 ± 6.1	7.3 ± 6.3
K₂ (mM)		1.4 ± 0.4	9.1 ± 0.2	6.6 ± 2.9	7.5 ± 6.6
R²	0.994	0.965	0.998	0.985	0.979
χ²	7.9	48.5	2.5	21.4	28.5
WT-SC					
n	2.0 ± 0.3 (1)	1+1	2		
K₁ (mM)	1 ± 0.1 (4.6 ± 0.7)	1.2	3.6 ± 0.7		
K₂ (mM)		0.05 ± 0.02	10.2 ± 2.7		
R²	0.918 (0.999)	0.957	0.952		
χ²	851 (0.044)	464	528		
WT					
n	2.02 ± 0.2	2	2		
K₁ (mM)	1.3 ± 0.1	0.12 ± 0.08	0.55 ± 0.09		
K₂ (mM)		2.1 ± 0.1	1.15 ± 0.08		
χ²	850	395	578		

The ITC data were fitted using **Eq. 2.10** and **Eq. 2.11** (as described in the text) to which the fractions of the metal bound enzyme monomers described in **(a) Eq. 2.6**, **(c) Eq. 2.7**, **(d) Eq. 2.9**, **(e) Eq. 2.12** and **(f) Eq. 2.13** were applied. The values are the averages of the independent fits of the datasets of direct Ca²⁺ titrations to 1.0, 0.75 and 1.2 mM WT|E68A-SC PvuII monomers and 0.5 μM WT-SC PvuII monomers, respectively. *Conditions*: 5 mM Hepes, 400 mM KCl, pH 7.5 at 25°C. The WT-PvuII data (Jose, et al., 1999) at 1 mM monomers are shown for comparison. The apparent Ca²⁺ binding constant for the WT-SC PvuII and the corresponding statistical values obtained by the competition experiment observing the Tb³⁺ luminescence are shown in parentheses in the n site model (the fraction of metal bound enzyme describe in **(b) Eq. 2.8** was applied and fitted in Kaleidagraph).

the WT subunit of the WTIE68A-SC heterodimer, the fit of the data is of lower quality, returning one Ca^{2+} site at 3.7 ± 0.2 mM and a second site at 1.4 ± 0.4 mM. The WT PvuII data (Jose, et al., 1999) fitted to the same model provided an affinity for Ca^{2+} at 0.12 ± 0.08 mM for one site and a second site of lower affinity for Ca^{2+} at 2.1 ± 0.1 mM (**Table 4.1**). Due to the relatively low quality of the fit to the independent site model for the WTIE68A-SC, it may be assumed that the hypothesis of two non-interacting sites within the WT subunit is not supported sufficiently. However the significantly better fit of the WTIE68A-SC data to the sequential two-site model returned two macroscopic binding constants at 150 ± 6 μM and 9.1 ± 0.2 mM which differ by a factor of 60. This indicates either the independent occupation of the two sites or the negative interaction between them, which would be significantly weak. Unlike the previously shown results for the WT PvuII, where the fits to an interacting and an independent site model were of the same quality (χ^2 at 578 and 395 respectively, **Table 4.1**) the WTIE68A-SC data fitted significantly better to the sequential model than the independent site model (χ^2 at 2.5 and 48.5 respectively, **Table 4.1**). An unambiguous pattern regarding the site interaction in the WT PvuII could not be supported leading to the conclusion that the interaction (if any) is weak (Jose, et al., 1999) which is also the case for the WT subunit of the WTIE68A-SC although due to the great difference in magnitude of the two sequential binding constants. Further observation of the magnitude of this difference indicates a stronger negative interaction (if present) between the two sites in the native WT (0.55 mM and 1.15 mM) compared to the potential interaction between the two sites in the WTIE68A-SC (0.15 mM and 9.1 mM respectively). It is thus concluded that two metal ions bind to the WT subunit of the WTIE68A-SC with lower affinity and pronounced

weaker communication between them compared to the native WT PvuII.

In the case of the WT-SC PvuII, the fit to the one set of independent sites model resulted in a number of 2.0 ± 0.3 sites each with a 1.0 ± 0.1 mM affinity, a result closely matching the corresponding result for the WT PvuII (**Table 4.1**). It is also noteworthy that the quality of the fit is the least good among the applied models, which is also the case for the WT PvuII (Jose, et al., 1999). The fit to the sequential model resulted in two sites at 3.6 ± 0.7 mM and 10.2 ± 2.7 mM, respectively, which differ by less than an order of magnitude (**Table 4.1**). This indicates marginally either the independent character of the two sites or the presence of interaction between the two sites, which in this case would be negative. The best fit to the two independent sites model returned one site with an affinity at 0.05 mM in the presence of a second site at 1.2 mM. The independent character of two Mg^{2+} , Co^{2+} and Mn^{2+} sites has been previously shown in the case of the bacteriophage T5 exonuclease in a similar divalent ion binding study performed by ITC in the absence of DNA (Feng, et al., 2004). Similarly in the case of the murine flap endonuclease-1 a set of two independent equivalent sites was shown through direct calorimetric titrations for Mn^{2+} ions although no further evidence of the independent character of the sites was supported (Zheng, et al., 2002). In both cases the analysis of the data did not involve a sequential model but the independent character of the sites was taken as obligatory. Whether there is negative interaction or not between the sites within the WT subunit, the fit to all three models indicates the binding of Ca^{2+} ions in a 2:1 stoichiometry with each site at low millimolar affinity. The similarity to the native WT PvuII regarding the affinity of the two sites (**Table 4.1**) demonstrates the minimal effect of the linker on the occupation of the apo-WT-SC PvuII by Ca^{2+} ions.

A further comparison of the fitted parameters (affinities and stoichiometries) for the binding sites within a WT subunit between the WT-SC and the WTIE68A-SC variants is performed. Due to the linker (and its overall effect) being present in both variants, the obtained parameters regarding a single WT subunit are expected to be of relative consistence. However the values are not consistent between the two variants (comparing the values across the independent and sequential models), although overall the presence of two metal ions is shown in both cases. The question arises on the origin of the observed discrepancy in the predicted affinities of the corresponding Ca^{2+} sites. It might be that it is not the lack of cooperativity between the two subunits in the WTIE68A-SC heterodimer or the different mode or absence of intrasubunit cooperativity in one or both variants leading to the observed difference. Instead it might be that the E68A subunit is also capable of binding Ca^{2+} ions, and a fraction of the higher concentration of metal ions observed for the saturation of the enzyme is also utilized for the partial occupation of the E68A subunit. This could lead to the observation of apparent binding to the WT subunit distinct from the ones observed in the case of the WT-SC variant. To explore this possibility, the data for the WTIE68A-SC PvuII were fitted regarding the E68A subunit as capable of binding Ca^{2+} ions. The total concentration of enzyme monomers was applied in this case including both the WT and E68A subunits. The two subunits are considered non-equivalent, while the sites involved in each subunit are identical. Two additional models were applied in the case of the WTIE68A-SC PvuII each describing two equivalent metal sites per WT subunit and one or two metal sites for the E68A subunit (the approach of two non-equivalent sites within each subunit could not be followed as the number of parameters cannot be sufficiently accounted for by the

obtained data). **Table 4.1** shows the results of the fits developed assuming the binding of Ca^{2+} ions to the E68A subunit. In both cases (with one and two metal sites in the E68A subunit) the best fitted values for the binding constants across the two subunits are shown to be equivalent. Either at 6.6 or 7.5 mM the models resulted in four (or three) equivalent sites (**Table 4.1**), which is unlikely due to the hypothesis of two non-equivalent sets of sites across the subunits of the heterodimer. It has been previously shown in the case of the E68A homodimer that the binding of Ca^{2+} cannot be detected by direct calorimetric titrations (not producing sufficient enthalpies) indicating the weakness of a potential Ca^{2+} binding site in the E68A subunit (Jose, et al., 1999). The binding of Mg^{2+} ions to the homodimeric E68A variant with a dissociation constant at 40 mM (20-fold weaker than the WT PvuII) further indicates the compromised metal binding affinity of the E68A subunit (Dupureur, et al., 2000). Thus it is expected by hypothesizing the binding of Ca^{2+} ions to the E68A subunit (in the case of the WT|E68A-SC heterodimer) that a weak site might be titrated although not with affinity comparable to the WT subunit. In both cases (one or two sites within the E68A subunit) the data fitted with similar convergence. However, the high errors associated with the fitted values, the high dependencies among the parameters, and the relatively low quality of the fits (as reflected in the R^2 and χ^2 values (**Table 4.1**)) are further indicative of the inappropriateness of the scenarios of the ligation of Ca^{2+} ions to the E68A subunit.

Further evidence for the apparent affinity of one Ca^{2+} binding site in the WT-SC PvuII with micromolar affinity is shown by the application of competition titrations of Ca^{2+} to an already formed Tb^{3+} -WT-SC PvuII complex and the observation of the Tyr-sensitized luminescence of the Tb^{3+} ions (**Fig. 4.4A**). The enzyme was applied at 2 μM

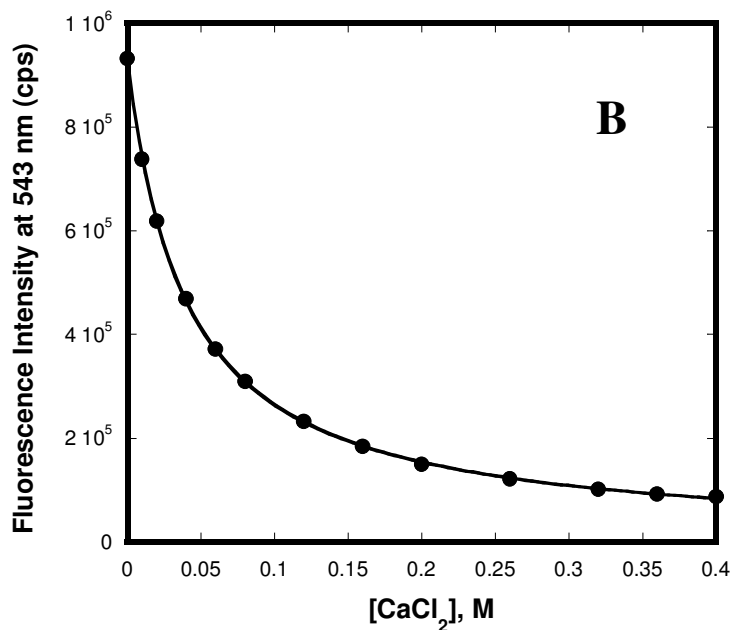
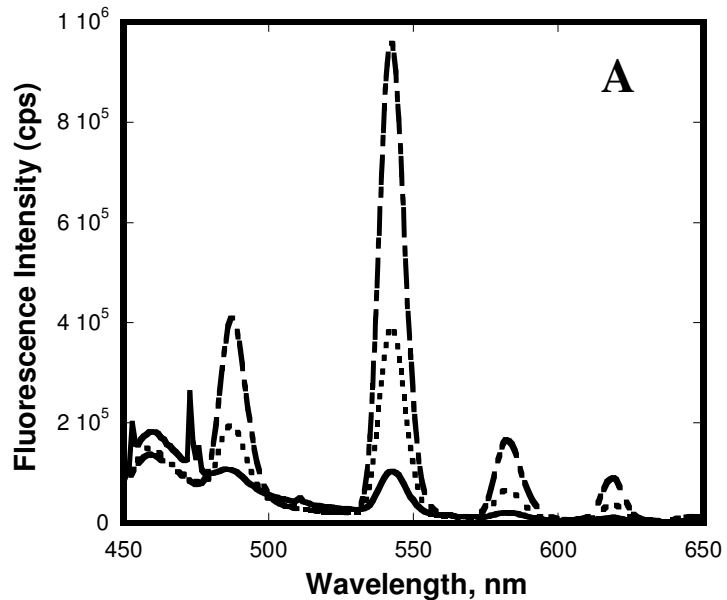


Figure 4.4 Ca²⁺ binding observed by Tyr-sensitized Tb³⁺ luminescence. A Spectra of the fluorescence emission of Tb³⁺ in the absence of Ca²⁺ ions (*dashed line*) and in the presence of 60 (*dotted line*) and 400 mM (*straight line*) Ca²⁺ ions. B. The titration curve obtained by the observation of the Tb³⁺ emission maximum at 543 nm. The data were fitted to the 1:1 competition model described by Eq. 2.8. The average of three independent measurements resulted in an apparent binding constant for Ca²⁺ at 4.6 ± 0.7 mM. *Conditions*: 20 or 18 μ M Tb³⁺, 2 μ M WT-SC PvuII monomers in 5 mM Hepes, 400 mM KCl, pH 7.5, 25°C.

monomers, while the Tb^{3+} ions were applied at 18 or 20 μM to ensure the saturation of a single Tb^{3+} site within the WT-SC monomers at 2 μM . The displacement of the Tb^{3+} ions by Ca^{2+} is evident in the decrease of the emission intensity of Tb^{3+} between 450-650 nm (**Fig. 4.4A**). The emission maximum at 543 nm (corrected for the buffer interaction) was used to obtain the isotherm shown in **Fig. 4.4B**. A binding constant was returned at 4.6 ± 0.7 mM (**Table 4.1** parentheses) via fit to a competition model with a 1:1 stoichiometry for the Ca:WT (monomer) complex (**Eq. 2.8**). This result is within the observed range of low millimolar affinity for a single Ca^{2+} binding site in the WT-SC PvuII shown by ITC further confirming the calorimetric results (**Table 4.1**).

4.3.1.2 Lanthanide binding in the absence of cognate DNA

Direct Tb^{3+} titrations have been performed for both the WT-SC and the WT|E68A-SC PvuII. The results are summarized in **Table 4.2**. For both variants, low micromolar concentrations of enzyme monomers were applied (0.25 μM WT monomers of the WT|E68A-SC heterodimer and 0.1-10 μM monomers of WT-SC PvuII). Tb^{3+} was effectively applied without observed precipitation up to 40 μM . The fits were performed only to the non-cooperative models described. The models describing two independent sites were successful yielding R^2 values close to unity. The two non-equivalent sites model and the one class of two equivalent sites (both calculated around 13 μM) do not unambiguously describe two sites considering the high error of the corresponding averages. The fits to the Hill model show a coefficient at 1.3 ± 0.3 which can be considered as proving the filling of a second weaker site. It has to be noted that the higher the concentration of the enzyme monomers the higher the n_H (achieved up to 1.9 at

Table 4.2. Tb³⁺ binding to the single chain PvuII variants.

WT-SC	Model		
	n equivalent sites	Two non equivalent sites	Hill
N	1.1 ± 0.05	2	1.3 ± 0.3
K ₁ (μM)	1.9 ± 1.6	1.1 ± 0.61	1.2 ± 1.2
K ₂ (μM)		10.3 ± 4.9	
R ²	0.994	0.998	0.996
WTIE68A-SC			
n	1.1 ± 0.06	2	1.1 ± 0.09
K ₁ (μM)	4.5 ± 4.9	4.9 ± 5.5	3.7 ± 3.8
K ₂ (μM)		80.3 ± 20.1	
R ²	0.994	0.994	0.993
WT			
n	1	2	
K ₁ (μM)	1.1 ± 0.6	2.3 ± 1.7	
K ₂ (μM)		117 ± 46	
R ²	0.986	0.988	

n is accordingly representing the number of sites in each model. The n and two site models describe independent sites. The WT PvuII Tb³⁺ binding data are presented for comparison (Bowen, et al., 2004).
Conditions: 5 mM Hepes, 400 mM KCl, pH 7.5 at 25°C

10 μM monomers) which would lead to the conclusion that a second site is indeed populated. The one site that is clearly monitored has identical affinity ($1.2 \pm 1.2 \mu\text{M}$) to the low micromolar site shown previously for the WT PvuII (Bowen, et al., 2004). As from the above it cannot be concluded that the WT-SC titrations prove the binding of only one Tb^{3+} ion, but as previously shown in the case of the WT PvuII (Bowen, et al., 2004), these titrations do not provide a definite approach regarding the affinity of a second site as well. In the case of the WT/E68A-SC PvuII, the direct titrations to 0.25 μM WT monomers show a Hill coefficient equal to 1.1 ± 0.09 , which does not allow for conclusions on a second site. It has to be noted that the WT subunit is considered as containing metal sites and the E68A subunit is considered metal free. This is particularly applied in the case of the lanthanide titrations, since the one weak site with an affinity at approximately 100 μM previously shown in the case of the E68A PvuII for Eu^{3+} can not be sufficiently populated at the working concentrations herein (Bowen, et al., 2004). From all the models it is shown that one site is titrated below 10 μM . A second site might also be occupied at lower affinity around $80 \pm 20 \mu\text{M}$, as it can be seen by the fit to the model describing two non equivalent sites (**Table 4.2**). The occupation of such a weaker site is more pronounced at higher enzyme concentrations and falls within the range of the WT PvuII weak site at $117 \pm 46 \mu\text{M}$ (Bowen, et al., 2004) although somewhat stronger. It may be (similar to the case of Ca^{2+}) that the loss of the subunit crosstalk results in alteration of the relationship between the sites regarding their affinities. In the present case, is not easy to interpret the hypothesis of a stronger site (as compared to the WT PvuII) when part of the cooperativity is lost. The similarity or minor weakness of the high affinity site compared to the WT PvuII (Bowen, et al., 2004)

is shown since despite the high errors associated with the values of the binding constants obtained from all the applied models, the values are in the low micromolar range.

4.3.2 DNA binding to the single chain PvuII variants

The WT-SC homodimers and the WT|E68A-SC heterodimers of PvuII were employed in DNA binding experiments as a function of the Ca^{2+} concentration using the non self complementary 14mer duplex DNA at 25°C as described in Chapter II. The binding constants for the WT-SC were obtained through nitrocellulose filter binding experiments at and above 0.5 mM Ca^{2+} (at and above 5 mM Ca^{2+} for the WT|E68A-SC), while fluorescence anisotropy measurements were applied at and below 0.5 mM Ca^{2+} (at and below 5 mM Ca^{2+} for the WT|E68A-SC). The profile of the association constants of WT|E68A-SC PvuII as a function of the Ca^{2+} concentrations is shown in **Fig. 4.5**. The corresponding profile for the native WT PvuII homodimer (Conlan, et al., 2002) and the values at 1 and 10 mM Ca^{2+} obtained for the E68A homodimer (Bowen, et al., 2003) are overlaid for comparison. The affinity for DNA under metal free conditions for the WT-SC is 10-fold higher (29 ± 14 nM) than that of the native WT PvuII (300 ± 150 nM), while for the WT|E68A-SC variant (450 ± 100 nM) the affinity is very similar to the WT PvuII (**Table 4.3**). In essence, the effect of the linker is shown by the comparison of these values. As it has been previously shown, the formation of the high affinity PvuII-DNA complex is promoted in the presence of the divalent Ca^{2+} ions (Nastri, et al., 1997; Conlan, et al., 2002) as the scissile site of the DNA is inserted to the active site of the enzyme and into the coordination sphere of the metal ion. However, several contacts between PvuII and the DNA substrate with the scissile and the flanking bases are formed

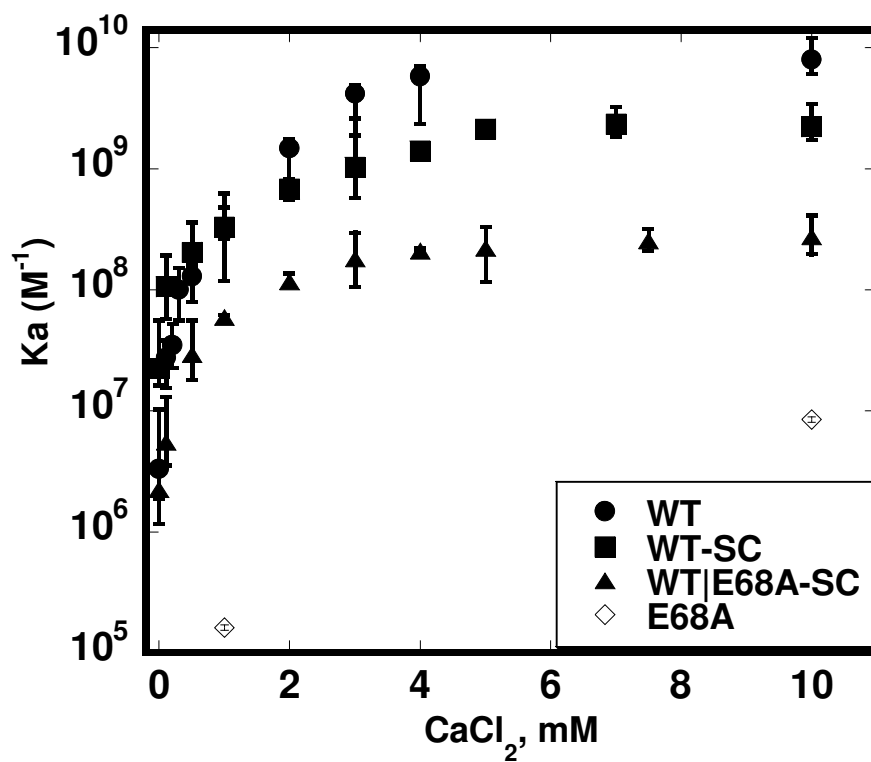


Figure 4.5 The Ca²⁺ dependence of the DNA association constants in the WT and variants of PvuII. The profiles of WT PvuII (●), WT-SC PvuII (■), WT|E68A-SC PvuII (▲) and E68A (◇) are overlaid. The difference in affinity above 1 mM CaCl₂ and the subsequent span of two orders of magnitude is shown among the PvuII variants.

Table 4.3 The DNA dissociation constants for the WT, WT-SC, WTIE68A-SC and E68A PvuII at different Ca²⁺ concentrations.

DNA dissociation constants (M)				
[Ca²⁺]	WT PvuII^{a,b}	WT-SC PvuII	WTIE68A-SC PvuII	E68A PvuII^b
0 mM	$(0.30 \pm 0.15) \times 10^{-6}$	$(0.03 \pm 0.01) \times 10^{-6}$	$(0.45 \pm 0.1) \times 10^{-6}$	$1.9 \pm 0.8 \times 10^{-6}$
1 mM	$(0.24 \pm 0.16) \times 10^{-9}$	$(3.04 \pm 0.9) \times 10^{-9}$	$(17.0 \pm 1.4) \times 10^{-9}$	$(6.2 \pm 4.6) \times 10^{-6}$
10 mM	$(82 \pm 61) \times 10^{-12}$	$(0.45 \pm 0.1) \times 10^{-9}$	$(3.7 \pm 1.3) \times 10^{-9}$	$(0.12 \pm 0.4) \times 10^{-6}$

The values correspond to the binding of PvuII to the non-self complementary 14mer described in Chapter II. Conditions: 50 mM Tris, pH 7.5 at 25°C. The ionic strength was maintained constant at the different Ca²⁺ concentrations by addition of NaCl. (a) (Conlan, et al., 2002), (b) (Bowen, et al., 2003)

even by the enzyme conformation not induced by the metal ions. This conformation for the WT-SC is clearly more effective in the formation of the necessary contacts than in the case of the native WT PvuII. The corresponding Gibbs free energies for the complexes formed at the different Ca^{2+} concentrations at 25°C are shown in **Table 4.4**. The WT-SC PvuII-DNA complex is stabilized by -10.3 kcal/mole, while the corresponding value for the WT PvuII is -8.9 kcal/mole and (similarly to the latter) equal to -8.65 kcal/mole for the WT E68A-SC (**Table 4.4**). These results indicate that the GSGG linker assists the WT-SC PvuII to adopt the necessary conformation that either enthalpically or entropically leads to a more stable complex with DNA by 1.4 kcal/mole than the complex formed by the WT-SC PvuII. In the case of the WT E68A-SC, the effect of the linker is compensated probably from the individual folding of the E68A subunit (see Discussion), and the complex of the variant with DNA is destabilized compared to the WT-SC.

In the presence of 1 mM Ca^{2+} ions the DNA bound complex of the WT-SC is stabilized compared to the metal free state by 1.32 kcal/mole. However the same concentration of metal ions lowers the free energy of the native WT PvuII-DNA complex by 4.2 kcal/mole compared to the metal free conditions. At this point the WT-SC and native WT-DNA complexes differ by 1.51 kcal/mole, although the native WT-DNA complex is more stable in this case (**Table 4.4**). It is thus shown that the ligation of metal ions is dominating over the covalent linker in the adoption of an enzyme conformation leading to increased stability of the PvuII-DNA complex. The effect of 1 mM Ca^{2+} ions on the DNA affinity of the WT E68A-SC variant is the stabilization of the complex by 2.0 kcal/mole compared to the metal free conditions (**Table 4.4**). This shows the significant contribution of the metal ions (even at one subunit only) to the formation of

Table 4.4 The apparent Gibbs free energies for the DNA-PvuII complexes at different Ca^{2+} ion concentrations.

ΔG° , kcal/mole (25°C)				
$[\text{Ca}^{2+}]$	WT PvuII ^{a,b}	WT-SC PvuII	WT/E68A-SC PvuII	E68A PvuII ^b
0 mM	-8.9	-10.3	-8.7	-7.5
1 mM	-13.1	-11.6	-10.6	-7.8
10 mM	-13.8	-12.7	-11.5	-9.5

The free energy values are calculated by application of the average values of the association constants of **Table 4.3** (retrieved from ^a(Conlan, et al., 2002) and ^b(Bowen, et al., 2003)) to the equation $\Delta G^{\circ} = -RT\ln K_a$.

the DNA complex in the presence of the linker. The poor free energy difference (only 0.35 kcal/mole) in the case of the E68A-DNA complex between 0 and 1 mM Ca^{2+} due to the limited metal ion occupancy of both subunits, additionally points to the constructive effect of the metal ions in the adoption of an enzyme conformation with high affinity to DNA.

At 10 mM Ca^{2+} ions, the WT-SC complex with DNA is 2.5 kcal/mole more stable than the metal free complex and only 1.01 kcal/mole less stable than the corresponding complex of the native WT (**Table 4.4**). Thus the effect of the linker on the DNA complex stabilization is shown to be overcome by the effect of the saturation by Ca^{2+} ions. In fact it is shown that although at low or no metal ions the enzyme subunits are positioned effectively by the linker, at saturating metal concentrations the conformation of the enzyme (driven by the metal ions) cannot lead to a DNA affinity similar to the native WT complex because of the restriction imposed by the linker. In the case of the native WT, the metal saturated DNA complex at 10 mM Ca^{2+} is more stable than the metal free complex by 4.86 kcal/mole (the highest $\Delta\Delta G^{\circ}$ among the variants presented). The $\Delta\Delta G^{\circ}$ between the two variants for the two states (metal free and 10 mM Ca^{2+}) at 2.4 kcal/mole represents the sum of the contributions of the linker to the affinity of the PvuII-DNA complex. The 2.4 kcal/mole energy difference consists of the 1.39 kcal/mole constructive contribution (at limited Ca^{2+}) and 1.01 kcal/mole destructive contribution (at saturating Ca^{2+}) of the linker (**Fig. 4.6**). At 10 mM Ca^{2+} , the higher occupation of the single WT subunit by Ca^{2+} ions in the WT|E68A-SC variant promotes the formation of the DNA complex which is 2.9 kcal/mole more stable than the corresponding complex in the absence of metal ions and also less stable (by 1.2 kcal/mole) than the corresponding

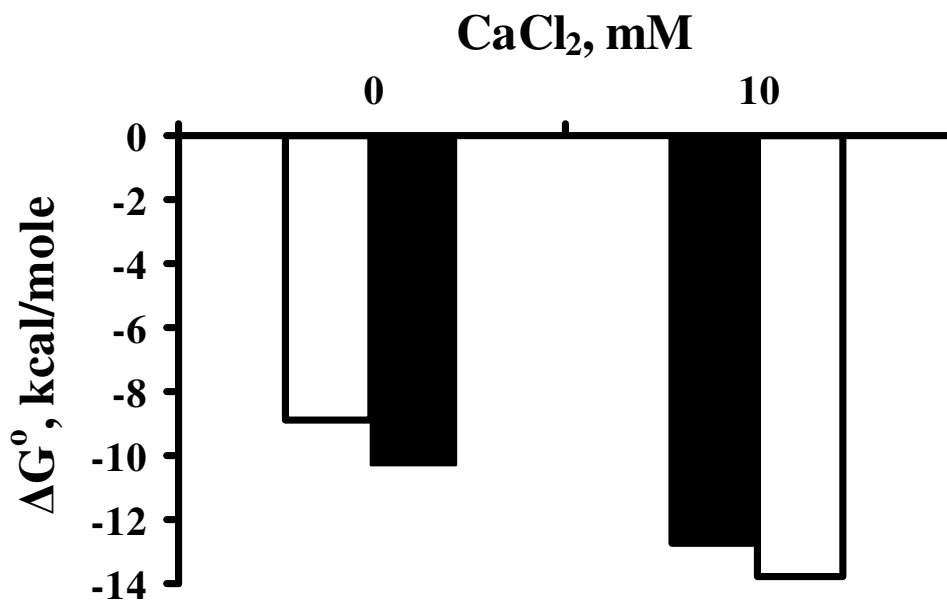


Figure 4.6 Energetic diagram of ΔG° for the DNA association with the WT PvuII variants (native and SC). The relative free energy values (ΔG°) as calculated in **Table 4.4** for the native WT PvuII (*White box*) and the WT-SC PvuII (*Black box*) are depicted and the stabilization of the DNA complexes in both variants from 0 to 10 mM Ca^{2+} is shown. The effect of the covalent linker is shown by the constructive $\Delta\Delta G^\circ$ value (-1.4 kcal/mole) for the WT-SC PvuII relative to the WT PvuII at zero Ca^{2+} and the corresponding destructive $\Delta\Delta G^\circ$ value (+1.0 kcal/mole) at 10 mM Ca^{2+} . The $\Delta\Delta G^\circ$ values are relative to the WT PvuII.

complex of the WT-SC variant. The high metal concentration has little effect on the DNA affinity of the E68A homodimer. The DNA complex of the variant is slightly more stable (only by 0.6 kcal/mole) than the native WT-DNA complex. This indicates that Ca^{2+} ions are required for the formation of the high affinity DNA complex but they cannot be ligated to the active site of PvuII in the presence of the Ala68 (Jose, et al., 1999; Bowen, et al., 2003). **Table 4.4** shows the hierarchy of PvuII variants according to their affinity to the cognate NSC 14mer, which is evidently dictated by the occupation of the PvuII subunits with metal ions. From left to right at each Ca^{2+} concentration, the affinities in **Table 4.3** and the free energies of the corresponding DNA complexes in **Table 4.4** are shown with respect to the decreasing functionality of the PvuII dimers in metal binding. For example at 10 mM Ca^{2+} , the ΔG° for the formation of the DNA complex of the WT-SC is -12.7 kcal/mole, while the introduction of the E68A mutation and the impairment of the metal binding by one subunit reduces the DNA complex free energy by 1.2 kcal/mole. A subsequent impairment of the second subunit reduces the free energy of the E68A-DNA complex by another 2.0 kcal/mole. It has to be noted though that the DNA affinity to the WT|E68A-SC might be higher in the absence of the linker and as such the 2.0 kcal/mole energy difference is due to the participation of the linker.

In order to explore quantitatively the extent of the communication of the metal binding sites across the PvuII subunits in the presence of cognate DNA, the binding constants for the metal and DNA association were extracted by fitting simultaneously the DNA equilibrium association data for the WT-SC and the WT|E68A- SC PvuII as a function of the metal ion concentration to the models of linked equilibria shown in

Scheme 4.1 using the software Dynafit. The fitted plots of 15 datasets for each of the WTIE68A-SC and WT-SC variants are shown in **Fig. 4.7** and **Fig. 4.8** respectively. For each dataset the individual fit to a 1:1 isotherm is shown along with the curve of the global fit with the two curves being overall in very good agreement. This reflects the success of the global fit in representing the metal dependence of the DNA binding. In the case of the WT-SC PvuII, the metal binding constants are used in the model with respect to the dimers of the enzyme assuming the sequential binding of two Ca^{2+} equivalents in each step of K_2 and K_3 (or K_6 and K_7 respectively) with one metal ion binding to each WT monomer of the WT-SC homodimer. The square of the values of K_2 and K_3 obtained by ITC were applied as fixed in the global fit of the DNA binding data. The results for all the metal binding constants with respect to the enzyme monomer are included in **Table 4.5**. The model shown in **Scheme 4.1** for the WT-SC PvuII resulted in a metal free DNA binding constant at 28.1 ± 1.3 nM (**Table 4.5**). The apparent sequential binding constants for the first and second equivalents of Ca^{2+} to a WT monomer in the presence of DNA are 1.5 ± 0.7 mM and 6.4 ± 1.9 mM respectively. As it results from the macroscopic definition of cooperativity in the presence of DNA, the ligation of the second equivalent within each subunit is not favored and a negative interaction is observed at the binding of the second set of sites with $K_6^2 - 0.25K_7^2 < 0$ (where K are the dissociation constants in **Table 4.5**). In the absence of DNA though, the two sequential constants at 3.6 ± 0.7 mM and 10.2 ± 2.7 mM (**Table 4.5**). The same definition also represents negative cooperativity for the two corresponding sets of sites with $K_2^2 - 0.25K_3^2 < 0$, although of lower magnitude. Assuming the free energy coupling between the two states of two sets of sites represented in

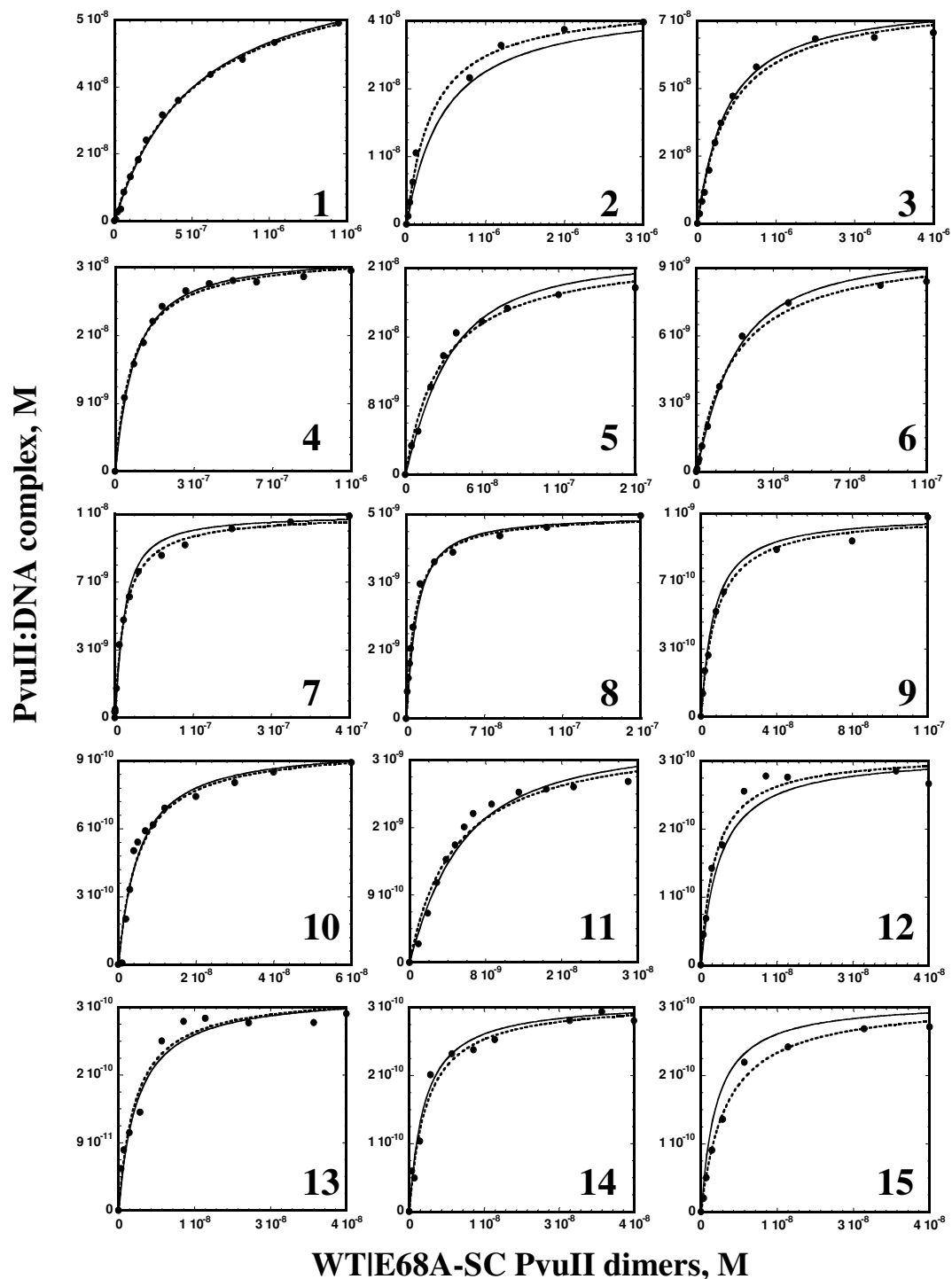


Figure 4.7 DNA binding to the WTIE68A-SC PvuII. Global fit (solid line) and individual fits (dotted line) for the PvuII titrations of the DNA duplex concentrations: 70 nM (1), 40 nM (2), 80 nM (3) duplex at 0 mM Ca^{2+} , 30 nM duplex at 0.1 mM Ca^{2+} (4), 25 nM duplex at 0.1 mM Ca^{2+} (5), 10 nM duplex at 1 mM Ca^{2+} (6,7), 5 nM (8) and 1 nM (9) duplex at 2 mM Ca^{2+} , 1 nM duplex at 3 mM Ca^{2+} (10), 3 nM duplex at 4 mM Ca^{2+} (11), 0.3 nM duplex at 5 mM Ca^{2+} (12,13), 0.3 nM duplex at 7.5 mM Ca^{2+} (14,15).

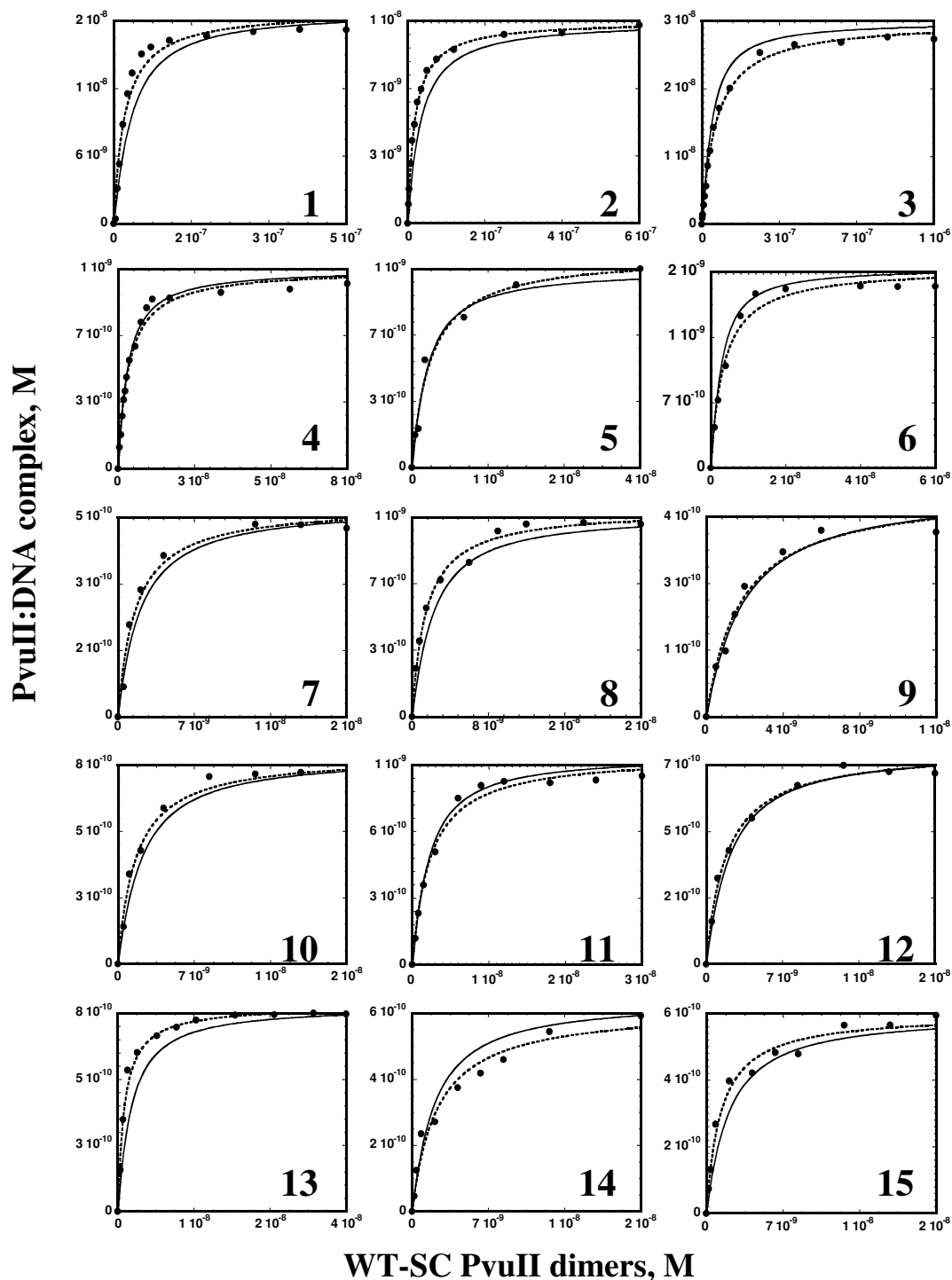


Figure 4.8 DNA binding to the WT-SC PvuII. Global fit (solid line) and individual fits (dotted line) for the PvuII titrations of the DNA duplex concentrations: 10 nM (1), 20 nM (2), 30 nM (3) duplex at 0 mM Ca^{2+} , 1 nM duplex at 0.1 mM Ca^{2+} (4), 1 nM duplex at 0.5 mM Ca^{2+} (5), 2 nM duplex at 1 mM Ca^{2+} (6), 0.5 nM (7) and 1 nM (8) duplex at 2 mM Ca^{2+} , 0.5 nM (9), 0.8 nM (10), 1 nM (11) duplex at 3 mM Ca^{2+} , 0.8 nM duplex at 4 mM Ca^{2+} (12), 0.8 nM duplex at 5 mM Ca^{2+} (13), 0.6 nM duplex at 7 mM Ca^{2+} (14,15).

Table 4.5 Ca^{2+} and DNA binding properties of the single chain variants of PvuII. Global analysis of the DNA binding data in the presence of Ca^{2+} .

Dissociation constant, M	WT-SC PvuII	WT/E68A-SC PvuII
K₁	$(28.1 \pm 1.3) \times 10^{-9}$	$(0.45 \pm 0.1) \times 10^{-6}$
K₂	$(3.6 \pm 0.7) \times 10^{-3}$	$(0.15 \pm 0.007) \times 10^{-3}$
K₃	$(10.2 \pm 2.7) \times 10^{-3}$	$(9.1 \pm 0.2) \times 10^{-3}$
K₄	$(4.9 \pm 2.6) \times 10^{-9}$	$(38.0 \pm 4.2) \times 10^{-9}$
K₅	$(1.9 \pm 1.2) \times 10^{-9}$	$(1.2 \pm 0.2) \times 10^{-9}$
K₆	$(1.5 \pm 0.7) \times 10^{-3}$	$(12.7 \pm 0.6) \times 10^{-6}$
K₇	$(6.4 \pm 1.9) \times 10^{-3}$	$(287.4 \pm 21.2) \times 10^{-6}$
RMS residual	8.7×10^{-10}	9.3×10^{-10}

K_1 , K_4 and K_5 are the DNA binding constants at 0, 1 and 2 Ca^{2+} equivalents per PvuII subunit. K_2 and K_3 are the binding constants for one and two equivalents of Ca^{2+} per enzyme subunit in the absence of DNA and K_6 , K_7 the corresponding values in the presence of DNA (**Scheme 4.1**). In the case of the WT/E68A-SC PvuII K_1 is fixed to the value obtained from the independent fitting of the DNA binding data under metal free conditions and K_2 , K_3 are fixed to the values obtained from the ITC experiments. In the case of the WT-SC PvuII only K_2 and K_3 are fixed to the values obtained from the ITC experiments. In both variants the values of K_4 and K_5 are pursued by the global fit of the data. The values of K_6 and K_7 are calculated from the values of the remaining five parameters in each case according to the relationships $K_1K_6=K_2K_4$ and $K_3K_5=K_4K_7$ (in the case of the WT-SC PvuII the presented values for the metal binding constants are the square roots of the values returned from the fit session, thus corresponding to the binding of Ca^{2+} to the WT monomer).

Scheme 4.2B and applying the squares of the values of **Table 4.5** in **Eq. 4.3** (involving in this manner the communication between the metal binding sites across and within the WT subunits), the least values for the interaction energies ($\Delta G^{\circ}_{\text{coop}}$) are calculated (as described in *Methods*). In the absence of DNA, the $\Delta G^{\circ}_{\text{coop}}$ is equal to +0.4 kcal/mole and equal to +0.9 kcal/mole in the presence of DNA. The agreement of the two approaches regarding the negative cooperativity between the two sets of sites is evident, and the unfavorable addition of a second equivalent within each WT subunit is confirmed. Despite the same extent of negative cooperativity in both the presence and absence of DNA, the affinity of the enzyme for each metal equivalent is improved in the tertiary complex of the DNA, showing the implication of the DNA backbone and the additional contacts that it offers to the active site for the formation of the bimetallic complex. The effect of the metal ions in the DNA complexation is also observed by the increasing affinity of the enzyme for DNA in the presence of the metal ions. In the presence of one metal equivalent in each subunit of the WT-SC PvuII, the DNA affinity is raised to 4.9 ± 2.6 nM, about 6-fold higher compared to the 28.1 ± 1.3 nM under metal free conditions (**Table 4.5**). The presence of a second equivalent in each subunit further increases the affinity for DNA to 1.9 ± 1.2 nM, although more modestly compared to the transition from the metal free to one metal equivalent per monomer states. In terms of the free energy associated with the formation of the complexes ED, EM₂D and EM₄D for the WT-SC PvuII from the corresponding DNA free enzyme species, the EM₂D complex (-11.3 kcal/mole) is more stable by 1.0 kcal/mole than the ED complex (-10.3 kcal/mole) while the EM₄D complex (-11.9 kcal/mole) is more stable than the EM₂D complex only by 0.6 kcal/mole (**Fig. 4.9**). It is thus shown that the principal effect to the DNA affinity

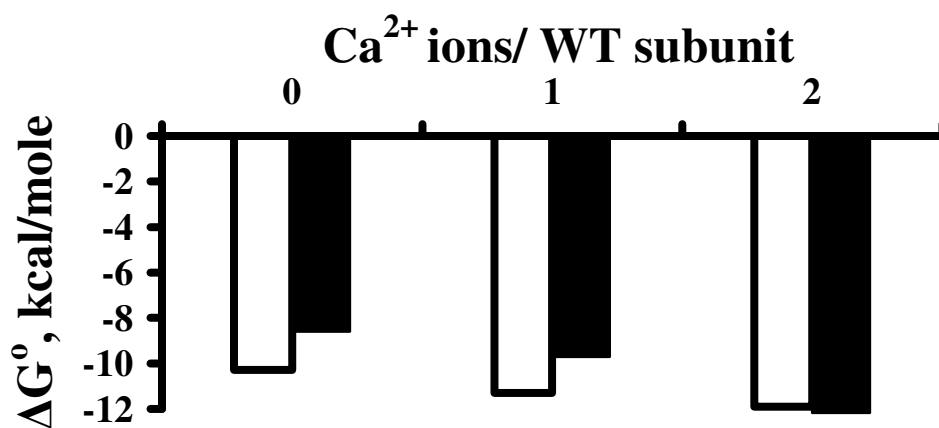


Figure 4.9 Diagram of ΔG° for the association of the WT-SC and WTIE68A-SC PvuII with DNA at different Ca^{2+} compositions. The free energy of the DNA complexes in the presence of Ca^{2+} ions for the WT-SC (*white bars*) is equivalent to the WTIE68A-SC (*black bars*) at each metal:WT subunit stoichiometry. Under metal free conditions the energy difference of the complexes between the two variants is at 1.6 kcal/mole.

comes from the presence of one metal ion per enzyme subunit, which probably signals the majority of the conformational alterations to the enzyme leading to the stabilization of the mononuclear Ca^{2+} -PvuII-DNA tertiary complex. The intrinsically unfavored addition of the second metal equivalent to the mononuclear metal complex also contributes to an active site conformation that further favors the DNA complexation but not to a substantial extent. Similar although roughly more extensive has been the stabilization of the binary complex of the two troponins C and I (analogous to the PvuII:DNA complexation) in the presence of Ca^{2+} ions at -2.8 kcal/mole (Wang, et al., 1985)

The application of the model for global fit of the WTIE68A-SC DNA binding data was performed using the equilibrium constant for the DNA association in the absence of Ca^{2+} ions at $0.45 \pm 0.1 \mu\text{M}$ (average of three independent values) along with the metal binding constants in the absence of DNA obtained by ITC as fixed parameters. The global fit of the data returned the DNA binding constants in the presence of one Ca^{2+} equivalent within the WT subunit at $38.0 \pm 4.2 \text{ nM}$, about 12-fold stronger than the metal free interaction of the heterodimer with DNA (**Table 4.5**). The addition of a second equivalent within the WT subunit resulted in a more dramatic increase for the DNA affinity with a DNA binding constant at $1.2 \pm 0.2 \text{ nM}$ (**Table 4.5**), which is about 32-fold stronger than in the presence of one metal equivalent. The affinity for DNA in the presence of two metal equivalents within one or two subunits is similar as it emerges from the comparison between the WT-SC and the WTIE68A-SC PvuII. The corresponding DNA complexes are stabilized at -11.9 and -12.2 kcal/mole (**Fig. 4.9**). This leads to the conclusion that the metal saturation of a second subunit is not necessary for the highest affinity PvuII-DNA complex in the case of the single chain variants. The

response of the WTIE68A-SC heterodimer to the ligation of each metal equivalent is significantly greater than in the case of the WT-SC. The DNA complex in the presence of one metal ion in the WT subunit (EMD) in the WTIE68A-SC (-10.1 kcal/mole) is stabilized by 1.5 kcal/mole compared to the metal free DNA complex (ED at -8.6 kcal/mole) while the second metal equivalent leads to a further stabilization by 2.0 kcal/mole (EM₂D at -12.1 kcal/mole) (**Fig. 4.9**). As such the conformational response of the WTIE68A-SC heterodimers to the addition of metal ions is more extensive than in the case of the WT-SC. However due to the largely weaker ED complex of the heterodimer compared to the ED complex of the WT-SC, the intermediate EMD of the heterodimer is not populated as extensively as in the WT-SC. It is thus shown that the apparent discrepancy in the DNA affinities observed at high Ca²⁺ concentrations in **Fig. 4.5** between the single chain variants are due to the greater accumulation of the EMD species in the case of the WT-SC PvuII, which contribute significantly to the measured signal. Nevertheless, the impact of the ligation of metal ions in one subunit is much greater than the metal ligation in both subunits and constitutes the only Ca²⁺-PvuII dimer interaction necessary to achieve a high affinity DNA complex. In the presence of DNA in a similar fashion as in DNA free conditions, the first and second equivalents of Ca²⁺ ions to the WT subunit of the WTIE68A-SC heterodimer bind with marked negative cooperativity. The affinity for the first metal ion is 12.7 ± 0.6 μM while the second metal ion binds at 287.4 ± 21.2 μM, about 22 times weaker and as such the anti-cooperative behavior may be assumed between the two sites (**Table 4.5**). This is also supported by the relationship between the macroscopic values of these metal binding constants (justifying the inequality $K_6 - 0.25K_7 < 0$, which denotes the negative cooperativity macroscopically,

(Wyman, et al., 1990)). However the presence of the DNA increased the affinity for each metal equivalent quite extensively compared to the DNA free conditions (first and second equivalent at 0.15 ± 0.007 mM and 9.1 ± 0.2 mM, respectively with $K_2 \sim 0.25K_3$) while it also decreased the difference between them (from ~ 60 to ~ 22 -fold). In the case of the WT-SC the difference of the corresponding values at the addition of DNA is relatively less dramatic (~ 3 - 4 fold) as the magnitude of the binding constants lies at low millimolar levels (**Table 4.5**). It is thus demonstrated that the apparent effect of the DNA is greater in the metal binding in one functional WT subunit than in the presence of the WT-SC homodimer. Due to the free energy coupling between the two sites represented in **Scheme 4.2A** for the WT E68A-SC, the application of the values of the metal binding constants of **Table 4.5** in **Eq. 4.3** leads to the calculation of the lower limits of the values of the interaction energies ($\Delta G^{\circ}_{\text{coop}}$). In the absence of DNA, the $\Delta G^{\circ}_{\text{coop}}$ is equal to +1.6 kcal/mole and in the presence of DNA equal to +1.0 kcal/mole. It follows that the presence of a second subunit capable of metal binding leads to the decrease of the unfavorable energy which is observed in the presence and absence of DNA at the ligation of the second metal ion (or set of ions, accordingly) within a WT subunit (or dimer). This is most probably due to the communication of the metal sites across the two subunits of the WT-SC homodimer.

As depicted in **Scheme 4.2B** for the WT-SC PvuII, the occupation of the second set of sites in the presence of the first two metal ions employs the intra-subunit interaction between each incoming metal ion and the pre-existing metal ion within the subunit. The interactions across the subunits are multiple and cannot be dissected per metal equivalent or set of sites. However, taking twice into account the free energy

coupling within a subunit ($\Delta G^{\circ}_{\text{coop}}$ for the WT|E68A-SC PvuII, $\Delta G^{\circ}_{\text{intra}}$), it follows that the total observed interaction energy observed in the case of the WT-SC ($\Delta G^{\circ}_{\text{WT}}$) would be equal to $2\Delta G^{\circ}_{\text{intra}} + \Delta G^{\circ}_{\text{inter}}$, where $\Delta G^{\circ}_{\text{inter}}$ is the total unresolved inter-subunit interaction energy observed at the simultaneous occupation of the two metal sites. It can thus be calculated from the values of $\Delta G^{\circ}_{\text{intra}}$ and $\Delta G^{\circ}_{\text{WT}}$ obtained above that in the absence of DNA the $\Delta G^{\circ}_{\text{inter}}$ is -2.8 kcal/mole (**Fig. 4.10**), while in the presence of DNA a value of $\Delta G^{\circ}_{\text{inter}}$ at -1.1 kcal/mole is obtained (**Fig. 4.10**). It is observed in the case of the occupation of a set of sites that the positive total interaction energy $\Delta G^{\circ}_{\text{WT}}$ referring to an anti-cooperative behavior stems from its two components, intra and inter-subunit, having opposite signs and relative magnitudes that lead to the prevalence of the unfavorable interactions.

4.3.3 Conformational analysis of the WT-SC PvuII

The global conformation of the WT-SC PvuII has been explored by ^1H - ^{15}N HSQC NMR spectroscopy, and the obtained spectra have been overlapped with the corresponding spectra of the native WT PvuII for comparison. The WT-SC was applied at 650 μM monomers in 25 mM Tris, 200 mM KCl, 10% D_2O , pH 7.7. Spectra of the apo-enzyme (**Fig. 4.11A**), and also in the presence of 10 mM Ca^{2+} ions (**Fig. 4.11B**), and in the presence of one equivalent of cognate DNA (**Fig. 4.11C**) were acquired. The dispersion of the peaks in the case of the apo-WT-SC shows that the individual subunits are allowed to fold in the WT-SC variant as in the case of the native WT without any interference by the linker, as predicted in the design of the linker for the formation of the single chain PvuII (Simoncsits, et al., 2001). The crosspeaks of the apo-native WT (blue)

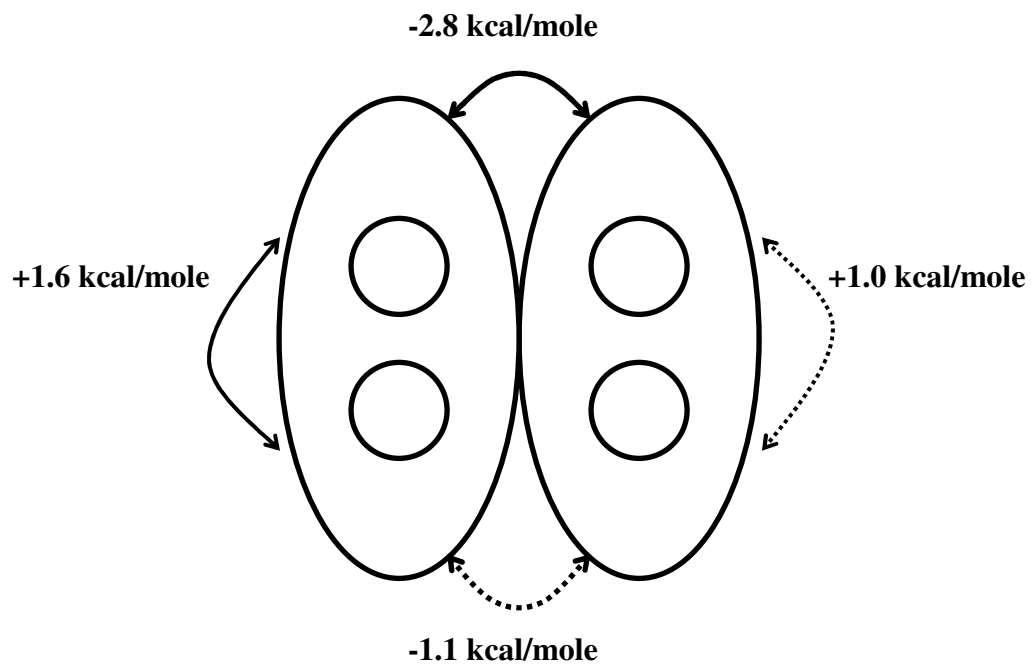


Figure 4.10 The intra and inter-subunit interaction among the metal binding sites in the WT-SC PvuII (obtained by the study of the single Chain PvuII variants). The WT subunits are shown, each with two metal binding sites. The lower limits of the intra-subunit free energies correspond to the single interaction between the two sites within the subunit. The lower limits of the inter-subunit free energies correspond to the multiple unresolved interactions across the subunits between two sets of sites. The free energy values are shown in the absence (*continuous line*) and in the presence of DNA (*dotted line*).

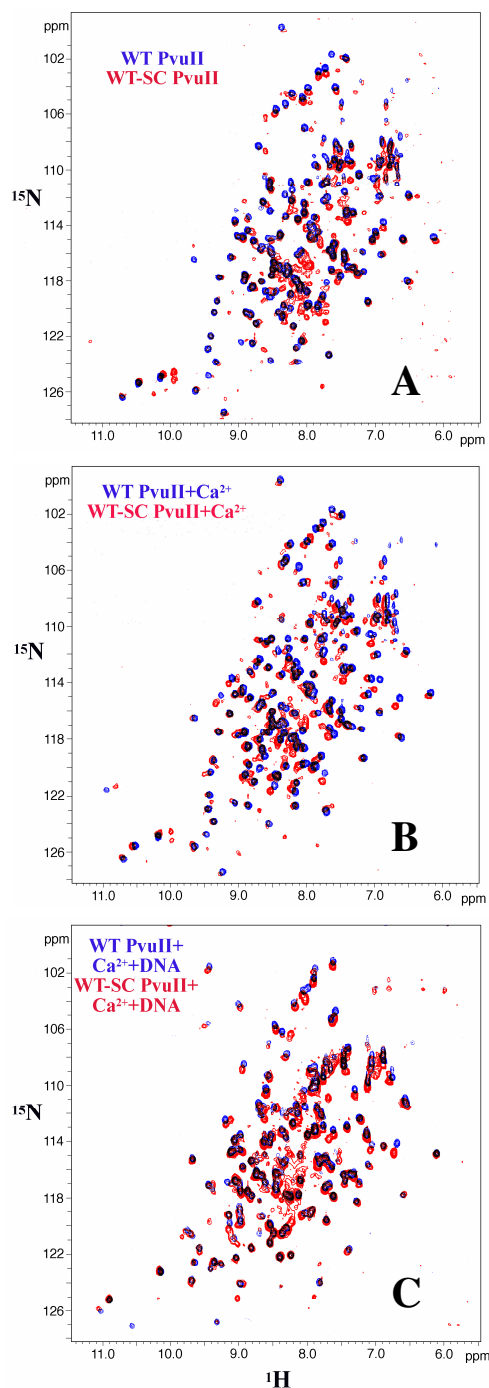


Figure 4.11. Overlays of the WT and WT-SC PvuII ^1H - ^{15}N HSQC spectra. A. Spectra of the apo-enzymes, B. in the presence of Ca^{2+} and C. in the presence of Ca^{2+} and cognate DNA (Blue: WT PvuII, Red: WT-SC PvuII). The A and B spectra are TROSY while the C is conventional. The enzyme was applied at 650 μM monomers in 25 mM Tris, 200 mM KCl, 10% D_2O , pH 7.7, and 25 $^\circ\text{C}$. Sequential additions of 10 mM Ca^{2+} in B and one equivalent of the cognate duplex in C are applied. The spectra result from 128 scans with each FID at 1024 (^1H) and 100 (^{15}N) points. The chemical shifts are relative to DSS.

and WT-SC PvuII (red) show significant overlap, although the least across the three states represented in the acquired spectra. The non-overlapping intensities between the apo-enzymes (located mostly in the square limited by 7.5-8.5 ppm in the ^1H axis and 115-120 ppm in the ^{15}N axis) (**Fig. 4.11A**) define the deviation of the overall conformation of the WT-SC variant from the conformation of the native WT PvuII due to the GSGG linker. Although no further quantification of the extent of the overlap has been applied, it is evident that the deviation of the overall conformation of the WT-SC from the native WT is minimal. In the presence of 10 mM Ca^{2+} ions, the crosspeaks of the metal saturated variants overlap extensively, suggesting that Ca^{2+} induces a global enzyme conformation which is also not significantly altered by the linker in the case of the WT-SC variant (**Fig. 4.11B**). In the presence of DNA, the effect of the linker in the WT-SC PvuII on the global conformation of the variant is obvious. The extent of the overlap is decreased compared to the apo and Ca^{2+} only states for the WT-SC and the native WT PvuII (**Fig. 4.11C**). The contacts of the WT-SC to the DNA which are critical in the absence of metal ions cannot be assessed. It might be, however, that their impact on the backbone conformation is not as extensive to be reflected in the HSQC spectra or if it is indeed reflected it is minimal (the crosspeak assignments of the residues would be quite helpful to explore this). Overall the effect of the linker to the global conformation of the single chain variants is shown to be more apparent in the DNA complex of the enzyme in the presence of Ca^{2+} ions than in the absence of DNA.

4.3.4 Catalytic activity of the single chain PvuII variants

The plasmid DNA Litmus 28i has been used as a substrate in kinetic experiments

in order to observe the nicking intermediate and measure the rate of its formation. This was previously performed in the PvuII endonuclease to demonstrate the nicking behavior (even at high Mg^{2+} concentrations) of the Y94F homodimer (Spyridaki, et al., 2003) and also the nicking behavior of the WTID34G-SC PvuII. The use of plasmid DNA as a substrate to PvuII allows for the cleavage of each strand to be monitored individually. As such, in the case of heterodimeric variants in which one subunit cannot bind metal ions, the kinetics of cleavage of a single DNA strand by the functional subunit can be studied independently. In the case of the half functional heterodimers, the rate of the cleavage performed on one strand of the duplex DNA under single turnover conditions should depend only on the rate of the cleavage event from the functional subunit. The rate measured for the cleavage of the second strand involves the dissociation of the heterodimer and its re-association or (under the single turnover conditions) the diffusion of a nearby non-specifically bound heterodimer at the right orientation to provide the second cleavage event. On the other hand as already mentioned, for a fully functional homodimer like the WT-SC PvuII and under single turnover conditions, the cleavage of the plasmid will depend only on the concentration of the metal ions (no dissociation and re-association of the dimeric enzyme to the scissile site is involved).

Reactions have been performed at 2 μ M dimers of single chain PvuII and 0.3 μ M Litmus 28i duplex at 37°C and different metal ion concentrations. In all the reactions performed only one pattern has been observed: the supercoiled plasmid is cleaved with the concomitant formation and disappearance of the nicked intermediate and also the formation of the linearized plasmid (at no metal concentration has there been only a linear product observed after the initiation of the reaction by the enzyme) (**Fig. 2.6** and

4.12). A hysteresis is observed for the formation of the linear plasmid depending on the concentration of the Mg^{2+} ions. The lower the concentration of Mg^{2+} , the slower is the appearance of the linear product. For both the WTIE68A-SC heterodimer and also for the WT-SC PvuII, the rates observed for the nicking (cleavage of the first strand) are significantly higher (about 10 fold) than the cleavage rates for the second strand, at low metal concentrations (**Table 4.6**). At higher metal concentrations, the two rates in both variants tend to equalize. These observations are in accordance with the sequential cleavage model for plasmid DNA also observed in other restriction endonucleases (Maxwell, et al., 1982; Halford, et al., 1988; King, et al., 1989; Sasnauskas, et al., 1999) under single turnover conditions in which the cleavage of the two strands is described by two sequential independent events (hence the appearance of the nicked intermediate). As expected, the cleavage rate of the first strand at low Mg^{2+} concentrations is similar between the two variants, which shows that the metal saturation of the WT subunit (the nicking subunit) in each variant is the same (**Fig. 4.13**). Profiles for the linearization step of each variant appear quite similar. As summarized in **Table 4.6** and taking into account the error associated with the nicking rate of the WT-SC variant, the values are similar for the cleavage of the first strand in both variants at 0.5 mM Mg^{2+} (0.03 and 0.01 s^{-1} respectively). The same holds for all Mg^{2+} examined up to 3 mM Mg^{2+} . However at 4 and 10 mM Mg^{2+} , the nicking rate is two and three fold higher in the case of the WT-SC than in the case of the WTIE68A-SC (**Table 4.6** and **Fig. 4.13**). This is consistent with the double probability of cleavage of a single strand in the case of two subunits rendered metal saturated (WT-SC) at high metal concentration compared to the probability of cleavage by enzyme dimers saturated with metal ions in only one subunit. A similar

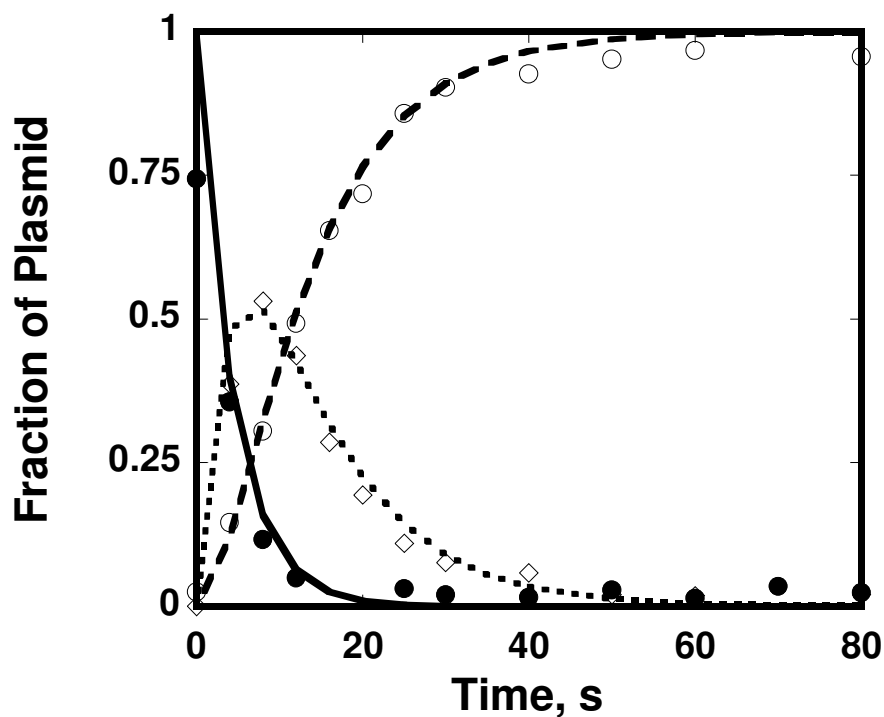


Figure 4.12 Cleavage of Litmus 28i by the WT-SC PvuII. The time course of the change in the fractions of each plasmid form is shown: fraction of supercoiled plasmid (f_{SC}) (continuous line-closed circles), fraction of open circles (f_{OC}) (short dashed line-rhombi) and fraction of linear product (f_L) (long dashed line-open circles). The three datasets were simultaneously fitted to equations (Eq. 2.14-2.16) yielding the nicking and linearization rates. The reaction was performed at 0.3 μM plasmid duplex, 2 μM WT-SC PvuII dimers, at 50 mM Tris-HCl, 118 mM NaCl, 4 mM MgCl_2 , pH 7.5 at 37°C.

Table 4.6 Single turnover reaction rates for the cleavage of the Litmus 28i plasmid by the single chain PvuII variants.

[Mg ²⁺]	WT-SC PvuII		WT/E68A-SC PvuII	
	k ₁ (s ⁻¹)	k ₂ (s ⁻¹)	k ₁ (s ⁻¹)	k ₂ (s ⁻¹)
0.5 mM	0.03 ± 0.01	0.006 ± 2e-4	0.01 ± 0.002	0.0003 ± 7.8e-5
4 mM	0.26 ± 0.03	0.1 ± 0.005	0.17 ± 0.016	0.08 ± 0.02
10 mM	0.66 ± 0.29	0.36 ± 0.006	0.23 ± 0.02	0.15 ± 0.06

The cases of limiting and high metal concentrations are shown. The nicking and linearization rates are denoted as k₁ and k₂ respectively. The conditions were 50 mM Tris, at pH 7.5 and 37°C while the ionic strength was maintained at 130 mM by addition of NaCl at the different Mg²⁺ concentrations. Quench flow experiments were conducted to obtain the rates at 4 and 10 mM Mg²⁺ while at 0.5 mM Mg²⁺ the reaction was performed on the bench.

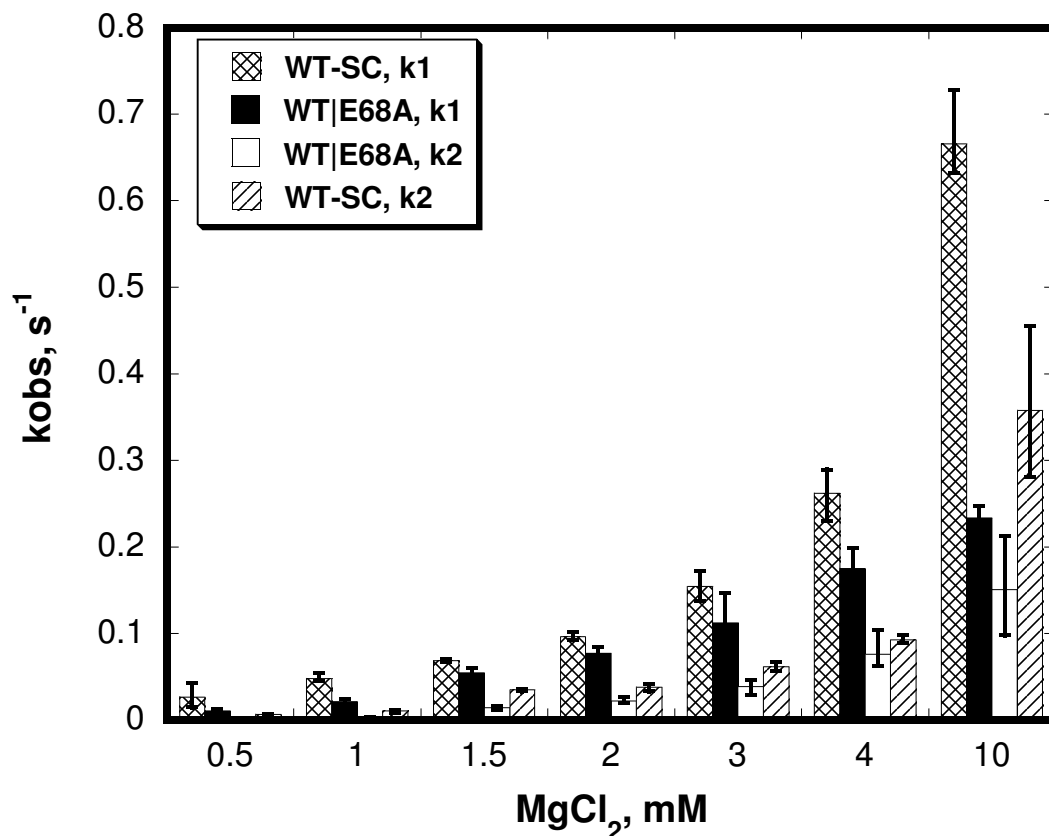


Figure 4.13 The Mg^{2+} dependence of the nicking (k_1) and linearization (k_2) rates of Litmus 28i by the WT-SC and WT|E68A-SC PvuII. The similar level of activity observed up to 4 mM Mg^{2+} ions is shown. The nicking activity of the WT-SC PvuII at 10 mM Mg^{2+} is clearly 2-3 fold higher than activity of the WT|E68A-SC variant and the subsequent linearization step occurs at a similar rate for both variants. The reactions were performed under single turnover conditions (2 μ M dimers PvuII, 0.3 μ M Litmus 28i) in 50 mM Tris, pH 7.5 at 37°C with the ionic strength maintained constant by addition of appropriate amount of NaCl. The reactions were performed using an SFM-400 Quench flow apparatus (Bio-Logic) from 3 mM Mg^{2+} and above while at lower metal concentrations the reaction was performed at the bench.

trend between the two single chain variants is observed in the case of the linearization rates. At limiting metal concentrations, this step is clearly slow for both variants, although there is a ten-fold difference between them (0.006 and 0.0003 s⁻¹ for the WT-SC and the WTIE68A-SC respectively at 0.5 mM Mg²⁺). The similarity between the values obtained for Mg²⁺ concentrations up to 4 mM is shown in **Fig. 4.13**. However at 10 mM Mg²⁺, there is a two-fold difference with the WT-SC cleaving the second strand at 0.36 s⁻¹ and the corresponding value being at 0.15 s⁻¹ for the WTIE68A-SC PvuII. As in the case of the cleavage of the first strand, the probability of the application of the nicked double stranded substrate to a population of metal saturated subunits is twice as much for the WT-SC variant than it is for the WTIE68A-SC. However this effect is observed only at 10 mM Mg²⁺. It might be that the expected hysteresis of the WTIE68A heterodimer due to the impaired metal binding is compensated at low metal concentrations by the fact that there is a large excess of enzyme dimers upon the duplex population (2 μM dimers on 0.3 μM DNA sites). As such, the series of events taking place in the case of the WT-SC homodimers is not significantly faster than the cleavage performed by the WTIE68A-SC (which has to dissociate from and re-associate to the nicked duplex, see *Discussion*) after the cleavage of the first strand. At 10 mM Mg²⁺ though, the effect of the availability of two functional subunits dominates.

4.4 Discussion

4.4.1 Preparation of PvuII heterodimers

The WT PvuII homodimer has been previously shown to bind to cognate DNA in the presence of Ca²⁺ ions, and in those measurements two metal ions were assigned per

enzyme active site ($n_H = 3.6$ for the PvuII dimer) (Conlan, et al., 2002). The sigmoidal dependence of the DNA binding profile on the Ca^{2+} concentration proves the synergistic mode by which the Ca^{2+} ions are ligated to the enzyme and assist the formation of the DNA-PvuII complex. Both inter-subunit and intra-subunit cooperativity might be involved in the binding of Ca^{2+} ions among the enzyme active sites, but no single quantitative answer for the contribution of each mode of cooperativity can be obtained by the profile of the WT-PvuII. In essence, the further investigation of Ca^{2+} binding to PvuII in the presence of DNA necessitates the dissection of the two modes of cooperativity. Similarly to the previously performed studies of asymmetrically mutant variants for the investigation of the communication within and among the EcoRV subunits (Stahl, et al., 1996; Groll, et al., 1997; Stahl, et al., 1998), or the PvuII subunits (Simoncsits, et al., 2001), we have prepared heterodimers of the PvuII endonuclease in an effort to study independently the two modes of cooperativity by which the metal binding is directed in the active sites of PvuII. Pursuing the creation of a PvuII dimer with one subunit inactive in metal binding, and thus abolishing the inter-subunit cooperativity, we employed the E68A mutation in heterodimers in which the two subunits are linked as previously described (Simoncsits, et al., 2001) to avoid the problem of the subunit exchange without tagging the protein with affinity chromatography tags.

4.4.2 The “metal free” E68A subunit

In the analysis of the behavior of the WT|E68A-SC PvuII heterodimers, the E68A subunit is assumed to be metal free. The investigation of the binding of Ca^{2+} ions to the WT|E68A-SC variant, considering the ligation of one or two metal ions to the E68A

subunit, did not return values of physiological significance for the affinities of these potential metal binding sites. The Mg^{2+} binding constant to the E68A subunit in the case of the E68A PvuII homodimer was previously measured by ^{25}Mg NMR to be at 40 mM (Dupureur, et al., 2000). Following these observations, the metal stoichiometry in the sequential scheme of the binding of Ca^{2+} ions and DNA in the case of the WT|E68A-SC variant (**Scheme 4.1**) refers to the WT subunit of the heterodimer only. The activity of the E68A monomer cannot be qualitatively associated with the phosphodiester cleavage performed by the WT subunit. The active site is not the same, and thus the mechanism may be different. Control experiments using the E68A homodimer are useful in considering the extent of the residual activity resulting from the binding of Mg^{2+} ions to the E68A variant. It has been previously shown that the E68A homodimer retains about 2.6% of the WT activity towards λ DNA (Dupureur, et al., 2000). However, in the case of the WT|E68A-SC heterodimers where the E68A subunit is participating, there cannot be a precise attribute of activity to the single E68A subunit resulting from rates observed for a E68A homodimer. This is especially true in the case of a plasmid where the two strands are cleaved sequentially and the initial orientation of the dimer bound to the duplex is important.

Assuming the Mg^{2+} binding constant to the E68A subunit under the single turnover conditions to be equal to 40 mM as in the absence of DNA (Dupureur, et al., 2000), then the fraction of the E68A subunits filled with one or two Mg^{2+} ions are as shown in (**Table 4.7**). At 0.5 and 10 mM Mg^{2+} there are 1.2 and 20% respectively of the 2 μ M E68A subunits (in 2 μ M WT|E68A-SC dimers) occupied by one Mg^{2+} ion. Regarding the E68A monomer as catalytically active when filled with one Mg^{2+} ion, then

Table 4.7 The metal saturation of the E68A subunit in the E68A homodimers.

Fraction (%) of E68A subunits filled with metal ions		
[Mg], mM	One Mg²⁺ ion (EM)	Two Mg²⁺ ions(EM₂)
0.5	1.2	0.016
10	19.9	5.9

The fractions (%) of E68A monomers EM(or EM₂)/E_{total} are shown, where EM (or EM₂) is the concentration of the E68A subunit occupied by one or two metal ions. The Mg²⁺ binding constant was applied at 40mM.

1.2% of the activity of the heterodimer at 0.5 mM (in either of the two sequential steps) is due to the E68A monomer and can be neglected. In the case of 10 mM Mg^{2+} though, when the activity of the heterodimer is higher, the fraction of E68A with one Mg^{2+} ion is at 20% and should not be neglected. However, in the case of each E68A subunit filled with two Mg^{2+} ions, the fractions of monomers are significantly lower: 0.016 and 5.9% at 0.5 and 10 mM Mg^{2+} respectively. It occurs then, in the reaction mixture at 10 mM Mg^{2+} , that 1.48 μM of the 2 μM of E68A monomers would be metal free, 0.4 μM should be occupied by one Mg^{2+} ion and the remaining 0.12 μM by two Mg^{2+} ions. Similar fractions are calculated for 4 μM monomers of E68A (i.e. 2 μM dimers of the E68A homodimer). If both the one and two metal occupied E68A subunits are considered to be contributing to the overall activity observed, then about 26% of the activity of the WT homodimer should be expected for the E68A heterodimer (assuming that a given concentration of metal saturated WT or E68A homodimers result in the same activity). However as previously stated the E68A homodimer has shown only 2.6% of the WT homodimer activity (on λ DNA) (Dupureur, et al., 2000), which is even lower than the 6% of the WT homodimer activity predicted for E68A with two Mg^{2+} ions. Accordingly, the observed rates suggest that either the Mg^{2+} binding constant in the presence of DNA is weaker than 40 mM for the E68A (though unlikely, see below), and/or the fractionation of E68A subunits with Mg^{2+} ions does not directly reflect the activity of the metal occupied subunits. In either case, it can be stated for WT|E68A-SC PvuII that the observed rates as a function of the Mg^{2+} concentration under single turnover conditions are not affected by the partial filling of the E68A subunit with metal ions (one or two). Consequently, the metal dependence observed in the plasmid cleavage rates involves

solely the metal occupancy of the active WT subunit of the WT|E68A-SC heterodimer and its effect on the activity of the enzyme.

Regarding the conformation of the active site of PvuII, it has been shown in the crystal structure of the WT enzyme in the presence of cognate DNA only ((Horton, et al., 1998) pdb:2PVI) that four water molecules form a hydrogen bonding network, three of which are within hydrogen bonding distance from the carboxylic oxygen atoms of Glu68 (**a.** 3.16 Å from Oε2, **b.** 2.87 Å from Oε2 and **c.** 3.21 Å from Oε1) (**Fig. 4.14**). The first two water molecules (a and b) are hydrogen bonded to the C(+1) and to the C(+1) and T(+2) respectively. The abolishment of this hydrogen bond network along with the lost coordination of the metal ions to the Glu68 carboxylate would result in the adoption of an overall different conformation of the active site compared to the WT PvuII. In this rearranged conformation though, in contrast to the DNA free conditions (for which the Mg²⁺ binding constant at 40 mM is measured), there are more ligands available to the metal ions. As it has been shown in the presence of cognate DNA and Ca²⁺ ions (Horton, et al., 2000), other possible ligation sites would include the oxygen O2P and an altered in this case but still possible hydrogen bond network formed by water molecules positioned by the DNA. Overall there are more sites for the Mg²⁺ ions to be ligated in the presence of DNA rather than in its absence, which would not favor the hypothesis that the binding constant for the Mg²⁺ ions might be weaker than 40 mM in the activity assays. An important aspect of the properties of the E68A subunit contributing to the DNA binding and cleavage performed by the WT|E68A-SC heterodimer is the distinct conformation and greater stability relative to the WT subunit. In ¹H-¹⁵N HSQC spectra obtained for the apo-E68A homodimer, the crosspeaks of the variant were perturbed compared to the WT

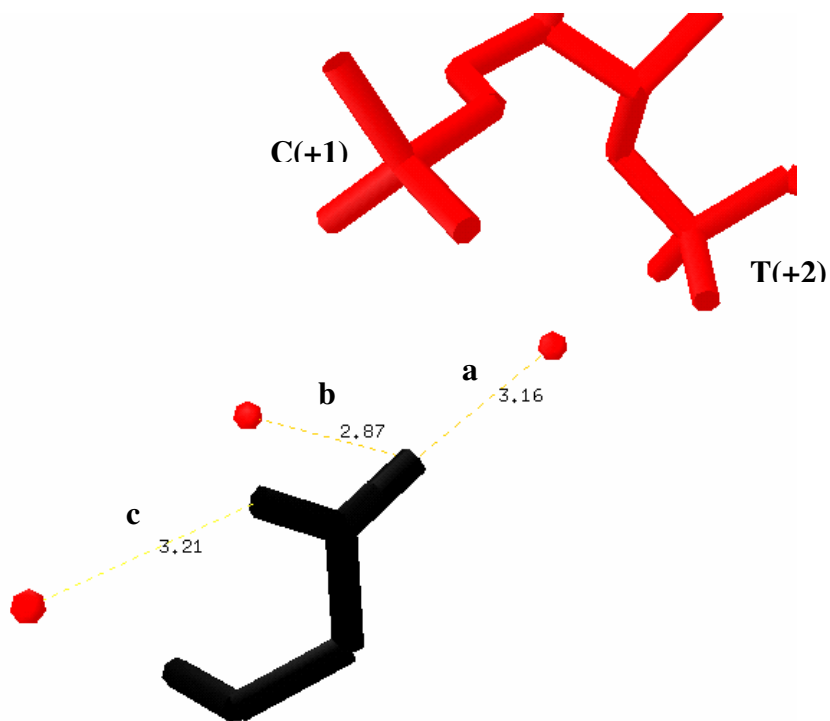


Figure 4.14 The environment of the Glu68 side chain in the WT PvuII complex with cognate DNA (pdb 2PVI) (Horton, et al., 1998). The relative positions of the water molecules in the hydrogen bond network are shown with a, b and c denoting the distances from the carboxylate oxygen atoms of Glu68 according to the text. The proximity of the backbone phosphate groups of the scissile C(+1) and T(+2) bases to the water molecules is also presented.

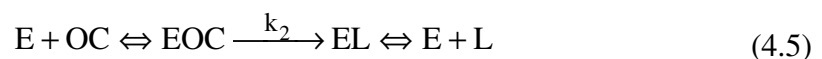
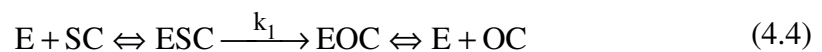
PvuII as demonstrated by the reduced spectral overlap between the two PvuII variants (Dupureur, et al., 2001). It was thus demonstrated that a conformation distinct to some extent from the WT PvuII is adopted by the E68A homodimer. In addition the chemical denaturation of the E68A variant at different pH values indicated that the removal of the side chain of Glu68 and its substitution by the non-polar Ala leads to greater conformational stability compared to the WT PvuII. It is evident that the electrostatic repulsion within the PvuII active site to which the Glu68 contributes is relieved at the substitution of the amino acid (Dupureur, et al., 2001)g. Due to these observations for the E68A homodimer, it may be assumed that the E68A subunit influences the folding and/or conformation of the WT|E68A-SC heterodimer in a manner that the non-metal mediated for the reduced affinity of the heterodimer to DNA, observed in the absence of Ca^{2+} ions compared to the WT-SC PvuII.

4.4.3 The nicking activity of the WT-SC PvuII

In the case of PvuII, the WT homodimer has been employed in plasmid cleavage experiments under steady state conditions (Spyridaki, et al., 2003) in which it has been shown that the cleavage has been concerted (the second strand is cleaved faster than the release of the nicked intermediate) and there is no nicking observed even at 5 mM Mg^{2+} . However, it is stated that at lower Mg^{2+} concentrations, the lower saturation of the monomers by metal ions leads to the loss of cleavage coordination by the subunits as mentioned above. Essentially the rates under steady state conditions observed by the disappearance of the supercoiled DNA at different Mg^{2+} concentrations led to the assumption that the cleavage of the duplex plasmid is dependent on four metal ions per

enzyme dimer (Spyridaki, et al., 2003). However in addition to the quantification of the supercoiled DNA, the measurement should involve the observed nicking rate at low metal concentrations which was quantitatively ignored. Essentially the measured rates involved the cleavage of the first strand only at low Mg^{2+} and the concerted linearization at high Mg^{2+} . In the current study, the nicking behavior under single turnover conditions is observed in the presence of either one or two active subunits at both high and low Mg^{2+} concentrations. The WT-SC PvuII shows significant accumulation of the nicked intermediate at all metal concentrations applied, which implies that either the linker affects the observed rates or the occupation by Mg^{2+} ions is not similar to the WT PvuII or does not lead to the same level of activity. It has to be noted that the activity on a contacts of the PvuII subunit to the DNA are perturbed. This may be the reason double stranded substrate by a functional dimer does not involve any other intermediate steps under the examined conditions. It may thus be concluded that unless the restrained conformation of the WT-SC (due to the linker) is involved in the observed rates, the cleavage activity might not be dependent on four metal ions as previously shown for the native WT PvuII.

The reaction scheme in **Fig. 2.6** to which the data are fitted is the form of the overall reaction model, which was deemed redundant under the reaction conditions. In such a model, the association and dissociation of the enzyme dimers should be taken into account as described in **Eq. 4.4-4.5**. The sequential independent events of cleavage of



(SC being the supercoiled plasmid, OC the open circles and L the linearized plasmid) each strand are preceded by the association and dissociation events whose rates would slow down the cleavage and thus the observed rates of product formation would not represent the chemistry steps (described by the rates k_1 and k_2). The large excess of the enzyme over the DNA in the case of the WT-SC variant ensures that the cleavage of the first strand does not depend on the association rate of the enzyme. As the enzyme has two functional subunits, it probably does not dissociate in order for the nicked intermediate to be linearized. The appearance of the intermediate at least at low metal concentrations shows that the orchestration of the cleavage events is indeed dependent on the metal ion concentration and the simultaneous metal saturation of both active sites. Similarly applied in the case of HhaII and EcoRI homodimers (Kaddurah-Daouk, et al., 1985; King, et al., 1989) the model described by **Eq. 4.4-4.5** may be reduced to **Eq. 2.14-2.16** to provide the rates k_1 and k_2 . In the case of the WTIE68A-SC variant, the cleavage of the first strand as in the case of the WT-SC, is observed due to the large enzyme excess over the DNA which renders the cleavage rate independent of the DNA association rate. However, carrying a single functional subunit, the heterodimer has to dissociate from the nicked substrate to allow for the intact DNA strand to become available for cleavage. A second enzyme dimer with the correct orientation of the single WT subunit has to be applied to the scissile site. As it is evident the rates of dissociation of OC and its re-association to enzyme (**Eq. 4.4** and **4.5** respectively) may limit the observed rate for the linearization step (k_2). Assuming that the enzyme concentration is sufficiently larger than the DNA sites, there should be an abundance of WTIE68A-SC dimers associated at non-specific sites in close distance to the nicked PvuII site of Litmus

28i. Alternatively, several enzyme dimers should be bound at more distant non-specific sites, which however may have a potential to reach the scissile site through a DNA loop. The 2,823 bp size of Litmus 28i allows for this to occur as two remote sites may be located at a distance greater than the 400bp threshold necessary for the thermally induced bending to occur (Halford, et al., 2004). Three potential mechanisms have been proposed for the facilitated diffusion of the DNA binding proteins to their cognate sites. The one dimensional diffusion (sliding) of the protein to the target site might be occurring, while the protein might also be associating and dissociating from non-cognate sites of relevant sequence (hopping), either simultaneously or independently of sliding until the target site is reached (von Hippel, et al., 1989; Halford, et al., 2004). In a third scenario a remote non-cognate site bearing a protein molecule might be juxtaposed towards the specific site through a loop created by the polynucleotide chain between the two sites (intersegmental transfer) (von Hippel, et al., 1989). It has been previously estimated that the association of the Lac repressor to its operator site occurs at a rate of $5 \times 10^{10} \text{ M}^{-1}\text{s}^{-1}$ (Riggs, et al., 1970; Hsieh, et al., 1997) which has also been the case for the Gal repressor-operator association (Hsieh, et al., 1997). However it has been shown in several other DNA binding proteins by measurement of their association rates to plasmid molecules by methods sensitive to the facilitated diffusion that the DNA association occurs at $\sim 3 \times 10^8 \text{ M}^{-1}\text{s}^{-1}$ (Halford, et al., 2004). Assuming that the WTIE68A-SC plasmid association rate is between $3 \times 10^8 \text{ M}^{-1}\text{s}^{-1}$ and $5 \times 10^{10} \text{ M}^{-1}\text{s}^{-1}$ it follows that the applied single turnover conditions ensure the facilitated diffusion of a second enzyme heterodimer properly oriented to the nicked scissile site at a rate that does not limit the linearization rate. It is practically inferred that as soon as the first strand cleavage occurs, the nicking enzyme

dimer is instantaneously replaced by the linearizing dimer. The model described by **Eq. 2.14-2.16** is thus justified in the case of both the WT/E68A-SC heterodimer and the WT-SC homodimer.

4.4.4 Energetics of the interaction of the SC PvuII variants with Ca^{2+} and cognate DNA

The GSGG linker introduced to connect the two PvuII subunits affects the conformation of the apo-single chain variants but as originally designed, the imposed perturbation is minimal (**Fig. 4.11**). However, the outcome of this perturbation is clearly reflected in the DNA binding properties of the native and single chain WT homodimers, as shown by their DNA binding affinities (**Table 4.4** and **Fig. 4.5**). Similar minimal influence of the perturbation imposed by the linker on the DNA binding and cleavage properties of the WT-SC variant have also been presented before (Simoncsits, et al., 2001). The restriction introduced in the overall dimer conformation by fixing the two subunits at 12 Å probably reduces the extent of the conformational space for the single chain PvuII variants, thus not allowing enough flexibility to scan a series of conformations in the presence of DNA. In essence, the introduction of the linker probably affects the dynamics of the dimer and subsequently the formed contacts to the DNA (leading to complexes of distinct stability), but not the absolute conformation of the enzyme. The combination of the WT subunit with the metal free E68A subunit resulted in a distinct profile for the Ca^{2+} dependence of the DNA binding from the WT-SC PvuII. Through calorimetric titrations the Ca^{2+} binding behavior to one or a pair of WT subunits was found to be negatively cooperative for the second metal equivalent. This correlates with the observation of the Ca^{2+} ions within 4 Å in the active site of PvuII (**Fig. 3.1**),

which would make the electrostatic repulsion due to the high ionic radius of the ion quite significant for the second equivalent. Thus as expected, the ligation of a second equivalent and the formation of the binuclear complex is not favored and this also holds in the case of two metal ions (with identical binding constants) binding simultaneously to a dimer of WT subunits. In addition to the observation of the Ca^{2+} -DNA-PvuII co-crystal structure, the primarily electrostatic character of the occupation of the active site has previously been shown through the large positive entropy change at the binding of Mn^{2+} and Co^{2+} ions in other nucleases (Zheng, et al., 2002; Feng, et al., 2004). The extent of the inhibition however is different in the two cases (with one or two functional WT subunits). In the case of a single functional WT subunit, the interaction energy is found at +1.6 kcal/mole, while +0.4 kcal/mole is the interaction energy between the two sets of sites in the presence of two functional WT subunits. It may thus be assumed that the presence of the second subunit and the communication of the metal sites across the subunits induces a conformational signal relieving the intrinsically anti-cooperative interaction within the PvuII active site.

The global analysis of the Ca^{2+} dependent DNA binding data provided the individual binding constants for each metal equivalent in the presence of DNA and also for each DNA equivalent to every metal loaded enzyme species. Unlike the formation of the binuclear metal complex and the antagonistic behavior of the metal ions, in the case of both the WT-SC and WT E68A-SC PvuII, the metal ions (present in only one or both subunits) facilitate the complexation of the enzyme to DNA. This synergistic effect is evident for both one and two metal equivalents in each WT subunit and more pronounced in the case of a single functional subunit. This indicates the dependence of the DNA

binding on the number of metal equivalents within a single subunit (32 and 12-fold affinity increase for the WT|E68A-SC vs 6 and 2-fold increase for the WT-SC at the subsequent metal ion equivalent per subunit). Despite the extensive synergy observed in the presence of one functional subunit, in the presence of a second metal loaded subunit the affinity to DNA is much higher (**Fig. 4.9**). A second WT subunit doubles the interactions of the enzyme active site with the DNA, contributing significantly to the stabilization of the corresponding complexes with one or two metal ions per subunit. The PvuII active site interactions with the DNA (**Fig. 3.1**) are thus shown to be of special importance in the context of all the contacts that are accomplished between the two macromolecules. From the co-crystal structures of the native WT PvuII in the absence and presence of Ca^{2+} ions (overlaid in **Fig 4.15**), it is evident that the overall fold and conformation of the dimer is identical in the absence and presence of Ca^{2+} ions. Assuming that all the essential contacts of the dimer with the DNA duplex are identically completed in both cases, the only missing contact in the absence of the metal ions is the bridging of the two metal centers by the scissile phosphate. Since the presence of the linker would introduce an identical restriction on the conformation of both the WT-SC homodimer and the WT|E68A-SC heterodimer, the same effect should be expected in the case of the single-chain variants. The duplication of the active site PvuII-metal ions-DNA interaction in the case of the WT-SC is thus the most probable explanation for the enhancement of the DNA affinity in the presence of metal ions compared to the half functional heterodimer. Further support for the significance of this interaction is provided by the DNA binding behavior of the E68A homodimer and its impaired DNA binding even at metal saturating conditions (**Fig. 4.5**) where the metal mediated contacts

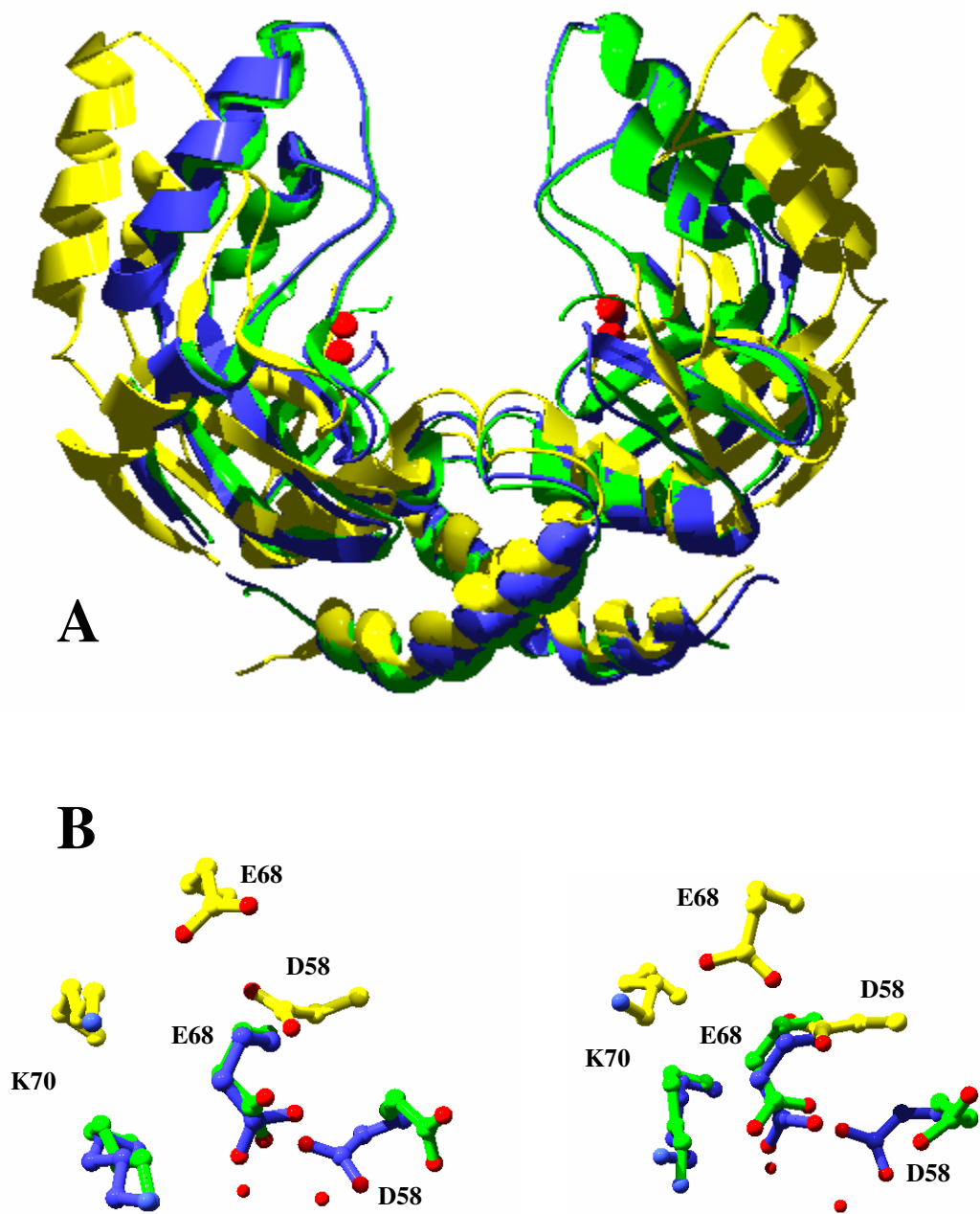


Figure 4.15 Superposition of the structures of the WT PvuII under different complexation states: apo-enzyme (*yellow*), in the presence of cognate DNA (*green*) and in the presence of Ca²⁺ ions and cognate DNA (*blue*) (pdb: 1PVU, 1PVI, 1F0O, respectively). A. The entire PvuII dimers (the DNA is omitted for clarity). B. The active site residues Asp58, Glu68 and Lys70 in the two enzyme subunits (*left and right*). The two Ca²⁺ ions (*red spheres*) from the 1F0O structure are included in A and B.

to the DNA within the active site (**Fig. 3.1**) have failed.

The impact of the presence of the DNA on the ligation of metal ions is also observed but not as dramatic as the effect of the metal ions on the DNA complexation. In both the WT|E68A-SC and the WT-SC the affinities of the ED complex for the first and second metal equivalents are increased compared to the corresponding binding constants in the DNA free enzyme. Again this is more pronounced for a single WT subunit and less significant in the case of the WT-SC. However negative cooperativity is also observed between the sites (or sets of sites) in this case. With +1.0 and +0.9 kcal/mole interaction energies between the two sites within the subunit and the two sets of sites, respectively, it is seen that the anti-cooperative effect of the electrostatics prevails in the presence of DNA as well. The presence of one or two subunits though does not make a difference to the unfavorable site interaction.

Taking a further step in characterizing the unfavorable ligation of a second metal equivalent or pair of metal ions, the exploration of the inter-subunit and intra-subunit contributions to the observed $\Delta G^{\circ}_{\text{coop}}$ for the WT-SC was attempted. Interestingly, the application of the corresponding $\Delta G^{\circ}_{\text{coop}}$ obtained by the WT|E68A-SC as the intra-subunit interaction energy revealed the favored inter-subunit communication among four metal ions within a WT-SC homodimer. In the absence of DNA, the $\Delta G^{\circ}_{\text{inter}}$ was found equal to -2.8 kcal/mole (**Fig. 4.10**), while in the presence of DNA a value of -1.1 kcal/mole was estimated. The magnitudes of the estimated interaction energies (intra and inter-subunit) in the absence of DNA are in agreement with the reported 0.9 kcal/mole cooperativity value in the case of the Ca^{2+} sites in oncomodulin (Henzl, et al., 1998), the -1.84 kcal/mole value in calbindin D_{9k} (Linse, et al., 1991), and the -0.93 and -2.22

kcal/mole for the two pairs of Ca^{2+} sites in calmodulin (Waltersson, et al., 1993). It has to be noted however that the latter three proteins do not form binuclear metal complexes like that exhibited in the active site of PvuII, which most probably contributes to rendering these interactions positive.

In this manner it is demonstrated that the two WT-SC PvuII subunits interact appropriately, after having ligated a single metal ion per subunit, and a signal is transmitted to the active sites favoring the ligation of a second metal ion. The extent of this positive interaction is larger in the absence of DNA (-2.8 kcal/mole) but also more dramatically reduced than in the presence of DNA (+0.4 vs +0.9 kcal/mole overall interaction energy in the absence and presence of DNA, respectively). This is due to the larger intra-subunit interaction energy in the presence of DNA (+1.6 kcal/mole) than in absence of DNA (+1.0 kcal/mole), which is doubled for the two sets of sites in the case of the WT-SC. This facilitating action of the inter-subunit communication is overcome by the large positive charge encountered by the second metal ion within the active site and as such the observed interaction is still unfavorable. It is thus concluded that the electrostatic repulsion of the two metal ions in the binuclear complex has a major impact which cannot be competed by any conformational change triggered either by the ligation of the first metal equivalent or the binding of DNA. In particular, the binding of DNA on one hand partially relieves this unfavorable effect between the two metal ions within the active site (+1.6 vs +1.0 kcal/mole per metal equivalent in the absence and presence of DNA, respectively). On the other hand, the DNA weakens the positive interaction across the two subunits (-2.8 vs -1.2 kcal/mole in the absence and presence of DNA). The net result is that the binding of the second metal equivalent becomes more unfavorable by 0.5

kcal/mole in the presence of DNA rather than in its absence. The conformational change in the overall structure of the native WT PvuII has been shown to be dramatic at the addition of DNA in the presence of Ca^{2+} ions while the backbone impact of Ca^{2+} ions to the apo-enzyme is also significant (Dupureur 2005). The inspection of the structure of the native WT PvuII active site residues at different metal and DNA complexed states provides an insight to the conformational outcome of the metal site interactions (**Fig. 4.15B**). It is noted that the correlation of any active site conformational changes with the binding of Ca^{2+} ions is hampered by the lack of a PvuII crystal structure in the presence of Ca^{2+} ions only. Although the exact conformational impact is not available, the fact that the backbone is perturbed at the binding of Ca^{2+} to the apo-enzyme shows that the inter-subunit energy estimated above translates in a structural alteration of the enzyme dimer. This alteration mediates the transmission of the signal among the side chains of the active site amino acids across the subunits affecting the metal ligation. The DNA binding cleft closes and encircles the DNA repositioning the whole PvuII active site irrespective of the presence of metal ions (**Fig. 4.15A**). The presence of Ca^{2+} leads to the orientation of the Asp58 carboxylate towards the pair of metal ions (in symmetry across the subunits), which is not observed in the case of metal free PvuII-DNA complex. The side chains of the remaining two residues Glu68 and Lys70 are appropriately positioned (also symmetrically) even in the absence of metal ions (**Fig. 4.15B**). The large conformational impact of the DNA on the active site of PvuII further supports the implication of the DNA in the ligation of the metal ions, the perturbation of their interaction and the energy by which this is represented. Similar alteration of the extent of cooperativity between Ca^{2+} sites in the presence of the substrate or an additive group is

the case of recoverin, an EF-hand protein in which the myristoyl moiety attached to the N-terminus induces the cooperative binding of Ca^{2+} in the otherwise independent binding sites (Ames, et al., 1995). In the scallop heavy meromyosin, the presence of ADP (substrate to the ATPase activity of the protein) induced the cooperative binding of Ca^{2+} ions (Kalabokis, et al., 1997). In the case of the extracellular EF-hands of the BM40 protein, it has been shown that the interactions between the several domains of the protein induce conformational changes that lead to the variation of the coupling energy between the Ca^{2+} sites from -2.1 to -4.4 kcal/mole (Busch, et al., 2000).

In the event of the availability solely of macroscopic data for a ligand binding interaction, the only achievable approach of the interaction energy is to assume that the two intrinsic binding constants (as denoted in **Scheme 4.2** for both variants) are equivalent. Although this might not be the case, the estimation of the coupling free energy provides the lowest limit of the interaction energy among the sites or sets of sites (Forsen, et al., 1995). The examination of macroscopic binding constants may be misleading in the exploration of the mode of cooperativity among two sites (Di Cera 1998). For example, the macroscopic binding constants may indicate the presence of positive cooperativity, although in reality a negative interaction might be present if the site-specific binding constants are examined. However the approach of calculating the free energy difference between the two states in the presence and absence of ligand in one of the interacting sites leads to an estimation of the increase or decrease of the affinity for a specific site without necessitating the measurement of site-specific binding constants (i.e. the ratio K_{ab}/K_b in **Scheme 4.2** may be calculated). Taking into account the equivalency of K_a and K_b as assumed in order to extract the $\Delta G^{\circ}_{\text{coop}}$ in each case, the

impact of the site-site interaction on the site-specific binding constants may be explored. Within this context, a 17-fold decrease of the binding constant for a single metal ion within the WT subunit of the WT-SC PvuII is observed in the absence of DNA and a 6-fold decrease in the presence of DNA. For a set of two sites the corresponding site-specific decreases in affinity are 2-fold and 5-fold respectively.

In conclusion through the quantification of the metal and DNA binding constants and also of the interaction energies among the metal binding sites of the PvuII endonuclease, it is demonstrated that the synergistic effect observed in the association of PvuII with DNA is dominated by the promotion of the DNA binding by the Ca^{2+} ions rather than the binding of Ca^{2+} ions being promoted by the DNA. Although the affinity for Ca^{2+} ions increases in the presence of DNA the metal site interactions remain unfavorable as in the absence of the substrate. The exact conformational impact on the PvuII structure attributed to the calculated energies would be of particular challenge.

REFERENCES

- Adelberg, E. A. and Umberger, H. E. (1953). "Isoleucine and valine metabolism in *Escherichia coli*. V. alpha-Ketoisovaleric acid accumulation." *J Biol Chem* 205: 475-82.
- Ames, J. B., Porumb, T., Tanaka, T., Ikura, M. and Stryer, L. (1995). "Amino-terminal myristoylation induces cooperative calcium binding to recoverin." *J Biol Chem* 270: 4526-33.
- Athanasiadis, A., Vlassi, M., Kotsifaki, D., Tucker, P. A., Wilson, K. S. and Kokkinidis, M. (1994). "Crystal structure of PvuII endonuclease reveals extensive structural homologies to EcoRV." *Nat Struct Biol* 1: 469-75.
- Bahar, I., Chennubhotla, C. and Tobi, D. (2007). "Intrinsic dynamics of enzymes in the unbound state and relation to allosteric regulation." *Curr Opin Struct Biol* 17: 633-40.
- Balendiran, K., Bonventre, J., Knott, R., Jack, W., Benner, J., Schildkraut, I. and Anderson, J. E. (1994). "Expression, purification, and crystallization of restriction endonuclease PvuII with DNA containing its recognition site." *Proteins* 19: 77-9.
- Beechem, J. M. (1992). "Global analysis of biochemical and biophysical data." *Methods Enzymol* 210: 37-54.
- Bennett, S. P. and Halford, S. E. (1989). "Recognition of DNA by type II restriction enzymes." *Curr Top Cell Regul* 30: 57-104.
- Bhat, M. G., Ganley, L. M., Ledman, D. W., Goodman, M. A. and Fox, R. O. (1997). "Stability studies of amino acid substitutions at tyrosine 27 of the staphylococcal nuclease beta-barrel." *Biochemistry* 36: 12167-74.
- Bird, R. E., Hardman, K. D., Jacobson, J. W., Johnson, S., Kaufman, B. M., Lee, S. M., Lee, T., Pope, S. H., Riordan, G. S. and Whitlow, M. (1988). "Single-chain antigen-binding proteins." *Science* 242: 423-6.
- Boros, I., Lukacsovich, T., Baliko, G. and Venetianer, P. (1986). "Expression vectors based on the *rac* fusion promoter." *Gene* 42: 97-100.
- Bowen, L. M. and Dupureur, C. M. (2003). "Investigation of restriction enzyme cofactor requirements: a relationship between metal ion properties and sequence specificity." *Biochemistry* 42: 12643-53.
- Bowen, L. M., Muller, G., Riehl, J. P. and Dupureur, C. M. (2004). "Lanthanide spectroscopic studies of the dinuclear and Mg(II)-dependent PvuII restriction endonuclease." *Biochemistry* 43: 15286-95.
- Bray, D. and Duke, T. (2004). "Conformational spread: the propagation of allosteric states in large multiprotein complexes." *Annu Rev Biophys Biomol Struct* 33: 53-73.
- Brent, R. and Ptashne, M. (1985). "A eukaryotic transcriptional activator bearing the DNA specificity of a prokaryotic repressor." *Cell* 43: 729-36.
- Busch, E., Hohenester, E., Timpl, R., Paulsson, M. and Maurer, P. (2000). "Calcium affinity, cooperativity, and domain interactions of extracellular EF-hands present in BM-40." *J Biol Chem* 275: 25508-15.
- Cheng, X., Balendiran, K., Schildkraut, I. and Anderson, J. E. (1994). "Structure of PvuII endonuclease with cognate DNA." *Embo J* 13: 3927-35.

- Cheng, X., Gonzalez, M. L. and Lee, J. C. (1993). "Energetics of intersubunit and intrasubunit interactions of Escherichia coli adenosine cyclic 3',5'-phosphate receptor protein." *Biochemistry* 32: 8130-9.
- Colandene, J. D. and Topal, M. D. (1998). "The domain organization of NaeI endonuclease: separation of binding and catalysis." *Proc Natl Acad Sci U S A* 95: 3531-6.
- Conlan, L. H. and Dupureur, C. M. (2002). "Dissecting the metal ion dependence of DNA binding by PvuII endonuclease." *Biochemistry* 41: 1335-42.
- Conlan, L. H. and Dupureur, C. M. (2002). "Multiple metal ions drive DNA association by PvuII endonuclease." *Biochemistry* 41: 14848-55.
- Conrad, M. and Topal, M. D. (1989). "DNA and spermidine provide a switch mechanism to regulate the activity of restriction enzyme Nae I." *Proc Natl Acad Sci U S A* 86: 9707-11.
- Cowan, J. A. (1998). "Metal Activation of Enzymes in Nucleic Acid Biochemistry." *Chem Rev* 98: 1067-1088.
- Deibert, M., Grazulis, S., Janulaitis, A., Siksnys, V. and Huber, R. (1999). "Crystal structure of MunI restriction endonuclease in complex with cognate DNA at 1.7 Å resolution." *Embo J* 18: 5805-16.
- Di Cera, E. (1998). "Site-Specific Thermodynamics: Understanding Cooperativity in Molecular Recognition." *Chem Rev* 98: 1563-1592.
- Dorner, L. F. and Schildkraut, I. (1994). "Direct selection of binding proficient/catalytic deficient variants of BamHI endonuclease." *Nucleic Acids Res* 22: 1068-74.
- Dupureur, C. M. (1999). "Metal ion-dependent DNA-induced conformational changes in PvuII restriction endonuclease." *SAAS Bull Biochem Biotechnol* 12: 43-47.
- Dupureur, C. M. (2005). "NMR studies of restriction enzyme-DNA interactions: role of conformation in sequence specificity." *Biochemistry* 44: 5065-74.
- Dupureur, C. M. and Conlan, L. H. (2000). "A catalytically deficient active site variant of PvuII endonuclease binds Mg(II) ions." *Biochemistry* 39: 10921-7.
- Dupureur, C. M. and Dominguez, M. A., Jr. (2001). "The PD...(D/E)XK motif in restriction enzymes: a link between function and conformation." *Biochemistry* 40: 387-94.
- Dupureur, C. M. and Hallman, L. M. (1999). "Effects of divalent metal ions on the activity and conformation of native and 3-fluorotyrosine-PvuII endonucleases." *Eur J Biochem* 261: 261-8.
- Engler, L. E., Sapienza, P., Dorner, L. F., Kucera, R., Schildkraut, I. and Jen-Jacobson, L. (2001). "The energetics of the interaction of BamHI endonuclease with its recognition site GGATCC." *J Mol Biol* 307: 619-36.
- Engler, L. E., Welch, K. K. and Jen-Jacobson, L. (1997). "Specific binding by EcoRV endonuclease to its DNA recognition site GATATC." *J Mol Biol* 269: 82-101.
- Feng, M., Patel, D., Dervan, J. J., Ceska, T., Suck, D., Haq, I. and Sayers, J. R. (2004). "Roles of divalent metal ions in flap endonuclease-substrate interactions." *Nat Struct Mol Biol* 11: 450-6.
- Forsen, S. and Linse, S. (1995). "Cooperativity: over the Hill." *Trends Biochem Sci* 20: 495-7.
- Fritz, J. S., Richard, M. J. and Karraker, S. K. (1958). "Potentiometric titrations with (ethylenedinitrilo)tetraacetate." *Analytical Chemistry* 30: 1347-50.

- Fuxreiter, M. and Simon, I. (2002). "Protein stability indicates divergent evolution of PD-(D/E)XK type II restriction endonucleases." *Protein Sci* 11: 1978-83.
- Gingeras, T. R., Greenough, L., Schildkraut, I. and Roberts, R. J. (1981). "Two new restriction endonucleases from *Proteus vulgaris*." *Nucleic Acids Res* 9: 4525-36.
- Gittelman, M. S. and Matthews, C. R. (1990). "Folding and stability of trp aporepressor from *Escherichia coli*." *Biochemistry* 29: 7011-20.
- Gormley, N. A., Bath, A. J. and Halford, S. E. (2000). "Reactions of BglII and other type II restriction endonucleases with discontinuous recognition sites." *J Biol Chem* 275: 6928-36.
- Groll, D. H., Jeltsch, A., Selent, U. and Pingoud, A. (1997). "Does the restriction endonuclease EcoRV employ a two-metal-ion mechanism for DNA cleavage?" *Biochemistry* 36: 11389-401.
- Gunasekaran, K., Ma, B. and Nussinov, R. (2004). "Is allostery an intrinsic property of all dynamic proteins?" *Proteins* 57: 433-43.
- Halford, S. E. and Goodall, A. J. (1988). "Modes of DNA cleavage by the EcoRV restriction endonuclease." *Biochemistry* 27: 1771-7.
- Halford, S. E. and Johnson, N. P. (1983). "Single turnovers of the EcoRI restriction endonuclease." *Biochem J* 211: 405-15.
- Halford, S. E. and Marko, J. F. (2004). "How do site-specific DNA-binding proteins find their targets?" *Nucleic Acids Res* 32: 3040-52.
- Hallewell, R. A., Laria, I., Tabrizi, A., Carlin, G., Getzoff, E. D., Tainer, J. A., Cousens, L. S. and Mullenbach, G. T. (1989). "Genetically engineered polymers of human CuZn superoxide dismutase. Biochemistry and serum half-lives." *J Biol Chem* 264: 5260-8.
- Henzl, M. T., Hapak, R. C. and Likos, J. J. (1998). "Interconversion of the ligand arrays in the CD and EF sites of oncomodulin. Influence on Ca²⁺-binding affinity." *Biochemistry* 37: 9101-11.
- Henzl, M. T., Larson, J. D. and Agah, S. (2003). "Estimation of parvalbumin Ca(2+)- and Mg(2+)-binding constants by global least-squares analysis of isothermal titration calorimetry data." *Anal Biochem* 319: 216-33.
- Hollis, M., Valenzuela, D., Pioli, D., Wharton, R. and Ptashne, M. (1988). "A repressor heterodimer binds to a chimeric operator." *Proc Natl Acad Sci U S A* 85: 5834-8.
- Horrocks, W. D., Jr. (1993). "Luminescence spectroscopy." *Methods Enzymol* 226: 495-538.
- Horton, J. R. and Cheng, X. (2000). "PvuII endonuclease contains two calcium ions in active sites." *J Mol Biol* 300: 1049-56.
- Horton, J. R., Nastri, H. G., Riggs, P. D. and Cheng, X. (1998). "Asp34 of PvuII endonuclease is directly involved in DNA minor groove recognition and indirectly involved in catalysis." *J Mol Biol* 284: 1491-504.
- Horton, N. C. and Perona, J. J. (1998). "Recognition of flanking DNA sequences by EcoRV endonuclease involves alternative patterns of water-mediated contacts." *J Biol Chem* 273: 21721-9.
- Hsieh, M. and Brenowitz, M. (1997). "Comparison of the DNA association kinetics of the Lac repressor tetramer, its dimeric mutant LacIadi, and the native dimeric Gal repressor." *J Biol Chem* 272: 22092-6.

- Hsu, M. and Berg, P. (1978). "Altering the specificity of restriction endonuclease: effect of replacing Mg²⁺ with Mn²⁺." *Biochemistry* 17: 131-38.
- Hu, J. C., O'Shea, E. K., Kim, P. S. and Sauer, R. T. (1990). "Sequence requirements for coiled-coils: analysis with lambda repressor-GCN4 leucine zipper fusions." *Science* 250: 1400-3.
- Huheey, J. E., Keiter, E. A. and Keiter, R. L. (1993). *Inorganic chemistry : principles of structure and reactivity*. New York, NY, HarperCollins College Publishers.
- Jack, W. E., Greenough, L., Dorner, L. F., Xu, S. Y., Strzelecka, T., Aggarwal, A. K. and Schildkraut, I. (1991). "Overexpression, purification and crystallization of BamHI endonuclease." *Nucleic Acids Res* 19: 1825-9.
- Jana, R., Hazbun, T. R., Fields, J. D. and Mossing, M. C. (1998). "Single-chain lambda Cro repressors confirm high intrinsic dimer-DNA affinity." *Biochemistry* 37: 6446-55.
- Jeltsch, A., Maschke, H., Selent, U., Wenz, C., Kohler, E., Connolly, B. A., Thorogood, H. and Pingoud, A. (1995). "DNA binding specificity of the EcoRV restriction endonuclease is increased by Mg²⁺ binding to a metal ion binding site distinct from the catalytic center of the enzyme." *Biochemistry* 34: 6239-46.
- Jen-Jacobson, L. (1997). "Protein-DNA recognition complexes: conservation of structure and binding energy in the transition state." *Biopolymers* 44: 153-80.
- Johnson, I. (1998). "Fluorescent probes for living cells." *Histochem J* 30: 123-40.
- Jose, T. J., Conlan, L. H. and Dupureur, C. M. (1999). "Quantitative evaluation of metal ion binding to PvuII restriction endonuclease." *J Biol Inorg Chem* 4: 814-23.
- Kaddurah-Daouk, R., Cho, P. and Smith, H. O. (1985). "Catalytic properties of the HhaII restriction endonuclease." *J Biol Chem* 260: 15345-51.
- Kalabokis, V. N. and Szent-Gyorgyi, A. G. (1997). "Cooperativity and regulation of scallop myosin and myosin fragments." *Biochemistry* 36: 15834-40.
- Kay, J., Moore, J. W. and Glick, M. D. (1972). "Structural studies of bridged lanthanide(III) complexes. Diaquotri(nicotinic acid)holmium(III) hexa(isothiocyanato)chromate(III) dihydrate and diaquotris(isonicotinato)lanthanum(III)." *Inorganic Chemistry* 11: 2818-27.
- Kim, Y. I. and Hu, J. C. (1995). "Operator binding by lambda repressor heterodimers with one or two N-terminal arms." *Proc Natl Acad Sci U S A* 92: 7510-4.
- King, K., Benkovic, S. J. and Modrich, P. (1989). "Glu-111 is required for activation of the DNA cleavage center of EcoRI endonuclease." *J Biol Chem* 264: 11807-15.
- Koshland, D. E. (1958). "Application of a Theory of Enzyme Specificity to Protein Synthesis." *Proc Natl Acad Sci U S A* 44: 98-104.
- Koshland, D. E., Jr. and Hamadani, K. (2002). "Proteomics and models for enzyme cooperativity." *J Biol Chem* 277: 46841-4.
- Koshland, D. E., Jr., Nemethy, G. and Filmer, D. (1966). "Comparison of experimental binding data and theoretical models in proteins containing subunits." *Biochemistry* 5: 365-85.
- Kostrewa, D. and Winkler, F. K. (1995). "Mg²⁺ binding to the active site of EcoRV endonuclease: a crystallographic study of complexes with substrate and product DNA at 2 Å resolution." *Biochemistry* 34: 683-96.

- Kozlov, A. G. and Lohman, T. M. (2006). "Effects of monovalent anions on a temperature-dependent heat capacity change for Escherichia coli SSB tetramer binding to single-stranded DNA." *Biochemistry* 45: 5190-205.
- Lagunavicius, A., Grazulis, S., Balciunaite, E., Vainius, D. and Siksnys, V. (1997). "DNA binding specificity of MunI restriction endonuclease is controlled by pH and calcium ions: involvement of active site carboxylate residues." *Biochemistry* 36: 11093-9.
- Lakowicz, J. R. (2006). *Principles of fluorescence spectroscopy*. New York, Springer.
- Li, H., Trotta, C. R. and Abelson, J. (1998). "Crystal structure and evolution of a transfer RNA splicing enzyme." *Science* 280: 279-84.
- Liang, H., Sandberg, W. S. and Terwilliger, T. C. (1993). "Genetic fusion of subunits of a dimeric protein substantially enhances its stability and rate of folding." *Proc Natl Acad Sci U S A* 90: 7010-4.
- Linse, S., Brodin, P., Drakenberg, T., Thulin, E., Sellers, P., Elmden, K., Grundstrom, T. and Forsen, S. (1987). "Structure-function relationships in EF-hand Ca²⁺-binding proteins. Protein engineering and biophysical studies of calbindin D9k." *Biochemistry* 26: 6723-35.
- Linse, S., Johansson, C., Brodin, P., Grundstrom, T., Drakenberg, T. and Forsen, S. (1991). "Electrostatic contributions to the binding of Ca²⁺ in calbindin D9k." *Biochemistry* 30: 154-62.
- Lukacs, C. M., Kucera, R., Schildkraut, I. and Aggarwal, A. K. (2000). "Understanding the immutability of restriction enzymes: crystal structure of BglII and its DNA substrate at 1.5 Å resolution." *Nat Struct Biol* 7: 134-40.
- Ma, B., Kumar, S., Tsai, C. J. and Nussinov, R. (1999). "Folding funnels and binding mechanisms." *Protein Eng* 12: 713-20.
- Maxwell, A. and Halford, S. E. (1982). "The SalGI restriction endonuclease. Mechanism of DNA cleavage." *Biochem J* 203: 85-92.
- Monod, J., Changeux, J. P. and Jacob, F. (1963). "Allosteric proteins and cellular control systems." *J Mol Biol* 6: 306-29.
- Mucke, M., Pingoud, V., Grelle, G., Kraft, R., Kruger, D. H. and Reuter, M. (2002). "Asymmetric photocross-linking pattern of restriction endonuclease EcoRII to the DNA recognition sequence." *J Biol Chem* 277: 14288-93.
- Nastri, H. G., Evans, P. D., Walker, I. H. and Riggs, P. D. (1997). "Catalytic and DNA binding properties of PvuII restriction endonuclease mutants." *J Biol Chem* 272: 25761-7.
- Neet, K. E. and Timm, D. E. (1994). "Conformational stability of dimeric proteins: quantitative studies by equilibrium denaturation." *Protein Sci* 3: 2167-74.
- Newman, M., Strzelecka, T., Dorner, L. F., Schildkraut, I. and Aggarwal, A. K. (1995). "Structure of Bam HI endonuclease bound to DNA: partial folding and unfolding on DNA binding." *Science* 269: 656-63.
- Nishino, T., Komori, K., Ishino, Y. and Morikawa, K. (2005). "Structural and functional analyses of an archaeal XPF/Rad1/Mus81 nuclease: asymmetric DNA binding and cleavage mechanisms." *Structure* 13: 1183-92.
- Nozaki, Y. (1972). "The preparation of guanidine hydrochloride." *Methods Enzymol* 26 PtC: 43-50.

- Oas, T. G., McIntosh, L. P., O'Shea, E. K., Dahlquist, F. W. and Kim, P. S. (1990). "Secondary structure of a leucine zipper determined by nuclear magnetic resonance spectroscopy." *Biochemistry* 29: 2891-4.
- Pace, C. N., Vajdos, F., Fee, L., Grimsley, G. and Gray, T. (1995). "How to measure and predict the molar absorption coefficient of a protein." *Protein Sci* 4: 2411-23.
- Pan, H., Lee, J. C. and Hilser, V. J. (2000). "Binding sites in Escherichia coli dihydrofolate reductase communicate by modulating the conformational ensemble." *Proc Natl Acad Sci U S A* 97: 12020-5.
- Pantoliano, M. W., Bird, R. E., Johnson, S., Asel, E. D., Dodd, S. W., Wood, J. F. and Hardman, K. D. (1991). "Conformational stability, folding, and ligand-binding affinity of single-chain Fv immunoglobulin fragments expressed in Escherichia coli." *Biochemistry* 30: 10117-25.
- Papadakos, G. A., Natri, H., Riggs, P. and Dupureur, C. M. (2007). "Uncoupling metallonuclease metal ion binding sites via nudge mutagenesis." *J Biol Inorg Chem* 12: 557-69.
- Pardee, A. B. and Yates, R. A. (1956). "Control of pyrimidine biosynthesis in Escherichia coli by a feed-back mechanism." *J Biol Chem* 221: 757-70.
- Percipalle, P., Simoncsits, A., Zakhariyev, S., Guarnaccia, C., Sanchez, R. and Pongor, S. (1995). "Rationally designed helix-turn-helix proteins and their conformational changes upon DNA binding." *Embo J* 14: 3200-5.
- Pingoud, A., Fuxreiter, M., Pingoud, V. and Wende, W. (2005). "Type II restriction endonucleases: structure and mechanism." *Cell Mol Life Sci* 62: 685-707.
- Pingoud, A. and Jeltsch, A. (2001). "Structure and function of type II restriction endonucleases." *Nucleic Acids Res* 29: 3705-27.
- Predki, P. F. and Regan, L. (1995). "Redesigning the topology of a four-helix-bundle protein: monomeric Rop." *Biochemistry* 34: 9834-9.
- Reuter, M., Schneider-Mergener, J., Kupper, D., Meisel, A., Mackeldanz, P., Kruger, D. H. and Schroeder, C. (1999). "Regions of endonuclease EcoRII involved in DNA target recognition identified by membrane-bound peptide repertoires." *J Biol Chem* 274: 5213-21.
- Riggs, A. D., Bourgeois, S. and Cohn, M. (1970). "The lac repressor-operator interaction. 3. Kinetic studies." *J Mol Biol* 53: 401-17.
- Roberts, E. L., Shu, N., Howard, M. J., Broadhurst, R. W., Chapman-Smith, A., Wallace, J. C., Morris, T., Cronan, J. E., Jr. and Perham, R. N. (1999). "Solution structures of apo and holo biotinyl domains from acetyl coenzyme A carboxylase of Escherichia coli determined by triple-resonance nuclear magnetic resonance spectroscopy." *Biochemistry* 38: 5045-53.
- Robinson, C. R. and Sauer, R. T. (1996). "Covalent attachment of Arc repressor subunits by a peptide linker enhances affinity for operator DNA." *Biochemistry* 35: 109-16.
- Robinson, C. R. and Sauer, R. T. (1996). "Equilibrium stability and sub-millisecond refolding of a designed single-chain Arc repressor." *Biochemistry* 35: 13878-84.
- Robinson, C. R. and Sauer, R. T. (1998). "Optimizing the stability of single-chain proteins by linker length and composition mutagenesis." *Proc Natl Acad Sci U S A* 95: 5929-34.

- Romier, C., Dominguez, R., Lahm, A., Dahl, O. and Suck, D. (1998). "Recognition of single-stranded DNA by nuclease P1: high resolution crystal structures of complexes with substrate analogs." *Proteins* 32: 414-24.
- Rule, G. S. and Hitchens, T. K. (2006). *Fundamentals of protein NMR spectroscopy*. Dordrecht, Springer.
- Sambrook, J., Maniatis, T. and Fritsch, E. F. (1989). *Molecular cloning : a laboratory manual*. Cold Spring Harbor, N.Y., Cold Spring Harbor Laboratory Press.
- Sasnauskas, G., Jeltsch, A., Pingoud, A. and Siksnys, V. (1999). "Plasmid DNA cleavage by MunI restriction enzyme: single-turnover and steady-state kinetic analysis." *Biochemistry* 38: 4028-36.
- Schmidt-Dorr, T., Oertel-Buchheit, P., Pernelle, C., Bracco, L., Schnarr, M. and Granger-Schnarr, M. (1991). "Construction, purification, and characterization of a hybrid protein comprising the DNA binding domain of the LexA repressor and the Jun leucine zipper: a circular dichroism and mutagenesis study." *Biochemistry* 30: 9657-64.
- Schulze, C., Jeltsch, A., Franke, I., Urbanke, C. and Pingoud, A. (1998). "Crosslinking the EcoRV restriction endonuclease across the DNA-binding site reveals transient intermediates and conformational changes of the enzyme during DNA binding and catalytic turnover." *Embo J* 17: 6757-66.
- Seeman, N. C., Rosenberg, J. M. and Rich, A. (1976). "Sequence-specific recognition of double helical nucleic acids by proteins." *Proc Natl Acad Sci U S A* 73: 804-8.
- Siksnys, V., Skirgaila, R., Sasnauskas, G., Urbanke, C., Cherny, D., Grazulis, S. and Huber, R. (1999). "The Cfr10I restriction enzyme is functional as a tetramer." *J Mol Biol* 291: 1105-18.
- Simoncsits, A., Bristulf, J., Tjornhammar, M. L., Cserzo, M., Pongor, S., Rybakina, E., Gatti, S. and Bartfai, T. (1994). "Deletion mutants of human interleukin 1 beta with significantly reduced agonist properties: search for the agonist/antagonist switch in ligands to the interleukin 1 receptors." *Cytokine* 6: 206-14.
- Simoncsits, A., Chen, J., Percipalle, P., Wang, S., Toro, I. and Pongor, S. (1997). "Single-chain repressors containing engineered DNA-binding domains of the phage 434 repressor recognize symmetric or asymmetric DNA operators." *J Mol Biol* 267: 118-31.
- Simoncsits, A., Tjornhammar, M. L., Kalman, M., Cserpan, I., Gafvelin, G. and Bartfai, T. (1988). "Synthesis, cloning and expression in Escherichia coli of artificial genes coding for biologically active elongated precursors of the vasoactive intestinal polypeptide." *Eur J Biochem* 178: 343-50.
- Simoncsits, A., Tjornhammar, M. L., Rasko, T., Kiss, A. and Pongor, S. (2001). "Covalent joining of the subunits of a homodimeric type II restriction endonuclease: single-chain PvuII endonuclease." *J Mol Biol* 309: 89-97.
- Sinha, S. P. and North Atlantic Treaty Organization. Scientific Affairs Division. (1983). *Systematics and the properties of the lanthanides*. Dordrecht ; Boston Hingham, MA, U.S.A., D. Reidel Pub. Co. ;
- Sold and distributed in the U.S.A. and Canada by Kluwer Academic Publishers.
- Spyridaki, A., Matzen, C., Lanio, T., Jeltsch, A., Simoncsits, A., Athanasiadis, A., Scheuring-Vanamee, E., Kokkinidis, M. and Pingoud, A. (2003). "Structural and

- biochemical characterization of a new Mg(2+) binding site near Tyr94 in the restriction endonuclease PvuII." *J Mol Biol* 331: 395-406.
- Sreedhara, A. and Cowan, J. A. (2001). "Catalytic hydrolysis of DNA by metal ions and complexes." *J Biol Inorg Chem* 6: 337-47.
- Stahl, F., Wende, W., Jeltsch, A. and Pingoud, A. (1996). "Introduction of asymmetry in the naturally symmetric restriction endonuclease EcoRV to investigate intersubunit communication in the homodimeric protein." *Proc Natl Acad Sci U S A* 93: 6175-80.
- Stahl, F., Wende, W., Jeltsch, A. and Pingoud, A. (1998). "The mechanism of DNA cleavage by the type II restriction enzyme EcoRV: Asp36 is not directly involved in DNA cleavage but serves to couple indirect readout to catalysis." *Biol Chem* 379: 467-73.
- Stahl, F., Wende, W., Wenz, C., Jeltsch, A. and Pingoud, A. (1998). "Intra- vs intersubunit communication in the homodimeric restriction enzyme EcoRV: Thr 37 and Lys 38 involved in indirect readout are only important for the catalytic activity of their own subunit." *Biochemistry* 37: 5682-8.
- Taylor, J. D., Badcoe, I. G., Clarke, A. R. and Halford, S. E. (1991). "EcoRV restriction endonuclease binds all DNA sequences with equal affinity." *Biochemistry* 30: 8743-53.
- Taylor, J. D. and Halford, S. E. (1989). "Discrimination between DNA sequences by the EcoRV restriction endonuclease." *Biochemistry* 28: 6198-207.
- Thielking, V., Selent, U., Kohler, E., Landgraf, A., Wolfes, H., Alves, J. and Pingoud, A. (1992). "Mg²⁺ confers DNA binding specificity to the EcoRV restriction endonuclease." *Biochemistry* 31: 3727-32.
- Toth, M. J. and Schimmel, P. (1986). "Internal structural features of E. coli glycyl-tRNA synthetase examined by subunit polypeptide chain fusions." *J Biol Chem* 261: 6643-6.
- Tsodikov, O. V., Enzlin, J. H., Scharer, O. D. and Ellenberger, T. (2005). "Crystal structure and DNA binding functions of ERCC1, a subunit of the DNA structure-specific endonuclease XPF-ERCC1." *Proc Natl Acad Sci U S A* 102: 11236-41.
- Venclovas, C., Timinskas, A. and Siksnys, V. (1994). "Five-stranded beta-sheet sandwiched with two alpha-helices: a structural link between restriction endonucleases EcoRI and EcoRV." *Proteins* 20: 279-82.
- Viadiu, H. and Aggarwal, A. K. (1998). "The role of metals in catalysis by the restriction endonuclease BamHI." *Nat Struct Biol* 5: 910-6.
- Vipond, I. B., Baldwin, G. S. and Halford, S. E. (1995). "Divalent metal ions at the active sites of the EcoRV and EcoRI restriction endonucleases." *Biochemistry* 34: 697-704.
- Vipond, I. B. and Halford, S. E. (1995). "Specific DNA recognition by EcoRV restriction endonuclease induced by calcium ions." *Biochemistry* 34: 1113-9.
- von Hippel, P. H. and Berg, O. G. (1989). "Facilitated target location in biological systems." *J Biol Chem* 264: 675-8.
- Waltersson, Y., Linse, S., Brodin, P. and Grundstrom, T. (1993). "Mutational effects on the cooperativity of Ca²⁺ binding in calmodulin." *Biochemistry* 32: 7866-71.
- Wang, C. K. and Cheung, H. C. (1985). "Energetics of the binding of calcium and troponin I to troponin C from rabbit skeletal muscle." *Biophys J* 48: 727-39.

- Weber, G. (1972). "Ligand binding and internal equilibria in proteins." *Biochemistry* 11: 864-78.
- Weber, G. (1975). "Energetics of ligand binding to proteins." *Adv Protein Chem* 29: 1-83.
- Weiss, J. N. (1997). "The Hill equation revisited: uses and misuses." *Faseb J* 11: 835-41.
- Wende, W., Stahl, F. and Pingoud, A. (1996). "The production and characterization of artificial heterodimers of the restriction endonuclease EcoRV." *Biol Chem* 377: 625-32.
- Wenz, C., Jeltsch, A. and Pingoud, A. (1996). "Probing the indirect readout of the restriction enzyme EcoRV. Mutational analysis of contacts to the DNA backbone." *J Biol Chem* 271: 5565-73.
- Wharton, R. P. and Ptashne, M. (1985). "Changing the binding specificity of a repressor by redesigning an alpha-helix." *Nature* 316: 601-5.
- Winkler, F. K., Banner, D. W., Oefner, C., Tsernoglou, D., Brown, R. S., Heathman, S. P., Bryan, R. K., Martin, P. D., Petratos, K. and Wilson, K. S. (1993). "The crystal structure of EcoRV endonuclease and of its complexes with cognate and non-cognate DNA fragments." *Embo J* 12: 1781-95.
- Wyman, J. and Gill, S. J. (1990). *Binding and linkage : functional chemistry of biological macromolecules*. Mill Valley, Calif., University Science Books.
- Zheng, L., Li, M., Shan, J., Krishnamoorthi, R. and Shen, B. (2002). "Distinct roles of two Mg²⁺ binding sites in regulation of murine flap endonuclease-1 activities." *Biochemistry* 41: 10323-31.
- Zhou, H. X. (2001). "Single-chain versus dimeric protein folding: thermodynamic and kinetic consequences of covalent linkage." *J Am Chem Soc* 123: 6730-1.

VITA

Grigorios A. Papadakos was born in Athens, Greece on May 29, 1978 to Athanasios and Eleni Papadakou. In 1996 Grigorios graduated from the Third Lyceum of Tripolis in Tripolis, Arcadia, Greece. He ranked first in the Panhellenic examinations in 1997 and entered the Chemistry department of the University of Athens where he received his Bachelor's degree in Chemistry in 2003. He entered the graduate program at the University of Missouri in St.Louis in the fall of 2003 where he earned his Master's degree in Biochemistry in May 2005.

Permanent address:
Grigorios Papadakos
Fotakou 10
Tripolis 22100
Greece

Publication

Papadakos, G. A., Nastri, H., Riggs, P. and Dupureur, C. M. (2007). "Uncoupling metallonuclease metal ion binding sites via nudge mutagenesis." *J Biol Inorg Chem* 12:557-69.